Oral lipid-based treatments for chronic liver disease: from formulation characterization to *in vitro* assays mimicking pathological conditions

Inaugural dissertation of the Faculty of Science,
University of Bern

presented by

Ivo Skorup

from Croatia

Supervisor of the doctoral thesis:

Prof. Dr. Paola Luciani

Department of Chemistry, Biochemistry and Pharmaceutical Sciences,

University of Bern



Oral lipid-based treatments for chronic liver disease: from formulation characterization to *in vitro* assays mimicking pathological conditions

Inaugural dissertation of the Faculty of Science,
University of Bern

presented by

Ivo Skorup

from Croatia

Supervisor of the doctoral thesis:

Prof. Dr. Paola Luciani

Department of Chemistry, Biochemistry and Pharmaceutical Sciences,

University of Bern

Accepted by the Faculty of Science.

Bern, August 30, 2023

The Dean

Prof. Dr. Marco Herwegh

Table of Contents

Chapter 1. Background and Purpose				
1.1 Liver – function and structure	2			
1.2 Chronic liver diseases – aetiology	4			
1.3 Potential therapies for chronic liver disease – essential phospho elafibranor and obeticholic acid	-			
1.3.1 Essential phospholipids	10			
1.3.2 Elafibranor	11			
1.3.3 Obeticholic acid	12			
1.4 Steatosis induction in <i>in vitro</i> models – hepatocytes as pivotal cell type	13			
1.5 Aim of the thesis	14			
Chapter 2. <i>In vitro</i> models of hepatic steatosis: current challenges and future dire				
2.1 Introduction	17			
2.2 Chronic liver diseases – NAFLD: the pathogenesis	18			
2.2.1 Lipid droplets – critical players in steatosis and NAFLD	19			
2.3 Hepatocytes in culture	23			
2.3.1 Cell lines overview	23			
2.3.2 System developments – co-culture systems, stem cell-derived hepato	-			
2.3.3 General remarks on cellular models	26			
2.4 Steatosis induction	27			
2.4.1 Free fatty acids, their salts, and lipid treatments	27			
2.4.2 Drugs and chemicals	32			
2.4.3 Steatosis-inducing compounds concentrations and incubation times	35			
2.4.4 Drug discovery for steatosis inhibition in vitro – state-of-the-art	36			
2.5 Outlook for drug discovery and early-stage drug formulations	37			
2.6 Conclusion	38			

Chapter 3. Polyenylphosphatidylcholines as bioactive excipient in tablets treatment of liver fibrosis	
Abstract	41
Graphical abstract	41
3.1 Introduction	42
3.2 Materials and methods	44
3.2.1 Materials	44
3.2.2 Powders and tablets preparation	45
3.2.3 Formulation development	45
3.2.4 Optimised formulation F70-5 – tablets preparation	48
3.2.5 Compendial powder quality tests	48
3.2.6 Compendial tablets quality tests	49
3.2.7 Gastro-resistant coating of tablets	49
3.2.8 Disintegration of gastro-resistant tablets	49
3.2.9 Thermogravimetry (TGA)	50
3.2.10 X-ray powder diffraction (XRPD)	50
3.2.11 Confocal Raman microscopy	50
3.2.12 S 80 M extraction from tablets	51
3.2.13 Preparation of protein-free chylomicrons (PFC)	51
3.2.14 Cell culture and general information about cell experiments	51
3.2.15 Direct treatment of LX-2 and PRHSC	52
3.2.16 Analysis of lipid droplet content ORO	53
3.2.17 Reactive oxygen species (ROS)	53
3.2.18 Cell proliferation assay (CCK-8)	54
3.2.19 Motional order of the cell membrane in adherent cells	54
3.2.20 qPCR gene expression analysis in LX-2 cells	55
3.2.21 Statistical tests and analysis	56

3.3 Results and discussion	56
3.3.1 Formulation development	56
3.3.2 Compendial quality assays of the final F70-	·5 formulation63
3.3.3 Thermogravimetry	64
3.3.4 X-ray powder diffraction (XRPD) and Rama	ın microscopy66
3.3.5 Modulation of LX-2 cell phenotype indicating	g antifibrogenic effects68
3.3.6 mRNA transcription of fibrosis markers	71
3.3.7 Motional order of the cell membrane in adh	erent LX-2 cells73
3.3.8 Modulation of cirrhotic PRHSCs phenotype	indicating antifibrogenic effects:
our proof of principle	75
3.4 Conclusion	78
Chapter 4. Secretome-mediated cross-talk between s stellate cells as <i>in vitro</i> model to evaluate lipid-bas	
disease	80
4.1 Introduction	81
4.1.1 Conditioned culture medium (CCM) as background and purpose	
4.1.2 Reported CCM models in various liver dise	ases – state-of-the-art 82
4.1.3 Final remarks on CCM – the rationale behi	nd our setup84
4.2 Materials and methods	84
4.2.1 Materials	84
4.2.2 Cell culture and general information about	cell experiments85
4.2.3 Preparation of stock solutions	86
4.2.4 Steatosis induction in Huh-7 cells	87
4.2.5 Preparation and characterisation of liposon	nes89
4.2.6 Dual cell culture model Huh-7 to LX-2	92
4.2.7 Dual cell culture model LX-2 to Huh-7 (Mo	odel E) – LX-2 cells treated with
controls and LX-2-CM on Huh-7 cells	95

4.2.8 Analysis of lipic	I droplet content (ORO)		95
4.2.9 Cell proliferatio	n assay (CCK-8)		96
4.2.10 qPCR gene ex	xpression analysis in LX	(-2 cells	96
4.2.11 Lipid and drug	g quantification – HPLC-	·CAD method	97
4.2.12 Statistical test	s and analysis		98
4.3 Results and discuss	sion		99
	tion in Huh-7 cells – cell	•	•
4.3.2 General remark	s on CCM treatment ex	periments	102
	X-2 phenotype after trea		
	ncubation with CCM and		-
_	re-treatments followed l	_	
-	Huh-7 CCM originating ions on naïve and quies		
4.3.7 Effect of contro	I-treated LX-2 CCMs on	ı steatotic Huh-7 cells (Model E) 118
4.4 Conclusion			120
Chapter 5. Conclusions a	nd Outlook		122
Appendix			127
Chapter 3			128
A3.1 Lipid quantificat	ion – HPLC method		129
A3.2 Preparation and	d characterisation of lipo	somes	130
Chapter 4			133
	nt of naïve Huh-7 with	•	
List of abbreviations			

Bibliography	143
Acknowledgements	162
Declaration of Consent	165

Chapter 1. Background and Purpose

1.1 Liver – function and structure

The liver is a complex organ central to numerous physiological and synthetical functions of the human body, such as protein synthesis, food digestion and macronutrient metabolism, carbohydrate metabolism, lipid storage regulation together with cholesterol homeostasis, xenobiotic detoxification, endocrine growth signalling pathways control, support and modulation of immunological activity, regulating blood volume and clearance of damaged erythrocytes.¹⁻⁷

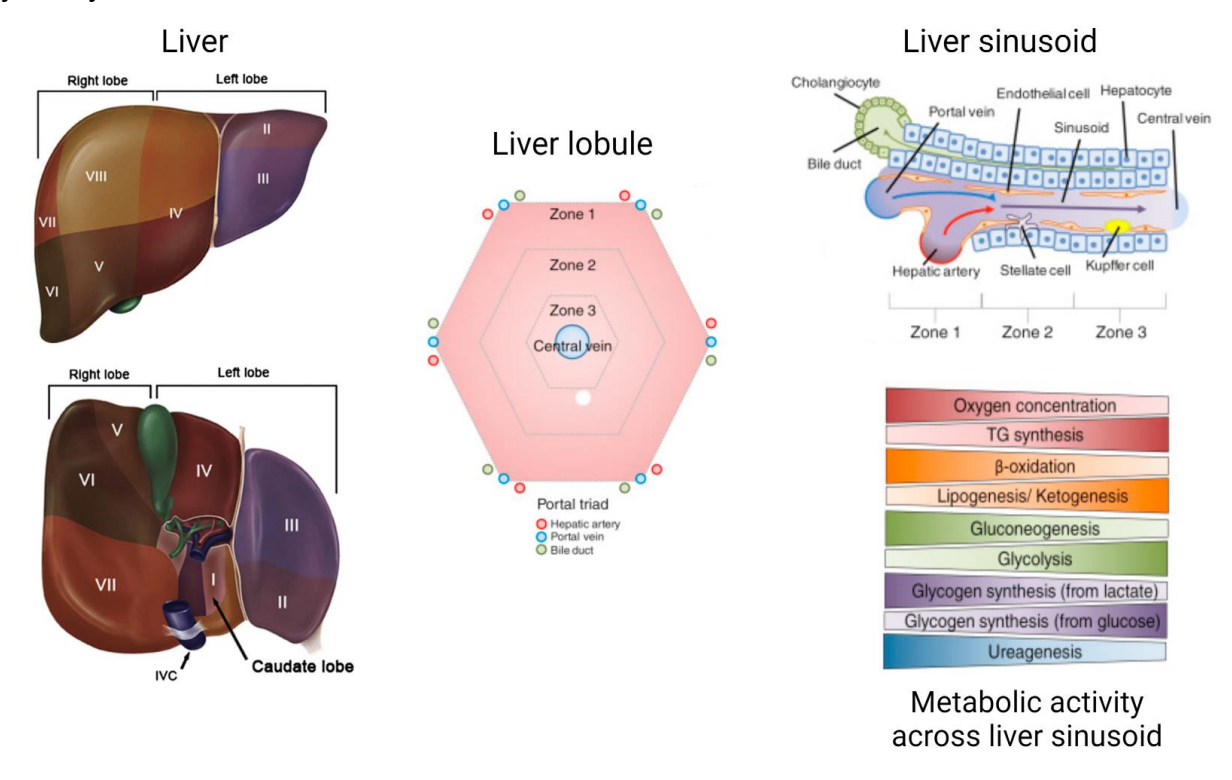


Figure 1.1. Liver anatomy, lobule, and sinusoid. The liver structure – two main lobes divided into eight segments containing hexagonal liver lobules connected to the sinusoids. The diagram under the sinusoid outline shows different metabolic activities along the sinusoid areas, whose intensities are represented by varying colour intensity. The figure was created using Biorender.com, adapted and reproduced from Trefts, E., Gannon, M. & Wasserman, D. H. The liver. (2007), DOI: 10.1016/j.cub.2017.09.019¹ and Abdel-Misih, S. R. & Bloomston, M. Liver anatomy. (2010), DOI: 10.1016/j.suc.2010.04.017⁸ both with permission from Elsevier that retains all rights on original figures.

The liver is the largest internal human body organ and its average mass is around 1500 g (838-2584 g).⁹ It is located just behind the ribcage in the right upper quadrant of the abdomen under the diaphragm within the Glisson's capsule.^{1,8} Highly organised structure with unique architecture consists of continuous parenchyma consisting of hepatocytes spotted with different cell types exerting various functions, penetrated by afferent and efferent circulation. The general structure of the liver is a large right lobe and smaller left lobe, sectioned into a

total of eight segments, each provided with biliary branches and vascularisation. 1,8 Lobules are the central organisational units of the lobes, consisting of hexagonally-arranged hepatocytes expanding from the central vein and delimited by six portal triads. 1,8,10. Each portal triad consists of a hepatic artery, portal vein, and bile duct ramifications (Figure 1.1).¹ Because of this anatomic structure, the liver possesses the most complex circulation of any with blood successively draining into а central vein across the organ, lobule. 11-13 The space of Disse (perisinusoidal space) is a place of contact between hepatocytes and sinusoids, mainly containing hepatic stellate cells (HSC) and dendritic cells, modulating the local immune response.¹⁴

Hepatocytes are major differentiated epithelial cells in the liver and present a high polarity. ¹⁵ They form a sieve plate around sinusoids, and hepatocytes' main function and morphology change based on their location across the lobule. ^{1,16-18} Hepatic acinus is a functional unit of the lobule formed from sinusoids and hepatocytes. ^{1,18} Basolateral side faces sinusoidal endothelial cells (LSEC), and the apical side is a secretory pole towards cholangiocytes and bile ducts. ^{15,19} Around 70% of all liver cells are hepatocytes which execute the liver's core functions of the lobule by performing various metabolic reactions. ² Since reactions are non-specific, a conversion of non-toxic molecules into toxic ones can occur, which is a potential cause of cell damage leading to chronic liver disease if unresolved. ⁶ Hepatocytes work collaboratively along non-parenchymal cells, such as hepatic stellate cells (Ito cells, HSC), LSEC, Kupffer cells (stellate macrophages), cholangiocytes (bile duct epithelial cells), biliary cells, liver-associated lymphocytes. Intercellular communication occurs via direct cellular contact or soluble factors. ^{1,19-21}

HSCs were described in 1876 by Kupffer for the first time and termed "Sternzellen".²² Located in the perisinusoidal space, their physiological cytoplasmatic processes receive systemic signalling from different organs via blood.²³ Because of this location, HSCs can be blood-targeted.^{1,23} Nerve endings collocate with blood vessels making HSCs susceptible to sympathetic nerve responses.²³ Different from hepatocytes of parenchymal cell type, HSC are mesenchymal cells and represent 5-10% of total liver cells.²²⁻²⁴ HSCs contain up to 80% of the human body's vitamin A (retinol), and retinoids reserve in the form of cytoplasmatic lipid droplets, which storage amount depends on the exact location of the cells inside of hepatic lobule.²³⁻²⁷ Nevertheless, they provide structural support to the liver lobule by physiological collagen and extracellular matrix (ECM) homeostasis. They are a significant source of cytokines and growth factors involved with normal liver development, hepatocyte mass preservation and drug and lipid metabolism.^{2,23,28,29} Although fibrosis development

depends on multifactorial causes, HSCs are responsible for liver fibrosis because of their central role as ECM production sites.^{23,30,31} Kupffer cells are resident macrophages filtering blood and performing immunoregulation.²

Even if the liver has an extraordinary regeneration ability, up to 70-90% of the tissue after the surgical resection, constant exposure to xenobiotics and by-products of metabolism, and antigenic and microbiological stimuli present a high risk of developing a chronic injury. 19,32 This might lead to a compensatory proliferation of hepatocytes and activation of other liver cells leading to regeneration exhaustion, progressing to liver insufficiency and can result in organ failure in severe cases. 19,33

1.2 Chronic liver diseases - aetiology

The gradual deterioration of liver function characterises chronic liver disease (CLD). This condition arises from sustained liver injury and the subsequent wound-healing response, which can lead to the irreversible alteration of liver structure and function.³⁴⁻³⁷

Based on aetiology, CLD is divided into alcoholic-associated and non-alcoholic fatty liver diseases (NAFLD), which are furtherly distinguished by non-alcoholic fatty liver (NAFL) and non-alcoholic steatohepatitis (NASH). ^{36,38-41} In June 2023, the European Association for the Study of the Liver (EASL), American Association for the Study of Liver Diseases (AASLD), and Latino-American Liver Study Association (ALEH) made a joint proposal to amend the NAFLD pathology nomenclature to metabolic dysfunction-associated liver diseases (MetALD), with respective changes to metabolic dysfunction-associated steatotic liver disease (MASLD) and metabolic dysfunction-associated steatohepatitis (MASH) to describe more precise these conditions and be less discriminatory. ⁴²⁻⁴⁴ Considering recent nomenclature introduction, for this dissertation, the old nomenclature, NAFLD and NASH, will be used throughout text.

NAFLD, the most common chronic liver condition, has a global prevalence of at least 25% with a constant increase and is becoming one of the significant pathologies of concern for the worldwide population. NAFLD occurs in individuals with a history of minimal to no alcohol consumption. AT

Major primary factors for developing NAFLD are metabolic disorders, such as type II diabetes mellitus (T2DM), metabolic syndrome, dyslipidaemias, and hypertension. Further attributing risks include genetics, autoimmune inflammation, viral infections, certain medications, starvation, environmental toxicity and celiac disease.⁴⁸⁻⁵⁰ As many factors influence the

initiation and progression of NAFLD pathogenesis, multiple parallel or sequential damaging "hits" have contributed to liver inflammation and damage on other organ systems^{41,49}, as proposed by Buzzetti,⁵¹ Tilg⁵² and Farrell.⁵³

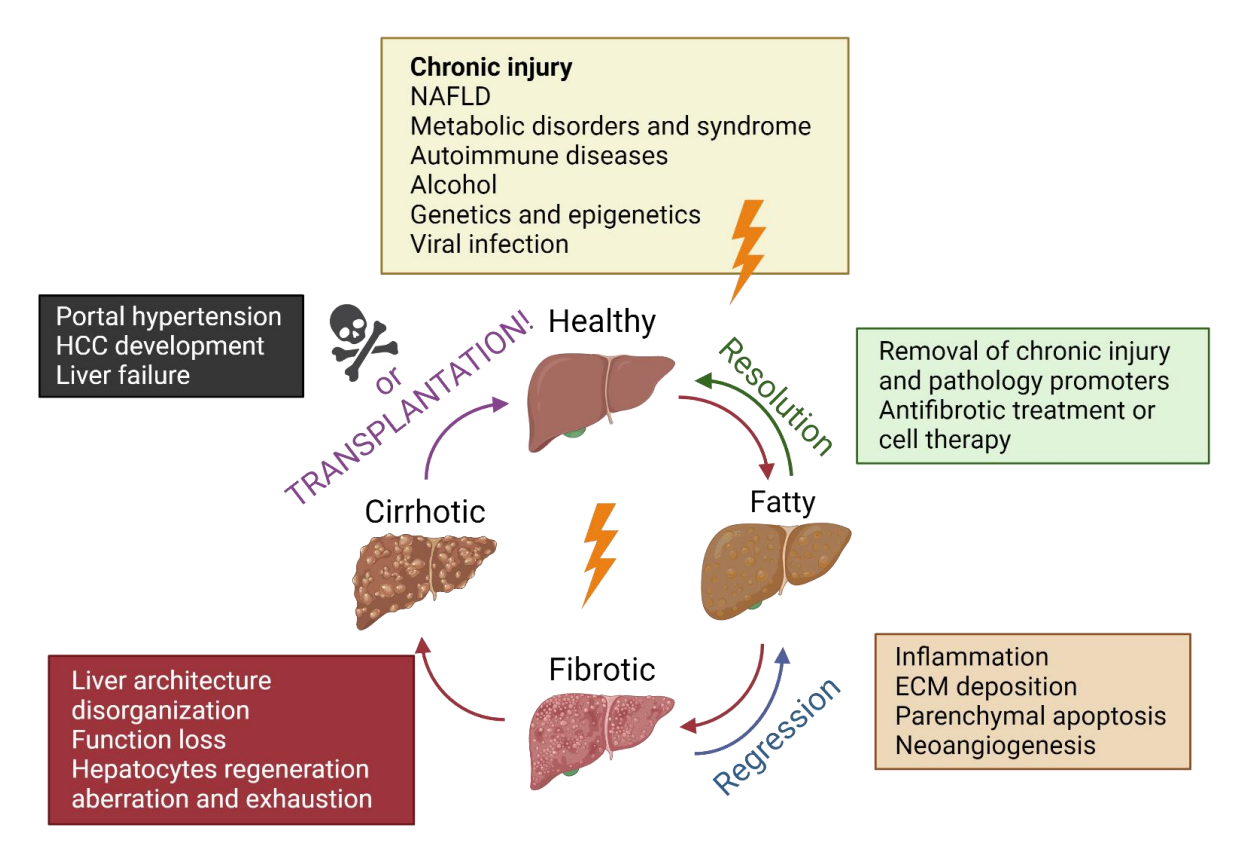


Figure 1.2. NAFLD spectrum circle of pathology. A healthy liver can progress towards a fatty liver state due to the influence of promoting factors. However, if liver damage promotors persist, the liver can advance to an advanced fibrotic state. If left untreated, this can lead to cirrhosis and a potential risk of developing hepatocellular carcinoma (HCC), which might require a liver transplant. In severe cases, pathology progression can even lead to death. The figure was created using Biorender.com and adapted partially from Pellicoro, A. et al. Liver fibrosis and repair: immune regulation of wound healing in a solid organ (2014), DOI: 10.1038/nri3623.³⁰

Based on histological liver tissue evaluation, as described by Matteoni⁵⁴ and integrated by Malnick⁴⁷, NAFLD expresses at least four levels of severity. The first two correspond to a more benign NAFL, and the second to a more advanced NASH characterised by tissue inflammation. While the progression of NAFL is considered only a minor risk, NASH progression could lead to a risk of severe fibrosis, cirrhosis, and, eventually, hepatocellular carcinoma (HCC), all of which might require an organ transplant as a therapeutic step because of the irreversible tissue damage.^{40,55,56} In most cases, NAFL is asymptomatic and

unexpectedly discovered in routine check-ups of liver enzymes, and its late discovery might lead to more pathological progression.^{57,58} Patients suffering from NAFLD reported altered fatty acid composition and phospholipid metabolism that was a direct consequence of pathological progression.⁵⁸ Inert triglycerides accumulate in the steatotic liver without producing damage.⁵⁹ but free cholesterol, saturated fatty acids, diacylglycerols (DAG), ceramide, and sphingomyelin migrate to mitochondria and exert lipotoxicity. 50,52,59,60 Lipid accumulation occurs as a disbalance of the lipid input and output or as a consequence of the reduced breakdown of free fatty acids (FFA). 50,61 As a result, mitochondrial dysfunction can occur and play a crucial part in hepatic steatosis development. 60,62,63 Production of reactive oxygen species (ROS) with respective production of free radicals and subsequent oxidative hepatocytes' damage by TNF-α (tumour necrosis factor-alpha) release. 50,52,59,60 In addition to steatosis characteristic of NAFL, in NASH, a more prominent clinical image is also characterised by the appearance of hepatocyte "ballooning" injury and lobular inflammation induced by lipotoxicity, ROS, oxidative and endoplasmic reticulum stress, conclude in apoptosis. 64,65 Chronic depletion of hepatocytes describes a crucial step that induces further progression instead of resolving the fibrosis. 66 Hepatocytes' apoptosis. and direct ROS, activate resident Kupffer cells releasing TNF-α, transforming growth factor β₁ (TGF-β₁), interleukin IL-1b, IL-6 and IL-13 and pro-fibrogenic factors with activation of the anti-fibrinolytic coagulation pathway. 30,52,66-69 Leukocytes are recruited to the injury site, phagocyting apoptotic hepatocytes, further amplifying the inflammatory reaction.³⁰ Cytokines released from dying hepatocytes act as pro-inflammatory mediators; their effect, combined with CTGF (connective tissue growth factor), PDGF (platelet-derived growth factor), and TGF-β1, stimulate the HSCs' activation. This activation elicits HSCs to undergo transdifferentiation, transitioning from a physiological, quiescent state to an activated, myofibroblast-like state, leading to a significant shift in their gene expression profile.^{24,30,66,68}-74

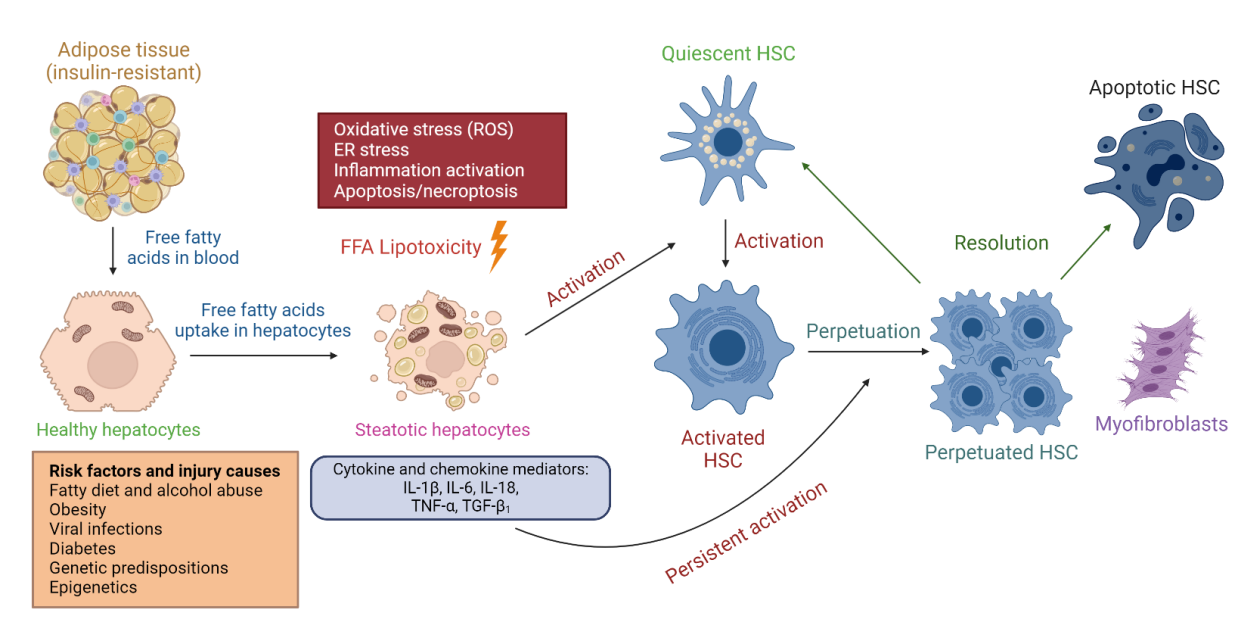


Figure 1.3 Hepatic interactions in NAFLD. Prolonged liver injury from various causes can lead to inflammation, finally resulting in fatty liver development. Throughout this process, hepatocytes uptake circulating free fatty acids, damaging the liver cells and releasing soluble mediators that activate HSCs. This activation leads to the transdifferentiation of HSCs into myofibroblast-like cells, perpetuating liver injury. However, this process can be reversed by eliminating the initial stimuli, allowing HSCs to return to a quiescent-like state or undergo apoptosis, ultimately resolving the condition. The figure was created using Biorender.com.

HSCs activation causing epigenetic changes can be distinguished into an initiation and a perpetuation phase bringing functional and morphological variations. 69,75,76 Pro-inflammatory initiation phase is the first early reply to damaged hepatocytes' signalling. From these paracrine signals, TGF- β_1 and TNF- α are the most responsible for increased collagen synthesis and accumulation, the hallmark of liver fibrosis. In particular, the targets of TGF- β_1 are bifunctional SMAD proteins, which activation stimulates ECM production while TNF- α regulates cell cycle and proliferation, co-modulates ECM, matrix metalloproteases (MMP) and adhesion molecules synthesis.

Successively, if various autocrine and paracrine stimuli are not resolved, HSCs can undergo lasting perpetuation.^{79,80} This perpetuation manifests as specific variations in the cells' behaviour, including increased proliferation, chemotaxis, higher contractility through increased expression of cytoskeletal filaments (α-smooth muscle actin [α-SMA]), and more outstanding production of collagen type I.^{77,78,80} To fuel increased ECM synthesis, activated HSCs lose their physiological lipid droplets by decreasing in size and breaking into smaller ones before completely disappearing.^{27,81,82} In the end, this process causes exhausted retinol and retinoid storage.²⁴

HSCs are considered a crucial factor in priming and sustaining liver fibrosis.^{22,83} Tissue fibrogenesis is typically reversible, but its outcome depends on the underlying cause. If the causing event is eliminated, early hepatic fibrosis can be resolved.⁸⁴⁻⁸⁶ Though, if the fibrosis' origin persists, it can gradually alter the liver's standard architecture and eventually lead to irreparable damage, compromising its function.³⁰ Fibrosis and subsequent cirrhosis result from an exaggerated wound-healing response caused by a continuous interplay between HSCs and consistently injured hepatocytes.^{26,87} The process of scar tissue accumulation is slow, taking up to 30 years to develop full-scale cirrhosis, so it is essential to prevent development to stop the pathology.³⁰

Once cirrhosis is established, the likelihood of reversing the process decreases significantly.³⁰ The hallmark of cirrhosis is the formation of hepatocellular nodules, where overgrown connective tissue encapsulates healthy liver tissue.⁸⁸ Consequently, liver stiffness impairs blood flow, leads to portal hypertension, and increases the liver decompensation risk or HCC, thereby increasing mortality.⁸⁹ At this damage state, to prevent liver failure or cancer development, the most effective current treatment is the transplantation.³⁰

Once activated HSCs can undergo a third pathway, resolution, in case the causing liver injury resolves. Part of the cells will undergo reversion/regression to quiescent status. At the same time, the other HSCs will submit to apoptosis through various pathways, some of which are still unidentified, to contain the caused damage.^{23,90}

Specific HSCs' location in perisinusoidal space just in-between blood vessels and hepatocytes makes them fibrosis primary mediators. Because of all this, HSCs can be considered a significant therapeutic target and provide a valuable tool for studying the effect and mechanisms of potential new antifibrotic therapies.^{68,79,91}

1.3 Potential therapies for chronic liver disease – essential phospholipids, elafibranor and obeticholic acid

There is no approved pharmacological treatment for NAFLD, but several potential active pharmaceutical ingredients (APIs) have been tested for the last 20 years. $^{92-97}$ Some considered APIs were glucose-lowering compounds targeting insulin resistance and lipid metabolism. Only recommended therapy by clinicians' guidelines currently are pioglitazone and vitamin E (α -tocopherol). $^{95-97}$

Pioglitazone is a peroxisome proliferator-activated receptor-gamma (PPAR-γ) agonist.⁹⁸⁻¹⁰⁰ It has shown promising results in improving liver histology in NASH, reducing steatosis and

inflammation in clinical trials (PIVENS study; NCT00063622).^{98,100,101} On the molecular level, pioglitazone acts as an insulin sensitiser and improves cytosolic lipolysis and autophagy by enhancing intracellular pathways.¹⁰² A decreased cytokines and chemokines production regulated by nuclear factor-κB (NF-κB) mediated secretion, with an increased adiponectin production, a peptide hormone involved in a pathology-positive carbohydrates and fatty acids metabolism regulation, has been observed after PPAR-γ pathway activation.^{92,103-105}

Vitamin E is a potent antioxidative agent. ^{106,107} As to PIVENS study results, alone or with pioglitazone, vitamin E improved liver histology in NAFLD-affected patients. ^{92,100} It modulates multiple molecular pathways, reducing oxidative stress by downregulating nicotinamide adenine dinucleotide phosphate (NADPH) oxidase and inducible nitric oxide synthase (iNOS), enhances glucose and lipid metabolism through the activation of the nuclear factor erythroid 2-related factor 2 – carboxylesterase 1 (Nrf2/CES1) pathway. ^{37,92,108,109}

Metformin is a biguanide API reducing blood glucose levels and hepatic gluconeogenesis and increases gastrointestinal glucose absorption. ^{92,103,104,110} By modulating carbohydrate metabolism and inducing weight loss in T2DM patients, it alleviates underlying risk factors for NAFLD progression but is not considered a valid therapeutic choice as it did not show any improvement in liver histology. ^{92,97,111}

Glucagon-like, incretin-mimetic, peptide 1 (GLP-1) receptor agonists, liraglutide, semaglutide, and exenatide, are antihyperglycemic APIs modulating glucose metabolism, inhibiting glucagon release, improving insulin secretion and resistance, consequentially hindering NAFLD development and progression.^{103,104,112-114} Liraglutide and semaglutide have been demonstrated to reduce liver fat content and improve the histological status, together with liver serum enzymes reduction without deterioration of fibrosis status.^{92,115} Sodium-glucose linked transporter 2 (SGLT2) inhibitors (dapagliflozin, empagliflozin, canagliflozin, ipragliflozin) block the SGLT2 protein located in the epithelium of proximal renal

tubules and enhance urinary glucose elimination, which as a consequence lowers circulating glucose independently of circulating insulin.^{97,116} Negative energy balance and metabolic change towards lipids as a principal energy source seem to be the main SGLT2 inhibitors' mechanism of action.¹¹⁶ A promising improvement in liver stiffness after using SGLT2 inhibitors has been observed in two small-scale clinical studies.¹¹⁶

Acetylsalicylic acid (Aspirin) is an interesting example of a traditional non-steroidal antiinflammatory drug and antiplatelet medication. It was investigated that reduced platelet accumulation and turnover in the liver after chronic Aspirin treatment caused the reduction in platelet-derived GPIba, identified as a contributing factor for NASH development and its subsequent progression to HCC independently from other coagulation factors.^{92,117} Another observational study showed that chronic Aspirin use by NAFLD patients attenuated the risk of severe fibrosis progression and improved liver histology status.^{92,118}

The investigational drugs elafibranor (Ela; PPAR- α/δ agonist),^{99,119} and obeticholic acid (Oca; farnesoid X receptor [FXR] ligand) are described in more detail in dedicated **Sections 1.3.2** and **1.3.3** (*vide infra*).^{120,121}

In the past, our research group investigated the co-formulation of Ela and Oca with PPC-rich liposomes, which mitigated not only the potentially damaging effects of the drugs on HSCs but also induced specific changes in the composition of cellular and extracellular vesicle (EV) phospholipids.¹²²

1.3.1 Essential phospholipids

Essential phospholipids (EPLs) are highly purified soybean extracts consisting of polyenylphosphatidylcholines (PPCs), with 1,2-dilinoleoyl-*sn*-glycero-3-phosphocholine (DLPC) being the major lipid in the mixture (content up to 52%). 123-127 Gundermann reviewed in 2016 EPLs use in liver disease, only for extracts containing 72-96% of PPC content. 125 Due to their antioxidant and anti-inflammatory properties, EPLs have been used to manage fatty liver disease since 1988. 125,128 They are named essential because the human body cannot synthesise them in enough quantity or at all. DLPC, which has a polyunsaturated 36:4 structure, is regarded as the primary active compound of PPCs. 129,130 For over 50 years, multiple investigations have examined the correlation between EPLs consumption and liver regeneration. However, the mechanism by which EPLs act against CLD is still not fully understood. 125,126,131,132 DLPC, the main component of EPLs, is commonly believed to be responsible for their antifibrotic effects by stimulating collagenase activity and reducing ROS levels induced by the TGF-β₁ effect in HSCs. 133-135 Furthermore, evidence suggests that PPCs can aid in preserving membrane fluidity and function through their incorporation into damaged portions of the hepatic cell's plasma membranes. 136 Despite these promising findings, a standardised understanding of EPLs' role is still lacking, and rigorous preclinical and clinical trials are necessary to determine the exact valuable effects of EPLs in liver fibrosis, which represents one of the most critical aspects of CLD.

Our group's previous research investigated the effect of PPCs formulated as unilamellar liposomes, particularly of lipid S 80 obtained from Lipoid (Ludwigshafen, Germany). S 80 containing 73-79% of PC demonstrated an *in vitro* potential to resolve fibrosis in an activated

human HSC model, LX-2.^{137,138} Furthermore, after S 80 treatment, LX-2 cells restored lipid droplets and have shown a decrease in significant fibrotic markers (collagen and α-SMA). The work described in this dissertation builds upon these studies, employing a modified version of the lipid S 80, Soluthin[®] S 80 M, magnesium-complexed salt of S 80. The task was to check if the EPLs bioactivity is retained and if this lipid, because of its better technical properties, can be employed to formulate a more patient-compliant pharmaceutical dosage form (tablets) to create a framework to potentially, in the future, co-formulate PPCs tablets with more potent new antifibrotic APIs.

Figure 1.4. Molecular structures of (a) DLPC, (b) elafibranor, (c) obeticholic acid.

1.3.2 Elafibranor

Elafibranor (Ela; GFT505) is a dual PPAR- α/δ agonist.^{119,139} PPARs are nuclear receptors comprising three families (alpha, delta and gamma) and play a critical role in metabolic homeostasis regulation, immune-induced inflammation, and cell differentiation.^{119,140}

PPAR- α regulates the liver's lipid metabolism by modulating fatty acid transport and β-oxidation, reducing triglycerides and increasing high-density lipoprotein (HDL) cholesterol levels. PPAR- α activation inhibits inflammatory gene expression induced by nuclear factor-κB (NF-κB). 119,141

PPAR-δ (sometimes reported as PPAR-β) activation improves fatty acids transport and oxidation, increasing HDL-cholesterol levels, improving insulin sensitivity, and constraining hepatic glucose output.^{94,142} Anti-inflammatory effects of PPAR-δ activation have been observed to reduce macrophage and Kupffer cells' activity.^{119,143} A selective PPAR-δ agonist GW501516 was found to decrease circulating triglycerides, apolipoprotein B, and low-density

lipoprotein (LDL) cholesterol but retain HDL cholesterol while improving insulin sensitivity and reducing y-glutamyltransferase (GGT) levels.¹⁴⁴

PPAR-γ is predominantly expressed in macrophages and adipose tissue. At the same time, liver expression is relatively low and is critical in adipogenesis, lipid metabolism, insulin sensitivity, inflammatory response and immune regulation. 103,140,145-147 However, fibrosis reversion was not consistent, and the drug caused severe side effects unsuitable for long-term therapy, including congestive heart failure, peripheral oedema, bone fractures, and substantial weight gain. 94

Ela's potential benefits rise from dual PPAR α/δ agonism, which could produce an effect as an insulin-sensitising agent and reduce hepatic steatosis, inflammation, and fibrosis while regulating glucose homeostasis. 94,119,139 While the Phase IIb clinical trials (GOLDEN-505, NCT01694849) showed positive results, 119 the Phase III studies involving almost 2000 patients (RESOLVE-IT, NCT02704403) were terminated early as Ela failed to meet the primary endpoint of NAFLD resolution without further fibrosis deterioration. 94,119,139,148 Ela, however, met the primary endpoint in Phase II clinical trial to treat primary biliary cholangitis by significantly reducing alkaline phosphatase (ALP) and will continue to Phase III studies (ELATIVE, NCT04526665) until 2028. 149 In January 2023, it has been announced that Phase II clinical trial with Ela will be conducted for patients affected by primary sclerosing cholangitis, a rare disease destroying bile ducts (ELMWOOD, NCT05627362).

1.3.3 Obeticholic acid

Obeticholic acid (Oca; 6α-ethyl-chenodeoxycholic acid; INT-747) is a potent FXR agonist and, after clinical trials, has been approved and indicated, with an orphan drug designation, for the primary biliary cholangitis (PBC) treatment.¹⁵⁰⁻¹⁵² By chemical structure, Oca is a synthetic derivative of chenodeoxycholic acid, a natural-occurring bile acid.¹⁵³

FXRs are a nuclear receptor family playing a crucial role in metabolic pathways regulation, including metabolism, in particular, glucose homeostasis, inflammation, bile acids, and fibrogenesis regulation. They are expressed in the liver, kidneys, intestines, and adrenal glands. Bile acid synthesis is affected by FXR activation that furtherly impacts hepatic lipogenesis and cholesterol synthesis and acts as a hepatoprotectant to bile acid-induced cytotoxicity. NASH-affected patients show an inverse association between liver FXR expression and disease severity.

In preclinical studies, Oca has been shown to improve hepatic steatosis, fibrosis, and portal hypertension. 120,155-157 In clinical trials with patients affected by T2DM and alleged NAFLD, Oca decreased serum alanine aminotransferase (AAT) concentrations and enhanced insulin sensitivity. 120,153

In contrast, clinical trials demonstrated that less lipophilic ursodeoxycholic acid (UDCA) presenting an insignificant binding affinity to FXR is not efficient in NASH patients. 120,158 Completed clinical trial FLINT (NCT01265498)120 and clinical trial REGENERATE (NCT02548351),121 which was supposed to run until 2025, have demonstrated that Oca can improve histologic severity and fibrotic status in NASH patients. These findings suggested that Oca may be approved as the first NASH-specific treatment. In June 2023, Intercept Pharmaceuticals, sponsor for Oca clinical trials, announced the receipt of a Complete Response Letter to their New Drug Application from the U.S. Food and Drug Administration (FDA) that reported that the drug in the present form could not be approved, and at least long term endpoint should be reached in the REGENERATE study after which they decided to cease all NASH-related operations with Oca.159

1.4 Steatosis induction in in vitro models – hepatocytes as pivotal cell type

To better understand the mechanisms fundamental to NAFLD and develop effective treatments, there is a pressing need for a reliable *in vitro* model of this disease.

The first distinguishing symptom of NAFLD is steatosis, which involves the abnormal accumulation of lipids in hepatocytes that can lead to cell toxicity due to the excess intracellular free fatty acids (FFAs), as previously described. Consequently, steatosis *in vitro* models are crucial for preclinical drug screening and can also aid in investigating novel therapeutic agents and their mechanisms of action.

The most used cell culture models for studying NAFLD include primary human hepatocytes from healthy donors, sometimes co-cultured with HSCs. Another widely used category is established hepatocarcinoma cell lines, which serve as substitute hepatocytes. These include Huh-7,^{73,160} HepG2,^{160,161} and HepaRG[™].¹⁶²⁻¹⁶⁴ Additionally, there is a growing trend towards using hepatocyte-like cells generated from induced pluripotent stem cells (iPSCs)^{165,166} or embryonic stem cells (ESCs)¹⁶⁷ as they provide a more representative cell model.

The scientific community has not yet agreed on the most effective methods for inducing steatosis. The literature contains a wide range of inducing compounds, concentrations, and

incubation times (ranging from a few hours to several weeks). Nevertheless, the standard protocol involves incubating hepatocyte-like cells with solutions of FFAs and their salts.

The most used FFAs for inducing steatosis are saturated palmitic acid (PA; C16:0), 160 typically used with or without monounsaturated oleic acid (OA; C18:1, ω -9), 160,162 at concentrations ranging between approximately 200 and 1000 μ M, which have been observed in patients or reported in the literature. Less frequently used fatty acids include other monounsaturated fatty acids, polyunsaturated fatty acids, and other lipids such as ceramide, 170 phosphatidylcholines, 171 and sphingomyelin 171 have been reported.

Furthermore, toxicology studies of commonly used hepatotoxic drugs can identify potential compounds for inducing steatosis. For instance, valproic acid, 172,173 tetracyclines, 174,175 amiodarone, 175 and cyclosporine A¹⁷⁶ are some alternative compounds used for this purpose.

1.5 Aim of the thesis

The main objective of this doctoral dissertation was to investigate new approaches in the treatment of NAFLD and fibrosis through the formulation of new soy PPC-based oral dosage form, testing it on fibrosis *in vitro* model, and *in vitro* disease modelling of steatotic hepatocytes and activated pro-fibrotic HSCs, to sincerely reproduce NAFLD and fibrosis pathophysiology by mimicking their mutual cross-talk by employing cell-conditioned medium (CCM). Given the absence of approved treatments specifically for NAFLD and fibrosis, there is an urgent necessity for developments in this area. To address this, we propose a therapy utilising soy PPC, a traditionally used compound, combined with experimentally investigated anti-NAFLD APIs, Ela and Oca.

Chapter 2 provides a comprehensive review of the current state-of-the-art steatosis induction *in vitro* models using human hepatocyte-like cell lines. The chapter critically examines various methodologies, including compounds and experimental parameters commonly employed in these models.

Chapter 3 focuses on developing and optimising antifibrotic PPC tablets based on a newly formulated soy PPC called Soluthin[®] S 80 M. The final tablet undergoes extensive physicochemical and pharmacopoeial tests to characterise its properties thoroughly. These tablets' bioactivity was evaluated in liver fibrosis *in vitro* models of immortalised human HSCs, LX-2, and primary cirrhotic rats HSCs.

Chapter 4 is dedicated to establishing and optimising NAFLD and fibrosis *in vitro* model that offers a critical insight into the cross-talk between hepatocytes and HSCs by employing CCM

in an asynchronous co-culture model using different incubation schemes. Steatotic hepatocytes and activated HSCs mimic the pathophysiology more accurately, compensating for the limitations of monoculture systems that fail to bring critical players into close contact. As previously observed, NAFLD and fibrosis are highly complex conditions and simultaneously interconnected pathologies involving various intracellular and extracellular elements and factors. However, the inconsistency of reported *in vitro* disease models calls for a more representative and reproducible model.

General experimental design involves inducing steatosis in Huh-7 cells, collecting their CCM-containing cell secretome, and using it to treat activated or quiescent-like-induced LX-2 cells. The study investigates different incubation sequences and experimental conditions with respective biological responses in detail. One experimental model assesses the bioactivity of CCM from steatotic Huh-7 cells, which were successively treated with formulations containing Ela and Oca encapsulated in PPC-base liposomes, and to observe the bioactivity of such obtained secretome on activated and quiescent-like LX-2 cells.

In conclusion, this doctoral research aimed to contribute to advancing NAFLD and fibrosis therapies by exploring new avenues, formulating challenging lipids into tablets, and developing improved *in vitro* disease models. The proposed pharmaceutical dosage form and the *in vitro* model offer a new perspective and solid framework for further investigation to address the pressing need for effective NAFLD treatment development.

Chapter 2.

In vitro models of hepatic steatosis: current challenges and future directions

Review article, ready for submission.

Skorup I, Luciani P

Author contribution

I.S. wrote the original manuscript; **P.L.** reviewed and edited the manuscript.

2.1 Introduction

The present chapter aims to recapitulate the state-of-the-art human cell culture models of steatosis, the treatments to reproduce the pathology *in vitro*, and the most recent therapeutic approaches tested in these models, thus providing a comprehensive guide in a vast area of liver steatosis research.

The importance of valid and representative *in vitro* cellular models of steatosis and NAFLD is of crucial significance to provide a robust screening platform for drug discovery and formulation development of potential drug candidates, so the efficiency of attenuation, prevention and reversion of the steatosis, and its further clinical progressions can be predicted. This is especially important when conducting the first biorelevant preclinical studies of new drug candidates to understand underlying physiological and pathological mechanisms of action. Practical therapeutic benefits can be screened at a more ethical, extensive, and reproducible scale to confirm proof of concept before passing further investigation towards more complex animal studies and finally human clinical trials.

A robust model can offer insight into identifying potential molecular targets to treat steatosis. Conclusive screening studies conducted on relevant and representative cell models can contribute to fewer animal studies and make research more 3R-compliant, with the three Rs standing for replacement, reduction, and refinement. In that way, only crucially relevant studies of the most promising new drugs can be performed.

As is often the case for *in vitro* cellular models, cellular systems mimicking chronic liver disease are hindered by several limitations. The scarce possibility of culturing together different cell types responsible for pathogenesis and disease progression and ensuring interaction because of different culturing conditions is one of the significant fallbacks. Cell culturing on plates and subjecting cells to various chemical agents may not accurately represent the actual effect on living organisms. Complex and multifactorial disease modelling, such as this one of steatosis, can present a significant challenge to design and mimic the entire pathological condition by employing simplified *in vitro* systems with available cell lines. In most cases, only selected aspects of pathophysiological mechanisms are investigated simultaneously. Nevertheless, they still represent a golden standard in preclinical research of new active pharmaceutical ingredients (APIs).

2.2 Chronic liver diseases - NAFLD: the pathogenesis

As reported in **Chapter 1**, NAFLD affects at least a quarter of the global population, with its prevalence steadily increasing, making it a significant global health concern. ^{38,41,45,177} Shortly, NAFLD is categorised into two types: NAFL, also known as fatty liver, and NASH, which are both characterised by lipid accumulation of at least 5% of the liver's weight, represented in triglyceride-rich lipid droplets. ^{36,38-41,62,178,179} NAFL is considered benign with a low risk of progression, with approximately 10-25% of all NAFL cases progressing to NASH, which can eventually advance to more severe conditions, such as increased fibrosis, cirrhosis, and liver cancer. ^{40,53,55,56,180}

Nowadays, it is well-known that NAFLD has multifactorial aetiology. Significant causes are unhealthy lifestyle and obesity, genetics, metabolic disorders, viral infection, autoimmune pathologies, and medical treatments involving intrahepatic and extrahepatic pathways.^{39,49} Its evolution is more precisely explained by multiple parallel or sequential damaging "hits", represented by an epiphenomenon of several diverse and contemporary injurious mechanisms.⁵¹⁻⁵³ Altered phospholipid metabolism and fatty acid composition profile have been observed in NAFLD patients.⁵⁸

The development of NASH is a consequence of intracellular liver lipotoxicity, driven by neo-synthesised DAGs, saturated FFAs, exogenous and free cholesterol, lysophosphatidylcholine, sphingolipids and ceramide (saturated FFAs esterified to sphingosine). All these elements play a significant role in lipid droplet formation, inflammation, and apoptosis induction. 50,52,53,59,60,111,181 Mitochondrial injury, followed by membrane disruption and dysfunction, leading to cytochrome c release, activation of apoptotic pathways and IL-6 and IL-8 release from hepatocytes constitute the primary mechanism of hepatocellular damage. 53,160,161,163,165,182,183 Activating the c-Jun N-terminal kinase (JNK) pathway impairs the β-oxidation of fatty acids in mitochondria, causing lipid metabolism disbalance. 50,52,59,60,184 Moreover, ROS-caused oxidative stress and TNF-α release also contribute to inflammation development. 50,52,59,60,163

Lipid droplets stored within hepatocytes consist of inert triglycerides, some derived from more toxic DAG that can upregulate phosphokinase C (PKC) and activate NF-κB pathways, resulting in enhanced inflammation.^{53,119,141} In both NAFL and NASH, there is evidence of highly reactive free cholesterol, able to downregulate specific CYP450 (CYP) isoforms responsible for metabolising the excess cholesterol.⁵³

NASH clinical image shows the hepatocytes "ballooning", namely the disruption of the cellular membrane and consequent morphological change of the cell.^{53,64,65,185,186} A different distribution of intracellular organelles and vesicles was observed, with an essential change in the cellular lipid profile content with the respective accumulation of triglycerides and cholesterol.^{53,186-189} An upregulated uptake of FFAs is caused by insulin resistance and higher circulating lipid concentration.⁵³ Inflammatory cytokines' secretion, such as TNF-α, various ILs, and TGF-β₁ from hepatocytes and Kupffer cells can activate fibrotic and inflammatory response in quiescent HSC, stimulate HSCs' activation to transdifferentiate from a physiological, quiescent state to an activated, myofibroblast-like one, expressing a radically different gene profile from physiological ones, with a certain number of most severely hit HSCs will go directly into apoptosis.^{24,30,53,66,68-74,152}

2.2.1 Lipid droplets – critical players in steatosis and NAFLD

Lipid droplets (LDs) are specialised organelles with a typical structure of a hydrophobic core, principally composed of sterol esters, triacylglycerols (TAG), and neutral lipids encased by a phospholipid monolayer containing proteins. LDs are not only passive storage for lipids but play a crucial role in various cellular functions across different cells and tissues, such as lipid storage and metabolism, energy balance and homeostasis, and cellular signalling.

2.2.1.1 Hepatocytes' LDs

Hepatic steatosis results from an excessive lipid accumulation caused by the disbalance between lipid catabolism and anabolism, dependent on increased dietary lipid intake, *de novo* lipogenesis, TAG synthesis and reduced lipid β-oxidation causing lipid accumulation in the form of LDs. ^{179,190,193} The main site of LDs genesis is the endoplasmic reticulum (ER), where neutral lipids accumulate in its membrane bilayer. TAG formation is catalysed by diacylglycerol acyltransferase 1 (DGAT1), having an active site inside the ER membrane. Nascent LD and ER-associated membrane phospholipid detach from ER and form cytosolic LDs. Fresh, small LDs can fuse with other LDs, a process regulated by cell death-inducing DFFA-like effector (CIDE) proteins with isoforms CIDEA and CIDEC upregulated in steatosis, and physiological isoform CIDEB downregulated. ¹⁹⁴⁻¹⁹⁶ LDs expansion can occur as a result of *de novo* lipogenesis, happening on the ER-LD membrane bridge to expand already present LDs. ^{194,197}

Steatosis can exhibit two distinct forms, microvesicular and macrovesicular, determined by the accumulated LDs size. 190 Main damage to hepatocytes occurs because of an increased FFAs conversion to lipid intermediaries, led by higher lipid intracellular content, impairs insulin signalling and provokes insulin resistance, causing lipotoxicity, resulting in increased inflammation and oxidative stress, causing chronic liver damage. 190,198 Initially, steatosis develops, potentially leading to steatohepatitis convoyed by disruptions in the ER, mitochondria and lysosome functions, which play a critical role in long-term disease progression. 190 Calcium homeostasis disruption caused by lipid metabolism disruption further fuels ER and oxidative stress in hepatocytes. 190,199,200 LDs stabilisation occurs through perilipin 2 (PLIN2) protein, and usually higher PLIN2 expression means higher mitochondrial activity. 190,201

Steatosis progression involves the significant participation of multiple LD-associated proteins. Differential protein expression profiles in the fatty liver include perilipin, adipophilin, TIP47, S3-12, OXPAT, and 17 β -hydroxysteroid dehydrogenase-13 (17 β -HSD13), all of which regulate LD size. TIP47 affects specifically budding LDs, while maturation and maintenance of LDs are regulated by adipophilin and perilipin. Significant upregulation of Fsp 27 and CIDEA regulates increased lipid storage and promotes LDs' fusion, characteristic of steatosis. T90,203 17 β -HSD13 potentiates steatosis phenotype by regulating LDs' size and number and activating liver X receptor α (LXR α) through the SREBP-1c pathway. T99,190,204,205

2.2.1.2 HSCs' LDs

Like hepatocytes' LDs, HSCs' LDs have various cellular functions, different from only storing lipids and rendering energy sources readily available. Their formation mechanism is comparable to that of hepatocytes. However, the lipid composition in HSCs is slightly different since HSCs' LDs contain a significant part of retinyl esters and represent a principal retinol reserve (approximately 75-80%) of the human body. 25,27,206 However, the LD abundance inside HSCs is a morphological indicator of quiescent HSCs. Contrarily, the loss of LDs signifies the activation of HSCs, representing an important visual marker for this transition. 80,82,206

HSCs' activation causes a depletion of physiological LDs, produces various lipid signalling precursors and instigates neo-synthesis of membrane phospholipids expanding ER and Golgi apparatus, critical for activated, transdifferentiated HSCs to produce substantial amounts of

extracellular matrix (ECM).^{206,207} Energy obtained from LDs metabolism, especially from HSCs' lipophagy, fuels cellular transdifferentiation, ECM synthesis, and development and progression of the fibrotic phenotype in hepatic diseases.^{80,206,208}

Since LDs hydrolysis yields not only TAGs but also all-trans and 9-cis retinoic acids, interacting with various retinoic acid (RAR) and retinoid X (RXR) receptors, directly and indirectly mediating transcription of more than 500 different HSCs' genes, which furtherly fortifies the fact that LDs are not only lipid storage but a significant player in cellular homeostasis.^{80,206,208,209}

Perilipins (PLIN), acting as LD-coating and stabilising proteins, are physiologically expressed in LDs, as already seen above. Reduction in general PLIN expression is directly correlated with LDs depletion and enables conditions for hepatic steatosis and fibrosis development and progression. The PLIN2 downregulation in NAFLD plays a crucial role in influencing widespread alterations in hepatic lipidomics, and these changes are believed to contribute to the process of SREBP-regulated *de novo* lipogenesis.^{206,210}

Immortalised human HSCs (LX-2) treated with retinol and palmitate have demonstrated a prominent Plin2 mRNA upregulation, consequentially enhanced PLIN2 protein levels and PLIN2-positive LDs containing retinyl palmitate are formed. PLIN2 induction reduced active HSCs molecular markers, namely collagen type I and α -smooth muscle actin (α -SMA), by simultaneously upregulating an ECM-digesting matrix metalloproteinase 1 (MMP-1) expression. The downregulation of HSC activation is endorsed by PLIN2 upregulation and is functionally linked to the fibrosis genomic and proteomic panel expression. α -206,211,212

Evaluating the histopathological status of human liver sections reveal numerous PLIN2-positive cytoplasmic LDs of distinguishable quiescent HSCs. However, in the fibrotic scarred liver, activated HSCs exhibit minimal LDs, thereby reducing PLIN2 immunoreactivity.²⁰⁶

2.2.1.3 Concluding remarks on LDs

LD metabolism is essential in steatosis and chronic liver diseases because of the dual nature of the lipid-driven effect on liver cells, in particular hepatocytes and HSCs. As described by Molenaar, lipids in the liver play Dr. Jekyll and Mr. Hyde, or as Mak nominates it, a "lipid paradox" occurs (**Figure 2.1**).^{206,213} Shortly, physiological state hepatocytes are virtually LD-free, while HSCs contain a significant LD content, which seems counterintuitive. Lipid quality, quantity and distribution in the liver are crucial when approaching NAFLD. Lipid-rich HSCs represent a healthy liver status, while lipid-rich hepatocytes obstruct physiological liver

function and give origin to steatosis, fibrosis and NAFLD. Lipid accumulation in hepatocytes or lipid depletion in HSCs can induce lipotoxicity and phenotype change characteristic of chronic liver diseases. Quiescent HSCs constitute significant retinyl esters reserve in the form of large LDs. However, once activated, these LDs are gradually digested and give rise to powering up liver fibrotic response. Treatment of NAFLD inconsiderately by targeting lipid accumulation in hepatocytes might provoke unwanted HSCs reaction and *vice versa* since the liver lipid metabolism is a finely balanced system that can easily skid towards a more pathological state. Here listed factors are why it is so difficult to reproduce steatosis and NAFLD as an *in vitro* model.

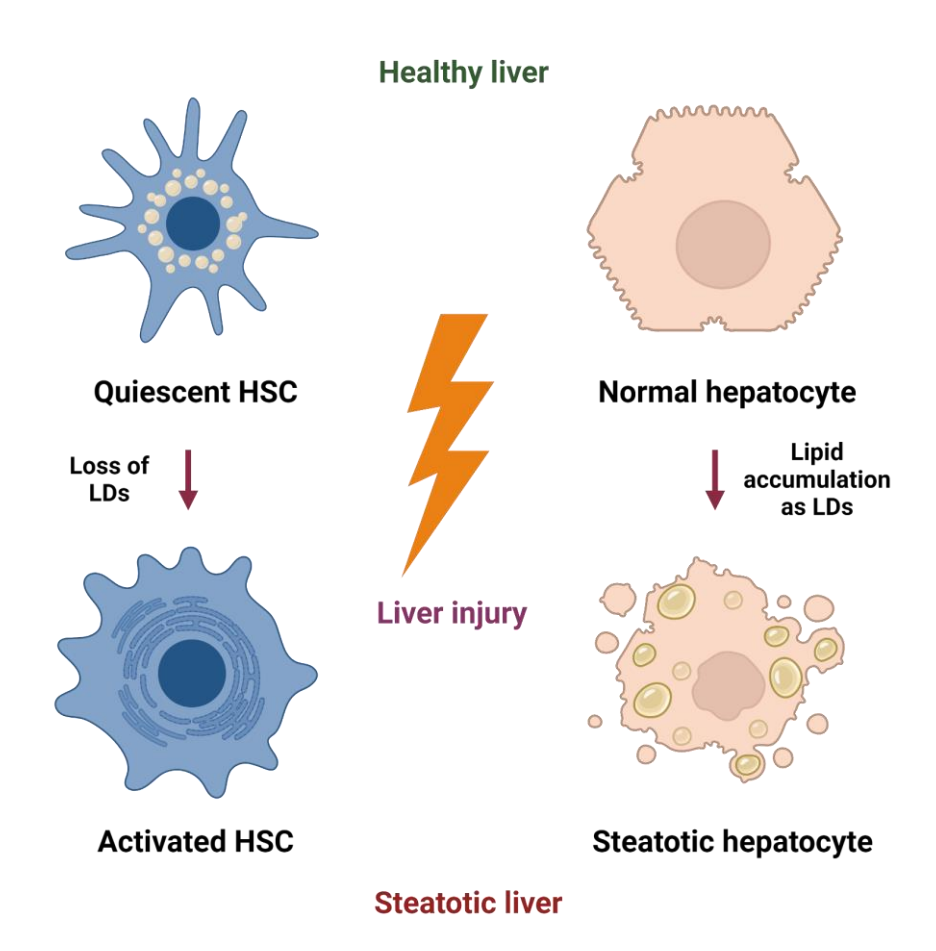


Figure 2.1. Lipid paradox in the liver. The lipid paradox consists of different effects of lipid accumulation in different liver cell types. Quiescent, healthy HSCs possess a substantial LDs population, and healthy hepatocytes present virtually no LDs. Once the liver sustains damage and a pathologic cascade starts, HSCs gradually lose their LDs, and hepatocytes fill up in LDs.

The figure was created using Biorender.com and adapted from Mak, K. M., Wu, C. & Cheng, C. P. Lipid droplets, the Holy Grail of hepatic stellate cells: In health and hepatic fibrosis. (2023), DOI: 10.1002/ar.25138.²⁰⁶

2.3 Hepatocytes in culture

2.3.1 Cell lines overview

In the human liver, hepatocytes represent approximately 60-70% of the organ and represent a significant metabolic centre of the human body.^{2,214} The isolation methods have been optimised over the last decades, reaching high yields and viability. 215,216 Therefore, the most common model used in modelling steatosis and underlying pathologies consists of PHH isolated from healthy and studied in vitro. 73,217,218 However, since the donor organ pool is scarce, other permanent cell lines have been established from hepatocarcinoma tissues.²¹⁹ Most notable examples are Huh-7 cells (Research Resource Identifiers [RRID], unique identifier of the cell line in the Cellosaurus database; CVCL 0336) from a 57-year-old Asian male,²²⁰ and **Huh-7.5** cells (RRID CVCL 7927), derived from Huh-7 cells, which demonstrate a permissiveness for the hepatitis C virus (HCV) RNA replication.²²¹ HepG2 (RRID CVCL 0027)²²² were isolated in 1979 from a 15-year-old white male and first identified as hepatocarcinoma.²²² In 2009, new genome expression profile research re-classified HepG2 as hepatoblastoma,²²³ but this misconception led to consider HepG2 as a problematic cell line since hepatoblastomas possess different cellular behaviour.²²³ Hepatocarcinoma cell line HepB3 (RRID CVCL 0326) was isolated from an 8-year-old African-American and contains at least 5 replicates of the hepatitis B virus (HBV) genome. 222 However, at the moment, there is no evidence suggesting that this cell line is capable of producing infectious HBV. 222,224 HepaRG™ cell line (RRID CVCL 9720) isolated from a female donor of unknown age suffering from hepatocarcinoma and hepatitis C infection resembles PHHs with the conserved metabolic array, in particular CYP system. 225,226 It can represent a reliable model to test liver metabolism, xenobiotics toxicity, and potentially drug-to-drug interactions. 225,226 HepaRG™ are considered bipotent liver progenitor cells able to differentiate toward hepatocyte- and biliary-like cells during their 2-week differentiation with dimethyl sulfoxide (DMSO) before conducting experiments.²²⁷

Other less commonly used cell lines include **HepG2/C3A** (RRID CVCL_1098), which is a clonal derivative of the HepG2 cell line, specifically chosen for its strong contact growth inhibition, high albumin and alpha-1-fetoprotein (AFP) production, besides the ability to grow in low-glucose cell culture medium.²²⁸ **KMCH-1** and **-2** cells (RRID CVCL_7970 and CVCL_7971), were isolated from middle-aged Japanese males. They represent combined hepato- and cholangiocarcinoma cell lines.^{229,230} **OR6** (RRID CVCL_VN30) is a more recent hepatocarcinoma cell line isolated from a 57-year-old Japanese male and supports consistent

hepatitis C virus (HCV) replication.²³¹ **PLC/PRF/5** (Primary Liver Carcinoma/Poliomyelitis Research Foundation/5; RRID CVCL_0485) is a hepatocarcinoma cell line isolated from a 24-year-old African male contains at least 7 copies of integrated HBV supporting enhanced carcinogenesis.^{232,233}

A comprehensive overview of the cell lines with steatosis-inducing fatty acids and conditions used to date and the corresponding references are reported in **Table 2.1**.

2.3.2 System developments – co-culture systems, stem cell-derived hepatocytes and 3D organoids

Hepatocytes are reported to be grown in co-culture with other cell types, with setups including direct simultaneous co-culture in a unique vessel (**Figure 2.2c**), 106,183,218,234,235 and using a Transwell® system (**Figure 2.2b**)183,217 where one cell type is cultured on a plate and another one on a cell insert, where cells communicate by exchanging soluble factors through a shared medium.

Hepatocytes are mainly co-cultured with HSCs, to connect two critical players in NAFLD progression. In particular, reported co-cultures are HepaRG™ with LX-2 (immortalised human HSCs; CVCL_5792)¹⁶³, Huh-7 with LX-2,^{183,235} PHH with primary human HSCs (PHHSC)^{73,217,218,236} also including primary human macrophages or 3T3-J2 mouse embryonic fibroblasts.^{217,236} Davidson *et al.* proposed this tri-culture model with mouse fibroblasts to stabilise the PHH phenotype since PHHSC could not perform it.²³⁶ Wobser *et al.* reported culturing HSCs with a conditioned medium of steatotic Huh-7 and HepG2, each time with immortalised human activated HSC cell line generated by ectopic (out-of-the-place) human telomerase reverse transcriptase (hTERT) expression.⁷³ These germline mutations in hTERT were observed in familial liver diseases and cirrhotic patients at a higher prevalence.^{237,238}

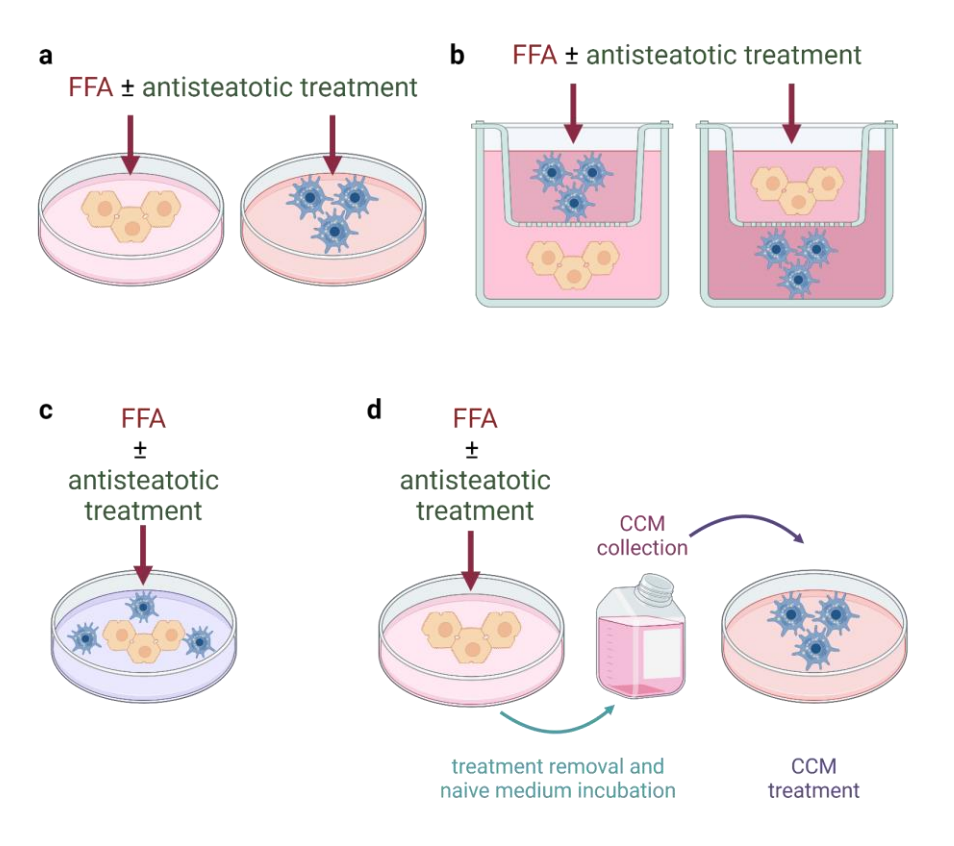


Figure 2.2. Cell culture protocols in steatosis in vitro models. Different culturing protocols: (a) Monoculture. (b) Transwell® co-culture. (c) Simultaneous co-culture. (d) Conditioned dual cell culture medium. The figure was created using Biorender.com and adapted from Barbero-Becerra, V. J. et al. The interplay between hepatic stellate cells and hepatocytes in an in vitro model of NASH. (2015), DOI: 10.1016/j.tiv.2015.07.010. 183

There are reports of **HLCs** derived from **iPSCs** and **ESCs**, sometimes cultured as organoids, offering a more consistent human NAFLD model. ^{165,166,234,239} Investigation of iPSCs-derived from NAFLD patients demonstrated a disease-specific gene expression profile, which provides new opportunities for more reliable pathology understanding and highlights the significance of individual and collective genetic factors in the disease process. ²⁴⁰ In addition, three-dimensional (3D) spheroid and organoid hepatocyte culture systems have been reported to simulate a more reliable liver environment condition, bringing hepatocytes into close contact. Reported spheroids were created from **PHHs**^{176,241,242} and **HepG2** cells, co-cultured with **LX-2** cells. ¹⁰⁶ Organoids derived from **iPSC-** and **ESC-**derived **HLCs** were reported. ^{165,234} Ouchi *et al.* also prepared **HepG2**, **THP-1** (human leukaemia monocytic cell line), and **LX-2** co-cultured 3D organoids with cell ratio 1:1:1. ²³⁴ Steatosis model in the form of a Liver-on-a-chip with **HepG2/C3A** cells was proposed by Gori *et al.* ²⁴³ For further details, additional information can be found in recent reviews. ²⁴⁴⁻²⁴⁷

2.3.3 General remarks on cellular models

As reported, no widely accepted immortalised human hepatocyte cell line is available. The most used human cellular models of hepatocytes are PHH, isolated from healthy patients, and liver carcinoma cell lines. Even if liver carcinoma possesses different genomic, proteomic and lipidomic profiles for intrinsic heterogenicity and different cellular origins, it does not consistently represent the physiological state. It cannot indeed recapitulate entire steatosis and NAFLD pathological pathways. However, these cell lines are still considered a golden standard in studies needing high reproducibility or high-throughput screening. PHH can be regarded as a better representative model for steatosis studies since they are actual hepatocytes from living donors. Still, the intrinsic heterogeneity of sources can bring variability and represent a limiting factor for extensive screening studies that might be prevented by pooling these cells.

In most cases, cells are grown as monolayers (**Figure 2.2a**). However, there are cases when hepatocytes are grown simultaneously (**Figure 2.2c**) or in a Transwell[®] co-culture (**Figure 2.2b**) with other cell types, usually HSCs.

Different cell types require different culturing conditions, so establishing a solid co-culture of hepatocytes, HSC, macrophages or other cell types, might present a significant challenge to keep the cells in their original expression state and give a reliable experimental model for steatosis screening. Therefore, cell identity validation in experimental culture conditions for two or more cell lines should be performed to ensure that cells represent the intended use to be part of the co-culture model. The realistic ratio between different cell types might represent an experimental challenge since this might change depending on the progression and intensity of the disease.

One of the solutions could be developing a co-culture model by conditioned dual cell culture medium (**Figure 2.2d**), as reported by Wobser *et al.* This model involves treating one cell type with a medium coming from the other one previously treated with FFAs and/or antisteatotic treatment or with its naïve state medium.⁷³

iPSC- and ESC-derived HLCs lack consensual derivation protocol and might present slightly inconsistent genomic and proteomic profiles based on the starting cells.

3D cell culture models, such as organoids and spheroids, might provide further development or an upgrade, especially of the co-culture model that puts different cell types in physical contact inside precisely engineered biocompatible scaffolds to reproduce even more closely the condition inside the human liver even more.

2.4 Steatosis induction

2.4.1 Free fatty acids, their salts, and lipid treatments

FFAs and their salts are the most used compounds to induce steatosis artificially in *in vitro* cell culture models. A significant part of dietary lipids, containing FFAs amongst other components, contributes to NAFLD pathogenesis, development and pathology reversion and prevention of the progression, depending on the lipid quality and composition.^{248,249} Approximately 15% of all hepatic TAGs originate from absorbed dietary intake and are substrates in hepatic lipogenesis.^{248,249} When building an experimental setup to mimic steatosis, one of the most convenient ways is to use these FFAs with already confirmed presence in the human diet and learned damage-inducing mechanism.

Although the human liver is usually exposed to a broad profile of circulating FFAs simultaneously, many studies used only one or two FFAs as a steatosis-induction agent, which might not provide a complete and realistic picture in screening cellular and molecular responses on a larger scale, but represent a valid and consistent model necessary to recreate pathological conditions *in vitro*. Therefore, single FFA induction provides a proper model for investigating specific aspects of steatosis induced strictly by that compound.

2.4.1.1 Single FFAs

Saturated **palmitic acid** (PA; C16:0) is commonly used alone or with oleic acid. PA has been shown to increase apoptosis by activating caspase 3 and 7 activity, leading to increased secretion of pro-inflammatory IL-8 and ROS, impaired insulin signalling, altered lipid and bile metabolism and enhanced CYP2E1 isoform in hepatocytes. $^{160,161,164,168,250-254}$ Increased expression of PPAR- α and decreased expression of PPAR- γ and sterol regulatory element-binding protein (SREBP-1), with activation of NF- κ B and activator protein 1 (AP-1) through higher JNK activation, has also been observed. $^{161-163}$ Induction of activin A by adiponectin, in its turn, increases TGF- β_1 level not regulated via NF- κ B. 255

Oleic acid (OA; C18:1, ω-9, *cis*) treatment increases the expression of PPAR- γ and SREBP-1 involved in FFA uptake, lipogenesis and cholesterol synthesis. ^{250,255} TGF- β ₁ level increases after an OA treatment and changes lipid and lipoprotein profiles, with increased triglyceride production and storage in lipid droplets form. Simultaneously, there is stimulation for higher DAG production. ^{164,250,255-260} Lipid droplets were reportedly increased compared to PA treatment. ²⁵⁰ Increased TNF- α production, lipid peroxidation, decreased PPAR- α expression, and cell proliferation have been observed in HepG2 cells. ²⁶¹ A lower amount of cytochrome

c diffusion from hepatocellular mitochondria accompanied by decreased apoptosis and JNK activation compared to PA and SA was kept.¹⁶⁰ Increased gene expression of glucose transporter 2 (GLUT2) has been observed upon OA treatment, affecting liver glucose output.²⁵⁸ In iPSC- and ESC-derived HLC increase in perilipin 2 (PLIN2), protein coating intracellular lipid droplets, has been observed, and many PPAR-α signalling pathway members were upregulated.¹⁶⁶

Stearic acid (C18:0, SA) has reportedly increased CYP2E1 activity and expression while decreasing CYP3A4 in HepaRG[™] cells.²⁶² Similarly to PA-treated cells, SA-treated cells show increased apoptosis through caspase 3 and 7 activations, and SA was even more toxic than PA in HepG2 cells.^{160,263}

Palmitoleic acid (C16:1, ω -7) induces lipid accumulation in Huh-7 cells but, when used together with PA, reduces apoptotic response provoked by PA.²⁶⁴

Elaidic acid (C18:1, ω-9, *trans*) is a *trans* isomer of OA, has not shown any difference in FFA load in hepatocytes compared to OA, but shows slightly smaller cell survivability and decrease in gene expression of ER stress marker and apoptosis-induced glucose-regulated protein (GRP78) and C/EBP homologous protein (CHOP).²⁶⁵

In screening for changes in different CYP450 isoforms, Madec *et al.* also reported using polyunsaturated FFAs: **arachidonic** acid (AA; C20:4 ω -6), **docosahexaenoic** acid (DHA; C22:6, ω -3), **eicosapentaenoic** acid (EPA; C20:5, ω -3), **linoleic** acid (C18:2, ω -6), and α -linolenic acid (C18:3, ω -3).¹⁶²

Linoleic acid (C18:2, ω -6) reverts increased IL-8 secretion when Huh-7 cells were treated simultaneously with PA but still increases intracellular lipid content.¹⁶⁹

Other lipids used were ceramide, phosphatidylcholine, sphingomyelin, ceramide, PA and cyclosporine A (drug, *vide infra*) combination has also been reported.²⁵²

2.4.1.2 Oleic and palmitic acid (OA+PA) combination

The most cited **combination** is **PA** with **OA**. These FFAs have the highest abundance among NAFLD and NASH patients and represent an optimal combination of unsaturated and saturated FFAs to employ in an *in vitro* system.^{266,267} It has also been observed that PA is a more apoptogenic lipid and OA is more steatogenic, attenuating the lipotoxic damage of PA, and why they are often used together, since they provide a synergistic effect on molecular pathways previously reported, to represent more reliably pathological condition in model cells.^{250,268} The mainly used ratio is 2:1 OA:PA with concentrations ranging from 200 µM to 2

mM, also depending on incubation time, often using fewer FFAs with more prolonged incubation and *vice versa*.

2.4.1.3 General remarks on FFAs

From the literature, it can be generally deduced that monounsaturated FFAs are more prone to cause steatosis, as they might favour aggregation of lipids in lipid droplets, and they are less apoptotic than saturated FFAs, which might favour the creation of oxidative stress via activating the mitochondrial pathways with respective apoptosis induction.^{53,250}

Lipid concentration values are usually chosen from the clinical values of fatty acids in NAFLD and NASH patients or based on studies performed during protocol optimisations. 98,254,268-270 To obtain different cellular and molecular responses, short- or long-term effects of named compounds studies need to be observed in that context. For example, certain research groups opted only to cause higher lipid uptake and metabolic pathways changes. In contrast, others intended to induce apoptosis and observe changes on a broader scale, also co-culturing other cells, such as HSC, to investigate the potential activation of pathology cascade even in collaboration with other cells.

All used fatty acids, various combinations, respective concentrations, and compounds for steatosis induction and eventual co-culture cases reported in the literature are summarised in **Table 2.1.** For simplicity, even if fatty acid salts were used, they are reported under the corresponding fatty acid.

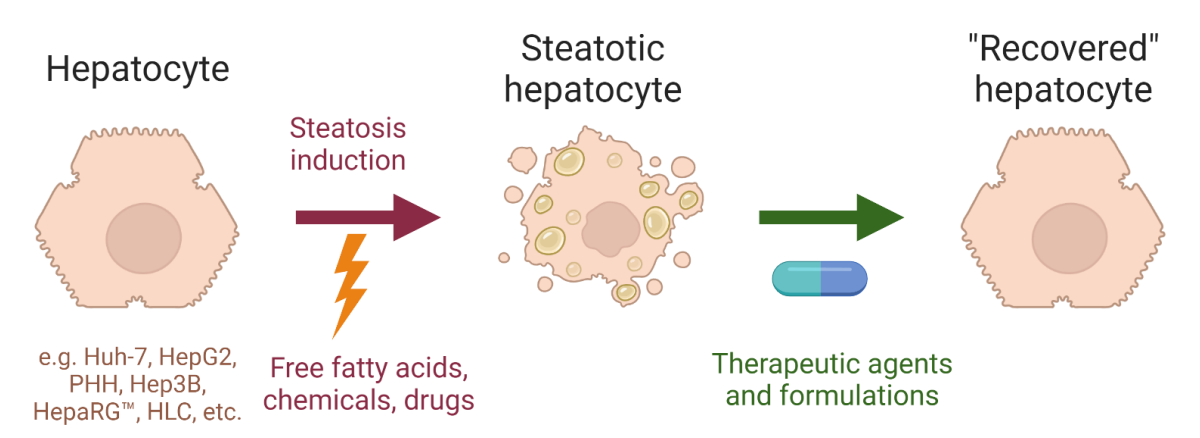


Figure 2.3. A proposal of the general steatosis induction and API screening in vitro model. Cultured hepatocytes are treated with steatosis inducer, after which they change their phenotype and genotype to pathological. Potential APIs are successively incubated with steatotic hepatocytes, and the effect is observed if hepatocytes manage to recover from steatosis. The figure was created using Biorender.com.

Table 2.1. Fatty acids used for steatosis induction. References are provided as an integral part of the following table, with data about cell lines and respective summarised induction conditions.

Compound	Concentration	Cell line	References
	Saturated fatty acids		•
	250-1000 μM for 8 h up to 24 h	Hep3B	251,255,264
	50-500 μM for 6 h up to 48 h or 7 days	HepaRG™	162-164,271
	50-1000 μM for 6 h up to 24 h, some reports of 10 μM for 24 h 36-180 μM for 12-24-48 h reported by Cao	HepG2	73,160,161,169,250- 253,255,259,272-280
	50, 100 or 200 μM for 6, 15 or 24 h	HepG2/C3A	162
Stearic acid C18:0	50-1000 μM for 6 h up to 24 h 500 μM for 48 h reported by Xiong	Huh-7	73,160,162,169,250,251,255, 259,264,268,274- 276,278,280-293
	400 or 800 μM 16 h or 24 h	KMCH	281
	200, 400 or 800 μM for 24 h	OR6	290
	100-800 μM for 8 h up to 24 h, some reports of 10 and 50 μM	PHH (⁷³ also with PHHSC and primary human macrophages)	73,253- 255,264,265,272,283,291,294 -297
	300 μM for 24 h	PLC	255
Stearic acid C18:0	50-200 μM for 6 h up to 24 h or 7 days	HepaRG™	162,262
	100-200 μM for 4, 16, 18 or 24 h	HepG2	160,263,298
	50, 100 or 200 μM for 6, 15 or 24 h	HepG2/C3A	162
	50-600 μM for 1 h up to 24 h	Huh-7	160,263,288,298
	100 μM for 7 days	PHH	262
	Monounsaturated fatty acid	ds	<u> </u>
Elaidic acid C18:1, ω-9, <i>tran</i> s	800 μM for 24 h	РНН	265
	300 μM for 24 h	Hep3B	255
	200 μM for 48 h after α-tocopherol 24 h pretreatment	HepaRG™	299
	50-1000 μM for 1 h up to 24 h, some report 1320, 1500, 2000 μM Ouchi reported 200-400-800 μM for 3-5 days in organoids	HepG2 Ouchi organoids HepG2:THP-1:LX-2 (1:1:1)	160,234,250,255- 259,261,263,286,298,300-303
	50, 100 or 200 μM for 6, 15 or 24 h	HepG2/C3A	162
Oleic acid C18:1, ω-9, <i>cis</i>	50 μM for 48 h or 800 μM for 3 days 200-400-800 μM for 3-7 days	iPSC HLCs (and organoids) Ouchi also reported ESC- derived HLCs and HepG:THP-1:LX-2 organoids	166,234
	50-800 μM for 1 h up to 24 h, or 72 h, reported 1000 and 1320 μM	Huh-7	160,162,250,255,259,263,268 ,284,285,288,289,298,301,30 4,305
	1000 μM for 48 h	Huh-7.5	260
	200-1000 μM for 1 h up to 24 h	PHH (Mahli also has it with PHHSC)	218,255,257,265,295
	300 μM for 24 h	PLC	255
	800 µM	Hep3B	264
Palmitoleic acid C16:1, ω-7	200 μM for 18 h	HepG2	160
, w .	200-800 μM for 9 h up to 18 h	Huh-7	160,264,284

Compound	Concentration	Cell line	References				
	800 μM	PHH	264				
	Polyunsaturated fatty acids	S					
Arachidonic acid C20:4 ω-6	50-200 μM for 6 h up to 24 h	HepaRG™, HepG2/C3A, Huh-7	162				
Docosahexaenoic acid C22:6, ω-3	50-200 μM for 6 h up to 24 h	HepaRG™, HepG2/C3A, Huh-7	162				
Eicosapentaenoic acid C20:5, ω-3	50-200 μM for 6 h up to 24 h	HepaRG™, HepG2, HepG2/C3A, Huh-7	162				
α-linolenic acid C18:3, ω-3	50, 100 or 200 μM for 6, 15 or 24 h, 500 μM for 9 h (Ito for Huh-7)	HepaRG™, HepG2/C3A, Huh-7	162				
	50, 100 or 200 μM for 6, 15 or 24 h	HepaRG™	162				
Linoleic acid	100-1000 μΜ	HepG2	169				
C18:2, ω-6	50, 100 or 200 μM for 6, 15 or 24 h	HepG2/C3A	162				
	50-1000 μM for 6 h up to 24 h	Huh-7	162,169,284				
	Combination of fatty acids Saturated and monounsaturated fa						
	50-500 μM for 6 h up to 48 h or 7 to 14 days usually 2:1 OA:PA ratio, 1:1 reported by Madec	HepaRG™	162,164,267,306				
	50-1000 μM (2:1 OA:PA) for 6 h up to 72 h, or 7 days; 2000 μM also reported by Gomez Lecheon and Ricchi, 1:1 OA:PA Breher-Esch, Patil	HepG2 reported by Pingitore spheroids also with LX-2	106,114,250,306-316				
	660+330 μM (OA:PA) for 24 or 48 h or 50, 100 or 200 μM (1:1 OA:PA) for 6, 15 or 24 h	HepG2/C3A Gori reported liver-on-a-chip	162,243				
	500+250 μM (OA+PA) for 3 days	iPSC-derived HLCs (and organoids)	165				
Oleic + palmitic acid	100-1200 μM for 6 h up to 24 h, or 72 h, 7 days; 50 μM by Madec; usually 2:1 OA:PA ratio, 1:1 reported by Breher-Esch, Madec and Sahini 300+200 uM or 100+400 uM OA:PA for 18 h reported by Infante-Menendez	Huh-7 reported by Anfuso and Barbero-Becerra with LX-2 (HSC)	114,162,182,183,235,250,268 ,287,289,307,310-312,317- 326				
	100-1000 μM for 24 h or 72 h (2:1 OA:PA)	Huh-7.5	322,324,327				
	800 μM 16 (WB) or 24 h	KMCH	319				
	100-1000 μM for 6 h up to 72 h, 7, 14 or 21 days; usually 2:1 OA:PA ratio, check respective publications, 1:1 Breher-Esch, Kozyra, Sahini 800+400 μM for 1-3-5-7 days reported by Rey-Bedon	PHH with primary human macrophages and PHHSC by Feaver spheroids by Kostrzewsky and Kozyra	114,217,241,242,262,307- 309,323,325,328-331				
Oleic + stearic acid	300 μM total FA, ratio OA:PA 1:1 for 12 to 14 days	HepaRG™, PHH	332,333				
Elaidic + oleic + palmitic acid	200+200+200μM for 24 h	PHH	265				
	Saturated and polyunsaturated fat	ty acids					
Eicosapentaenoic + oleic acid	100+100, 100+200, 200+200 μM for 20 h	HepG2, Huh-7	263				
Linoleic + palmitic acid	100-1000 μM + 500 μM for 9 h	HepG2, Huh-7	169				
Palmitic + palmitoleic	600+600 μM (PA:PO) up to 8 h	Нер3В, РНН	264				
acid 800+400 μM (PA:PO) up to 8 h		Huh-7					
Monounsaturated and polyunsaturated fatty acids							
Linoleic + oleic acid	300 μM final concentration for 24 h	HepG2	334				
	Saturated, monounsaturated, and polyunsat	turated fatty acids					
Linoleic + oleic + palmitic acid	250 μM final concentration for 48 h (refresh after 24 h)	PHH (+cholangiocytes, HIEC)	170				
	Saturated fatty acids and dru	ug					
Palmitic acid + cyclosporine A	100-200-300-400-600-800 μM + 1, 3, 10, 30 μM for 24 h	HepG2	252				

Compound	Concentration	Cell line	References				
Other lipids							
Ceramide (C2Cer or C6Cer) Ceramide C2DCer (inactive)	up to 100 μM for 48 h, 50 μM effective and analysed	Huh-7	335				
Ceramide Phosphatidylcholine Sphingomyelin	10 and 30 μM for 24 h	Huh-7	171				
Lithocholic Acid	10 μM for 4 days	hESC-I3, Human fetal hepatocytes	167				
Sodium L-lactate + sodium pyruvate + octanoic acid (C8:0)	10 mM + 1 mM + 2 mM for 48 h	iPSC-derived HLCs	239				

2.4.1.4 FFAs solubilisation vehicles

There is a need to solubilise highly hydrophobic FFAs with the help of co-solvent vehicles in a cell culture medium to transport them to cells in the culture. There is no consensus on which or if any compound should be used for this purpose, but there is a clear need for this step. The most commonly reported compounds in literature are bovine serum albumin (BSA)^{164,242,251,264,273,284,285,287,304,309,315,336}, fat-free BSA,^{161,162,170,268,313} DMSO,^{183,235} methanol,^{243,250,308}, ethanol and decanol,¹⁷¹ and isopropanol.^{160,265,289,317} The concentration of named co-solvents, such as solubilisation protocols, is variable or not reported.

BSA is an albumin derived from bovine blood serum and appertains to a family of naturally occurring transport proteins in blood plasma and is involved with non-specific xenobiotic transport. It is indicated to be a primary FFAs transport vehicle in extracellular fluids since it possesses 7 non-specific sites with different affinities for different FFAs. In that way, albumin presence regulates FFAs bioavailability and contributes to a human body lipid turnover through this shuttle system.³³⁷ Since alcoholic steatosis presents similar signs and symptoms to a non-alcoholic one, but partially different cellular pathways are involved, to discriminate an influence of alcoholic co-solvents such as methanol, ethanol, decanol, and isopropanol, we would recommend avoiding them. DMSO is a commonly used co-solvent in cell culture, but it is unclear if it affects steatosis-involved intracellular mechanisms.

2.4.2 Drugs and chemicals

From empirical toxicity and pharmacovigilance studies of registered drugs, side effects regarding liver toxicity with an accumulation of fatty acids (steatosis) were observed. If this first liver damage strike is unresolved, it can progress into a more severe pathological state and alter clinically relevant patients' liver parameters and profiles. Identifying these drugs is

vital since they are used for a broad therapeutic range, not at all connected with liver conditions. These drug categories include antiepileptic, antiarrhythmic, analgetic, antipsychotic, anxiolytic, antibiotic, and HIV/AIDS antiviral APIs, which ultimately were proven to be hepatotoxic.

In vitro testing of steatosis-inducing drugs reproduced specific parameters and conditions observed in patients. Those experiments were performed to understand the pathological mechanism, genomic, proteomic and lipidomic profile changes, and potential point of attack in cellular pathways that can be exploited to contain and revert the pathology. Thus, chemical agents and drugs can be an attractive alternative to the classical steatosis induction model with FFAs.

Furthermore, one emerging problem of those compounds resulted in their apparent induction or repression of specific molecular pathways with higher affinity than "pure" FFAs, provoking steatosis consequently. On the other side, understanding the steatosis-induction mechanism of these APIs might help treat steatosis caused by these specific compounds and prevent their toxicity when usually therapeutically employed.

Using drugs and chemicals in steatosis induction can induce comparable effects on cellular and molecular metabolism and lipidic and lipoprotein profiles, similar to those observed with fatty acids. This similarity arises from the shared involvement of specific pathways, particularly those related to mitochondrial lipid metabolism. These compounds might provide a valid alternative for steatosis induction in previously listed human *in vitro* models.

2.4.2.1 Most commonly used drugs and chemicals

Valproic acid (VA), also in the form of its sodium salt, an antiepileptic API, is reported to inhibit mitochondrial activity since VA is structurally analogous with FFAs and competes with them to bind to the carnitine shuttle system, which is responsible for bringing FFAs to mitochondria for β-oxidation. ^{173,338-342} Once in the mitochondrion, VA competes with enzymes responsible for endogenous FFAs metabolisation, which concludes with diminished oxidative FFA phosphorylation. ^{164,173,342-344} VA can induce mitochondrial membrane permeability and inhibit triglyceride transport outside the cell, causing FFA accumulation due to reduced breakdown and elimination. ^{173,339} Those remaining FFAs are transformed into triglycerides and ceramides, forming lipid droplets, in more pronounced cases, causing hepatocyte "ballooning". ^{164,173,338,339,342,345}

Tetracyclines are a family of broad-spectrum antibiotics inhibiting bacterial ribosomes inhibiting mitochondrial FFAs β-oxidation.^{174,175,346} **Amiodarone** is a class III antiarrhythmic agent, pharmacologically acting as a calcium and potassium channel blocker, affecting the mitochondrial respiration cycle, preventing FFAs' physiological metabolism and causing their intracellular accumulation.^{344,347} **Cyclosporine A** is an immunosuppressant used in rheumatoid arthritis, psoriasis or to prevent organ rejection following the transplantation.³⁴⁸ Cyclosporine causes a metabolic change in hepatocytes, majorly with the CYP450 system, increasing ROS generation and FFA accumulation leading to lipotoxicity.^{349,350}

Paracetamol (acetaminophen), one of the most common antipyretic and analgetic drugs worldwide, is safe to use in strictly delimited doses since its high doses can cause and worsen the steatosis through significant depletion of glutathione (GSH), necessary in its complete metabolisation, to remove newly generated ROS. 351,352 Oxidative stress induces JNK pathway and inhibits FFAs β-oxidation in mitochondria. 352 This condition is especially emphasised in obese and NAFLD patients. 351

Furthermore, as summarised in **Table 2.2**, chemicals such as bisphenol A and TCDD have been reported to induce liver toxicity and steatosis in hepatocytes. Several studies were performed to establish the damage those compounds exerted on hepatocytes and understand the underlying mechanisms.^{353,354} There is an extensive study on steatogenic pesticides in HepaRG[™] cells by Lichtenstein *et al.*³⁵⁵

Table 2.2. Drugs and chemicals used for steatosis induction.

Compound	Concentration	Cell line	References
	Chemicals		
AMPK activator	500 μM for 24 h	HepaRG™, PHH	262
Diambanal A	0.2, 2, 20, 200, and 2000 nM for 3 weeks	HepaRG™	353
Bisphenol A	0.02, 0.2, 2 μM for 48 h	HepG2	356
Cyproconazole	25, 50, 100, 200 μM for 24 or 72 h	HepaRG™, HepG2	357
TCDD - 2,3,7,8- tetrachlorodibenzo- p-dioxin	0.001, 0.01, 0.1, 1, 10, or 100 nM TCDD for 12 and 24 h, time course studies were conducted for 1, 2, 4, 8, 12, 24 and 48 h, treated with DMSO vehicle or 10 nM TCDD.	РНН	354
	Drugs		
	20 μM for 24 h or 14 days	HepaRG™	174,175
Amiodarone	200 μM for 2-8 h	HepG2 and PHH	358
	5, 10, 20, 40, 80 μM for 24-72 h	Huh-7	305
Chlorpromazine	1, 10, 20, 30, 40, 50 μM for 24 h (viability) 0.02, 0.1, 0.2, and 1 μM for 13 days with a daily refresh (transcriptome)	РНН	359
Cyclosporine A	30 μM for 48 h	PHH spheroids (+ non- parenchymal cells)	176
Insulin	0, 0.01, 0.5 ug/mL for 7 days	HepaRG™, PHH	262

Compound	Concentration	Cell line	References
Lamivudine (3TC)	8 μM for 24, 48 or 72 h	HepG2, Huh-7, PHH	360
Methotrexate	1.9, 63 µM	HepaRG™+IHSC	361
Midazolam	1 μg/mL for 3 h	PHH, Huh-7	325
Paracetamol (acetaminophen)	5-40 mM for 12 or 24 h	HepaRG™ with or without IHSC, PHH	262,361
Stavudine (d4T)	3 μM for 24, 48 or 72 h	HepG2, Huh-7, PHH	360
Tetracycline	50 μM for 24 h or 14 days (refresh every 2-3 days)	HepaRG™	174,175
Thapsigargin	0.5, 1, 1.5 μM for 6 h up to 24 h	HepG2, Hep3B, Huh-7	172,251
Tunicamycin	5, 10, 20 ug/mL for 6 h up to 24 h	Huh-7	172
	47-10.000 μg/mL for 72 h (665 ug/mL for 72 h) 250-10.000 μg/mL for 24 h (2.300 ug/mL for 24 h)	HepaRG™	173
Valproic acid Sodium valproate	1, 2.5, 5 mM for 12, 24, 48 h or 14 days 0.5, 1, 2 mM for 24-48h reported by Yan	HepG2	300,361,362
•	500 μM for 30 min	Huh-7	363
	0-30 mM for 24 h and 48 h, 15 mM for the main experiment 5 days + 3 days washout	PHH	364
Vitamin K2	10 μM for 4 d	hESC-I3, Human fetal hepatocytes	167
Zidovudine (AZT/ZDV)	6 µM for 24, 48 or 72 h	HepG2, Huh-7, PHH	360

2.4.3 Steatosis-inducing compounds concentrations and incubation times

The reported values of a broad range of reported steatosis-inducing agents' concentrations, lipids, drugs, and chemicals retrieved from analysing the literature are inconsistent. Therefore, in case of a new investigation, it is highly recommended to perform a series of pilot experiments to determine the realistic steatosis induction effect and extension in a specific model.

The time of incubation reported in the literature shows a high variability but, in general, could be classified as short-term, up to 24 h, and long-term, up to 14 days. Short-term incubation, sometimes as short as 1 to 3 h but most commonly lasting from 6 to 24 h, can reproduce an acute change in the cellular response to the induction agent. Longer exposure times that last from 2 to 21 days are usually reported in specific cell lines (HepaRG[™]) and might provide an insight into what chronic exposure to an inducing agent might change in cellular pathways. However, various investigations have proven that specific genomic, proteomic, and lipidomic profile expressions only occur during a specific, sometimes shorter or more extended timeframe.

The external agents' exposure might affect further aspects of constant gene expression that are permanent after a longer time. Long-term incubation might provide a better insight into

how the pathology develops and how the model replies to prolonged exposure to the pathological agent concentration – observing if the cascade can be stopped and overturned towards the physiological functional state.

2.4.4 Drug discovery for steatosis inhibition in vitro – state-of-the-art

Multiple molecules have been tested on cellular models, as summarised in **Table 2.3**. Some molecules are marketed as lipid-modifying agent drugs, ezetimibe and fluvastatin, and glucagon-like proteins, like exendin-4. These "known" drugs might prove helpful as a therapy touchstone, as there are available clinical data. In addition, some plant-derived molecules, such as classic silymarin extract compounds, iso-alpha acid from hops, and berberine, were reported to be effective in attenuating steatotic symptoms. One exciting example is the "defatting cocktail" used by Boteon *et al.*,¹⁷⁰ consisting of several API classes. This treatment might shed light on the generation of new antisteatosis therapy, as these are active on newly identified pathological pathways.

Refer to recent reviews for comprehensive insights into the current perspectives and strategies within NASH/NAFLD drug pipelines, including *in vitro* and *in vivo* investigations and clinical trials. 50,365-368

Table 2.3. Molecules used to attenuate or revert steatosis in steatosis-induced human cells

Therapeutic compound	Compound concentration and dissolution vehicle	Cell line	References
5-Aminolevulinic acid	200 μM together with FFA treatment for 4-8 h	Huh-7	293
n to comb and (Alternia E)	25 nM for 24 h pretreatment	HepaRG™	299
α-tocopherol (Vitamin E)	10, 25, 50 µM for 48 h pretreatment to prevent steatosis reported by Pingitore	HepG2 (+LX-2) spheroids PHH spheroids	106,176
Andrographolide from <i>Andrographis paniculata</i>	14 μM for 24 h together with FFA treatment in 0.01% (v/v) DMSO	HepG2	314
Ascorbic acid (Vitamin C)	25, 50, 100, 200, 1000 μg/mL for 24 h together with FFA treatment	HepG2	315
Berberine from <i>Berberis</i> plants	10 μM in DMSO	HepG2, Huh-7	311
Bouchardatine-analogue (R17) with the side chain of N,N-dimethyl-1,3-propane diamine, from <i>Bouchardatia neurococca</i> (<i>Rutaecae</i>)	1 μM in cell medium (DMEM)	HepG2, Huh-7	259
Cinnabarinic acid	30 μM together with FFA treatment for 24 h	HepG2	316
Compound K (derived from ginsenoside)	0.1, 0.5, 1 μM vehicle not specified	Huh-7	321

Therapeutic compound	Compound concentration and dissolution vehicle	Cell line	References
Curcumin from <i>Curcuma Longa</i>	5 μM for 24 h together with FFA treatment in 0.01% (v/v) DMSO	HepG2	314
Defattening cocktail of PPAR α-ligand GW7647, PPAR δ-ligand GW501516, adipokine visfatin, forskolin, PXR-ligand hypericin, CAR ligand scoparone (6,7- dimethoxycoumarin) and L-carnitine	respectively 0.001 mM, 0.001 mM, 0.4 ng/mL, 0.01 mM, 0.01 mM, 0.01 mM, 0.01 mM, cell medium	PHH (+cholangiocytes, HIEC)	170
Elafibranor	10, 25, 50 µM for 48 h pretreatment to prevent steatosis reported by Pingitore	HepG2 (+LX-2) spheroids	106
Exendin-4	10 nM (Gupta and Sharma) 50 or 100 nM (Lee) vehicle not specified	HepG2, Huh-7, PHH	114,265,275
Ezetimibe	10 μM, vehicle not specified	Huh-7	282
Fluvastatin	1,5, 10, 20 µM, vehicle not specified	HepG2	272
Icaritin	5, 10, 20, 50 µM for 48 h together with FFA treatment	Huh-7	292
iso-alpha acids (from hops)	10 or 20 μg/mL, vehicle not specified	PHH	218
Liraglutide	1, 10, 20 μM for 48h pretreatment	HepG2 (+LX-2) spheroids	106
Enagiatide	5, 10, 20 nM for 24-72 h together with OA and amiodarone treatment	Huh-7	305
Niacin (Vitamin B3)	250-500 μM, vehicle not specified	HepG2, PHH	253
Obeticholic acid	10, 25, 50 μM for 48 h pretreatment	HepG2 (+LX-2) spheroids	106
Silibinin, Silymarin from S <i>ylibum marianum</i>	5-7.5 μM (Anfuso) 200 μM (Song)	HepG2, Huh-7+LX-2	235,273
Sodium nitrite	10 μM in cell medium	HepG2 PHH spheroids	336
Soluble tumour necrosis factor-like weak inducer of apoptosis (sTWEAK)	100 ng/mL	PHH immortalised	297
Toyocamycin	1 μM, vehicle not specified	Huh-7	289
Withaferin A	1, 2.5, 5 μM for 24 h	HepG2, Huh-7	298

2.5 Outlook for drug discovery and early-stage drug formulations

PHH and cell lines such as HepG2, Huh-7, and HepaRG[™] are the core models to mimic steatotic conditions and test potential new therapeutic agents. In future research, steatosis induction could be reproduced in iPSC-derived hepatocytes, similar but more representative to the observations made in conventional "classic" cell models. Co-cultures of any type and 3D models that will contain hepatocytes, hepatic stellate cells, and macrophages, although more complex to develop and validate than simple cell lines, can provide a more realistic model of the pathological human liver microenvironment and, consequently, soon a more reliable platform for pharmacological screening and drug discovery.

2.6 Conclusion

From the overview of the currently available studies on *in vitro* steatosis in humans, the most conclusive results arise from the use of using PHH. However, since primary cell results can be highly variable, based on the parameters of the cell donor, they are usually correlated to another model of choice, such as the hepatic carcinoma cell line. In addition, differentiated HepaRGTM cells also contain a portion of primitive bile duct cells to represent a better system mimicking the physiological situation in the liver. iPSC-derived HLCs might give more valuable insight into the progression of the pathology. However, a more foetal and immature type of hepatocytes expressing a slightly different panel of genes and proteins may represent a significant drawback in some investigations. Indeed, to our knowledge, no reliable and reproducible protocol to render them "more mature", i.e., expressing a complete adult genomic and proteomic array, is currently available.

Regarding the steatosis-induction methods, we would consider the "golden combination", OA and PA combination, total FFA concentration between 200 and 1000 μ M, with a ratio 2:1 (OA:PA), solubilised with the help of fat-free BSA for at least 24 h, up to several days. It seems to be the most effective and consistent steatosis-inducing treatment so far tested. According to steatosis induction studies performed in our research group, presented in **Chapter 4**, it was decided to use 300 + 150 μ M of OA:PA for 24 h in Huh-7 cells, grown in the serum-free culture medium supplemented by 30 μ M BSA as a solubilising agent.

Should a chemical compound other than fatty acid be preferred, a good approach would be to use valproic acid, amiodarone, paracetamol, or some HIV/AIDS retroviral therapeutics, as their effects have been mainly studied. When using steatosis-inducing drugs, particular attention should be paid to the possible "side effects" on other cellular and molecular mechanisms of the drug and its effect on metabolomic, genomic, proteomic and lipidomic profiles. These variations might not correlate directly with the drug's capability to only induce steatosis.

Time exposure for short-term effect studies should be considered in a range of 12-24 h. If chronic studies should be performed, 7 or 14 days might be very valid time points that might give insight into the cellular pathways' "re-adaptation" due to the steatosis. A classic single-cell culture model should always be considered a good starting approach. The use of co-cultures with extension to spheroids/organoids could be considered when there is interest in mirroring the functionality of the hepatic tissue more confidently. There is no widespread use

of described co-culture models, especially simultaneous cell culturing, since the major limitation in employing these are very different culturing conditions and how reliably the actual system could be represented if internal system changes are not investigated and validated in detail. Because of the reasons mentioned above, we decided to develop and optimise a conditioned dual cell culture medium (**Figure 2.2d**) of Huh-7 hepatocarcinoma cell line with LX-2 immortalised human HSCs, described in **Chapter 4**.

Current developments in metabolomic, genomic, proteomic and lipidomic studies provide valuable detailed information on changes and expression levels of various intracellular actors and pathological markers. In the future, these parameters will be screened by researchers and clinicians to establish a correlation between the treatment *in vitro* and *in vivo* and the advancement of the pathology phase. A remarkable additional advantage of studying steatosis-induced cells offers the possibility of using specific inducing agents to mimic a well-defined pathology phase (NAFLD, NASH or cirrhosis), thus allowing the chance to test specific therapeutics acting precisely on imbalanced pathways or only on the specific reactions.

Chapter 3.

Polyenylphosphatidylcholines as bioactive excipient in tablets for the treatment of liver fibrosis

Parts of this chapter are submitted as a research article manuscript, currently under revision in the *International Journal of Pharmaceutics*.

Skorup I*, Valentino G*, Aleandri S, Gelli R, Ganguin AA, Felli E, Selicean SE, Marxer RA, Gracia-Sancho J, Berzigotti A, Ridi F, Luciani P; "Polyenylphosphatidylcholines as bioactive excipient in tablets for the treatment of liver fibrosis", 2023.

* These authors contributed equally

Author contributions

I.S. devised and performed all the tabletting and *in vitro* and *ex vivo* experiments, developed methodology, analysed the data, co-wrote the original draft; **G.V.** conceived the original project, devised and performed pilot experiments, developed methodology, co-wrote the original draft; **S.A.** devised experiments and methodology, contributed to data curation, wrote parts of the original draft of the manuscript; **R.G.** performed physicochemical analysis (TGA, XRPD, Raman), co-wrote the original draft; **A.A.G.** devised qPCR methodology and help performing and analysing qPCR experiments; **E.F.** devised methodology with rat primary cells, consulted on data analysis; **R.A.M.** devised and validated methodology; **S.E.S.** devised methodology with rat primary cells; **J.G.S.** and **A.B.** provided resources and funding, revised and edited the manuscript; **F.R.** supervised R.G. research work, revised and edited the manuscript; **P.L.** conceived and supervised the original project, provided funding, administered the project, reviewed and edited the manuscript.

Parts of this chapter have been submitted as a Master thesis:

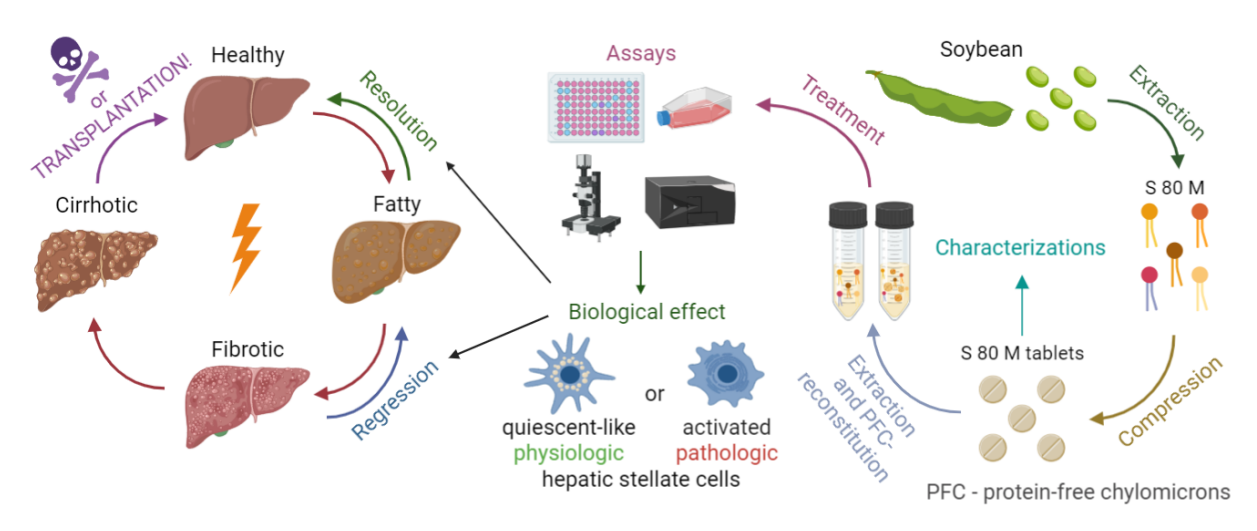
Marxer, RA; "Design of novel lipid-based solid oral formulations for the therapy of liver fibrosis", 2021.³⁶⁹

R.A.M. devised and validated methodology, ran early formulation optimisation studies (Formulations Ref_GV, 1, 2, 3, 4, and S80M + Sily).

Abstract

Liver fibrosis is characterised by the accumulation of extracellular matrix (ECM) arising from the myofibroblastic transdifferentiation of hepatic stellate cells (HSCs) occurring as the natural response to liver damage. To date, no pharmacological treatments have been approved explicitly for liver fibrosis. We recently reported a beneficial effect of polyenylphosphatidylcholines (PPCs)-rich formulations in reverting fibrogenic features of HSCs. However, unsaturated phospholipids' properties constantly challenge to the development of tablets as the preferred patient-centric dosage form. Profiting from the advantageous physical properties of the PPCs-rich Soluthin[®] S 80 M, we developed a tablet formulation incorporating 70% w/w of this bioactive lipid. Tablets were characterised via Xray powder diffraction, thermogravimetry, and Raman confocal imaging and passed the major compendial requirements. To mimic physiological absorption after oral intake, phospholipids extracted from tablets were reconstituted as protein-free chylomicron (PFC)-like emulsions and tested on the fibrogenic human HSC line LX-2 and primary cirrhotic rat hepatic stellate cells (PRHSC). Lipids extracted from tablets and reconstituted in buffer or as PFC-like emulsions exerted the same antifibrotic effect on both activated LX-2 and PRHSCs as observed with plain S 80 M liposomes, showing that the manufacturing process did not interfere with PPCs' bioactivity.

Graphical abstract



The figure was created using Biorender.com.

3.1 Introduction

Natural phospholipids, extracted from soybean or egg, are frequently used as excipients in developing new pharmaceutical products. These phospholipids, characterised by a low batch-to-batch variability, are derived from renewable sources, produced with ecologically sustainable procedures, and available on a larger scale at a relatively low cost compared to synthetic ones, which found application only in a few pharmaceutical products. 124,128

Soybean extracts of polyenylphosphatidylcholines (PPCs), belonging to the broad family of essential phospholipids (EPL), have already been formulated in dietary supplements to support the therapy of chronic liver diseases. Pemarkably, these "generally recognised as safe" (GRAS) lipids do not exert their function only as an excipient but also as a bioactive component, as demonstrated in previous studies. PLs are commonly used in some countries, like Russia and Poland, for patients suffering from non-alcoholic fatty liver diseases (NAFLD) and steatohepatitis (NASH), 132,370,371 due to their alleged antioxidant and anti-inflammatory effect. However, their mechanism of action is not fully understood yet.

EPLs are commercially available as hard or soft capsules. Both pharmaceutical dosage forms are favoured by EPLs' suitability as a liquid filler due to phospholipids' physicochemical properties. Tompared to soft capsules, hard gelatine capsules offer advantages for liquid and semi-solid formulations, as they do not require additional plasticisers and can be filled at higher temperatures. While the lipid amount can reach 100% in soft and hard capsule systems, tabletting significantly reduces the lipid amount per dosage unit. Tipid excipients often compromise conventional compressed tablets' physical integrity and mechanical strength. At ambient temperature, mono- and polyunsaturated lipids are in a liquid crystalline state 124, and storage conditions and handling require strict humidity and temperature control and oxidation prevention precautions. Only with a careful fine-tuning of the formulation composition a consistent compendial quality of the manufactured tablets could be achieved, as recently emphasised in the case study by Koch *et al.* on using lipid excipients to produce lipid tablets with optimal properties.

Compressing tablets majorly composed of unsaturated, bioactive phospholipids – the recommended daily dose of EPLs is 1.05 and 1.80 g following oral intake, for instance^{125,132} – may thus be considered a breakthrough in pharmaceutical manufacturing.

Recently, our group showed that PPC nanodispersions could revert activated, profibrogenic LX-2, immortalised human hepatic stellate cells (HSCs) to a quiescent-like status.¹³⁷

Specifically, we screened the antifibrotic effects of PPC liposomes, both in the presence and absence of silymarin, by using LX-2 cells. More recently, we identified the secreted protein acidic and rich in cysteine (SPARC), a matricellular protein, as a fibrogenesis-associated factor in extracellular vesicles (EVs). 138 The direct treatment of LX-2 with two experimental antifibrotic drugs, elafibranor and obeticholic acid, increases the secreted SPARC in EVs. 122 However, the damaging drugs' effect on HSCs could be mitigated when formulating them with PPC. Proteomics and lipidomics profiling pointed out specific changes in the cellular and EVs phospholipid composition, and biological assays indicated that the beneficial antifibrotic features of our PPC treatments could be transferred from the parent cells to the EVs. 122 Among the several PPC-rich phospholipids commercially available, Soluthin® S 80 M, a magnesium chloride lecithin analogue of the phospholipid S 80,¹³⁷ shows flow properties remarkably suitable for tabletting. Here, we blended S 80 M with microcrystalline cellulose (MCC, filler), magnesium alumino-metasilicate (oils adsorbent), and sodium croscarmellose (disintegrant in direct compression), generating a powder mixture that could be directly compressed into high-quality tablets complying with the compendial requirements.³⁷⁷ Thermogravimetric analyses estimated the amount of water absorbed by the tablets and their components after equilibrating at relative humidity (RH) of 75%. In addition, via X-ray powder diffraction (XRPD) performed before and after tabletting, we assessed if and how the compression step affected the bulk property of the powder and its crystalline state. Finally, Raman imaging was also employed to evaluate the tablet's homogeneous S 80 M distribution.

Finally, we investigated whether tabletting PPC could affect the antifibrotic bioactivity of S 80 M testing tablets extracts on activated human HSCs immortalised cell model (LX-2) and on primary hepatic stellate cells (PRHSC) obtained from cirrhotic rats to validate the ability of these formulations to revert fibrotic features not only in a cell line but also in primary cells.

3.2 Materials and methods

3.2.1 Materials

Soluthin® S 80 M (S 80 M; soybean phospholipid 80% complexed with MgCl₂) and 1,2dioleoyl-sn-glycero-3-phosphocholine (DOPC) were a kind gift from Lipoid GmbH (Ludwigshafen, Germany). The LX-2 cells immortalised human HSC line (RRID CVCL 5792) were purchased from Merck Millipore (Darmstadt, Germany). Dulbecco's Modified Eagle Medium (DMEM-HG; 4.5 g/L glucose, with phenol red and pyruvate, no glutamine), 4-(2hydroxyethyl) piperazine-1-ethanesulfonic acid sodium (HEPES) solution, DMSO (dimethyl sulfoxide), 4',6-diamidino-2-phenylindole (DAPI), Roti®-Histofix 4% (acid-free, pH 7.4, % w/v phosphate-buffered formaldehyde solution) were purchased from Carl Roth (Arlesheim, Switzerland). Iscove's Modified Dulbecco's Medium (IMDM; with phenol red and Lglutamine), phosphate buffer saline (PBS) (pH 7.4, without Ca/Mg), L-Glutamine, Penicillin-Streptomycin, microcrystalline cellulose (MCC), hydrochloric acid (HCl), sodium hydroxide (NaOH), chloroform (CHCl₃), ethanol (EtOH), trifluoroacetic acid (TFA), isopropanol, acetone, methanol (MeOH), acetonitrile (ACN), TRIzol™ reagent, RNAse-free water were purchased from Fisher Scientific (Reinach, Switzerland). Foetal bovine serum (FBS), Accutase[®], Cell Counting Kit-8 (CCK-8), 1,6-Diphenyl-1,3,5-hexatriene (DPH), N,N,N-trimethyl-4-(6-phenyl-1,3,5-hexatrien-1-yl)-phenyl-ammonium-p-toluolsulfonate (TMA-DPH), cholesterol, Oil Red O (ORO; 0.5% w/v in propylene glycol), collagen type I (from rat tail), triethyl citrate, palmitic acid, fumed silica (Aerosil[®] 200), silymarin extract (Sily), and glycogen were bought from Sigma Aldrich (Buchs, Switzerland). Myritol® 318 triglycerides (produced by BASF Personal Care and Nutrition GmbH, Monheim am Rhein, Germany) were obtained from Impag (Zürich, Switzerland). Cell culture plates and flasks were from Sarstedt (Nümbrecht, Germany), TPP (Trasadingen, Switzerland) and Nunc (Roskilde, Denmark). ROS-ID® Total ROS/Superoxide detection kit was from Enzo Life Science (Lausen, Switzerland).

Neusilin® US2 (Fuji Chemical Industries Co., Ltd., Toyoma, Japan) was a kind gift from IMCD (Zürich, Switzerland). Primellose® was a kind gift from DFE Pharma (Goch, Germany). The enteric methacrylic acid copolymer Eudragit® L100-55 was a kind gift from Evonik (Essen, Germany). Biorelevant dissolution media, FaSSIF (fasted simulated state intestinal fluid), and FaSSGF (fasted state simulated gastric fluid) were purchased from Biorelevant (London, UK).

3.2.2 Powders and tablets preparation

All the formulations described below were manually prepared by mixing S 80 M via dry granulation with a determined amount of other components, depending on the relevant formulation. First, S 80 M was ground in the mortar with the pestle and then blended with other excipients until obtaining a homogenous mixture. Turbula T 2 F 3D mixer (Willy A. Bachofen, Muttenz, Switzerland) was employed for 5 min to ameliorate the mixture's homogeneity. Afterwards, the mixture was sieved (1400 µm) into a plastic container where inert nitrogen gas was flushed, and the container was sealed and kept at +4 °C until the compression. Tabletting was then carried out using a single punch press XP1 from Korsch (Berlin, Germany), and tablets were manually compressed using 11 mm matrix and round concave stamps from Natoli Engineering Company (Saint Charles, MO, USA), insertion and filling depth of 5 mm and 5.5 mm, respectively. Both powder mixing and tabletting were performed at room temperature or in an air-conditioned room at +15 °C, as indicated per specific experiments. Tablets were kept at +4 °C under an inert nitrogen atmosphere.

3.2.3 Formulation development

3.2.3.1 Preliminary formulations

A former research group member, Dr. Gina Valentino, reported in her dissertation³⁷¹ that S 80 M could be formulated as granules with the appropriate choice of excipients. Starting from these findings, we further optimised the manual process to understand whether tablets could be produced from the direct compression of granules. The first optimisation step was replacing Aerosil[®] 200, used in the original formulation, with Neusilin[®] US2.

A pilot formulation of S 80 M with silymarin (Sily), a known hepatoprotectant acting as an antioxidant and radical scavenger, was also produced based on Formulation 3, replacing a percentage of microcrystalline cellulose (MCC) content with Sily to investigate if we can incorporate another active ingredient in our formulation since there are reported hepatoprotective products containing both PPC and Sily. 378,379

Table 3.1. Preliminary formulations composition

	Component - % (w/w)						
Formulation	S 80 M	МСС	Mannitol Magnesium stearate Neusilin® US2		Silymarin	Batch size mass (g)	
Ref_GV T > 25°C	50.55	40.50	8.20	8.20 0.25 0.50 Aerosil® 200 ,		0.00	10.00
Ref_GV T < 25°C	50.55	40.50	0.20	0.25	not Neusilin® US2	0.00	6.00
1	50.55	40.50	8.20	0.25	0.50	0.00	10.00
2	50.55	40.00	8.20	0.25	1.00	0.00	6.00
3	25.00	74.00	0.00	0.00	1.00	0.00	60.00
4	37.50	61.50	0.00	0.00	1.00	0.00	8.00
S80M + Sily	25.00	49.00	0.00	0.00	1.00	25.00	10.00

All the formulations were produced, and tablets from Formulations 3, 4, and S 80 M + Sily were also successfully obtained via direct compression at room temperature.

3.2.3.2 Design-of-experiment (DoE) formulations

Further formulations' optimisations to maximise S 80 M content in the granules have been calculated with a DoE in Minitab 18.1 statistical software (Minitab LLC, State College, PA, USA) to safeguard the quality-by-design (QbD) approach. The DoE method changes component variables simultaneously to observe the specific effect on the product quality by calculating the minimum number of necessary formulations to prepare. Lower and upper components' limits are given in the extreme vertices mixture design employed in this case (**Table A3.1**). The software calculated the composition of the most-favourable formulations inside the given constraints, and various components' proportions had to add up to one.³⁸⁰ It represented them as the hyper-polyhedron (**Figure A3.1**).³⁸¹ DoE provided 13 different formulations for further studies (**Table 3.2**).

Table 3.2. Formulations' compositions obtained from DoE calculation based on pre-set component content constraints

	Co			
Formulation	S 80 M	мсс	Neusilin [®] US2	Batch size mass (g)
DoE 1	39.50	50.00	10.50	5.00
DoE 2	30.00	50.00	20.00	5.00
DoE 3	64.00	35.00	1.00	5.00
DoE 4	54.50	35.00	10.50	5.00
DoE 5	49.00	50.00	1.00	5.00
DoE 6	69.50	20.00	10.50	5.00
DoE 7	57.25	27.50	15.25	5.00
DoE 8	60.00	20.00	20.00	5.00
DoE 9	79.00	20.00	1.00	5.00
DoE 10	45.00	35.00	20.00	5.00
DoE 11	66.75	27.50	5.75	5.00
DoE 12	42.25	42.50	15.25	5.00
DoE 13	51.75	42.50	5.75	5.00

A mass of 5 g of each formulation was produced in one replicate. Based on powder characterisation, to examine in detail, 10 g batches of formulations DoE 5 and DoE 11 were produced in triplicate, and the corresponding tablets were also successfully obtained via direct compression at room temperature.

3.2.3.3 Optimisation of 70% S 80 M containing formulation

The most favourable formulation with a high S 80 M content from the DoE formulations, specifically DoE 11, was chosen to optimise the formulation further. Five formulations were optimised for better technological properties (**Table 3.3**).

Table 3.3. Composition of further optimised formulations based on DoE 11 formulation.

	Component - % (w/w)					
Formulation	S 80 M	Batch size mass (g)				
F70-1	70.00	29.00	1.00	0.00	5.00	
F70-2	70.00	27.00	1.00	2.00	5.00	
F70-3	70.00	24.00	1.00	5.00	5.00	
F70-4	70.00	28.00	2.00	0.00	5.00	
F70-5	70.00	23.00	2.00	5.00	5.00	

A mass of 5 g of each formulation was produced in one replicate and directly compressed into tablets in an air-conditioned room at +15 °C.

3.2.4 Optimised formulation F70-5 – tablets preparation

Three 35 g batches of final formulation F70-5 containing 70% (w/w) of S 80 M, 23% (w/w) MCC, 2% (w/w) Neusilin[®], and 5% (w/w) Primellose[®] were produced. Both powder mixing and tabletting were performed in an air-conditioned room at +15 °C. Tablets were kept at +4 °C under an inert nitrogen atmosphere.

3.2.5 Compendial powder quality tests

The mixture flow analysis was performed per the Ph. Eur. monographs 2.9.16. and 2.9.36. using an Erweka GTL granules and powder flow tester (Langen, Germany) equipped with one hopper of 480 mL and a nozzle of 25 mm.

The bulk volume (V_0) of the mixture was measured in a 100 mL measuring cylinder as well as the volume after 10 taps (V_{10}), 500 taps (V_{500}) and 1250 taps (V_{1250}) using an Erweka SVM 222 tapped density tester (Langen, Germany). As a result, bulk and tapped densities were calculated as 25 g/ V_0 and 25 g/ V_{1250} , respectively. As indicated by Ph. Eur. 2.9.36, the compressibility index (CI) was calculated from the bulk and tapped density using the following equation (Eq. (1)):

$$CI = 100 \times [(V_0 - V_{1250})/V_0]$$
 (1)

While the Hausner ratio (HR) was calculated using the following formula (Eq. (2)):

$$HR = V_0/V_{1250}$$
 (2)

Bulk and tapped densities were calculated using the following formula (Eq. (3,4)), where m stands for the mass of weighted powder ~25 g that the test was performed on:

$$BD = V_0/m \tag{3}$$

$$TD = V_{1250}/m$$
 (4)

Powders from all the formulations described in **Section 3.2.3** (except Formulation 3) were tested using the same parameters, only measuring the amount of powder produced.

3.2.6 Compendial tablets quality tests

Twenty tablets were randomly chosen from a population and weighed on an analytical balance (Kern ADB 200-4; Ballingen, Germany), and their average mass was determined. Approximately 6.5 g of tablets were weighed on an analytical balance and tested with Erweka TAR 120 tablet friability and abrasion tester (Langen, Germany) with a setting of 100 revolutions, with a defined velocity of 25 rpm, as prescribed by Ph. Eur. 2.9.7. Tablets were weighed again, and the mass difference has been calculated. Furthermore, 10 tablets were arbitrarily tested for hardness on Erweka TBH 125 tablet hardness tester (Langen, Germany), using a constant speed setting (2.3 mm/s). Maximum, minimum, and mean values have been determined following Ph. Eur. 2.9.8.

For the tablets obtained from formulations reported in **Table 3.3**, mass was measured for 13-16 tablets, friability was measured on 4.0-4.7 g of tablets, and hardness was measured on 5 tablets.

3.2.7 Gastro-resistant coating of tablets

Compressed tablets were coated with a functional enteric coating Eudragit[®] L100-55, by modifying the manufacturer's dip-in protocol. First, the coating suspension was prepared by mixing solvents (acetone, isopropanol, ultrapure water, 30:46:4% w/w of total) to which triethyl citrate and Eudragit[®] were added (3.33:16.67% w/w) gradually and stirred with Polytron[®] PT 2500 E (Kinematica, Malters, Switzerland) for about 1 h until the suspension did not become transparent and homogenous. Next, tablets were manually inserted in coating suspension for approx. 10 sec, air-dried for 20-30 min and then reinserted 5 times (layers). Coated tablets were kept at +4 °C under an inert nitrogen atmosphere.

3.2.8 Disintegration of gastro-resistant tablets

Gastro-resistant tablets were tested for disintegration using the Automated Disintegration System G7962A from Agilent (Santa Clara, CA, USA) to check the targeted location of tablet disintegration obtained. Experimental conditions were followed from Ph. Eur. 2.9.1, 5.17.1 and Tablets monography³⁷⁷ (medium temperature: 37 °C; medium volume: 900 mL; 6 tablets per test), were left to disintegrate in the apparatus for 2 h in HCl 0.1 M without discs and transferred for 1 h in phosphate buffer pH 6.8 (PB) with added discs.

3.2.9 Thermogravimetry (TGA)

Thermogravimetry evaluated the amount of water absorbed by the tablet and by the tablet's components upon equilibration at RH 75%. The analyses were conducted using a Discovery SDT 650 from TA Instruments (New Castle, DE, USA). Samples were loaded in aluminium pans and were heated from room temperature (RT) to 500 °C, at 10 °C/min, in an N_2 atmosphere (flow 100 mL/min). The weight loss between RT and 150 °C was used to estimate the amount of water in the samples, calculated as the difference between the weight loss of the same sample equilibrated at RH 75% and that of the freeze-dried one. The equilibration process was done by placing small aliquots of powders or tablets in a hermetically closed chamber with NaCl-saturated solution, at +4 °C, for one week. The freeze-drying process was conducted by freezing the samples in liquid N_2 (-196 °C) and lyophilising them at -50 °C and 50 mTorr for 24 h (VirTis Benchtop freeze-dryer, Gardiner, NY, USA).

3.2.10 X-ray powder diffraction (XRPD)

XRPD analyses were conducted using a D8 Advance powder diffractometer from Bruker (Billerica, MA, USA) equipped with a Cu X-ray source (λ =1.54 Å) at 40 kV and 40 mA. Samples were ground with agate mortar and pestle and flattened on a Si low background sample holder. The diffraction patterns were collected in the 20 range of 3-50°, with an increment of 0.03°, a time *per* step of 0.3 s, and with a 0.6 mm slit.

3.2.11 Confocal Raman microscopy

Confocal Raman measurements were conducted on a Renishaw inViaTM QontorTM confocal Raman microscope (Wotton-under-Edge, UK) equipped with a 785 nm laser, a front-illuminated CCD camera, and a research-grade Leica DM 2700 microscope. The spectra of the tablet's components were collected using a 20x objective (numerical aperture 0.40, working distance 1.15 mm) in the 200-3200 cm⁻¹ range, a laser power of 10 mW, and an exposure time of 10 s with 5 accumulations. The tablet's chemical map was obtained with a 5x objective (numerical aperture 0.12, working distance 14 mm) using the StreamLineTM mode, which allows for the fast imaging of large sample areas. In this case, the laser power was 100 mW, the exposure time 15 s with 1 accumulation, and the Raman shifts range 680-1730 cm⁻¹. Four maps of 1.8 mm x 1.0 mm were collected (step along x: 20 μm, step along y: 14.2 μm), resulting in a total imaged area of 3.6 x 2.0 mm. The S 80 M distribution within

the tablet was obtained considering the intensity at 1658 cm⁻¹, which is the peak maximum characteristic only of the lipid.

3.2.12 S 80 M extraction from tablets

S 80 M from tablets was extracted by crushing them in the mortar and dissolving them in 1 mL of a 3:1 (v/v) ratio of methanol:chloroform solution. Samples were then vortexed (5 min) and sonicated (10 min) at 37 °C. Further centrifugation (10 min at 3400 *g*) allowed the separation of the supernatant containing lipids. The solution was left to rest in an upright position for 5 min. The extraction step was repeated four times until a clear supernatant was obtained. Organic solvents in the supernatant were evaporated under an inert nitrogen gas and later under reduced pressure (12 h) to eliminate residual solvent traces. The dried lipids were reconstituted and diluted in pure methanol prior to analysis. Lipids were reconstituted in HEPES buffer (10 mM, pH 7.4) for cell culture treatments to reach 50 mM S 80 M concentration.

Tablet extracts were also used to quantify the lipids content in each sample using an HPLC-CAD gradient method (see **Appendix Section A3.1**)

3.2.13 Preparation of protein-free chylomicrons (PFC)

PFCs were prepared by modifying previously described emulsions.³⁸² Briefly, 70% (w/w) S 80 M extracted from tablets, 3% (w/w) triglycerides from saturated fatty acids, 2% (w/w) cholesterol, and 25% (w/w) DOPC were dissolved in a 3:1 (v/v) ratio of methanol:chloroform solution. Solvents were evaporated under a stream of nitrogen before an overnight vacuum to eliminate residual solvent traces. The dried lipid mixture was dissolved in HEPES buffer (10 mM, pH 7.4) to reach 50 mM S 80 M and 18 mM DOPC concentration, respectively, and sonicated for 20 min at 37 °C. Control emulsions without S 80 M (PFC) were also produced with 10% (w/w) triglycerides from saturated fatty acids, 6.7% (w/w) cholesterol, and 83.3% (w/w) DOPC and diluted to 18 mM DOPC concentration. PFC treatments were further diluted in a serum-free experimental cell culture medium (*vide infra*, **Section 3.2.14**) 1:10 to treat the cells to reach final S 80 M and DOPC concentrations of 5 mM of 1.8 mM, respectively.

3.2.14 Cell culture and general information about cell experiments

LX-2 cells were grown at 37 °C in a 5% CO₂ humidified atmosphere in an LX-2 complete medium: DMEM-HG (4.5 g/L glucose, phenol red, no L-glutamine, pyruvate) supplemented

with 1% (v/v) penicillin/streptomycin mixture (penicillin: 10'000 U/mL, streptomycin: 10'000 μg/mL), 1% (v/v) of L-glutamine (2 mM), and 2% (v/v) FBS. According to the manufacturer's instructions, subcultivation was performed with Accutase[®] at about 80-90% cell confluency. LX-2 at passages 8 to 14 were used for cell experiments. LX-2 cell experimental medium was a serum-free complete medium.

For experiments, LX-2 cells were seeded either in 24-well microtiter plates with 0.5 mL/well at a density of 50'000 cells/well or in 96-well microtiter plates with 100 μ L/well at a density of 12'500 cells/well and cultured 18 h at 37 °C, 5% CO₂ to ~90% confluency. Treatments were always performed with 0.5 mL/well for 24-well plates or 100 μ L/well for 96-well plates at 37 °C, 5% CO₂.

Primary rat hepatic stellate cells (PRHSC) were isolated according to established protocols. PRHSCs were isolated from the livers of cirrhotic Sprague Dawley rats treated with thioacetamide (TAA) for 12 weeks. Animal experiments were approved by the Veterinary Office of the Canton of Bern, Switzerland, under License n. BE 90 2021 and followed accepted guidelines and regulations. After isolation, cells were seeded on assay microplates and grown at 37 °C in a 5% CO₂-humidified atmosphere for 7 days in a PRHSC complete medium containing IMDM (phenol red, L-glutamine) supplemented with a 1% (v/v) penicillin/streptomycin mixture (penicillin: 10'000 U/mL, streptomycin: 10'000 μg/mL) and 10% (v/v) FBS. PRHSC cells were grown for 7 days, not passaged, and used for cell experiments. PRHSC cell experimental medium was serum-free complete medium.

For experiments, PRHSC were directly seeded either in 24-well microtiter plates with 0.5 mL/well at a density of 50'000 cells/well or in 96-well microtiter plates with 100 μ L/well at a density of 12'500 cells/well and cultured 7 days at 37 °C, 5% CO₂ to reach 70–90% confluency. Cells were washed, and the medium was exchanged first at 24 h after seeding and then every 48 h until Day 7. Treatments were always performed with 0.5 mL/well for 24-well plates or 100 μ L/well for 96-well plates at 37 °C, 5% CO₂.

3.2.15 Direct treatment of LX-2 and PRHSC

For LX-2 cells, the medium from seeded cells was discarded the day after cell seeding, the cells were rinsed once with PBS, and a fresh complete medium was added. Then, treatments of cells in microtiter plates were performed directly. Briefly, the formulations were mixed with the experimental medium without FBS to reach a total lipid concentration of 5 mM, and cells

were incubated at 37 °C in a 5% CO₂ humidified atmosphere with this solution for 24 h and assayed.

For PRHSC, the day before the treatment (Day 7), the medium from seeded cells was discarded, and the cells were rinsed once with PBS. Then, treatments of cells in microtiter plates were performed directly. Briefly, the formulations were mixed with the experimental medium without FBS to reach a total lipid concentration of 5 mM, and cells were incubated with this solution for 24 h and assayed.

3.2.16 Analysis of lipid droplet content ORO

After cell treatment, both LX-2 and PRHSC cells in 24-well plates were washed three times with PBS, fixed with 500 μ L/well Roti®-Histofix 4% for 10 min at RT, and washed once with PBS. Cells were stained with a 0.5% w/v ORO solution in propylene glycol (500 μ L/well) for 15 min at RT. Carefully removed using a pipette and rinsed with PBS. Nuclei were then counterstained with a DAPI solution (3.6 μ M) in PBS for 5 min at RT. Afterwards, cells were rinsed with PBS. Fluorescence and brightfield image acquisition was performed using a Nikon Ti2-E (Nikon Instruments, Melville, NY, USA) inverted microscope with 20x magnification. DAPI filter (λ_{ex} 360 nm, λ_{em} 460 nm) and TxRed filter (λ_{ex} 560 nm, λ_{em} 645 nm) were used. The fluorescent binary area in the TxRed field was examined using FIJI/ImageJ software.³⁸⁴ Shortly, for each image, the qualitative interpretation of images was supplemented by quantification of fluorescence to have a transparent comparative purpose and confirm observed results. A fluorescent ORO relative intensity (FRI) was obtained by normalising the fluorescent binary area (μ m²) in the fluorescent field to the number of objects (cell nuclei number) in the DAPI field.

3.2.17 Reactive oxygen species (ROS)

After treatments, LX-2 and PRHSC cells in 96-well plates were washed with PBS (100 μ L/well) and incubated with ROS-ID® Total ROS detection kit following the manufacturer's instruction.

Briefly, cells were washed and incubated with ROS solution and the positive control (100 μ L/well) for 2 hours at 37 °C, 5% CO₂. After the incubation, the fluorescence was measured (λ ex=488 nm, λ em=520 nm) with an Infinite 200 Pro M-Nano plate reader (Tecan, Männedorf, Switzerland).

3.2.18 Cell proliferation assay (CCK-8)

The CCK-8 assay was used following the manufacturer's instructions. Briefly, after treatments (100 μ L/well; 96 well plate), LX-2 and PRHSC cells were washed once with PBS. A volume of 90 μ L of serum-free experimental medium and 10 μ L of CCK-8 was added to each well. Next, cells were incubated for 2 h at 37 °C, 5% CO₂. Afterwards, the absorbance was measured at 450 nm with an Infinite® 200 Pro M-Nano plate reader.

To calculate the cell metabolic activity in per cent, the following equation was used (Equation (5)):

Cell metabolic activity (%) = (OD sample/OD control)
$$\times$$
 100 (5)

"OD sample" refers to the optical density of the cells treated with the substances, and "OD control" refers to cells exposed to a serum-free experimental medium.

3.2.19 Motional order of the cell membrane in adherent cells

Stock solutions of the fluorescent probes DPH and TMA-DPH in DMSO were stored at -20 $^{\circ}$ C and protected from light until use. Working solutions of DPH (8 μ M) or TMA-DPH (5 μ M) in PBS were prepared fresh before experiments from aliquots of the corresponding fluorophore.

After cell treatments for 24 h, the adherent LX-2 and PRHSC cells were washed three times with PBS, and 100 μ L of DPH or TMA-DPH were added to each well of the 96-well plate (black bottom and wall). LX-2 cells were further incubated at 37 °C, 5% CO₂ with DPH (2 h) or TMA-DPH (10 min). After one PBS wash (100 μ L/well), all the remaining solution was aspirated from the wells, and fresh PBS was added to each well. The fluorescent anisotropy was measured with an Infinite 200 Pro F-Plex plate reader (Tecan, Männedorf, Switzerland) equipped with polarisation filters (monochromator mode, λ_{ex} = 360 nm, λ_{em} = 430 nm) and calculated by applying the following formula (Equation (6)):

$$r = \frac{G \times I_{\parallel} - I_{\perp}}{G \times I_{\parallel} + 2I_{\perp}}$$
 (6)

where the calibrated G factor (G) was 1.026, r is a calculated fluorescent anisotropy, I_{\parallel} parallel fluorescent intensity, and I_{\perp} perpendicular fluorescent intensity.

3.2.20 qPCR gene expression analysis in LX-2 cells

After LX-2 cell treatment for 24 h, a total RNA was isolated using TRIzol™ reagent following the manufacturer's protocol. Briefly, cells were lysed with TRIzol™ directly on the 24-well plate and transferred to 1.5 mL reaction tubes. Chloroform volume equivalent to one-fifth of the total TRIzol™ volume was added to the samples. The tube was vortexed vigorously for 10 sec and was incubated at room temperature for 10 min before being centrifuged for 20 min at 4°C and 16'000 *g*. The upper phase was transferred to a new reaction tube, and 1 µL glycogen and one volume of isopropanol were added and mixed well before the RNA precipitation on ice for 10 min. Next, the RNA was pelleted by centrifugation for 10 min at 4 °C and 24'000 *g*. The supernatant was discarded, and the pellet was washed with 1 mL of 70% EtOH in RNAse-free water. The centrifugation was repeated twice, and the final pellet was resuspended in RNAse-free water after air drying for a few minutes. The RNA concentration was measured with a NanoDrop (ThermoFisher, USA).

The isolated RNA was reverse-transcribed into cDNA. Briefly, 1000 ng of RNA were diluted in RNAse-free water and incubated for 5 min at 65 °C after adding 3 μL of a 150 ng/μL random hexamer (Microsynth, Switzerland). After 10 min incubation at RT, 13.5 μL of pre-mixed reverse transcription master mix was added (**Table A3.3**), and the samples were incubated for another 10 min at RT, followed by a 1 h incubation at 50 °C and 20 min incubation at 75 °C. RNAse-free water was added to reach a theoretical concentration of 8 ng/μL cDNA.

The primers (**Table A3.4**) were diluted in RNAse-free water to a primer pair solution of 2.5 μ M of forward and reverse primer each. The remaining reagents (polymerase, nucleotides, buffer, fluorophore) for qPCR were in the Brilliant III Ultra-fast SYBR Green qPCR master mix (MM; Agilent, USA). The cDNA samples were measured in duplicate for each gene and cDNA dilution. A pipetting robot (Corbett Robotics, USA) was used for pipetting the samples (3 μ L cDNA, 7.5 μ L 2x MM, 3 μ L primer mix, 1.5 μ L water). The samples were then transferred to the qPCR analyser centrifuge (Rotor-Gene Q 2Plex System, Qiagen, Germany), which performed 40 amplification cycles at 95 °C and 60 °C. The fluorescence was always measured at 60 °C (λ ex 470 nm, λ em 510 nm). After the 40 cycles, the melting curve of each sample was measured. The data were analysed using the RotorGene Q version 2.3.5 software and Microsoft Excel 365. The qPCR data were analysed using the delta-delta CT method. GAPDH was used as a reference gene.

3.2.21 Statistical tests and analysis

All experiments were performed in three independent replicates, and samples were freshly prepared if otherwise stated. Statistical analysis was carried out using GraphPad Prism version 9.5.1. Multiple comparisons between the groups were performed by an ordinary one-way ANOVA with *post-hoc* Tukey's multiple comparison analysis, respectively (statistical significance note as **** p < 0.0001, *** p < 0.001, ** p < 0.01, *p < 0.05). If not stated otherwise, the data are presented as mean \pm S.D. (standard deviation calculated from independent samples). qPCR data are presented as mean \pm S.E.M. (standard error of the mean).

3.3 Results and discussion

3.3.1 Formulation development

3.3.1.1 Preliminary formulations

The properties of the reference formulation (Ref_GV) were not compatible with direct compression to obtain tablets. Investigations to obtain a directly compressible formulation started by replacing Aerosil® 200 (fumed silica) with Neusilin® US2, magnesium aluminometasilicate, marketed by FIJI Chemicals and reported in the literature, as amorphous large surface area oil adsorbent with superior direct compressibility and mixture stabilisation able to improve powder flow. Formulations 1 and 2, powders containing 0.5% and 1% of Neusilin® were successfully produced, not compressible into tablets, but with improved powder properties. Compressibility index (CI) and Hausner ratio (HR), used as indirect methods to estimate the flow character, were decreased to 1.07 and 1.04, and 6.67 and 4.17, respectively, categorising powders as "excellent", the best category in the scale of flowability reported in Ph. Eur. 2.9.36.377 Doubling the Neusilin® quantity resulted in a better powder. All the results are reported in **Table 3.4**.

Table 3.4. Powder properties of preliminary and reference formulations

Formulation	Powder flow [g/s]	Bulk density [g/mL]	Tapped density [g/mL]	Hausner ratio	СІ	Note
Ref_GV T > 25°C	10.4 ± 2.2	0.33 ± 0.01	0.40 ± 0.01	1.22 ± 0.00 - Fair	17.86 ± 0.00 - Fair	only powder
Ref_GV T < 25°C	23.3 ± 1.7	0.38 ± 0.00	0.44 ± 0.00	1.15 ± 0.00 - Good	13.33 ± 0.00 - Good	only powder
1	20.3 ± 5.0	0.38 ± 0.00	0.41 ± 0.00	1.07 ± 0.00 - Excellent	6.67 ± 0.00 - Excellent	only powder
2	23.6 ± 3.8	0.36 ± 0.00	0.38 ± 0.01	1.04 ± 0.03 - Excellent	4.17 ± 2.95 - Excellent	only powder
3	12.6 ± 2.7	0.56 ± 0.00	0.70 ± 0.00	1.23 ± 0.02 - Fair	18.79 ± 1.04 - Fair	

^{*}CI – compressibility index. Mean ± SD, n = 3.

No powder characterisation for Formulation 4 and S80 + Sily.

In Formulation 2, the most abundant excipient MCC was reduced by 0.5% to double Neusilin[®] quantity to 1%. A slight decrease in MCC amount was considered negligible since its primary function was filler.

The following stage involved creating a powder formulation by reducing the initial quantity of S 80 M by half to 25% to investigate the potential of achieving a compressible powder formulation through decreased S 80 M amount. Furthermore, we removed mannitol and magnesium stearate from the mixture to produce a simple formulation. Mannitol, a carbohydrate, was removed from the formulation since it could potentially increase its water content, to which a highly hygroscopic S 80 M might respond with worse technical properties. Magnesium stearate, even if in discrete amounts and technically relevant, could potentially produce an unwanted saturated fatty acid biological effect on the liver. The sum of the S 80 M and MCC percentages was kept constant, with 1% Neusilin to reduce changing multiple factors simultaneously during the manual formulation optimisation. The final composition of Formulation 3 was set to 25% S 80 M, 74% MCC and 1% Neusilin. The obtained powder had shown only a "fair" flow, the third-best category by Ph. Eur., where Cl was 1.23 and HR 18.79. This formulation could be directly compressed into tablets and was considered successful. BD and TD values of formulations Ref GV, 1, and 2 were consistent at 0.33-0.38 g/mL and 0.40-0.44 g/mL, respectively. However, Formulation 3 had 0.56 (BD) and 0.70 g/mL (TD). Since we aimed to maximise S 80 M lipid content in tablets, we formulated a middle-ground formulation with 37.5% S 80 M, which falls in-between original granules (50.55%) and successfully compressed tablets (25%). Therefore, the sum of the S 80 M - MCC percentages was kept constant (37.5% S 80 M and 61.50% MCC), with Neusilin® again at 1%.

To perform a proof-of-concept investigation that it is possible to incorporate other ingredients in the PPC formulation, a formulation containing a well-known hepatoprotectant mixture Sily was prepared. Since EPLs are often recommended for NAFLD-affected patients, alone or in combination with other hepatoprotective ingredients. Sily is a commonly investigated EPL-associated ingredient that is bioactive in liver diseases. This lipophilic extract from *Silybum Marianum* seeds decreases inflammatory cascade by reduction of proinflammatory cytokines, diminishes HSCs activation, exerts antioxidant effect and acts as a radical scavenger.^{378,379} There is a recent report of the ongoing clinical study treating patients with PPC, vitamin E and silymarin formulation that should prove a beneficial effect of this therapeutical combination in NAFLD patients (Siliver; NCT03749070).³⁹³

Formulation 3 was modified by reducing MCC content by 25% and substituting it with the same amount of Sily.

Formulations 4 and S 80 M + Sily were not tested for powder characterisation but yielded once more successfully tablets.

Table 3.5. Tablet properties of preliminary formulations

Formulation	Mass [g]	Friability [%]	Minimum hardness [N]	Maximum hardness [N]	Mean hardness [N]
3	0.3293 ± 0.0121	0.05 ± 0.04	10	39	25.20 ± 7.42
4	0.2419 ± 0.0090	0.04 ± 0.04	n/a	n/a	n/a
S 80 M + Sily	0.2856 ± 0.0028	0.04 ± 0.02	11	25	16.10 ± 3.89

n/a – not available. Hardness was not measurable. Mean \pm SD, n = 3.

Tablets obtained from a powder containing 25% S 80 M (Formulation 3) were ~25% heavier than those obtained from Formulation 4 with 37.5% S 80 M, while Sily tablets were ~14% lighter than the only lipid tablets (**Table 3.5**). It was observed that higher lipid content tablets were not measurable for the resistance to crushing since they proved themselves to be too soft. Formulation 3 and S 80 M reported a mean hardness of 25.20 N and 16.10 N, respectively. Friability was always low, under the Ph. Eur. requirement of 1%. Positive results from the S 80 M + Sily formulation, in line with S 80 M-only formulations, confirmed the hypothesis of incorporating other ingredients in the PPC formulation, paving the way for further, more complex formulation development and optimisation.

3.3.1.2 DoE formulations

Based on preliminary investigation results, it was decided to run a DoE calculation to obtain a reasonable starting point for further formulation optimisation. Based on wanted S 80 M lipid content and the observed effect of different excipients on preparing different powders, the constraints were set as shown in **Table A3.1**, S 80 M 30 - 79%, MCC 20 - 50%, and Neusilin[®] 1 - 20%, with the final amount that had to sum up to 100%.³⁸¹ 13 formulations (**Table 3.2**) were prepared in a single replicate to evaluate if the formulation could be manually produced and measure each formulation's powder flow character.

Table 3.6. Powder properties of DoE formulations

Formulation	Powder flow [g/s]	Bulk density [g/mL]	Tapped density [g/mL]	Hausner ratio	CI
DoE 1	5.93	0.51	0.69	1.36 - Poor	26.32 - Poor
DoE 2	13.17	0.43	0.53	1.22 - Fair	18.18 - Fair
DoE 3	13.43	0.54	0.64	1.20 - Fair	16.67 - Fair
DoE 4	13.67	0.52	0.61	1.19 - Fair	15.79 - Fair
DoE 5	9.67	0.61	0.70	1.14 - Good	12.50 - Good
DoE 6	13.67	0.55	0.70	1.29 - Passable	22.22 - Passable
DoE 7	10.97	0.50	0.62	1.25 - Fair	20.00 - Fair
DoE 8	15.03	0.47	0.58	1.24 - Fair	19.05 - Fair
DoE 9	14.87	0.54	0.61	1.13 - Good	11.11 - Good
DoE 10	17.90	0.43	0.52	1.21 - Fair	17.39 - Fair
DoE 11	13.67	0.58	0.65	1.13 - Good	11.76 - Good
DoE 12	14.87	0.49	0.57	1.18 - Good	15.00 - Good
DoE 13	11.30	0.54	0.65	1.20 - Fair	16.67 - Fair

Measurements for 1 replicate.

The powder flow character of obtained formulations was examined (**Table 3.6**) together with organoleptic appearance during the production process. CI of these formulations was inbetween 1.14 and 1.36, and HR between 11.11 and 26.32. One formulation each had a "poor" and "passable" flow. Seven formulations were "fair", but only four, DoE 5, 9, 11 and 12, were characterised as "good". BD ranged from 0.43 to 0.61 g/mL, and TD from 0.52 to 0.70 g/mL in these formulations. Based on the production experience and obtained powders, DoE 5 and 11 were chosen to be produced in a bigger triplicate batch to examine the formulation properties and their compressibility more reliably into tablets.

Table 3.7. Powder properties of selected DoE formulations

	Formulation	Powder flow [g/s]	Bulk density [g/mL]	Tapped density [g/mL]	Hausner ratio	CI
	DoE 5	18.78 ± 4.22	0.58 ± 0.01	0.68 ± 0.01	1.17 ± 0.00 - Good	14.78 ± 0.35 - Good
Γ	DoE 11	17.97 ± 4.31	0.57 ± 0.03	0.69 ± 0.01	1.21 ± 0.03 - Fair	17.25 ± 2.15 - Fair

 $Mean \pm SD$, n = 3.

DoE 5 kept its "good" flow character, with a reported CI of 14.78 and HR of 1.17. Simultaneously, there was a slight deterioration in DoE 11 powder character, "fair" with CI 17.25 and HR 1.21 (**Table 3.7**), which could be expected since there is a substantial quantity of S 80 M lipid in this formulation, which amounted to 49.00% (DoE 5) and 66.75% (DoE 11). BD and TD were slightly higher than in pilot DoE formulations, but this might be attributed to larger batch size, amounting to 0.58 and 0.57 g/mL for BD, and 0.68 and 0.69 g/mL for TD, in DoE 5 and DoE 11 formulations, respectively. Higher amounts of Neusilin® did not seem to improve the powder quality since it would separate from the mixture, which the eye could

observe. Slight variations in the powder properties could be attributed to uncontrolled room air temperature and humidity.

Table 3.8. Tablet properties of selected DoE formulations

Formulation	Mass [g]	Friability [%]	Minimum hardness [N]	Maximum hardness [N]	Mean hardness [N]
DoE 5	0.3886 ± 0,0176	0.07 ± 0.05	27	51	40.03 ± 5.63
DoE 11	0.4031 ± 0.0136	0.04 ± 0.01	30	65	46.50 ± 7.82

Mean \pm SD, n = 3.

Both powders yielded tablets, with the ones compressed from DoE 5, yielded ~3.5% lighter tablets (0.3886 g) than DoE 11 (0.4031 g) (**Table 3.8**). Friability, as usual, was at a negligible level of 0.07% and 0.04%. DoE 11 tablets were harder than DoE 5, with the mean hardness being 46.50 N compared to 40.03 N.

These results provided a direction for further optimisation of the formulation DoE 11, containing 66.75% of S 80 M, which provided a high-lipid content and the possibility to compress them into the tablets directly.

3.3.1.3 Optimisation of 70% S 80 M containing formulation

Based on the DoE 11 formulation containing 66.75% S 80 M, 27.50% MCC, and 5.75% Neusilin®, S 80 M content was rounded up to 70%, Neusilin® percentage was set to 1 or 2%, and a disintegrant, Primellose®, croscarmellose sodium, was added in the amount of 2 or 5%, as recommended by the manufacturer for the demanding formulations (**Table 3.3**). It acted as an absorbent hydrophilic but insoluble material with exceptional swelling and wicking properties, used as a disintegrant.³⁹⁴

Table 3.9. Powder properties of optimised DoE formulations

Formulation	Powder flow [g/s]	Bulk density [g/mL]	Tapped density [g/mL]	Hausner ratio	CI
F70-1	12.30	0.50	0.59	1.17 - Good	14.29 - Good
F70-2	16.40	0.51	0.58	1.14 - Good	12.50 - Good
F70-3	13.77	0.50	0.56	1.11 - Good	10.20 - Good
F70-4	12.40	0.53	0.63	1.21 - Fair	17.02 - Fair
F70-5	13.67	0.51	0.63	1.23 - Fair	18.75 - Fair

Measurements for 1 replicate. Formulations' compositions reported for convenience:

F70-1: S 80 M 70.00%, MCC 29.00%, Neusilin® US2 1.00%, Primellose® 0.00% F70-2: S 80 M 70.00%, MCC 27.00%, Neusilin® US2 1.00%, Primellose® 2.00% F70-3: S 80 M 70.00%, MCC 24.00%, Neusilin® US2 1.00%, Primellose® 5.00% F70-4: S 80 M 70.00%, MCC 28.00%, Neusilin® US2 2.00%, Primellose® 0.00% F70-5: S 80 M 70.00%, MCC 23.00%, Neusilin® US2 2.00%, Primellose® 5.00%

All formulations yielded "good" (F70-1, F70-2, and F70-3) or "fair" (F70-4 and F70-5) flowing powders with CI ranging 1.11-1.23 and HR 10.20-18.75. BD was consistent in the 0.50-0.53 g/mL range, the same as TD, with reported values of 0.58-0.63 g/mL (**Table 3.9**). They were successfully directly compressed into tablets. All the production and characterisation have been performed in an air-conditioned room at +15°C.

Table 3.10. Tablet properties of optimised DoE formulations

Formulation	Mass [g]	Friability [%]	Minimum hardness [N]	Maximum hardness [N]	Mean hardness [N]
F70-1	0.2774 ± 0.0183	0.16	15	30	22.20 ± 5.45
F70-2	0.2779 ± 0.0239	0.08	11	33	17.20 ± 9.01
F70-3	0.2860 ± 0.0199	0.02	10	15	12.20 ± 2.17
F70-4	0.3096 ± 0.0141	0.08	22	36	27.00 ± 5.92
F70-5	0.3039 ± 0.0183	0.03	12	24	18.00 ± 5.24

Measurements for 1 replicate. Mass and hardness means are reported with SDs to display intra-batch variability.

From the data reported in **Table 3.10**, tablets of the first three formulations were ~8-10% lighter than those of the latter two. The friability of all formulations was consistently under the required 1% by Ph. Eur. Tablets' hardness was slightly lower than previously observed. However, it can be attributed to the different quality and composition of the mixture. It ranged from 12.20 N to 27.00 N.

These tablets were submitted to a preliminary disintegration study. The disintegration test was run as described in **Section 3.2.7**, but using 900 mL of Biorelevant dissolution media FaSSIF and FaSSGF with disintegration discs, prepared per manufacturer's instructions. Three tablets of F70-1 and F70-2 and two of F70-3, F70-4, and F70-5 were used. These media simulated wanted human body compartment's liquid composition, fasted intestine and stomach. Since tablets disintegrated in FaSSGF and FaSSIF, which was an undesirable effect, since we wanted the disintegration to occur only in the small intestine, the enteric tablet coating was considered for the following optimisation step.

3.3.1.4 Final remarks on formulation development

Based on preliminary, low-percentage S 80 M content and DoE formulations, this extensive optimisation study yielded only partially satisfying formulation. Therefore, the highest-lipid content formulation from DoE, acceptable according to our criteria, was chosen and manually optimised for different components and quantities to obtain the tested one. Based on all the reported results, F70-5 was defined as a formulation of choice to produce a larger batch and test on *in vitro* models of LX-2 HSCs and cirrhotic PRHSCs.

3.3.2 Compendial quality assays of the final F70-5 formulation

The present work aimed to formulate compendium-compliant tablets containing a high percentage of S 80 M. One of the main challenges in developing an EPL-based tablet is the high lipid percentage needed to reach the daily hepatoprotective dose, reported to be 1.05-1.80 g.^{125,132} Based on optimisations described previously, we could incorporate 70% (w/w) soy phospholipid via dry granulation due to the physicochemical properties of PPC with low melting points.^{124,395} Considering the demanding nature of EPL's formulation, the choice and quantity of excipients were critically important. MCC (23%, w/w) was chosen as a classical filler, binder, and anti-caking agent. In addition, its plasticity enables efficient binding to other materials, especially poorly tabletable active pharmaceutical ingredients.^{396,397} Primellose® (5%, w/w), croscarmellose sodium, is an absorbent hydrophilic but insoluble material with exceptional swelling and wicking properties and, as such, used as a disintegrant.³⁹⁴ Neusilin® was added as an oil adsorbent due to its large surface area and ability to stabilise the mixture, improve the powder flow, and thus achieve a direct lipid tablet compression.³⁸⁶⁻³⁸⁸

As shown in **Table 3.11**, the measured bulk and tapped density were 0.58 g/mL and 0.66 g/mL, respectively. The resulting HR and CI confirmed the "good" powder flow. The obtained HR and CI values were similar to those obtained in the study from Kolbina *et al.*³⁹⁸ (CI 12.64 \pm 1.21 and HR 1.15 \pm 0.02), where saturated phosphatidylcholine (SPC) was formulated as a matrix for the extended-release dosage form.

Table 3.11. Powders' mixture properties. Mean \pm S.D. (n=3)

Property	Experimental values
Powder Flow	28.0 ± 4.2 g/s
Bulk density	0.5787 ± 0.0085 g/mL
Tapped density	0.6598 ± 0.0010 g/mL
Hausner Ratio	1.14 ± 0.02 – Good flow
Compressibility Index	12.30 ± 1.16 – Good flow

The measured powder flow was 28.0 g/s, a value in agreement with the good flow character assessed by HR and CI evaluation. Therefore, based on these findings, this powder mixture was suitable for further tabletting.

The ensuing powder mixture was further compressed into tablets and analysed following Ph. Eur. tests.

The obtained friability of the tablets was low (0.09%, **Table 3.12**), mirroring the good mechanical properties of our solid dosage form and shape and mass conservation, of pivotal

importance, especially during processes imminently after production, such as packaging, transportation, and use. Despite the excipients' softness, the tablets' hardness was 21.80 N, ranging from 12 to 41 N.

Table 3.12. Tablets' properties measured according to Ph. Eur. 11. Mean \pm S.D. (n=3)

Property	Experimental Values
Mass	0.2950 g ± 0.0151
Friability	0.09% ± 0.04
Minimum Hardness	12 N
Maximum Hardness	41 N
Mean Hardness	21.80 N ± 6.20

The Ph. Eur. disintegration test was carried out to determine the speed at which the tablet breaks down into smaller particles, allowing for a greater surface area and absorption of the phospholipid in the small intestine. Uncoated tablets entirely disintegrated after less than 1 h and evidently did not comply with the pharmacopoeial gastro-resistance requirement of at least 2 h in HCl 0.1 M. Considered that EPLs' absorption and uptake occur with other lipids *via* retinyl esters and chylomicrons, starting from the small intestine, ³⁹⁹⁻⁴⁰¹ to avoid the disintegration and release of tablets in the stomach, the choice was to provide the tablets with a gastro-resistant coating to modulate their release. We manually dip-coated tablets as proof of principle, and disintegration tests were performed again to verify the efficiency of the coating layer. Coated tablets resisted HCl 0.1 M for 2 h and showed no structural damage. After their transfer to PB pH 6.8, complete disintegration occurred within the prescribed 1 h (**Figure A3.2**). We could thus demonstrate that with enteric coating, we can modulate the tablet disaggregation in the small intestine compartment as desired.

3.3.3 Thermogravimetry

The hygroscopicity of the tablets and their components was assessed using TGA. Aliquots of samples were either freeze-dried or equilibrated at RH 75% (see the **Materials and Methods** section for further details) to quantify water absorption upon incubation in a humid environment. For TGA analysis, the samples were heated at 10 °C/min, and their weight loss as a function of temperature was monitored (**Figure 3.1**).

The difference between the weight loss from RT to 150 °C of each sample, either freezedried or equilibrated at RH 75%, was taken as an indication of the amount of water present in the sample due to equilibration at RH 75%. The results in **Table 3.13** reveal that the lipid

S 80 M is remarkably hygroscopic, as expected, since after equilibration at RH 75%, it consists of about 19% w/w of water. On the other hand, MCC is the least hygroscopic component of the formulation, while the other excipients, the powder mixture and the uncoated tablet, display a water % ranging from ~14% to 17%.

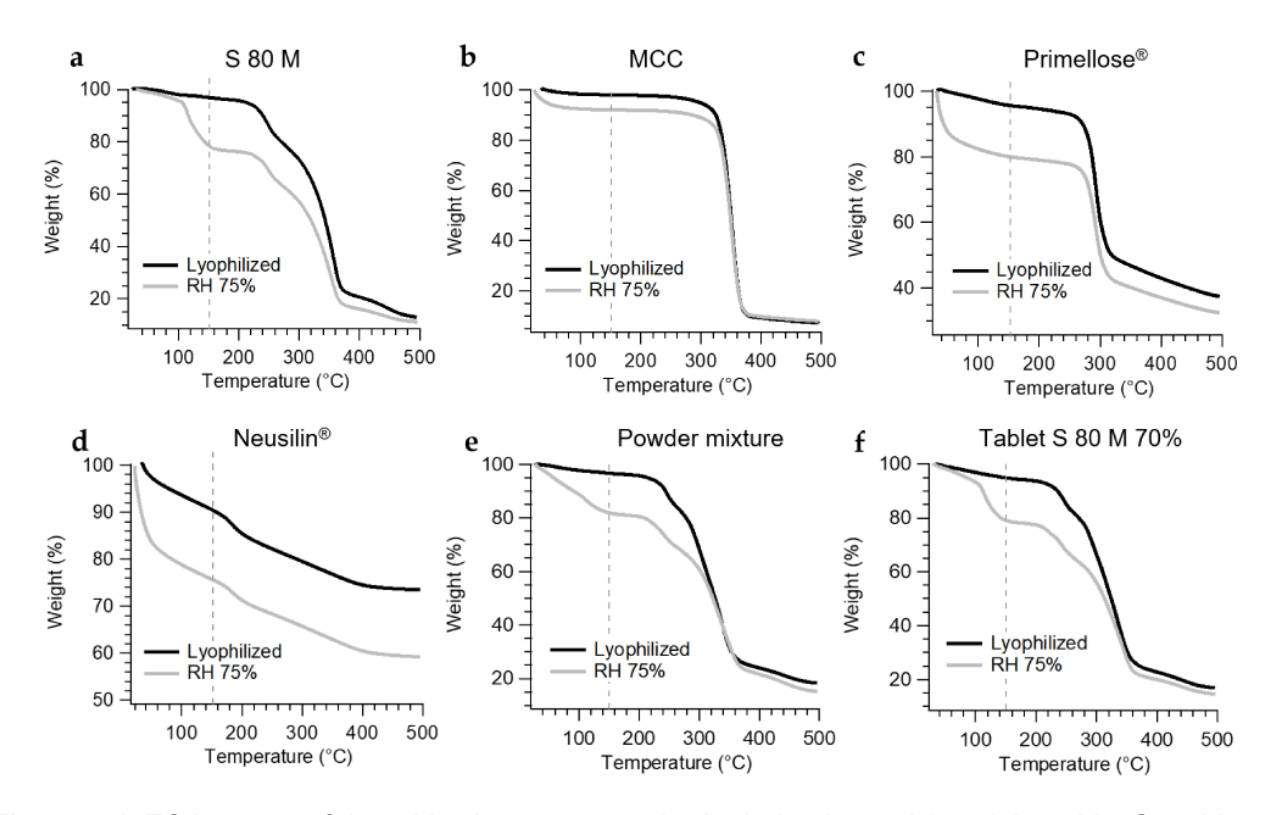


Figure 3.1. TGA curves of the tablets' components (**a-d**), their mixture (**e**) and the tablet S 80 M 70% (**f**). The black curves indicate the freeze-dried samples, while the grey ones refer to those equilibrated at RH 75%. The dashed line at 150 °C indicates the point chosen for estimating the water amount gained upon equilibration at RH 75%.

Table 3.13. Water % (w/w) in the samples after equilibration at RH 75% was obtained as the difference between the weight loss % at 150 °C of samples equilibrated at RH 75% or freeze-dried. Mean \pm S.D. (n=3).

Sample	Water % (w/w)
S 80 M	19.3 ± 2.9 %
MCC	4.6 ± 1.2 %
Primellose®	17.4 ± 2.9 %
Neusilin [®]	14.1 ± 1.9 %
Powder mixture	17.0 ± 3.3 %
Tablet S 80 M 70%	16.8 ± 0.9 %

3.3.4 X-ray powder diffraction (XRPD) and Raman microscopy

The samples were also characterised by employing XRPD to understand if the water uptake or the tabletting process would impact the crystallinity. The diffraction patterns of the tablets' components are given in **Figures 3.2a-d**. S 80 M displays sharp diffraction peaks at low angles, which reveal its liquid crystalline nature. The excipients are characterised by broad peaks that are diagnostic of a low degree of crystallinity, as expected, given their polymeric nature. The patterns reveal that no significant difference between the freeze-dried and the equilibrated at RH 75% samples is observed, except for minor variations in the S 80 M peaks intensity and position, which are reasonably due to the different amount of water present in the samples: it is indeed well known that the number of water molecules per phosphatidylcholines influences their diffraction pattern.⁴⁰²

The XRPD pattern of the sample S 80 M 70% equilibrated at RH 75% before and after tabletting is given in **Figure 3.2f**. Both samples show the narrow and intense peaks of S 80 M at low 2θ, together with broader signals at higher angles due to MCC and Primellose[®]. No differences were observed between the pattern of the tablet and the powder mixture, suggesting that the compression occurring during the tabletting procedure does not influence the crystallinity of the formulation components. Such patterns refer to samples equilibrated at RH 75%, but the same considerations can be drawn for the freeze-dried samples, whose diffractograms are shown in **Figure 3.2e**. Kolbina *et al.* published similar findings, showing that after producing and characterising matrices extruded from hydrogenated soybean phosphatidylcholine (HSPC), a change in HSPC's crystallinity was not observed.⁴⁰³

The lipid distribution within the tablet was analysed with confocal Raman mapping. We initially collected the Raman spectra for the different components constituting the formulation, shown in **Figure 3.3a**. S 80 M shows a variety of signals in its spectrum, which are consistent with stretching and bending modes of vibration of phosphatidylcholines. The spectra of MCC and Primellose® are similar, which is reasonable considering that the two polymers derive from cellulose; the sharper peaks of MCC might be related to its more crystalline nature (see **Figure 3.2**). Neusilin®, on the other hand, shows very weak and broad signals. The lack of distinctive peaks is consistent with its chemical nature, a synthetic amorphous form of magnesium alumino-metasilicate, and agrees with literature reports. The lack of distinctive reports of the sharper peaks is consistent with its chemical nature, a synthetic amorphous form of magnesium alumino-metasilicate, and agrees with literature reports.

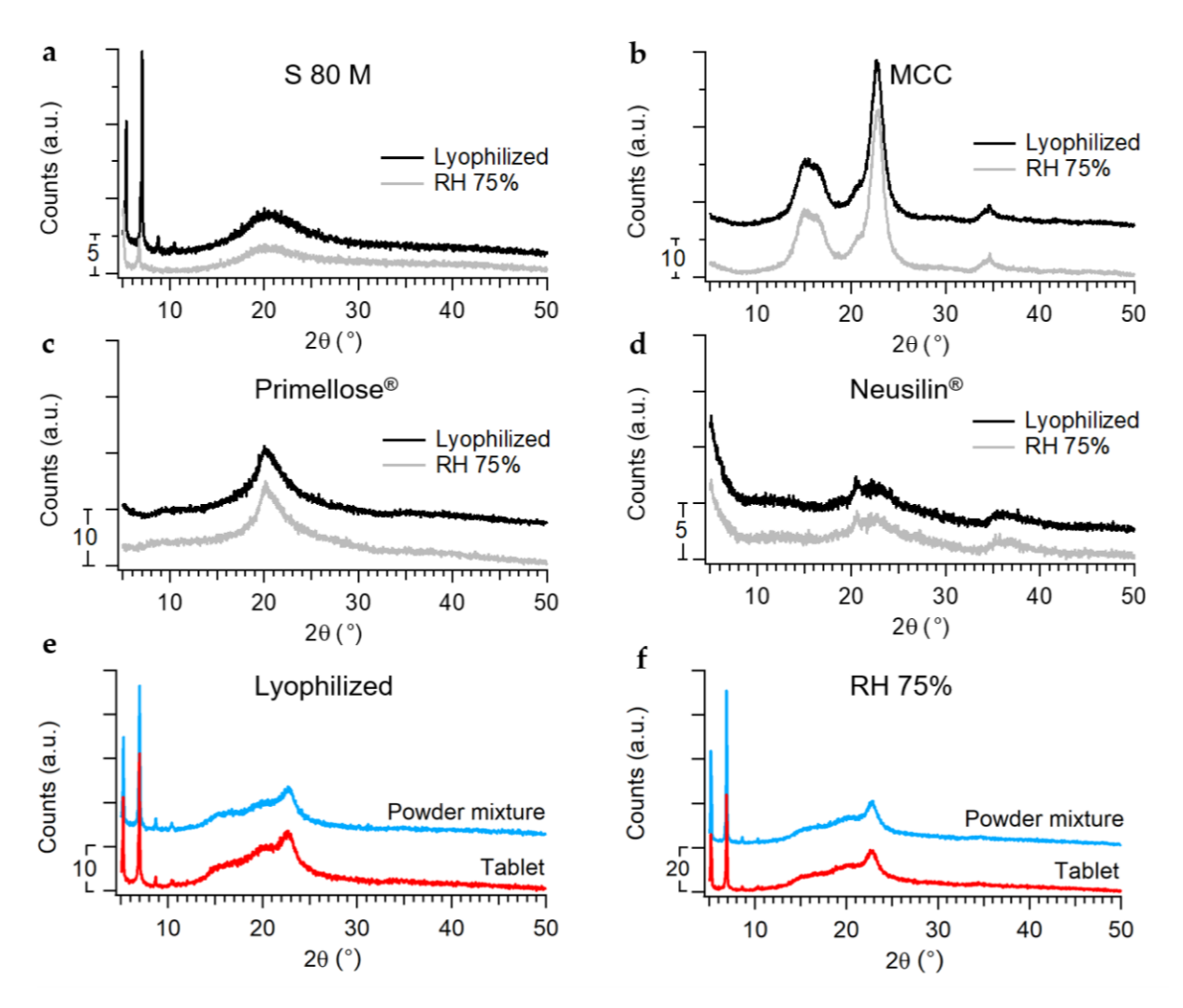


Figure 3.2. XRPD diffractograms of (a) S 80 M, (b) MCC, (c) Primellose[®], (d) Neusilin[®]. The black patterns refer to the freeze-dried samples, while the grey ones belong to the samples equilibrated at RH 75%. (e) freeze-dried tablet S 80 M 70% (red) and powder mixture before tabletting (blue) samples. (f) tablet S 80 M 70% before (blue) and after (red) tabletting equilibrated at RH 75%. All the diffractograms have been vertically offset for display purposes.

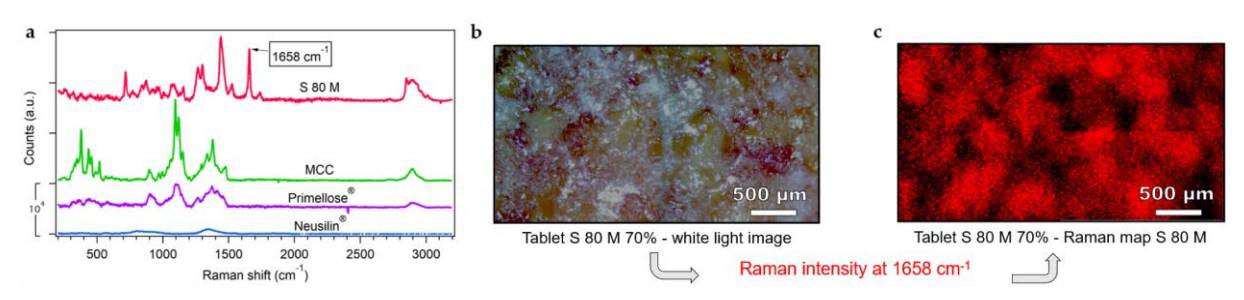


Figure 3.3. (a) Raman spectra of the components present in the tablets. From top to bottom: S 80 M, MCC, Primellose® and Neusilin®. The spectra have been vertically offset for display purposes. (b) and (c) refer to the confocal Raman characterisation of the Tablet S 80 M 70%. (b) White light image of the area under investigation. (c) Raman map showing the intensity at 1658 cm⁻¹ indicates the S 80 M distribution within the tablet.

To perform a Raman mapping and to discriminate between the components of a multi-phase sample, it is fundamental to identify regions where no overlay between the signals of the different components is present: to our purposes, the peak at 1658 cm⁻¹ of S 80 M, which corresponds to C=C stretching of unsaturated fatty acids,⁴⁰⁶ is particularly well suited to observe the distribution of this component within the tablet since MCC, Primellose[®] and Neusilin[®] do not display any signal in this region. Therefore, we analysed a large area of the tablet (3.6 x 2.0 mm), collecting a white light image (**Figure 3.3b**) in which the S 80 M distribution was obtained by observing in each pixel the intensity of the Raman spectrum at 1658 cm⁻¹ (**Figure 3.3c**). The lipid appears homogeneously distributed within the tablet on the tens of µm length scale, as only hundreds of µm domains can be observed. Notably, S 80 M-rich regions correlate with the yellowish areas visible in the white light image (**Figure 3.3b**).

3.3.5 Modulation of LX-2 cell phenotype indicating antifibrogenic effects

Solid dosage forms cannot be tested as such on cells. Therefore, we decided to extract the phospholipids from tablets using the Bligh-Dyer method⁴⁰⁷ and reconstitute the lipids in a buffer. The efficiency of the extraction process of the lipids from the other excipients was assessed via HPLC-CAD, revealing $102.8\% \pm 2.7$ lipid content recovery (**Figure A3.3**).

For a better understanding and comparison of the *in vitro* antifibrotic effect of S 80 M successfully extracted from tablets, control treatments of S 80 M liposomes were produced via the film hydration method and extrusion through polycarbonate membranes as previously reported (see **Appendix Section A3.2**).^{137,408} To simulate a more physiologically relevant lipid transport method, extracted S 80 M from tablets was also reconstituted as a PFC-like emulsion.^{399-401,409}

The bioactivity of the extracted S 80 M was tested over a 24 h incubation time, fixing the total S 80 M lipid concentration at 5 mM on cells for all the treatment conditions on naïve LX-2 immortalised hepatic stellate cells following our optimised *in vitro* model.¹³⁷

All the treatments did not interfere with LX-2 cell viability, excluding thus any possible toxicity of S 80 M (**Figure 3.4a**), as expected from our previous studies.¹³⁷ S 80 M liposomes and extracts did not contribute to oxidative stress, as the ROS level did not increase after treatment (**Figure 3.4b**).

After establishing the effect of PPC on metabolic activity and toxicity, we quantified the changes in lipid droplet storage, evaluated variations in cellular membrane motional order,

and followed the gene expression for the most important fibrosis factors as a function of the lipid treatments.

The Oil Red O (ORO) staining of neutral lipid droplets in LX-2 cells reveals their content in fluorescence, and it is among the golden standard methods to rapidly quantify the reversion of HSCs from an activated, profibrogenic status, depleted of lipid droplets, to a non-fibrogenic quiescent-like phenotype, characterised by distinct storage of lipid droplets.⁸²

As expected, LX-2 incubation with control conditions DMEM, DOPC, and PFC induced the formation of lipid droplets only to a negligible, non-significant amount (**Figures 3.4cd**); on the contrary, all the S 80 M treatments (Lipo, Tbl 70%, Tbl 70% + PFC) contributed to a significant increase (p < 0.0001) in the number of HSCs' lipid droplets, clearly visible as red spots in fluorescent images, with a ~36-fold FRI increase compared to untreated LX-2 (DMEM) (57.1 FRI, 58.8 FRI and 59.7 FRI for Lipo, Tbl 70% and Tbl 70% + PFC treatments, respectively) in agreement with what previously observed.¹³⁷ The differences in-between different S 80 M treatments were not significant.

These data convey that both S 80 M extracts retained significant bioactivity even after extensive technical processing. Findings entirely agree with previous observations¹³⁷ and confirm PPC-specific bioactivity in reverting activated HSCs in a quiescent-like phenotype by restoration of lipid droplet content.

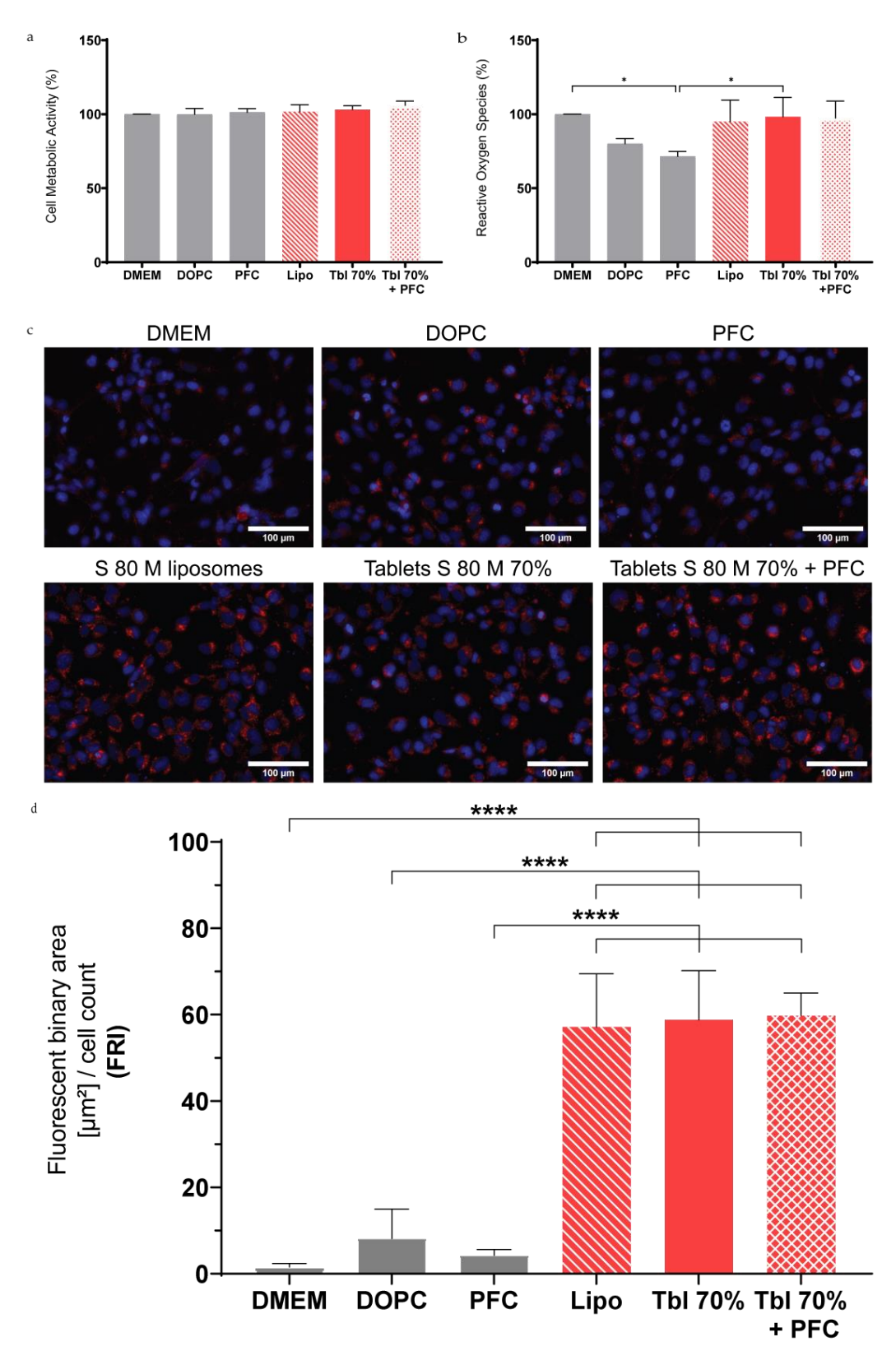


Figure 3.4. (a) LX-2 cell viability (%) using CCK-8 assay. (b) LX-2 ROS production. (c-d) ORO staining of LX-2 cells treated with various phospholipid treatments: DMEM experimental medium (untreated); DOPC: inactive phospholipid used as negative control; PFC: protein-free chylomicron-like emulsions without S 80 M; Lipo: S 80 M liposomes; Tbl 70%: S 80 M tablet extract in buffer; Tbl

70% + PFC: tablet extract reconstituted as PFC-like emulsions. (c) Representative fluorescence images of LX-2 cells in which lipid droplets can be visualised as red spots and the nuclei are counterstained with blue DAPI. (d) Quantification of the ORO fluorescence normalised to the number of LX-2 cells in the DAPI field (FRI). Cell number per image was in the range of ~50-160 cells. Mean \pm S.D. (n=3). p-values (**** p < 0.0001, * p < 0.05) from ordinary one-way ANOVA with post-hoc Tukey's multiple comparison analysis.

3.3.6 mRNA transcription of fibrosis markers

To further assess PPC lipid extracts' bioactivity, we chose to analyse the mRNA transcription of some prominent markers of fibrosis, namely PLIN2, PDGFRB, ACTA2 coding for α -smooth muscle actin – α -SMA, COL1A1 for collagen type I, and SPARC, a membrane-associated protein, recently reported by our group¹³⁸ to be associated with extracellular vesicles harvested and purified from activated LX-2. PLIN2 (perilipin 2) is a cytoplasmatic protein involved in lipid droplet formation, stabilisation and lysis, and its upregulation leads to a regulation of lipid droplet metabolism that are depleted in fibrotic pathological condition. The upregulation of PLIN2 has been shown to correlate with decreased activation of HSCs and is associated with a reduction in specific prominent fibrotic markers (for example, collagen type I, α -SMA, matrix metalloprotease 2 – MMP-2) via still unknown intracellular mechanisms.

Platelet-derived growth factor receptor- β (PDGFR- β) is a tyrosine kinase transmembrane protein. This specific isoform mediates the activation and increases profibrogenic transdifferentiation of HSCs into myofibroblasts during hepatic fibrosis. 411-413 It has been identified to rapidly increase expression to sustain pathological progression by modulating multiple intracellular pathways. 411-413 Its expressional decrease is correlated with a decrease in HSC activation and ameliorating of the fibrosis progression, 411 namely reverting HSCs to a quiescent-like phenotype.

Cells treated with S 80 M extracts significantly maximised PLIN2 mRNA expression of 2.8-fold, 2.6-fold and 3.0-fold for Lipo, Tbl 70% and Tbl 70% + PFC, respectively. As PLIN2 expression is connected with lipid droplet metabolism, the observed upregulation of this gene confirms the increase in fluorescence quantified with the ORO staining (**Figure 3.4b**).

In the case of PDGFRB mRNA expression, cells treated with S 80 M showed a decrease of ~45%, ~49% and ~42% (Lipo, Tbl 70% and Tbl 70% + PFC, respectively), which means lipid extracts managed to revert cells to quiescent-like phenotype by reducing the mRNA transcription. PDGFR-β activation leads to enhanced signalling along the Fas-MAPK

pathway and further to the PI3K-AKT/PKB pathway with the involvement of PKC family members. 411,414 Particularly, the activation of the ERK2 and ERK5 (part of the MAPK family) axis has been associated with increased cell migration, proliferation, transdifferentiation and inflammation. 415,416 Expression of soluble PDGFR-β in blood has been studied to be used as a valid parameter in the clinical prognosis of the fibrosis state of patients by Lambrecht *et al.* 413 To confirm the validity of system expression levels of PDGFRB were assessed and were found to be notably lower in healthy/quiescent HSCs (primary human and mouse HSCs). PDGFR-β antagonism is considered a desirable target to treat hepatic fibrosis. 411,417-419 It has been demonstrated that imatinib mesylate (a tyrosine kinase inhibitor, Gleevec®), a potent inhibitor of PDGFR-β, could inhibit HSCs activation and sequentially reduce early fibrosis. However, the progression of the pathology was not prevented. 420

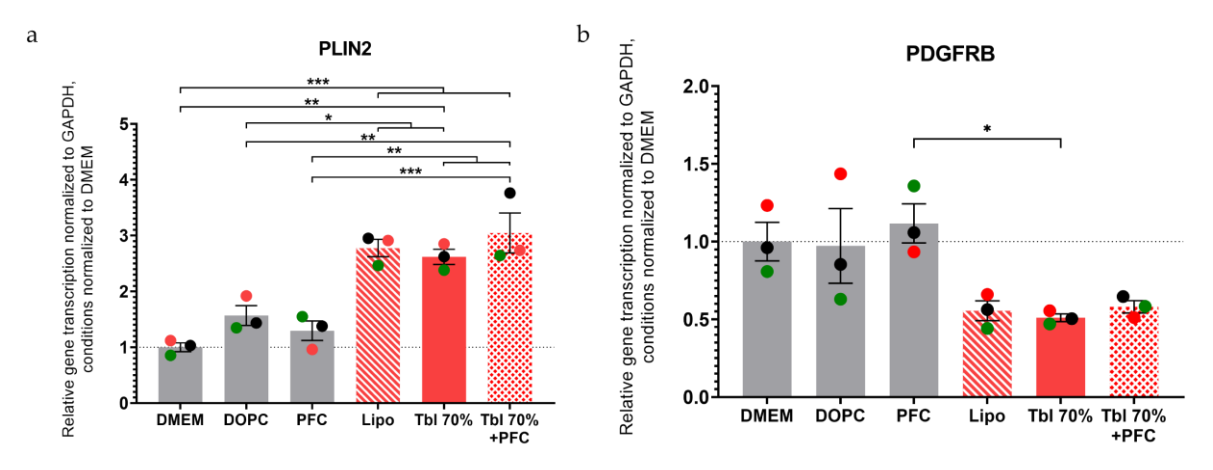


Figure 3.5. Relative mRNA transcription in LX-2 cells of two fibrosis markers (**a**) PLIN2 and (**b**) PDGFRB, normalised to GAPDH mRNA transcription and normalised to the DMEM condition after different phospholipid treatments: DMEM experimental medium (untreated); DOPC: inactive phospholipid used as negative control; PFC: protein-free chylomicron-like emulsions without S 80 M; Lipo: S 80 M liposomes; Tbl 70%: S 80 M tablet extract in buffer; Tbl 70% + PFC: tablet extract reconstituted as PFC-like emulsions. Mean \pm S.E.M. (n=3). p-values (*** p < 0.001, ** p<0.01, * p < 0.05) from ordinary one-way ANOVA with post hoc Tukey's multiple comparison analysis.

SPARC is a matricellular glycoprotein whose primary function is exerted by mediating the interactions between cells and their extracellular matrix with respective tissue remodelling, including those undergoing wound repair or morphogenesis. 121-423 Its upregulation in hepatic fibrosis pathways has been previously demonstrated in LX-2 cells and human biopsies 124-426, suggesting that downregulating SPARC could be part of a therapeutic approach to revert the

pathology. SPARC is associated with the plasma membrane in the extracellular space, and we recently reported that EVs from LX-2 cells treated with S80, a PPC-rich lipid analogue to S 80 M, have a remarkably lower level of SPARC associated with their membrane measured via fluorescence nanoparticle-tracking analysis. 122,138

In our experimental design, no statistically significant change in mRNA transcription of ACTA2, COL1A1, and SPARC markers could be observed. However, it could be observed that all the S 80 M treatments contributed to a slight decrease in the relative values with respect to naïve cells (**Figure A3.5**).

Since liver fibrosis employs more than 150 differently expressed markers in HSCs, ⁴²⁷ looking at only a few *ad hoc* selected markers and assays could give us a rapid insight into the PPC bioactivity but cannot preclude that a broader biological effect of S 80 M treatments could take place. Nevertheless, the observed decrease in PDFGRB and increase in PLIN2 mRNA transcription levels and the lipid droplets recovery in ORO staining upon incubation with S 80 M suggest that PPC contributes to restoring a quiescent-like status, as also observed by other groups^{211,428}, and that handling the PPCs to manufacture tablets does not interfere with their biological activity. Further extensive transcriptomics and proteomics studies will shed light on the pathways involved and understand whether a proper de-activation of HSCs occurs.

3.3.7 Motional order of the cell membrane in adherent LX-2 cells

The dynamic properties of membrane lipids to the treatments were assessed by calculating the anisotropy of DPH and TMA-DPH from fluorescence polarisation experiments. DPH is a probe known to arrange itself in the inner core of the bilayer, while TMA-DPH is at the interface region owing to its amphiphilic nature. Therefore, DPH could be employed to estimate the motional order of the hydrophobic membrane region. At the same time, TMA-DPH senses a change in motional order in the region at the interface with the extracellular space. Independently of the probe used, a decrease of anisotropy corresponds to an increased motional order of the cell membrane and, thus, to a higher membrane fluidity. All S 80 M treatments significantly increased the motional order of the inner membrane layer, shown in **Figure 3.6a**, compared to DMEM. Lipo, Tbl 70% and Tbl 70% + PFC caused a decrease in measured DPH anisotropy from 0.224 (untreated) to 0.208 (-7.1%), 0.204 (-8.9%) and 0.199 (-11.5%), respectively.

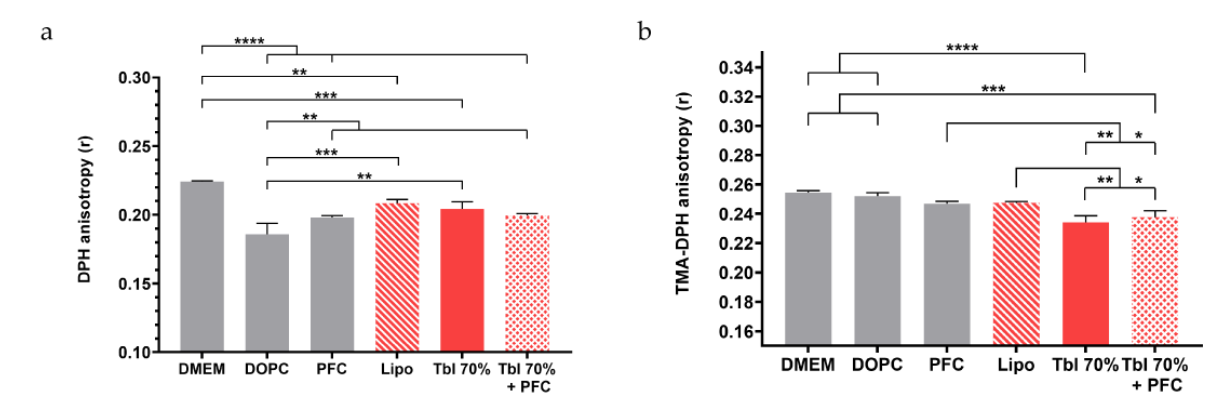


Figure 3.6. PPC treatment effect on the motional order of LX-2 cell membrane employing anisotropy of (a) DPH (inner membrane) and (b) TMA-DPH (interfacial membrane) as a function of different phospholipid treatments: DMEM experimental medium (untreated); DOPC: inactive phospholipid used as negative control; PFC: protein-free chylomicron-like emulsions without S 80 M; Lipo: S 80 M liposomes; Tbl 70%: S 80 M tablet extract in buffer; Tbl 70% + PFC: tablet extract reconstituted as PFC-like emulsions. Mean \pm S.D. (n=3). p-values (**** p < 0.0001, *** p < 0.001, ** p < 0.05) from ordinary one-way ANOVA with post hoc Tukey's multiple comparison analysis.

At the interfacial region (**Figure 3.6b**), Tbl 70% and Tbl 70% + PFC significantly increased the motional order of the membrane with respect to untreated DMEM. Measured TMA-DPH anisotropy was decreased from 0.255 to 0.248 (-2.8%, Lipo), 0.234 (-8.1%, Tbl 70%) and 0.238 (-6.5%, Tbl 70% + PFC). Overall, PPC treatments of LX-2 cells affected the motional order of the cell membrane more at the interfacial level than in the hydrophobic core.

The increase in liver tissue stiffness observed in fibrosis and caused by HSCs myofibroblastic transdifferentiation and extracellular matrix (ECM) accumulation⁴³⁰⁻⁴³² is related to a change in the cell membrane motional order. Our measurements of fluorescent anisotropy on living adherent cells provided us with a one-of-a-kind insight into the effects of treatments with PPC tablet extract on cell membrane fluidity. The SPARC mRNA transcription results (**Figure A3.5c**), though, suggest that the beneficial action of S 80 M does not interfere with the mRNA expression itself but rather with the mesoscale properties of the cell membrane – namely its stiffness at the interface (**Figure 3.6b**) – the region where SPARC docks to exert its ECM orchestrating function.

3.3.8 Modulation of cirrhotic PRHSCs phenotype indicating antifibrogenic effects: our proof of principle

The biological tests to establish the possible hepatoprotective function of PPC tablets were all conducted on LX-2 cells, a model of activated human immortalised HSCs. In an attempt to move a step toward preclinical studies, we decided to validate our findings in primary rat HSCs from cirrhotic rats.³⁸³

Although liver fibrosis does not always proceed to end-stage liver disease, we hypothesised that demonstrating that our formulations could de-activate highly fibrogenic HSCs could be a compelling first piece of data for upcoming *in vivo* studies.

We screened the treatments on cirrhotic PRHSCs adopting the same experimental design used in LX-2 cells. Briefly, S 80 M extracted from tablets was reconstituted and tested on cells over a 24 h incubation, fixing the total lipid concentration at 5 mM.

We observed in PRHSCs the same trends observed in LX-2 (**Figure 3.4**). Specifically, none of the treatments interfered with cell viability, excluding thus any possible toxicity of S 80 M (**Figure 3.7a**). In addition, S 80 M liposomes and extracts did not contribute to oxidative stress, as proven by the ROS level, which did not increase after treatment (**Figure 3.7b**).

Cirrhotic PRHSCs treated with Lipo showed a significant increase in the number of lipid droplets. Simultaneously, Tbl 70% and Tbl 70% + PFC followed the same trend and were of similar magnitude but did not reach statistical significance. Lipid treatments induced a ~14-fold FRI increase compared to IMDM (51.0 FRI, 46.3 FRI and 44.31 FRI for Lipo, Tbl 70%, and Tbl 70% + PFC treatments, respectively; **Figures 3.7ab**). S 80 M Lipo had a slightly higher impact on lipid droplet content, but the difference was insignificant compared to other S 80 M treatments.

Rat quiescent HSCs physiologically express lipid droplets in the cytoplasm as a storage for physiological retinoic esters similar to what was observed in HSCs from other sources (human, murine). Lipid droplets disrupt once HSCs transdifferentiate in case of injury to the liver, a phenomenon that ultimately may lead to a change in the cellular architecture and ECM accumulation.²⁷ Recovery of lipid droplets in cirrhotic PRHSCs is analogous with one observed in directly treated activated LX-2 cells that implicates that S 80 M had a similar effect on lipid metabolism of PRHSCs, even if general pathological cell state was more advanced since usually, rat HSCs express similar metabolic pathways as the human ones. The motional order of the membrane of primary cells was also quantified (**Figure 3.8**) to investigate whether PPC treatment would exert the same fluidifying effect observed in LX-2

cells. Tbl 70% and Tbl 70% + PFC significantly increased the motional order of the inner membrane layer compared to IMDM (**Figure 3.8a**). Lipo, Tbl 70%, and Tbl 70% + PFC caused a decrease in measured DPH anisotropy from 0.269 (untreated) to 0.211 (-21.5%), 0.166 (-38.3%) and 0.166 (-38.4%), respectively. The other S 80 M treatments were not significantly different. Lipo appears to have only a moderate effect on inner membrane motility. The reduction of stiffness of the PRHSC membrane seemed to be induced in its deep hydrophobic core, as at the interfacial region (**Figure 3.8b**), S 80 M extracts did not induce any significant variation.

PFC had the most potent effect on decreasing both DPH and TMA-DPH anisotropy, allowing a higher degree of cellular membrane motility. However, this effect was not additive to the tablet extract treatment. In this latter case, the anisotropy values remained unchanged when the extracted lipids were reconstituted in PFC emulsions (**Figure 3.8ab**).

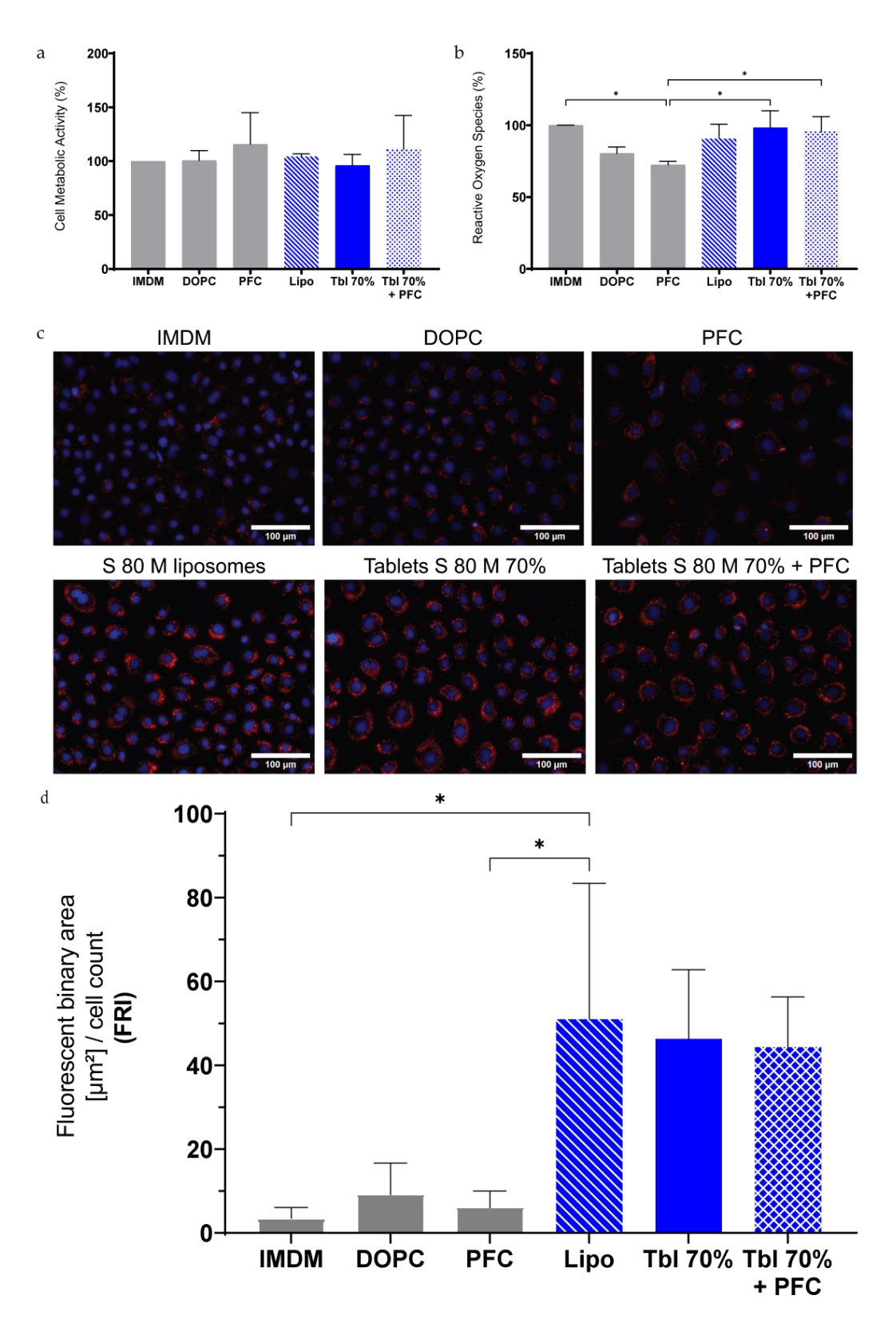


Figure 3.7. (a) PRHSCs cell viability (%) using CCK-8 assay. (b) PRHSCs ROS production. (**c-d**) ORO staining of cirrhotic PRHSCs treated with various phospholipid treatments: IMDM: experimental medium; DOPC: inactive phospholipid used as negative control; PFC: protein-free chylomicron-like emulsions without S 80 M; Lipo: S 80 M liposomes; Tbl 70%: S 80 M tablet extract in buffer; Tbl 70%

+ PFC: tablet extract reconstituted as PFC-like emulsions. (c) Representative images of PRHSCs. (d) Quantification of the ORO fluorescence normalised to the number of PRHSCs in the DAPI field (FRI). Cell number per image was in the range of \sim 5-150 cells. Mean \pm S.D. (n=3). p-values (* p < 0.05) from ordinary one-way ANOVA with post hoc Tukey's multiple comparison analysis.

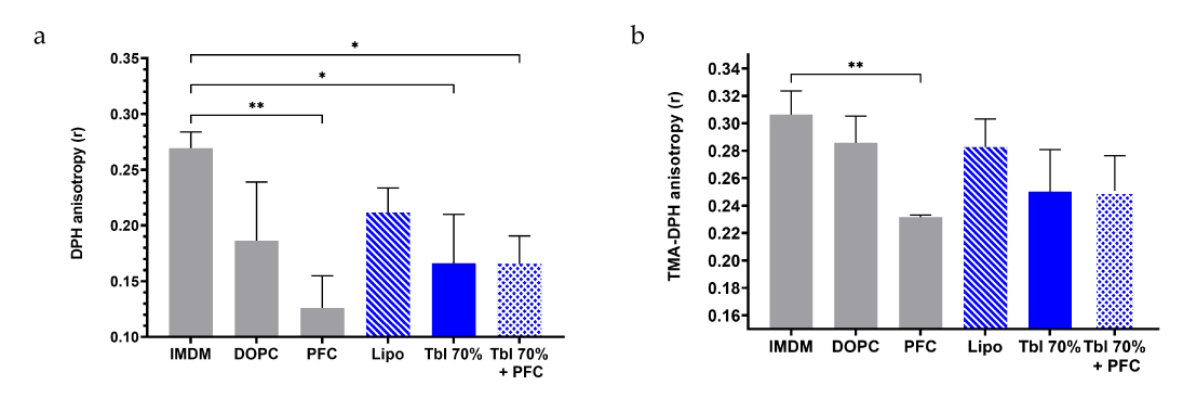


Figure 3.8. PPC treatment effect on the motional order of PRHSC cell membrane employing anisotropy of (a) DPH (inner membrane) and (b) TMA-DPH (interfacial membrane) as a function of different phospholipid treatments: IMDM experimental medium (untreated); DOPC: inactive phospholipid used as negative control; PFC: protein-free chylomicron-like emulsions without S 80 M; Lipo: S 80 M liposomes; Tbl 70%: S 80 M tablet extract in buffer; Tbl 70% + PFC: tablet extract reconstituted as PFC-like emulsions. Mean \pm S.D. (n=3). p-values (** p < 0.01, * p < 0.05) from ordinary one-way ANOVA with post hoc Tukey's multiple comparison analysis.

3.4 Conclusion

The PPC-rich soy phospholipid S 80 M has physical properties suitable to generate a lipid powder mixture via dry granulation. The good flowability of the lipid powder was also maintained with 70% of bioactive lipids, and the subsequent compression of the lipid mixture in tablets led to a dosage form complying with the major pharmacopoeial requirements. PPCs extracted from tablets were tested with a dynamic fibrogenic cell model of human immortalised HSCs and cirrhotic rat PRHSCs. In all cases, the PPC treatments reverted the fibrogenic phenotype of HSCs, resulting in increased lipid storage and increased membrane fluidity correlated with the improved fibrotic state of HSCs. mRNA transcription data showing an increase in PLIN2 and a decrease in PDGFRB levels in LX-2 cells supports our hypothesis of an antifibrotic effect of S 80 M treatments. Mimicking the uptake of PPCs in remnant chylomicrons using chylomicrons-like emulsion was comparable to pure PPCs in both LX-2 and PRHSCs in all experimental conditions.

Our findings shed new light on the understanding that sensitive, complex, technically challenging, yet bioactive phospholipids, such as the natural PPC-rich S 80 M, can be formulated in a more patient-centric, simple-to-manufacture pharmaceutical dosage form: tablets. Furthermore, PPC retained their physicochemical and bioactive properties, as demonstrated by our combination of technological characterisation and biological assays performed on two different *in vitro* models of liver fibrosis (and cirrhosis). The bioavailability and pharmacological action of these lipid-based products will be clarified by upcoming *in vivo* studies, which will provide more information on the potential of PPC tablets for the pharmacological management of chronic liver diseases.

Chapter 4.

Secretome-mediated cross-talk between steatotic hepatocytes and hepatic stellate cells as *in vitro* model to evaluate lipid-based treatments for chronic liver disease

Parts of this chapter are manuscript in preparation to be submitted for publication.

Skorup I, Widak A, Valentino G, Aleandri S, Luciani P.

Author contributions

I.S. devised and performed all *in vitro* experiments, developed methodology, analysed the data, wrote the original draft; **A.W.** prepared and characterised liposomal formulations; **G.V.** developed methodology; **S.A.** devised experiments and methodology with steatogenic stock solutions, contributed to data curation; **P.L.** conceived and supervised the original project, provided funding, administered the project, reviewed and edited the manuscript.

4.1 Introduction

4.1.1 Conditioned culture medium (CCM) as a NAFLD in vitro model – background and purpose

Authentic replication of non-alcoholic fatty liver disease (NAFLD) in an *in vitro* system represents a significant challenge. A finely tuned interplay between hepatocytes and hepatic stellate cells (HSCs) modulates pathology progression or regression, as described in **Chapters 1** and **2**. Since various cell lines require diverse culturing conditions, this poses a considerable obstacle to maintaining cells' original expression state, creating a reliable experimental setup, and establishing a robust multicellular, pathologically relevant model. For instance, using different culture media might be necessary, and longer incubation times in non-native medium might induce significant changes in cells' behaviour and expression patterns. Therefore, validating cell identity or reducing transdifferentiation possibilities under the experimental culture conditions for two or more cell lines is crucial to ensure that the cells accurately represent their intended use within the co-culture model. Another experimental challenge of simultaneous co-culture is determining the ratio between different cell types representative of the disease that might skew once the cells are culture together and the difficulty to objectively assay both cell types once mixed in the culturing vessel.

Ramos *et al.*²⁴⁶ reported in their recent review that NAFLD research is predominantly done in monocultures (59.4% of the cases) following more complex models of co-cultures (14%), spheroids (9.7%), organoids (7.3%), liver-on-a-chip (7.8%), collagen gel sandwiches (1.2%), and micropatterned cultures (0.6%). They also report that many investigations are conducted in parallel in an *in vivo* model to ensure the significance of the experimental setup.²⁴⁶ Established cell lines are pivotal in research and drug development, offering significant advantages over *in vivo* models.²⁴⁶ In comparison to animal studies, the advantages of cell experiments are that they can be conducted on a larger scale cost-efficiently and have extended longevity, surpassing the typical lifespan of current NAFLD *ex vivo* models, which usually range from approximately 5 to 15 days.^{246,433,434}

As reported in **Chapter 2**, there is sporadic use of the co-culture model, usually simultaneous co-culture of primary hepatocytes and hepatic stellate cells. In this specific case, we propose an asynchronous co-culture model mediated by the transfer of cell-conditioned medium (CCM) to investigate the cross-talk between steatotic hepatocytes and activated hepatic stellate cells (HSCs) in liver fibrosis. The treatment of HSCs was performed with a conditioned medium from hepatocytes, treated with steatosis-inducing free fatty acids (FFAs) and/or

antisteatotic/antifibrotic treatment. Standard culture medium (DMEM) represents an internal control on the treatment effect of cells incubated only with an experimental medium.

CCM, also known as cell secretome, is a biological fluid enriched with a group of proteins comprising signal peptides secreted through classical pathways originating from the Golgi apparatus and endoplasmic reticulum. In addition, CCM includes proteins shed from the cell membrane and surface together with non-classical-secretion intracellular proteins or exosomes. A wide array of cytokines, growth factors, hormones, enzymes, and other soluble factors can be found within this secreted protein pool. These proteins play a central role in diverse intra- and intercellular processes, including cell proliferation, invasion, differentiation, angiogenesis, extracellular matrix (ECM) modulation, and cell-to-cell interactions. In our study, CCM is a vehicle for the hepatocytes' cell secretome, representative of the steatotic cell expression profile, and responsible for hepatocytes-HSCs intercellular cross-talk. By employing CCM, we reduce intra-system variability factors of different mediums, foetal bovine serum amount, and various supplement concentrations when keeping incubation times relatively short.

4.1.2 Reported CCM models in various liver diseases – state-of-the-art

Reported uses of CCM in various, not only NAFLD, liver diseases are only sporadic, but some are listed here to demonstrate the strength of this experimental approach. Wobser *et al.* reported one of the rare specific steatosis/NAFLD CCMs on the human model from the literature. Here, immortalised human activated HSC cell line generated by ectopic (out-of-the-place) human telomerase reverse transcriptase (hTERT) expression. These cells were treated for 2 or 72 h with a CCM from naïve or palmitic acid (PA)-treated PHH, HepG2, and Huh-7 cells. Consequently, due to this incubation, an increase in mRNA of pro-fibrotic markers specific to activated HSCs, collagen type I (COL1A1), α -smooth muscle actin (α -SMA), transforming growth factor β (TGF- β), matrix metalloprotease 2 (MMP-2), metallopeptidase inhibitor 1 and 2 (and -2) was reported. Decreased HSC doubling time and NF-kB and MCP-1 pathways activation, involved in the inflammatory response and macrophage recruitment, were also described among the outcomes.

CCM from human hepatocyte organoids treated with PA and oleic acid (OA) stimulated LX-2 cells activation through vascular endothelial growth factor A (VEGFA) signalling, a compelling pathway regarding the potential development of hepatocarcinoma (HCC) starting

from NAFLD. In CCM-treated LX-2, an increase in α -SMA and TIMP-1 mRNA transcription levels is reported, consistent with the activated HSCs' fibrotic state. 436

CCM from hydrogen peroxide-induced senescent HepG2 cells was used on PHHSCs that were activated. An increase in inflammatory (tumour necrosis factor- α [TNF- α] and IL-1 β) and fibrotic (TIMP-1, α -SMA, and procollagen) markers was reported. A higher concentration of platelet-derived growth factor (PDGF) has been observed in senescent-HepG2 CCM.⁴³⁷

HepG2 cells were treated with a high concentration of glucose, and CCM-derived from these cells was used to treat primary mice HSCs, that, after 12 and 24 h of CCM incubation, have shown an increase in pro-fibrotic markers (COL1A1, COL1A2, ACTA2). CTGF in CCM is a hepatocyte-derived pro-fibrogenic enhancer, once inhibited or silenced in HSCs, resulting in diminished HSCs activation and alleviating fibrotic response.⁴³⁸

Hepatotoxic substances (tetrachloromethane, thioacetamide, ethanol, paracetamol) were used to treat HepG2 to induce an apoptotic but not necroptotic cell state. PHHSC treated with this apoptotic-HepG2 CCM decreased HSCs proliferation, increased activation of platelet-derived growth factor receptor- β (PDGFR- β) and TGF- β II receptor, increased mRNA transcription of desmin and α -SMA, all hallmarks of activated pro-fibrotic HSCs, meaning that seriously damaged or dying hepatocytes' secretome strongly sustains HSCs' pro-fibrotic activation.

There have been several reports of using CCM in other liver conditions. Conditioned medium originating from hepatitis C virus (HCV)-infected Huh-7 cells able to replicate the virus, was able to induce a fibrotic response in PHHSC by modulating mRNA expression of fibrotic markers, increasing CTGF, procollagen α1(I), TIMP-1, and MMP-1, and by reducing MMP-2 mRNA. MMP-1 collagenase activity also was significantly decreased in treated cells. 440 Marti-Rodrigo *et al.* transferred the secretome from HSCs to hepatocyte-like cells using treated PHH and Hep3B cells with CCM originating from LX-2 cells treated with rilpivirine (RPV). RPV is a common antiretroviral HIV drug possessing good tolerability and efficacy, with a pronounced safety profile related to liver toxicity, more favourable than the rest of antiretroviral agents, as several are reported as steatosis-inducing drugs in **Chapter 2**. 441 RPV-treated LX-2 cells exhibited increased apoptosis and its CCM managed to activate Janus kinase – signal transducer and activator of transcription 3 (JAK-STAT3) pathway as a response to IL-6 in hepatocytes. 441 JAK-STAT3 pathway activation is involved with enhanced liver reparation and regeneration by promoting hepatocyte survival and anti-steatogenic activity. 442

4.1.3 Final remarks on CCM – the rationale behind our setup

All the previously reported CCM models provided insight into an interconnected NAFLD/steatosis/fibrosis pathology spectrum, shedding light on complex pathophysiological interactions. By simplifying the multifactorial NAFLD, these models may reveal essential discoveries and confirm hypotheses on pathway regulations.

For these reasons and considering the results obtained from various reported CCM studies, we chose to establish a new setup based on the transfer of secretome from a human hepatocarcinoma Huh-7 cell line to an immortalised human HSCs LX-2 cells to obtain a simplified yet representative *in vitro* model of NAFLD. Steatosis was induced by incubating Huh-7 cells with oleic and palmitic acid, and the resulting CCM was collected and transferred to LX-2 cells. To investigate the bidirectional cross-talk between hepatocytes HSC, also activated LX-2, either naïve or treated with control conditions or with our proposed bioactive antifibrotic soybean essential phospholipid (EPL) treatment combined with silymarin extract, 137,371 were incubated with Huh-7-derived CCM. We tested different incubation sequences and treatments with control and experimental conditions (*vide infra*, **Models A-E**, **Figures 4.2-4.6**). Cells were assayed using cell metabolic activity, lipid droplet staining, and transcriptomics.

In the most therapeutically relevant experimental design (Model E), steatotic Huh-7 cells were treated consecutively with PPC-based liposomal formulation containing Ela and Oca, experimental antisteatotic APIs, to investigate if CCM obtained from these cells had a beneficial effect on activated LX-2.

4.2 Materials and methods

4.2.1 Materials

Soybean phospholipid with 75% phosphatidylcholine (S 80), Soluthin[®] S 80 M (S 80 M, soybean phospholipid 80% complexed with MgCl₂), and 1,2-dioleoyl-*sn*-glycero-3-phosphocholine (DOPC) were a kind gift from Lipoid GmbH (Ludwigshafen, Germany). Elafibranor (Ela) and obeticholic acid (Oca; 6-ethylchenodeoxycholic acid) were purchased from MedChemExpress (Sollentuna, Sweden).

The LIPEX® extruder used to manufacture liposomes was from Transferra Nanosciences Inc. (Burnaby, B.C., Canada). Polycarbonate membranes were from Sterlitech (Auburn, WA, USA), and drain discs were from Whatman (Maidstone, UK). The LX-2 cells immortalised human hepatic stellate cell line (RRID: CVCL_5792) were purchased from Merck Millipore

(Darmstadt, Germany) and the Huh-7 cells human hepatocellular carcinoma cell line (RRID: CVCL_0336) were purchased from Sekisui Xenotech (Hamburg, Germany). Dulbecco's Modified Eagle Medium (DMEM-HG, 4.5 g/L glucose, with phenol red and pyruvate, no glutamine), Dulbecco's Modified Eagle Medium (DMEM-LG, 1.0 g/L glucose, with phenol red and pyruvate, no glutamine), phosphate buffer saline (PBS) (pH 7.4, without Ca/Mg), 4',6-diamidino-2-phenylindole (DAPI), Roti®-Histofix 4% (acid-free, pH 7.4 % w/v phosphate-buffered formaldehyde solution), 4-(2-hydroxyethyl)piperazine-1-ethane sulfonic acid sodium (HEPES) solution, dimethylsulphoxide (DMSO) and trifluoroacetic acid (TFA) were purchased from Carl Roth (Arlesheim, Switzerland). Penicillin/streptomycin mixture (PenStrep; penicillin: 10'000 U/mL, streptomycin: 10'000 μg/mL), L-glutamine (L-Glu; 200 mM), Trypsin-EDTA (0.25%), chloroform (CHCl₃), ethanol (EtOH), methanol (MeOH), acetonitrile (ACN), TRIzol™ reagent, and RNAse-free water were from Fisher Scientific (Reinach, Switzerland).

Foetal bovine serum (FBS), bovine serum albumin (>98% lyophilised powder, essentially fatty acid-free [BSA]), Accutase®, Oil Red O (ORO; 0.5% (w/v) in propylene glycol), transforming growth factor-beta 1 (TGF- β_1), oleic acid (OA), palmitic acid (PA), silymarin extract (Sily), retinol (Rol), and Cell Counting Kit-8 (CCK-8) were bought from Sigma Aldrich (Buchs, Switzerland). Random hexamers and qPCR primers were synthesised by Microsynth (Balgach, Switzerland). qRT-PCR Brilliant III SYBR Master Mix was from Agilent (Santa Clara, CA, USA). Cell culture plates and flasks were from Sarstedt (Nümbrecht, Germany) and TPP (Trasadingen, Switzerland).

4.2.2 Cell culture and general information about cell experiments

4.2.2.1 LX-2 cell culture

LX-2 cells were grown at 37 °C in a 5% CO₂ humidified atmosphere in an LX-2 complete medium (LX-2-CM): DMEM-HG (4.5 g/L glucose, phenol red, no L-glutamine, pyruvate) supplemented with 1% (v/v) penicillin/streptomycin mixture (penicillin: 10'000 U/mL, streptomycin: 10'000 μg/mL), 1% (v/v) of L-glutamine (2 mM), and 2% (v/v) FBS. According to the manufacturer's instructions, subcultivation was performed with Accutase[®] at a cell confluency of about 80-90%. Cells at passage number 8 to 16 were used for cell experiments. LX-2 cell experiment medium (LX-2-EM) was serum-free, prepared with DMEM-HG and supplemented with 1% (v/v) penicillin/streptomycin and 1% (v/v) L-glutamine.

For experiments, LX-2 cells were seeded either in a 12-well plate with 1.0 mL LX-CM/well with a density of 100'000 cells/well, 24-well plates with 0.5 mL LX-2-CM/well at a density of 50'000 cells/well, or in transparent 96-well plates with 100 μL LX-2-CM/well at a density of 12'500 cells/well, and cultured 18 h at 37 °C, 5% CO₂ to 70–90% confluency. Treatments were always performed with 1.0 mL/well for 12-well plate, 0.5 mL/well for 24-well plates or 100 μL/well for 96-well plates at 37 °C, 5% CO₂.

4.2.2.2 Huh-7 cell culture

Huh-7 cells were grown at 37 °C in a humidified atmosphere containing 5% CO₂ in a Huh-7 complete medium (Huh-7-CM): DMEM-LG (1.0 g/L glucose, phenol red, no L-glutamine, pyruvate) supplemented with 1% (v/v) penicillin/streptomycin mixture (penicillin: 10.000 U/mL, streptomycin: 10.000 μg/mL), 2% (v/v) of L-glutamine (4 mM), and 10% (v/v) FBS. According to the manufacturer's instructions, subcultivation was performed with Trypsin-EDTA 0.25% at a cell confluency of about 80-90%. Cells at passage number 6 to 20 were used for cell experiments. Huh-7 cell experiment medium (Huh-7-EM) was serum-free, prepared with DMEM-LG and supplemented with 1% (v/v) penicillin/streptomycin and 2% (v/v) L-glutamine.

For experiments, Huh-7 cells were seeded either in a 12-well plate with 1.0 mL LX-CM/well with a density of 75'000 cells/well, 24-well plates with 0.5 mL LX-2-CM/well at a density of 50'000 cells/well, or in transparent 96-well plates with 100 μ L LX-2-CM/well at a density of 12'500 cells/well, and cultured 18 h at 37 °C, 5% CO₂ to 70–90% confluency. Treatments were always performed with 1.0 mL/well for 12-well plate, 0.5 mL/well for 24-well plates or 100 μ L/well for 96-well plates at 37 °C, 5% CO₂.

4.2.3 Preparation of stock solutions

Stock solutions of DOPC, S 80, and S 80 M were prepared at a concentration of 100 mM in MeOH. Sily, Ela, and Oca stock solutions were prepared in MeOH at 50 mM, 0.5 mM, and 0.5 mM, respectively. Rol, PA and OA stock solutions were prepared in DMSO at 10 mM, 75 mM, and 500 mM, respectively. The TGF- β_1 stock solution was prepared in BSA 0.1% (w/V) at 10 μ g/mL concentration. BSA stock solution was prepared fresh in Huh-7-EM at 30 mg/mL (corresponding to ~454 μ M) by adding BSA in Huh-7-EM, vortexing for 10 min at RT, and kept at 37°C until use.

4.2.4 Steatosis induction in Huh-7 cells

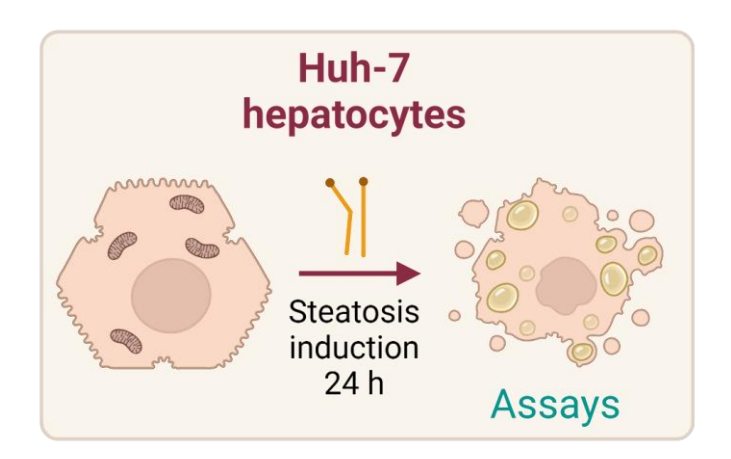


Figure 4.1. Steatosis induction in Huh-7 cells. Cultured hepatocytes are treated with OA and PA, changing their phenotype and genotype to the steatotic one and expressing pathologic secretome in a conditioned medium. The figure was created using Biorender.com.

4.2.4.1 Stock solutions of OA and PA supplemented to Huh-7-EM (Model 1)

Huh-7-EM experimental serum-free medium was supplemented directly with FFA DMSO stock solution of OA, PA, and a combination of OA and PA in a 2:1 ratio. Concentrations tested were 75 and 150 μ M (PA), 150 and 300 μ M (OA), and 150+75 and 300+100 μ M (OA+PA). The steatogenic treatment medium was successively vortexed for 10 min at room temperature (RT), kept at 37°C until use and shortly vortexed directly before use.

4.2.4.2 Stock solutions of OA and PA sonicated with Huh-7-EM – micelles-like vesicles (Model 2)

The steatogenic medium was prepared as described above with the addition of the sonication step in the water bath for 30 min at 40 °C to enhance FFAs solubility and homogenisation in an aqueous cell culture medium. This process should produce FFA-derived micelles-like vesicles in the solution. The prepared medium was kept at 37°C until use and shortly vortexed directly before use. Concentrations tested were, as mentioned above, with additional being 300 μ M (PA), 600 μ M (OA), and 600+300 μ M (OA+PA). These micelles-like vesicles were not characterised.

4.2.4.3 Stock solutions of OA and PA supplemented with BSA in Huh-7-EM (Model 3)

To further enhance the solubility and homogeneity of the steatogenic medium, a non-specific serum transport protein, fatty acid-free bovine serum albumin (BSA), was used. Huh-7 serum-

free experimental medium was first supplemented with BSA stock solution to reach the final 30 μ M BSA concentration, the approximate concentration in regularly used FBS to culture cells as per manufacturers specification. This dispersion was consecutively vortexed for 10 min at RT, kept at 37 °C for 10 min before adding the appropriate amount of FFA in DMSO stock solution, vortexed again for 10 min at RT, kept at 37 °C until use and shortly vortexed directly before use. The concentrations tested were the same as in **Section 4.2.4.2**. Steatogenic Huh-7 medium in CCM experiments containing OA+PA 300+150 μ M was produced with this method.

4.2.4.4 Steatogenic treatment with test solutions

The medium from seeded Huh-7 cells was discarded the day after cell seeding, the cells were washed once with PBS, and the steatogenic medium, prepared as described above, was added. Cells were incubated at 37 °C in a 5% CO₂ humidified atmosphere for 24 h. Control wells received equal volumes of naïve control Huh-7-EM. Cells were assayed for viability and lipid droplets. Huh-7 cells were seeded in 24- and 96-well plates for these experiments.

4.2.4.5 Huh-7 steatotogenesis for CCM harvesting

To obtain steatotic Huh-7 cell-conditioned medium (CCM) containing naïve and steatotic secretome used to treat LX-2, the medium from seeded cells was discarded the day after cell seeding, the cells were washed once with PBS, and the steatogenic medium, prepared as described in **Section 4.2.4.3**, was added. Cells were incubated at 37 °C in a 5% CO₂ humidified atmosphere for 24 h. Control wells received equal volumes of naïve control Huh-7-EM.

Huh-7 steatogenic medium was discarded, cells were washed three times with PBS, and fresh naïve Huh-7-EM was resupplied to all the cells, which were left for the following 24 h. After these 24 h, control naïve and steatotic Huh-7 CCM was collected and used to directly incubate LX-2, sequence-depending on the specific model (*vide infra*).

4.2.4.6 Huh-7 steatogenesis and successive antisteatotic liposomal treatment for CCM harvesting

In the case of Huh-7 CCM prepared to treat LX-2 in **Model D** (**Section 4.2.6.4**), as described above, after 24 h steatogenesis, the medium was discarded, and cells were washed three times with PBS. Liposomal formulations containing non-bioactive control, PPC, Ela, and Oca,

listed in **Table 4.2**, were diluted in Huh-7-EM and successively transferred to cells for a 24 h incubation. The treatment medium was discarded, cells were washed three times with PBS, and fresh naïve Huh-7-EM was resupplied to all the cells, which were left for the following 24 h. After this 24 h, treated control naïve and steatotic Huh-7-CCM was harvested and used to incubate LX-2 directly.

4.2.5 Preparation and characterisation of liposomes

4.2.5.1 S 80, S 80 M, and DOPC liposomes preparation

Liposomes containing S 80 and S 80 M soybean-derived phospholipid and DOPC were prepared using the film hydration extrusion method (**Table 4.1**). ^{137,408} Briefly, an appropriate aliquot of lipid stock solution in MeOH was evaporated under a nitrogen stream until dry. The resulting thin lipid films were kept under a vacuum overnight to remove further traces of solvent. After hydration with HEPES buffer (10 mM, pH 7.4), the large multilamellar vesicles with a final lipid concentration of 50 mM were extruded through a 200 nm polycarbonate membrane 10 times at RT using a LIPEX® extruder.

4.2.5.2 S 80 + Sily liposomes preparation

Liposomes containing S 80 and Sily were produced starting from the dry lipid film, as described above, with the only difference being that the final S 80 concentration was 25 mM. A corresponding aliquot of Sily stock solution was added to the dried lipid film to acquire a final theoretical S 80-to-Sily molar ratio of 11:1 to silybin B. MeOH was evaporated under nitrogen stream until dry, and the resulting silymarin-lipid film was hydrated with HEPES buffer (10 mM, pH 7.4). The resulting lipid films with Sily were hydrated, and liposomes were extruded, as described above.

Table 4.1. Liposomal formulations prepared for the treatment of CCM Model C

Formulation	Liposomal concentration	Concentration "on-cells"
DOPC (non-bioactive control)	50 mM	5 mM
S 80	50 mM	5 mM
S 80 M	50 mM	5 mM
S 80 + Sily (lipid-to-Sily molar ratio 11:1)	25 mM	2.5 mM

4.2.5.3 DOPC, S 80 M, Ela, Oca liposomes preparation

Liposomes containing DOPC or S 80 M with drugs Ela, Oca or Ela and Oca together (**Table 4.2**) were produced by adding a necessary amount of the lipid to reach 50 mM. At this stage, the necessary amount of hydrophobic drug stock solution (Ela and/or Oca) was mixed with a lipid stock so that the final drug concentration in the formulation would be 1.5 μ M. Films were dried and hydrated, and liposomes were extruded, as described above.

Table 4.2. Liposomal formulations prepared for the treatment of CCM Model D

Formulation	Liposomal concentration	Concentration "on-cells"
DOPC (non-bioactive control)	50 mM	5 mM
DOPC + Ela	50 mM + 1.5 μM	5 mM + 150 nM
DOPC + Oca	50 mM + 1.5 μM	5 mM + 150 nM
DOPC + Ela + Oca	50 mM + 1.5 μM + 1.5 μM	5 mM + 150 nM + 150 nM
S 80 M	50 mM	5 mM
S 80 M + Ela	50 mM + 1.5 μM	5 mM + 150 nM
S 80 M + Oca	50 mM + 1.5 μM	5 mM + 150 nM
S 80 M + Ela + Oca	50 mM + 1.5 μM + 1.5 μM	5 mM + 150 nM + 150 nM

The effect of direct treatment with these formulations for 24 h has been tested in naïve Huh-7 cells, and cell viability and lipid droplet content has been assayed, as reported in **Appendix Section A4.1**.

4.2.5.4 Liposomal characterisation (hydrodynamic diameter and zeta potential)

Liposomes were analysed for the hydrodynamic diameter and the polydispersity index (PDI) with the LitesizerTM 500 (Anton Paar, Austria). A volume of 10 μL of liposomes was diluted in 2 mL of HEPES buffer (10 mM, pH 7.4). Intensity size distribution was typically uni-modal; therefore, the autocorrelation function was analysed using the cumulant method. For zeta potential (ZP) measurements, 200 μL of the sample was used in Omega cuvettes for 100 runs.

Table 4.3. Schematical overview of investigated cell-conditioned medium (CCM) models reported in Sections 4.2.6 and 4.2.7

	<u>Huh-7 → LX-2</u>						
	Cell line	Day 1	Day 2	Day 3	Day 4	Day 5	Day 6
Model A	Huh-7	Seeding	Steatosis induction with FFAs	CCM formation	CCM harvest ↓		
	LX-2			Seeding	Treatment with Huh-7 CCM	Treatment with LX-2 controls	Assays
Model B	Cell line	Day 1	Day 2	Day 3	Day 4	Day 5	
	Huh-7	Seeding	Steatosis induction with FFAs	CCM formation	CCM harvest ↓		
	LX-2			Seeding	Simultaneous treatment Huh-7 CCM + LX-2 controls	Assays	
Model C	Cell line	Day 1	Day 2	Day 3	Day 4	Day 5	
	Huh-7	Seeding	Steatosis induction with FFAs	CCM formation	CCM harvest ↓		
	LX-2		Seeding	Pre-treatment with LX-2 controls and PPC-based liposomes	Treatment with Huh-7 CCM	Assays	
	•					•	
Model D	Cell line	Day 1	Day 2	Day 3	Day 4	Day 5	Day 6
	Huh-7	Seeding	Steatosis induction with FFAs	Treatment with DOPC/S 80 M + Ela/Oca	CCM formation from treated steatotic cells	CCM harvest ↓	
	LX-2			Seeding	"Preconditioning" LX-2-EM (activated, naïve LX-2), Rol+PA (quiescent-like LX-2)	Treatment with Huh-7 CCM	Assays
	<u>LX-2</u> → Huh-7						
Model E	Cell line	Day 1	Day 2	Day 3	Day 4	Day 5	
	LX-2	Seeding	Treatment with LX-2 controls	CCM formation	CCM harvest ↓		
	Huh-7		Seeding	Steatosis induction with FFAs	Treatment with LX-2 CCM	Assays	

4.2.6 Dual cell culture model Huh-7 to LX-2

Huh-7 cells were seeded in 12-well plates and LX-2 cells in 24- and 96-well plates in the following experiments.

4.2.6.1 LX-2 cells treated with Huh-7 CCM and successively with control treatments (Model A)

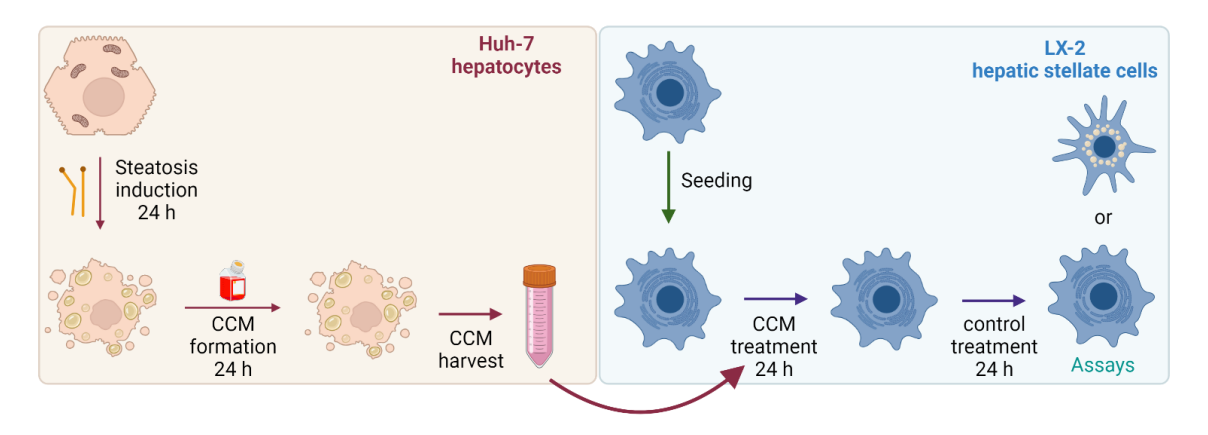


Figure 4.2. Model A schematics – First treatment with Huh-7 CCM 24 h and then control LX-2 treatments 24 h. The figure was created using Biorender.com.

The day after the LX-2 cells were seeded, the medium was discarded, and the cells were washed once with PBS. LX-2 were treated with CCM harvested from naïve control and steatotic Huh-7 for 24 h. Afterwards, cells were washed three times with PBS and incubated for 24 h with Rol + PA treatment to revert LX-2 cell activation and fibrogenesis and to induce a quiescent-like phenotype, following the previous reports. ^{137,211} Rol + PA stock solutions were vortexed vigorously for 10 min at RT with LX-2-EM to reach final concentrations of 10 μM Rol and 300 μM PA. LX-2 also were treated with TGF-β₁ to simulate a perpetuation of the fibrotic state of LX-2, transdifferentiating them to myofibroblasts. ^{66,137,443-445} TGF-β₁ treatment was prepared by mixing the stock solution with LX-2-EM to obtain a final 10 ng/mL concentration, shortly vortexed and kept at 37 °C until use. Control wells received equal volumes of naïve LX-2-EM. Before use, treatments were kept at 37 °C until use and cells were incubated for 24 h and were assayed afterwards.

4.2.6.2 LX-2 cells treated contemporary with Huh-7 CCM and control treatments (Model B)

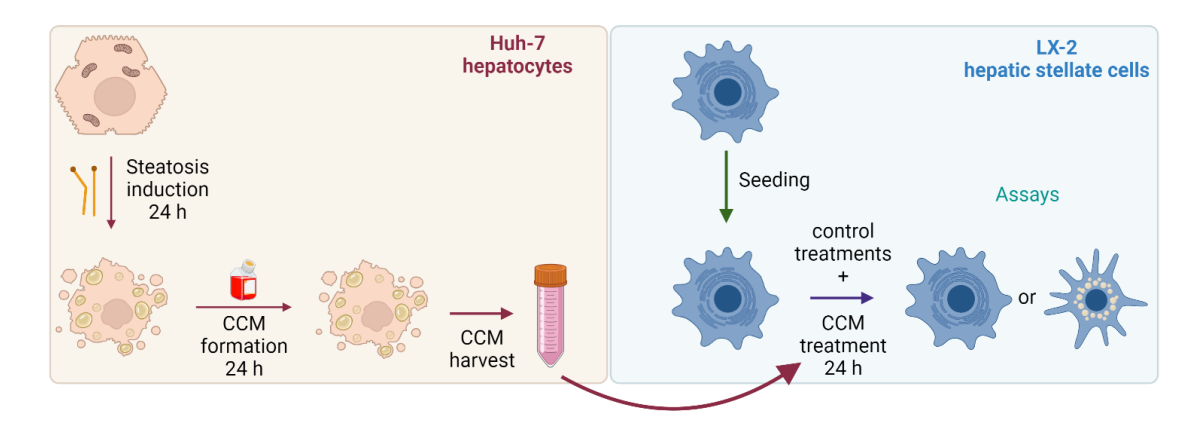


Figure 4.3. Model B schematics – Treatment of LX-2 cells with Huh-7 CCM mixed with LX-2 control treatments for 24 h. The figure was created using Biorender.com.

The day after LX-2 cells were seeded, the medium was discarded, and the cells were washed once with PBS. Differently from **Model A**, cells were treated with Rol+PA and TGF- β_1 controls mixed directly with harvested naïve control and steatotic Huh-7 CCM for 24 h. In Model B, Huh-7 control and steatotic CCMs were split in different tubes, mixed with control stock solutions, employing the same concentrations as in Model A, and shortly vortexed. Control wells received equal volumes of naïve LX-2-EM and naïve non-steatotic Huh-7 CCM. Before use, treatments were kept at 37 °C. After 24 h incubation time, cells were assayed.

4.2.6.3 Pre-treating LX-2 cells with PPC-based formulations and subsequently with Huh-7 CCM (Model C)

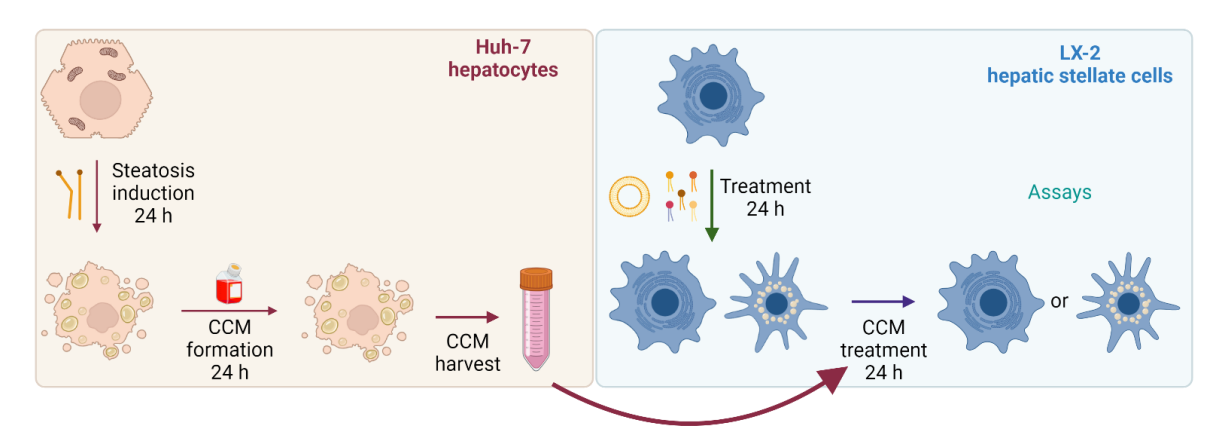


Figure 4.4. Model C schematics – 24 h PPC pre-treated LX-2 cells were incubated with Huh-7 CCM for 24 h. The figure was created using Biorender.com.

Each liposomal formulation (**Table 4.1**) was mixed with LX-2-EM to obtain a treatment medium with 5 mM lipid concentration or 2.5 mM in the case of S 80 + Sily (LX-2-TM). The

medium was discarded a day after seeding, and LX-2 were washed three times with PBS and incubated with LX-2-TM for 24 h. Control wells received equal volumes of naïve LX-2-EM. Before use, treatments were prepared fresh and maintained for 5-10 min at 37°C until the cell incubation occurred. After 24 h, cells were washed three times with PBS, incubated with CCM from naïve control and steatotic Huh-7 for 24 h, and then were assayed.

4.2.6.4 Activated and quiescent-like LX-2 cells treated with Huh-7 CCM originating from PPC, Ela, and Oca-treated steatotic cells (Model D)

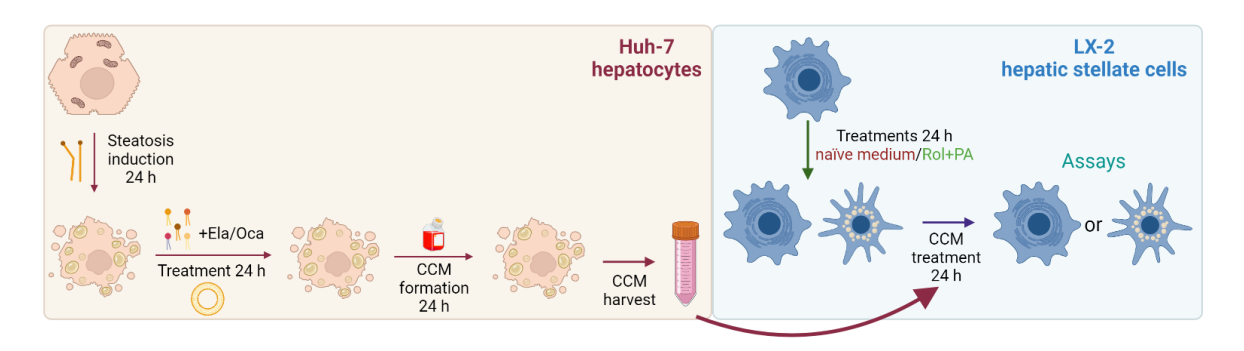


Figure 4.5. Model D schematics – LX-2 cells (naïve and quiescent-like) pre-treated for 24 h were then treated with Huh-7 CCM originating from steatotic cells treated with liposomal formulations containing PPC, Ela, and Oca. The figure was created using Biorender.com.

The day after the LX-2 cells were seeded, the medium was discarded and washed once with PBS and treated for 24 h with LX-2-EM and Rol+PA to keep them activated or revert them to a quiescent-like state. On the following day, the treatment-containing medium was discarded, and cells were washed three times with PBS, incubated with CCM from treated naïve control and steatotic Huh-7 for 24 h and assayed. Control wells received equal volumes of naïve LX-2-EM and naïve non-steatotic Huh-7 CCM. Before use, treatments were kept at 37 °C.

4.2.7 Dual cell culture model LX-2 to Huh-7 (Model E) – LX-2 cells treated with controls and LX-2-CM on Huh-7 cells

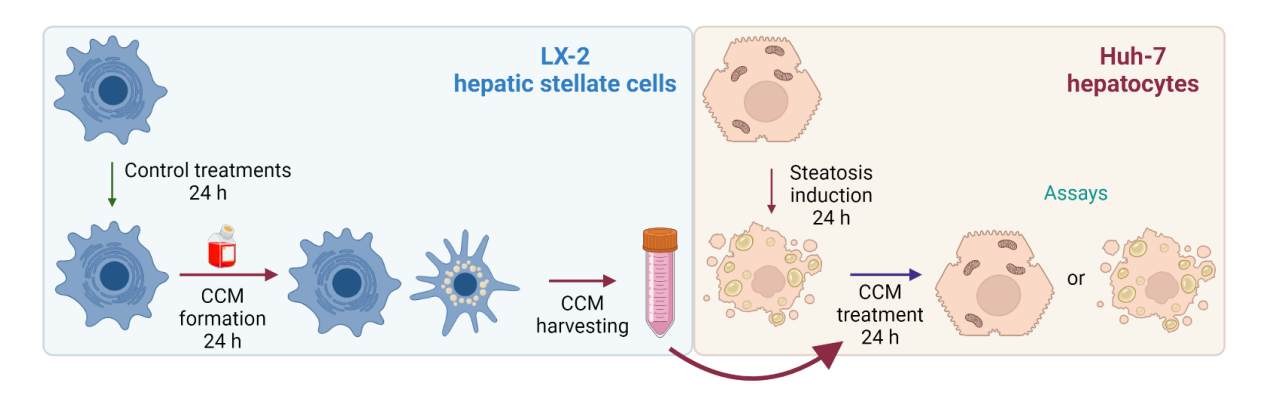


Figure 4.6. Model E schematics – Huh-7 steatotic cells were treated with LX-2 CCM from cells incubated with controls. The figure was created using Biorender.com.

In this experiment, LX-2 cells were seeded in 12-well plates and Huh-7 in 24- and 96-well plates.

The day after the LX-2 were seeded, the medium was discarded, and the cells were washed once with PBS and treated for 24 h with LX-2-EM, Rol+PA, and TGF- β_1 to keep them activated, revert them to a quiescent-like state or to perpetuate them. On the following day, the treatment-containing medium was discarded, cells were washed three times with PBS, and fresh naïve LX-2-EM was resupplied to all the cells, which was left for the following 24 h. After this 24 h, LX-2 CCMs were harvested to incubate Huh-7 cells directly.

Medium from seeded Huh-7 cells was discarded the day after cell seeding, the cells were washed once with PBS, and the cells were incubated for 24 h with steatogenic medium, prepared as described in **Section 4.2.4.3**. Control wells received equal volumes of naïve control Huh-7-EM. Huh-7 steatogenic medium was discarded, cells were washed three times with PBS and incubated with LX-2 CCMs for 24 h and assayed.

4.2.8 Analysis of lipid droplet content (ORO)

After cell treatment, both LX-2 and Huh-7 cells in 24-well plates were rinsed with PBS three times, fixed for 10 min at RT with 500 μ L/well Roti®-Histofix 4%, and rinsed once with PBS. Cells were stained with ORO solution for 15 min at RT. Carefully removed using a pipette and rinsed with PBS. Nuclei were then counterstained with a DAPI solution (3.6 μ M) in PBS for 5 min at RT. Afterwards, cells were rinsed with PBS. Fluorescence images were acquired using a Nikon Ti2-E (Nikon Instruments, Melville, NY, USA) inverted microscope with 20x magnification. DAPI filter (λ ex 360 nm, λ em 460 nm) and TxRed filter (λ ex 560 nm, λ em 645 nm)

were used. The fluorescent binary area in the TxRed field was examined using FIJI/ImageJ software. Shortly, for each image, the qualitative interpretation of images was supplemented by quantification of fluorescence to have a transparent comparative purpose and confirm observed results. A fluorescent ORO relative intensity (FRI) was obtained by normalising the fluorescent binary area (μ m²) in the fluorescent field to the number of objects (cell nuclei number) in the DAPI field.

4.2.9 Cell proliferation assay (CCK-8)

The CCK-8 assay was used following the manufacturer's instructions. Briefly, after treatments (100 μ L/well; 96-well plate), LX-2 and Huh-7 cells were washed once with PBS. A volume of 90 μ L of serum-free experimental medium and 10 μ L of CCK-8 was added to each well. Next, cells were incubated for 2 h at 37 °C, 5% CO₂. Afterwards, the absorbance was measured at 450 nm with an Infinite® 200 Pro M-Nano plate reader.

To calculate the cell metabolic activity in per cent, the following equation was used (Equation (1)):

Cell metabolic activity (%) = (OD sample/OD control) \times 100 (1)

"OD sample" refers to the optical density of the cells treated with different treatments, and "OD control" always refers to cells exposed to a naïve serum-free experimental medium.

4.2.10 qPCR gene expression analysis in LX-2 cells

From LX-2 cells treated with CCM for 24 h according to **Model D**, a total RNA was isolated using TRIzol™ reagent following the manufacturer's protocol. Briefly, cells were lysed with TRIzol™ directly on the 24-well plate and transferred to 1.5 mL reaction tubes. Chloroform volume equivalent to one-fifth of the total TRIzol™ volume was added to the samples. The tube was vigorously vortexed for 10 sec and was incubated at RT for 10 min before being centrifuged for 20 min at 4°C and 16'000 *g*. The upper phase was transferred to a new reaction tube, and 1 µL glycogen and one volume of isopropanol were added and mixed well before the RNA precipitation on ice for 10 min. Next, the RNA was pelleted by centrifugation for 10 min at 4 °C and 24'000 *g*. The supernatant was discarded, and the pellet was washed with 1 mL of 70% EtOH in RNAse-free water. The centrifugation was repeated twice, and the

final pellet was resuspended in RNAse-free water after air drying for a few minutes. The RNA concentration was measured with a NanoDrop (ThermoFisher, USA).

The isolated RNA was reverse-transcribed into cDNA. Briefly, 1000 ng of RNA were diluted in RNAse-free water and incubated for 5 min at 65 °C after adding 3 μ L of 150 ng/ μ L random hexamers. After 10 min incubation at RT, 13.5 μ L of pre-mixed reverse transcription master mix was added (**Table A3.3**), and the samples were incubated for another 10 min at RT, followed by a 1 h incubation at 50 °C and 20 min incubation at 75 °C. RNAse-free water was added to reach a theoretical concentration of 8 ng/ μ L cDNA.

The primers (**Table A3.4**) were diluted in RNAse-free water to a primer pair solution of 2.5 μ M of forward and reverse primer each. The remaining reagents (polymerase, nucleotides, buffer, fluorophore) for qPCR were in the qRT-PCR Brilliant III SYBR Master Mix (MM). The cDNA samples were measured in duplicate for each gene and cDNA dilution. A pipetting robot (Corbett Robotics, USA) was used for pipetting the samples (3 μ L cDNA, 7.5 μ L 2x MM, 3 μ L primer mix, 1.5 μ L water). The samples were then transferred to the qPCR analyser centrifuge (Rotor-Gene Q 2Plex System, Qiagen, Germany), which performed 40 amplification cycles at 95 °C and 60 °C. The fluorescence was always measured at 60 °C (λ ex 470 nm, λ em 510 nm). After the 40 cycles, the melting curve of each sample was measured. The data were analysed using the RotorGene Q version 2.3.5 software and Microsoft Excel 365. The qPCR data were analysed using the delta-delta CT method. GAPDH was used as a reference gene.

4.2.11 Lipid and drug quantification – HPLC-CAD method

Liposomal formulations of S 80 M and DOPC, including their combination with Ela and Oca, as Ela and Oca stock solutions, were diluted in MeOH, and analysis was performed as follows. An Ultimate 3000 HPLC system (Fisher Scientific, Reinach, Switzerland) equipped with a quaternary pump (LPG-3400SD), an autosampler (WPS-3000), a thermostatted column compartment (TCC-3000), a DAD (DAD-3000) and a CAD (Corona Veo RS) was used for lipid quantification. The following method has been adapted from the method developed in our lab: 446 Reprospher 200 C18-DE 150 x 2mm with a particle size of 2 μ m and a pore size of 200 Å (Dr. Maisch, Ammerbuch, Germany) was used at 50 °C as the stationary phase. During the analysis, samples were refrigerated at 6 °C in the autosampler. The injection volume was 5 μ L, and the flow rate was constant at 0.5 mL/min. Three different eluents, eluent A: acetonitrile + 0.2 v/v% trifluoroacetic acid (TFA), eluent B: methanol + 0.2

v/v% TFA and eluent C: ultrapure water + 0.2 v/v% was used to create a linear gradient as described in **Table 4.4**. For the Corona Veo RS, the gas evaporation temperature was adjusted to 45 °C, data collection was 10 Hz with filter 3.6, and the response rate was set to 100 pA. Palmitic acid (100 μ g/mL) was used as an internal standard (IS). Data were analysed using the software Chromeleon (Thermo Scientific, version 7.2).

Table 4.4. The method used for the analysis of lipids was adapted from⁴⁴⁶.

Time (min)	Eluent A (%)	Eluent B (%)	Eluent C (%)
0	25	65	10
27	9.2	89.3	1.5
28	25	65	10
32	25	65	10

4.2.12 Statistical tests and analysis

All experiments were performed in three independent replicates, and samples were freshly prepared if otherwise stated. Statistical analysis was carried out using GraphPad Prism version 9.5.1. Multiple comparisons between the groups were performed via an ordinary one-way ANOVA with *post-hoc* Tukey's multiple comparison analysis, respectively (statistical significance noted as **** p < 0.0001, *** p < 0.001, ** p < 0.01, *p < 0.05). All p-values from ordinary one-way ANOVA with *post-hoc* Tukey's multiple comparison analysis are reported in supplementary tables to this Chapter. If not stated otherwise, the data are presented as mean ± S.D. (standard deviation calculated from independent samples). qPCR data are presented as mean ± S.E.M. (standard error of the mean).

4.3 Results and discussion

4.3.1 Steatosis induction in Huh-7 cells – cell metabolism and lipid droplet content

Steatosis in hepatocytes is characterised by a visible lipid accumulation in the cytoplasm caused by a disbalance of the lipid input and output or by the reduced breakdown of FFAs.^{50,61} Extreme lipid accumulation leads to mitochondrial dysfunction, playing a pivotal role in the advancement of hepatic steatosis and the progression of NAFLD, representing the initial stage of the disease's pathology.^{60,62,63,193}

Huh-7 is a human adult hepatocellular carcinoma cell line extensively used as a hepatocytes cell model and for steatotic **NAFLD** in vitro modelling. 160,162,179,250,255,259,263,268,284,285,288,289,298,301,304,305 As reported in the literature, steatosis can be induced in vitro in Huh-7 by incubating various combinations of fatty acids and other lipid classes, as reported systematically in Chapter 2. To choose the most robust experimental setup based on FFAs' steatosis-inducing capacity, a 2:1 molar ratio of OA (in a concentration range of $150-600 \mu M$) and PA (in a concentration range of $75-300 \mu M$) were incubated with cells over 24 h incubation time, varying concentrations, incubation times, and solubilisation vehicles using what reported in the literature as starting point. These high FFA concentrations are not readily dispersible in cell culture medium and pose a significant challenge to obtaining standardised and replicable preparation and incubation conditions. In our case, Huh-7 were treated with steatogenic medium prepared by mixing FFA with medium, micelle-like vesicles containing FFAs, and by solubilisation of FFA with BSA (Model 1, 2, and 3, respectively).

All three steatogenic treatments did not interfere with Huh-7 cell viability, excluding thus any substantial FFA toxicity in given experimental conditions (**Figure 4.7 a, c, e**). The minor variability in cell metabolism can be observed in cells treated with **Model 3** medium. In contrast, the highest variability is observed when treated with **Model 2** medium, especially with combined lipids. Two significant changes in cell metabolism rate were observed in **Model 3** treated cells and are related to vehicle control (DMSO+BSA) between two single lipid treatments (PA 300 μM and OA 600 μM). They demonstrated a decrease compared to vehicle control. This vehicle control also numerically increased cell metabolism compared to the control (LX-2-EM) condition.

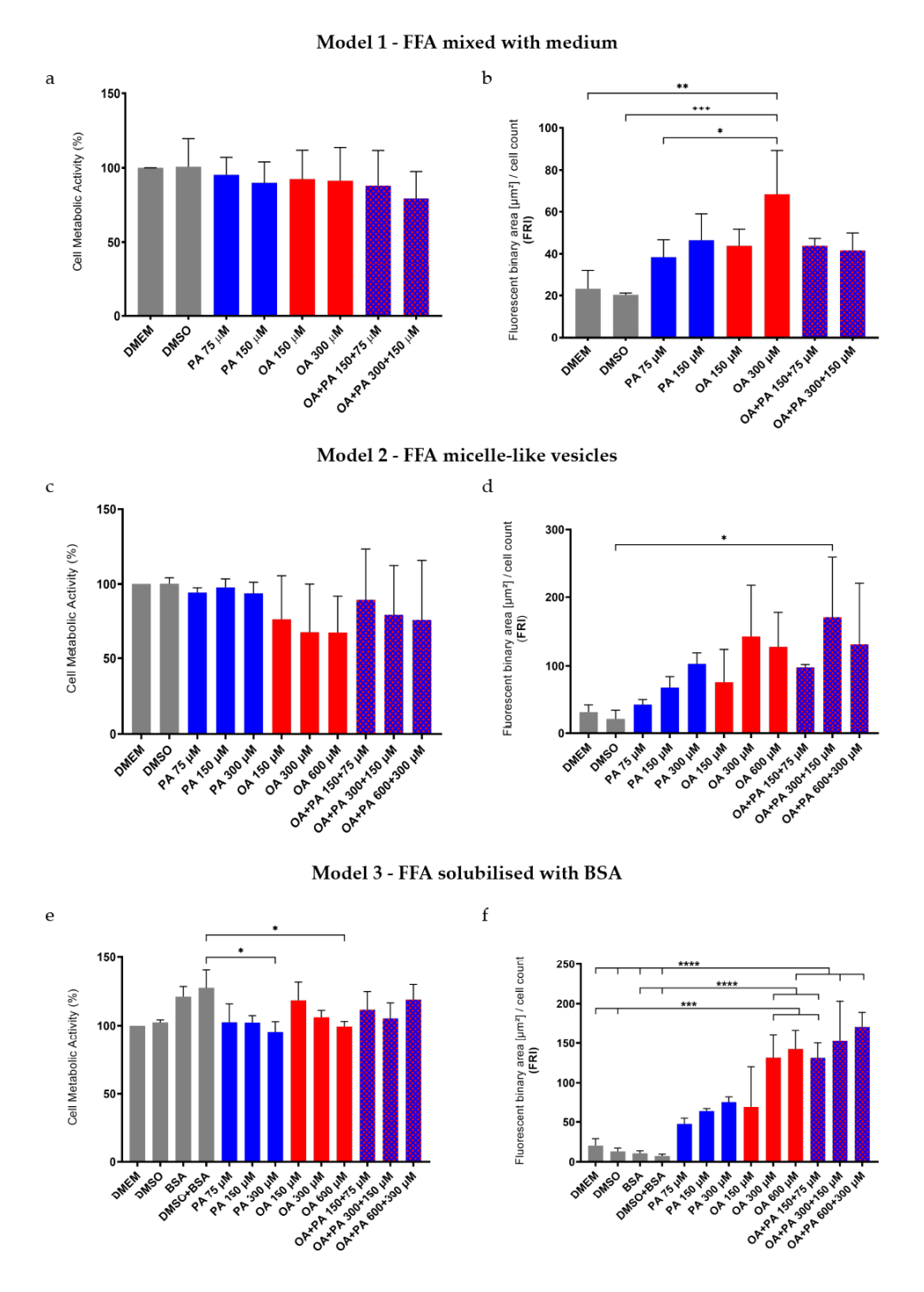


Figure 4.7. (**a**, **c**, **e**) Huh-7 cell viability (%) using CCK-8 assay after treatment with (**a**) Model 1, (**c**) Model 2, and (**e**) Model 3. (**b**, **d**, **f**) Quantification of the ORO fluorescent staining of Huh-7 cells treated with various steatogenic treatments normalised to the number of Huh-7 cells in the DAPI field (FRI). (**b**) Model 1, (**d**) Model 2, (**f**) Model 3. Mean \pm S.D. (n=3). p-values: **** p < 0.0001, *** p < 0.001, ** p < 0.05. All p-values from ordinary one-way ANOVA with post-hoc Tukey's multiple comparison analysis are reported in supplementary tables to this Chapter. Representative fluorescent microscopy images of lipid droplet staining are reported in **Appendix** to this Chapter (**Figures A4.1-3**).

We quantified lipid droplet storage using Oil Red O (ORO), a fluorescent dye staining neutral lipid droplets, considered among the golden standard methods to quantify the hepatocytes' lipid accumulation.^{73,162,170,174,275}

We established that naïve Huh-7 also expressed a basal level of lipid droplets but in a significantly reduced amount compared to other steatosis-induced cells. Three experiments report FRI of 23.18, 32.86, and 20.38. Vehicle controls in all setups reduced lipid content numerically, expressing a bland antisteatotic effect, but not significantly, compared to medium control cells.

Overall, the extent of steatosis was considerably lower in magnitude in cells treated with **Model 1** medium compared to **2** and **3**. For example, in the case of OA 300 μ M treatment, reported FRI value in **Model 1** treated cells of only 68.26 \pm 21.01, when **Model 2** and **3** displayed 142.50 \pm 74.79, and 131.60 \pm 29.43, respectively. Another observation is that cells treated with **Model 1** (FFA mixed with medium) and **Model 2** (FFA micelle-like vesicles) medium expressed more variability in lipid droplet content (**Figure 4.7 b, d, f**) when compared to **Model 3** (FFA solubilised with BSA).

As expected, OA had more steatogenic power than PA, which presents a more apoptogenic one, 250 especially when **Model 3** medium was used, with almost double the potency of OA compared to PA to increase lipid droplet content (for example, an FRI of 64.54 ± 3.11 was obtained with PA 150 μ M while 131.60 \pm 29.43 and with OA 300 μ M). The combinations of OA and PA were not superior to their single-component treatments in increasing cellular lipid content, inferring that they affect not only lipid droplet content but also an entire panel of lipid metabolism and factors involved. However, FFAs' combination of various fatty acids represents a more realistic pathological setup, with multiple FFAs reaching the liver simultaneously. 248,249 OA+PA 600+300 µM treatment did not show superiority in steatosis induction. However, quantitatively increased cell metabolism more than OA+PA 300+150 µM, as proven by the FRI obtained with the steatogenic medium Model 3 170.70 ± 18.20 compared to 152.60 ± 50.44 of OA+PA 300+150 µM. Based on these preliminary studies' findings, we chose the combination of OA+PA 300+150 μM prepared according to Model 3 (BSA supplementation) to induce lipid accumulation and apoptotic stress in Huh-7 to have a consistent, reproducible and straightforward steatogenic medium preparation with a commonly used solubilisation vehicle that is not significantly affecting cell viability.

4.3.2 General remarks on CCM treatment experiments

Tests were performed to investigate the effect of CCM collected from steatotic hepatocytes (treated or not with antisteatotic treatment) on activated or quiescent-like HSCs in different sequences. These experiments aimed to understand the secretome-mediated cross-talk between the two critical factors in steatosis and fibrosis, assessing their response to treatment. Additionally, the purpose was to establish an *in vitro* model of the pathology, serving as a screening tool for potential antisteatotic and antifibrotic therapies. For our formulations of interest, we chose PPC-derived essential soybean phospholipids (EPLs), S 80 and S 80 M, combined with the hepatoprotective Sily on LX-2 and S 80 M with the investigational antisteatotic drugs, Ela and Oca on Huh-7.

A "lipid paradox" theory, as described in **Chapter 2**, explains that healthy hepatocytes present no visible droplets inside the cells, and healthy HSCs present an abundance of retinyl ester lipid droplets with opposing situations. Hence fatty hepatocytes and fat-free HSCs give rise to a pathologic condition. Specific importance lies in the lipid metabolism in the liver, a precisely tuned system that, upon specific chronic injury, may progress into a pathological state such as steatosis and fibrosis, strongly interconnected conditions.^{206,213}

To validate the CCM system, in the first three models, we used control protocols for LX-2 well established in our laboratories, namely Rol+PA (10+300 μ M) to revert activated LX-2 to a quiescent-like state and TGF- β_1 (10 ng/mL) to perpetuate them towards the myofibroblastic transdifferentiated stage. ^{137,211,443-445}

4.3.3 Modulation of LX-2 phenotype after treatment with steatotic CCM incubation followed by control conditions treatments (Model A)

In the CCM-mediated study Model A, we investigated whether activated LX-2 could be reverted to a quiescent-like state following treatment with steatotic Huh-7 secretome.

The treatment with Huh-7 CCMs did not induce any changes in LX-2 cell viability. Only differences to direct treatment of LX-2 with controls and Rol+PA treatment increased cell metabolic activity to $162.40\% \pm 44.64$, $164.40\% \pm 53.22$, and $166.50\% \pm 45.92$ when treated with LX-2-EM, naïve control, and steatotic Huh-7 CCM, respectively, not reaching statistical significance (**Figure 4.8a**). Changes in cell viability and metabolic rate could also be an acute effect caused by changing the medium type. Huh-7 is grown in DMEM with low glucose and more glutamine, and LX-2 in DMEM with high glucose and lower glutamine. Substrates in each medium are slightly different, transitorily modifying cellular metabolic pathways caused

by acute incubation but did not induce any significant metabolic change comparing two control conditions on LX-2 cells. Noticeable is that the CCM medium contains not only different composition but also the secretome from naïve or steatotic Huh-7, so in general, in these experimental conditions, CCM was not apoptotic to the LX-2 cells, which is a favourable premise since we want to observe the bioactivity of this balanced system.

Rol+PA-treated cells managed to re-establish the quiescent-like status of LX-2 in all conditions, as shown by the significantly increased lipid droplets with FRI values of 58.99, 63.54, and 50.83 when LX-2 were pre-treated with LX-2-EM, naïve control, and steatotic Huh-7 CCM, respectively (**Figure 4.8bd**). Quiescent-inducing LX-2 control was also effective in the case of incubation with another, not native but containing other cells secretome (both naïve and steatotic) originating from Huh-7, meaning there is a certain intrinsic tolerance and paved pathways that are not affected even with this additional cell-induced stress. Controls and TGF- β_1 treatments did not induce recovery of lipid droplets, as expected, since they sustained the prolonged activated state of LX-2 cells. In the case of TGF- β_1 , there is a solid driving force toward permanent transdifferentiation towards myofibroblast-like cells, not expressing any lipid droplets but nourishing increased ECM synthesis.

In conclusion, any effect caused by steatotic CCM on activated LX-2 can be considered reversible, as Rol+PA still managed to revert LX-2 to express lipid droplets even after this 24 h treatment without significantly affecting cell viability.

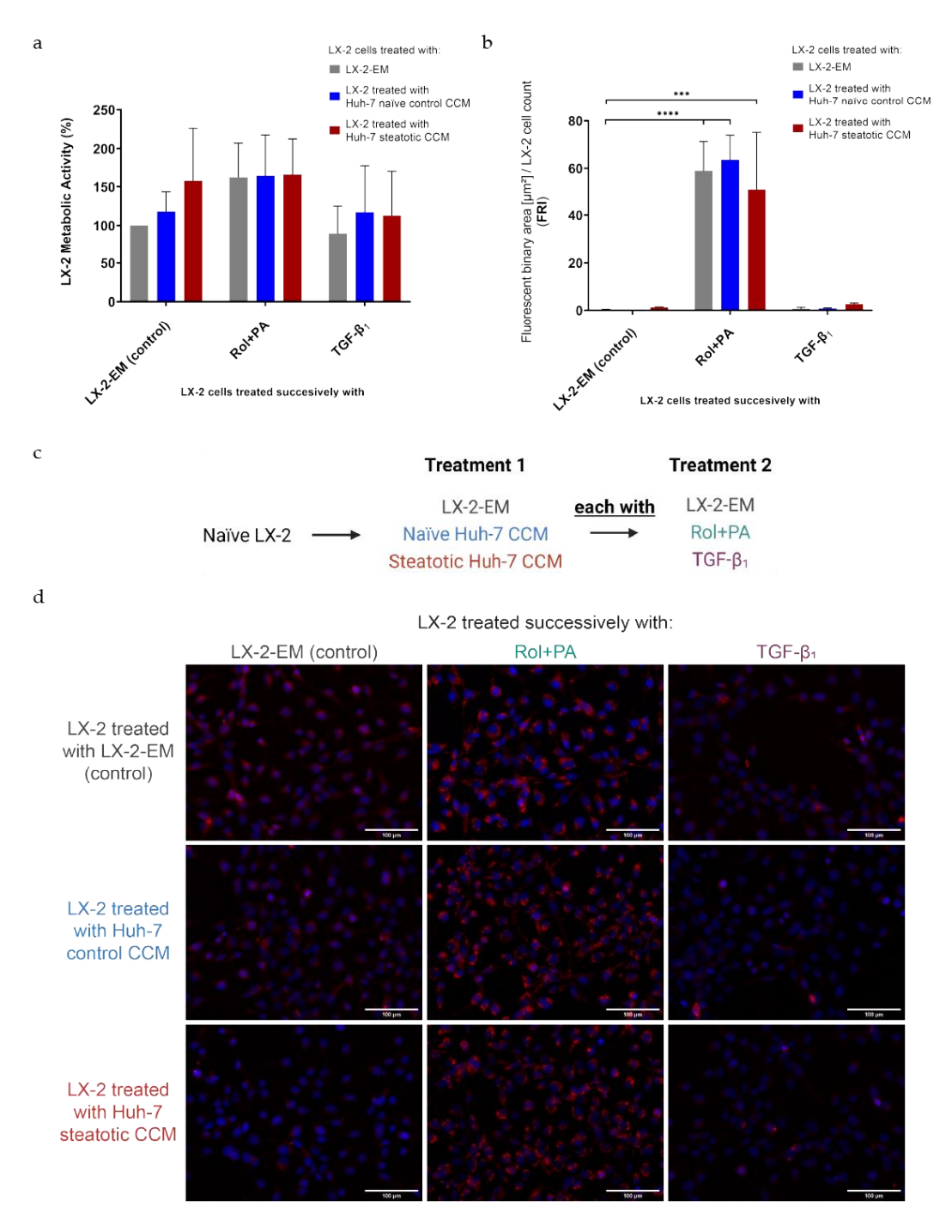


Figure 4.8. (a) LX-2 cell viability (%) using CCK-8 assay. (b, d) ORO staining of LX-2 cells treated first with control or Huh-7 CCMs and then with their control conditions: LX-2-EM experimental medium (untreated); Huh-7 naïve control and steatotic CCM; Rol+PA positive control, reverting to quiescent-like state; TGF-β1 negative control, pro-fibrotic fibrotic, progressing the cell to perpetuated state. (b) Quantification of the ORO fluorescence normalised to the number of LX-2 cells in the DAPI field (FRI). (c) Schematic of the experimental setup of Model A. (d) Representative fluorescence images of LX-2 cells in which lipid droplets can be visualised as red spots and the nuclei are counterstained with blue DAPI. Mean \pm S.D. (n=3). All comparisons in **Figure 4.8a** are not statistically significant. In **Figure 4.8b**, only p-values to LX-2-EM (control) are reported for convenience. p-values: ***** p <

0.0001, *** p < 0.001. All p-values from ordinary one-way ANOVA with post-hoc Tukey's multiple comparison analysis are reported in supplementary tables to this Chapter.

4.3.4 Simultaneous incubation with CCM and control conditions bioactivity on LX-2 cells (Model B)

Model B investigation was designed to investigate whether LX-2 can be reverted to a quiescent-like state with simultaneous treatment of Rol+PA with steatotic Huh-7 CCMs.

The same trend from **Model A** was observed here. The combined treatment of LX-2 controls and Huh-7 CCMs did not induce any changes in LX-2 cell viability (**Figure 4.9a**). The only significant differences were observed when TGF- β_1 supplemented CCMs significantly decreased cell viability to $83.09\% \pm 23.56$ and $80.90\% \pm 1.47$, when treated together with LX-2-EM and naïve control Huh-7 CCM, respectively. This decrease can be attributed to the "normal" TGF- β_1 perpetuating effect, HSCs taking a path towards the myofibroblast-like cells, where an inevitable part of HSCs end up in apoptosis, unable to differentiate phenotypically, affecting regular HSCs turnover.

Also, steatotic CCM mixed with Rol+PA quantitatively increased lipid droplet content, with FRIs of 60.46, and it demonstrated a higher ability to induce the production of lipid droplets concerning what was observed in **Figure 4.8b** (FRI 50.83), but it was not statistically significant. When comparing Rol+PA treatment efficiency for restoration of lipid droplet content directly in-between **Models A** and **B** (sequential and simultaneous treatment with Rol+PA), there is no significant difference when comparing Rol+PA with LX-2-EM and CCM from steatotic Huh-7. However, there was a significant improvement (p=0.0454, unpaired test with Welch's correction) when Rol+PA treatment was performed following the incubation with CCM from naïve Huh-7 compared to direct mixing with CCM.

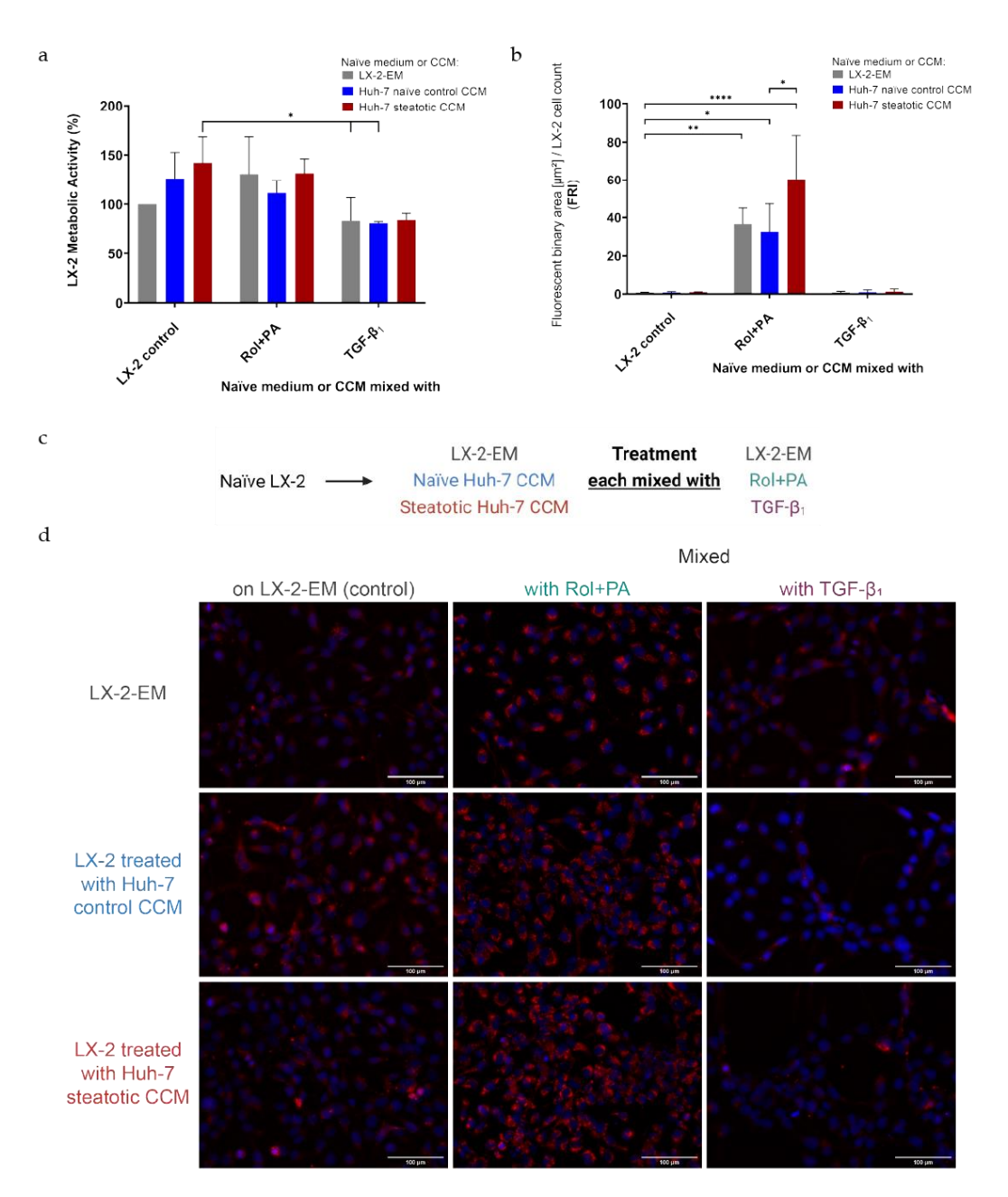


Figure 4.9. (a) LX-2 cell viability (%) using CCK-8 assay. (**b**, **d**) ORO staining of LX-2 cells treated with control or Huh-7 CCMs together with their control conditions: LX-2-EM experimental medium (untreated); Huh-7 naïve control and steatotic CCM; Rol+PA positive control, reverting to quiescent-like state; TGF-β1 negative control, pro-fibrotic fibrotic, progressing the cell to perpetuated state. (**b**) Quantification of the ORO fluorescence normalised to the number of LX-2 cells in the DAPI field (FRI). (**c**) Schematic of the experimental setup of Model B. (**d**) Representative fluorescence images of LX-2 cells in which lipid droplets can be visualised as red spots and the nuclei are counterstained with blue DAPI. Mean ± S.D. (n=3). In **Figure 4.9b**, only p-values to LX-2-EM (control) and between Rol+PA treated cells are reported for convenience. p-values: **** p < 0.0001, **p < 0.01, *p < 0.05. All p-values from ordinary one-way ANOVA with post-hoc Tukey's multiple comparison analysis are reported in supplementary tables to this Chapter.

In the setup of **Model B**, the Rol+PA effect is readily opposed by the pro-fibrogenic action of CCM from steatotic Huh-7, and there are no two consecutive system adaptations related to each treatment condition separately.

In contrast, pure steatotic CCM on naïve LX-2 had shown no effect, exhibiting FRI 1.05. TGF- β_1 and other controls had a negligible effect on lipid droplet content, consistent with data obtained in **Model A**.

In conclusion, Rol+PA mixed with all mediums reverted LX-2 to produce new lipid droplets in the amount comparable to post-treatment with Rol+PA (**Model A**), also when mixed directly with CCM from steatotic Huh-7, without significantly affecting LX-2 viability.

4.3.5 Effect of PPC pre-treatments followed by steatotic CCM incubation on LX-2 cells (Model C)

From our previous studies, direct treatments with Rol+PA and liposomal PPC formulations (S 80, S 80 M, and S 80 + Sily) induced a quiescent-like phenotype in LX-2, with a significant increase of lipid droplets and a decrease in α -SMA determined by immunocytochemistry. This was confirmed in studies described in **Chapter 3**, where S 80 M tablet extracts efficiently reverted activated LX-2 and cirrhotic PRHSCs towards lipid-rich, quiescent-like HSCs phenotype.

In **Model C**, we wanted to determine whether PPC-treated LX-2 could retain their quiescent-like status following the treatment with CCM from steatotic Huh-7.

PPC liposomal formulations were prepared by the film hydration method and extruded as previously reported (see **Section 4.2.5.1-2**). 122,137,138,408 Following 24 h incubation of LX-2 with 5 mM of PPC lipids (2.5 mM lipid in case of S 80 + Sily), cells were successively washed and incubated with steatotic CCM for an additional 24 h. We complemented one formulation of PPC with Sily, which is the bioactive hepatoprotective ingredient and commonly investigated PPC-associated component that exerts an antioxidant effect, reduces HSCs activation and acts as a radical scavenger to observe which potential protective activity it will exert on LX-2 once treated with steatotic CCM. 378,379

As expected from previous model studies, all PPC treatments did not interfere with LX-2 cell viability, even after being treated with CCM from steatotic Huh-7, excluding any possible toxicity (**Figure 4.10a**). Only a decrease in cell metabolic activity was observed in cells treated with pro-fibrotic TGF- β_1 control, consistent with results obtained in **Model A** and **B**, which could be due to enhanced transdifferentiation due to doubled culturing time towards

the myofibroblast-like state and apoptotic destiny of specific HSCs population part, not identifiable by the assays we performed.

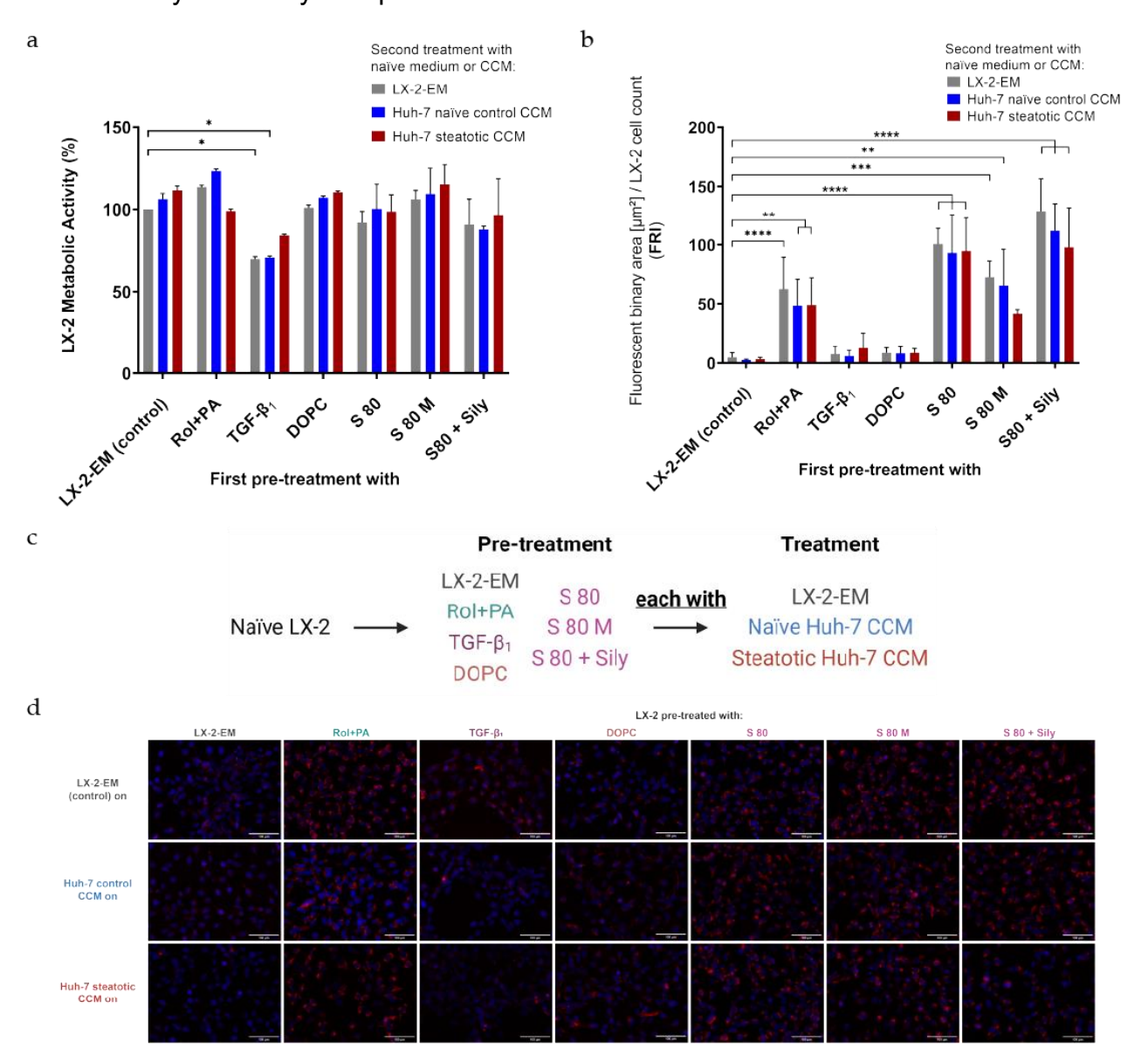


Figure 4.10. (a) LX-2 cell viability (%) using CCK-8 assay. (b, d) ORO staining of LX-2 cells treated with control or Huh-7 CCMs together after being treated with their control conditions and PPC-based formulations: LX-2-EM experimental medium (untreated); Huh-7 naïve control and steatotic CCM; Rol+PA positive control, reverting to quiescent-like state; TGF-β₁ negative control, pro-fibrotic fibrotic, progressing the cell to perpetuated state; DOPC inactive phospholipid used as negative control; S 80 and S 80 M liposomal PPC formulations; S 80 + Sily, liposomal and hepatoprotectant formulation. (b) Quantification of the ORO fluorescence normalised to the number of LX-2 cells in the DAPI field (FRI). (c) Schematic of the experimental setup of Model C. (d) Representative fluorescence images of LX-2 cells in which lipid droplets can be visualised as red spots and the nuclei are counterstained with blue DAPI. Mean ± S.D. (n=3-6). In **Figure 4.10b**, only p-values to LX-2-EM (control) are reported for convenience. P-values: ***** p < 0.0001, **** p < 0.001, **p < 0.05. All p-values from ordinary

one-way ANOVA with post-hoc Tukey's multiple comparison analysis are reported in supplementary tables to this Chapter.

Control non-bioactive conditions of LX-2 incubation (LX-2-EM, DOPC, and TGF-β₁) after the CCM incubation brought only a formation of negligible, non-significant amounts of remanent lipid droplets (**Figures 4.10bd**), consistent with previously reported results. All PPC treatments, S 80, S 80 M, S 80 + Sily, and Rol+PA, significantly increased the quantity of remaining LX-2 lipid droplets in all conditions compared to naïve control. Accumulation of lipid droplets is visible in fluorescent images (**Figure 4.10d**), causing ~21-fold, ~15-fold, ~27-fold, and ~13-fold FRI increase compared to control naïve LX-2, with an FRI of 100.60 (p<0.0001), 72.97 (p=0.0013), 129.20 (p<0.0001), and 62.38 (p<0.0001) for S 80, S 80 M, S 80 + Sily, and Rol+PA treatment, respectively.

Different PPC treatments, and Rol+PA positive control, were not significantly different from each other, even if numerically noticeable. S 80 and S 80 + Sily were significantly better (p=0.0483 and p=0.0002, respectively) than Rol+PA in increasing the remaining lipid droplets in LX-2 after steatotic CCM treatment.

When considering cells treated with steatotic CCM and considering it a control, PPC formulations increased FRI by \sim 30-fold (p<0.0001), \sim 13-fold (p=n.s.), and \sim 31-fold (p<0.0001) for S 80, S 80 M, and S 80 + Sily. Rol+PA treatment increased FRI value by \sim 16-fold (p=0.0043).

PPC formulations were able to retain a quiescent-like state by inducing not readily depletable lipid droplets storage in LX-2 cells, no matter which experimental CCM treatment was successively used, as observable from the data mentioned above, meaning that the treatment with CCM from steatotic Huh-7 is not able to hinder the antifibrogenic activity of PPC in this experimental setup. However, there seems to be a slight decrease of lipid droplets following the treatment with steatotic secretome in cells previously treated with S 80 M and S 80 + Sily in comparison to naïve medium control that might be attributed to potentially lower efficacy of S 80 M in direct comparison to S 80 in this experimental setup, that was not statistically significant. In S 80 + Sily case, it is worth mentioning that a direct comparison of S 80 and S 80 + Sily should be taken with reserve since we used only half of the usual PPC concentration because of technical reasons of difficulty extruding Sily-containing formulation (2.5 mM instead of 5 mM on cells). Sily content is directly dependent on lipid amount since the lipid-to-drug molar ratio was fixed at 11:1. If Sily were employed at higher concentration, it might exert more beneficial bioactivity, in line or even superior to plain S 80 treatment across

all conditions, as it has been observed with naïve LX-2-EM treated cells even at lower concentration (**Figure 4.10b**).

4.3.6 Bioactivity of Huh-7 CCM originating from steatotic cells treated with antisteatotic formulations on naïve and quiescent-like LX-2 cells (Model D)

To further explore the potential of our CCM-mediated dual cell culture model, we first induced steatosis in Huh-7, and subsequently, we treated the cells with new investigational drugs (Ela and Oca) formulated in the liposomal formulation of antifibrotic PPC (S 80 M). The CCM of Huh-7 subjected to this treatment was then used to treat activated and quiescent-like LX-2. We aimed to understand whether this more complex CCM transfer could affect the ability of activated LX-2 to be inactivated into a quiescent-like state and if quiescent-like cells can retain their lipid-rich phenotype without significantly increasing fibrotic markers' mRNA transcription levels.

PPC liposomal formulations were prepared by the film hydration method and extruded as previously reported (see **Section 4.2.5.1 and 4.2.5.3**). 122,137,138,408 Based on our previous studies, lipid amount was kept consistent at 5 mM on cells, eventually adding 150 nM antisteatotic drug. 122,137,138 DOPC formulations were used as inactive phospholipids (negative control).

All CCMs from steatotic Huh-7 did not affect LX-2 cell viability without any evident toxicity or cell metabolic rate change (**Figure 4.11a**).

As for the ORO staining of neutral lipid droplets, all CCMs originating from steatotic but antisteatotic-treated Huh-7 did not induce an increase in lipid droplet numbers and did not revert LX-2 to quiescent-like state (**Figure 4.11b and 4.12**), but we also did not observe an increase in LX-2 activation from the data we collected. For example, we assessed that naïve LX-2 treated with CCMs obtained from steatotic Huh-7 treated with S 80 M, S 80 M + Ela, S 80 M + Oca, and S 80 M + Ela + Oca gave FRI of 0.75, 1.55, 0.64, and 0.61, respectively, compared to naïve control FRI 0.47. Interestingly, no further increase was observed when the same CCMs were used to treat quiescent-like LX-2, presenting lipid droplets in the cytoplasm (**Figure 4.11b and 4.12**). However, the amount remained relatively constant, indicating the preservation of lipid storage directly connected with the quiescent-like state of LX-2. FRI of LX-2 treated with CCMs from PPC-treated steatotic Huh-7 (S 80 M, S 80 M + Ela, S 80 M + Oca, and S 80 M + Ela + Oca) was 24.78, 27.95, 23.35, and 28.87, respectively and quiescent-like control's FRI was 33.80, slightly, but not significantly higher.

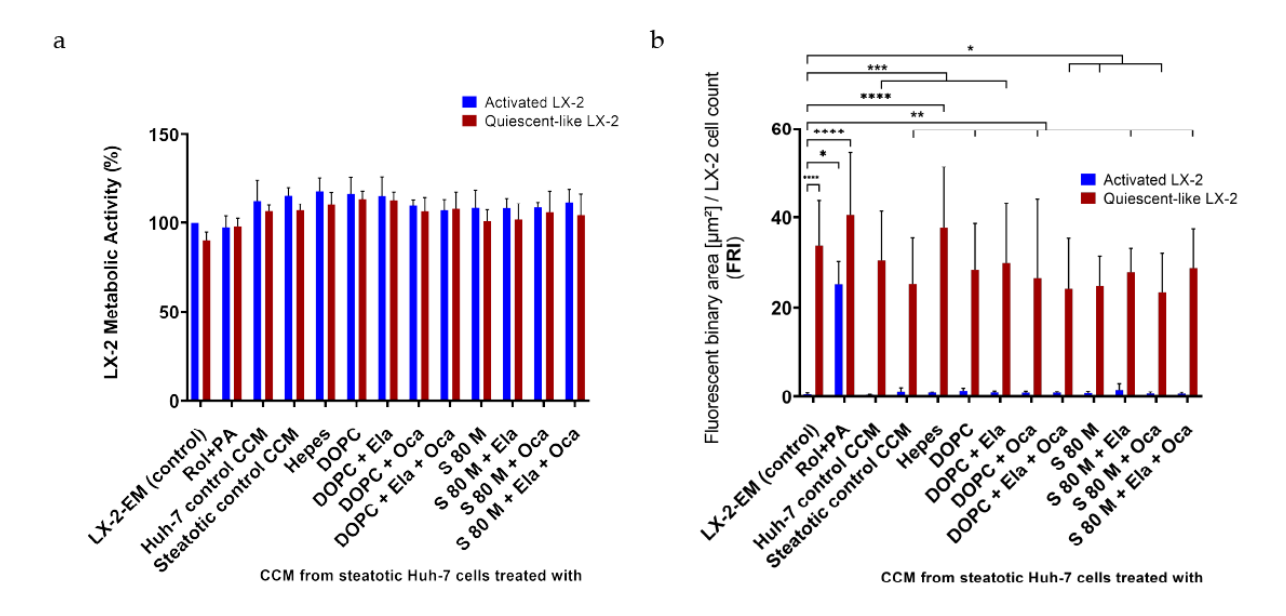


Figure 4.11. (a) LX-2 cell viability (%) using CCK-8 assay. (b) Quantification of the ORO staining fluorescence normalised to the number of LX-2 cells in the DAPI field (FRI). Naïve activated (blue) and induced quiescent-like (red) LX-2 cells treated with control or Huh-7 CCMs from steatotic Huh-7 cells treated successively with various antifibrotic/antisteatotic formulations (represented as individual columns on the x-axis): LX-2-EM experimental medium (untreated); Huh-7 naïve control and steatotic CCM; DOPC inactive phospholipid used as negative control; S 80 M liposomal PPC formulation. DOPC/S 80 M + Ela, DOPC/S 80 M + Oca, DOPC/S 80 M + Ela + Oca combinations of DOPC and S 80 M with Ela and Oca, antisteatotic drugs. Mean \pm S.D. (n=3). All comparisons to activated LX-2-EM in Figure 4.11a are not statistically significant. In Figure 4.11b, only p-values to activated LX-2-EM (control) are reported for convenience. p-values: **** p < 0.0001, *** p < 0.001, **p < 0.01, *p < 0.05. All p-values from ordinary one-way ANOVA with post-hoc Tukey's multiple comparison analysis are reported in supplementary tables to this Chapter.

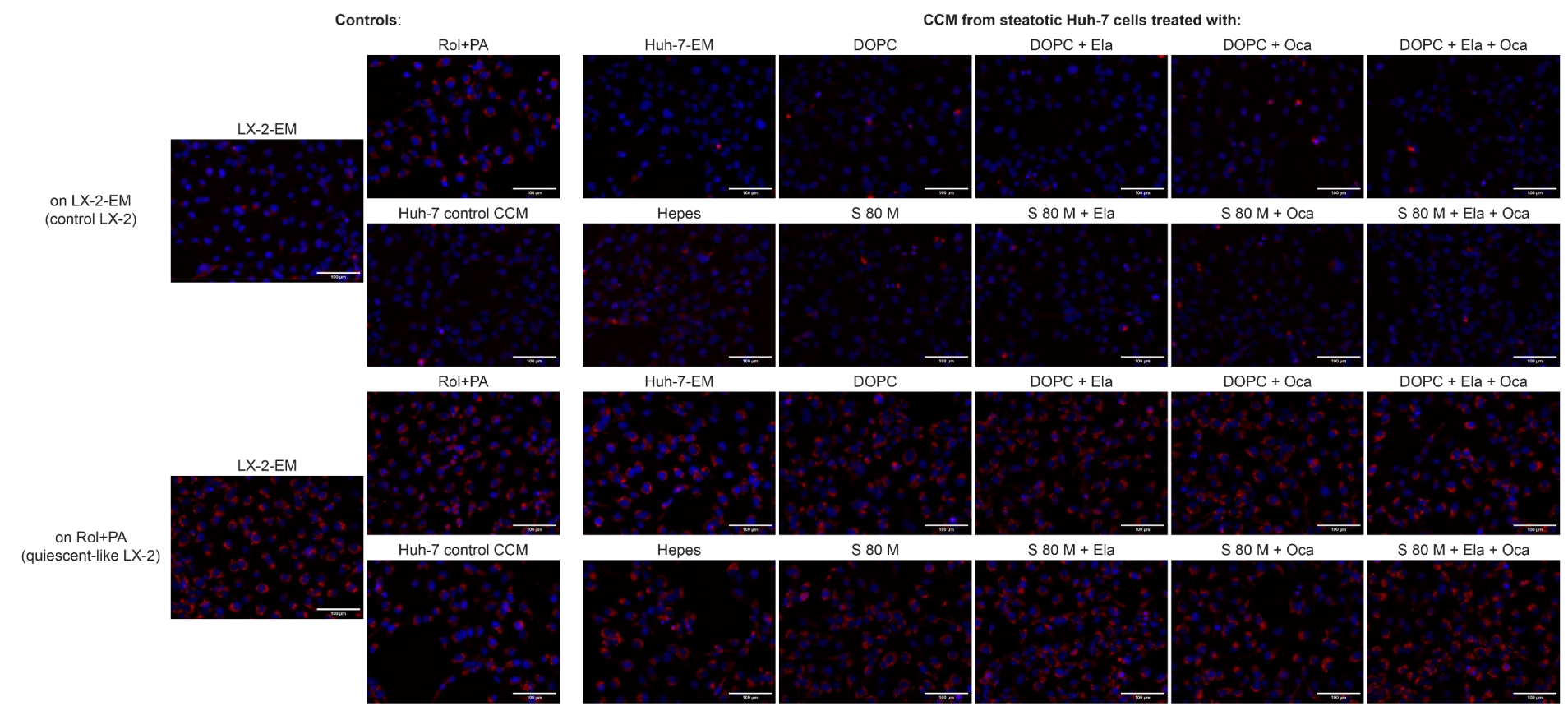


Figure 4.12. Representative fluorescence images of LX-2 cells from **Model D** in which lipid droplets can be visualised as red spots and the nuclei are counterstained with blue DAPI. LX-2-EM experimental medium (untreated); Huh-7 naïve control and steatotic CCM; DOPC inactive phospholipid used as negative control; S 80 M liposomal PPC formulation. DOPC/S 80 M + Ela, DOPC/S 80 M + Oca, DOPC/S 80 M + Ela + Oca combinations of DOPC and S 80 M with Ela and Oca, antisteatotic drugs.

In conclusion, the CCM from treated steatotic Huh-7 could not deplete the lipid content of quiescent-like LX-2. However, it remained relatively constant across all conditions, meaning quiescent-like LX-2 were not reactivated once treated with steatotic CCM from antisteatotic-treated Huh-7. There is a delicate numerical, but not statistically significant decrease between treatment with CCM from only steatotic Huh-7 compared to CCM originating from Huh-7 additionally treated with antisteatotic treatments, for example, S 80 M + Ela + Oca (FRI 25.19 and 28.87, respectively), meaning that quiescent-like LX-2 are less susceptible to reduce their lipid droplets content once in contact with medium originating from a steatotic cell treated with investigative therapy.

4.3.6.1 mRNA transcription of fibrosis markers

As already reported in **Chapter 3**, PLIN2, PDGFRB, ACTA2 coding for α -SMA, COL1A1 for collagen type I, and SPARC, a membrane-associated protein, recently reported by our group¹³⁸ to be associated with harvested and purified extracellular vesicles originating from activated pro-fibrotic LX-2, were all analysed as hallmark fibrotic markers.

Perilipin 2 (PLIN2) is a protein playing a crucial role in the formation, stabilisation, and breakdown of lipid droplets within cells. PLIN2 upregulated is correlated with the regulation of lipid droplet turnover, which is often decreased in fibrosis. 207,211,410 Studies have shown that the higher level of PLIN2 expression is associated with reduced HSCs activation, and it is also linked to the decrease in several crucial fibrosis markers, including α -SMA, collagen type I, and matrix metalloprotease 2 (MMP-2). However, the exact mechanisms through which PLIN2 influences these processes are not yet fully understood. 211

Control, activated LX-2 treated with CCM from steatotic Huh-7 originating from cells treated with S 80 M, S 80 M + Ela, S 80 M + Oca, and S 80 M + Ela + Oca even showed a non-significant 16%, 18%, 20%, and 23% PLIN2 expression decrease (**Figure 4.13a, Table 4.5**) compared to a control condition LX-2 confirmed by variably low lipid storage capacity in these cells as stained by ORO (**Figure 4.11b**).

In quiescent-like LX-2, there was no significant change in PLIN2 expression, 3.21-fold (S 80 M), 3.98-fold (S 80 M + Ela), 3.30-fold (S 80 M + Oca), and 3.38-fold (S 80 M + Ela + Oca) increase was observed, slightly lower (S 80 M + Ela excluded) compared to quiescent-control (3.53-fold) which were all consistent with the data obtained from ORO staining. PLIN2 upregulation in quiescent-like LX-2 generally confirms the increase in ORO staining

quantified fluorescence (**Figures 4.11b** and **4.12**), corroborating retained quiescent-like cell status.

Rol+PA control treatment directly on activated cells increased PLIN2 by 2.41-fold, consistent with ORO staining and expected from previous results. Interestingly, quiescent-like LX-2 reincubated with Rol+PA expressed ~70% less PLIN2 mRNA than control ones treated with LX-2-EM control, suggesting that prolonged exposure to Rol+PA might reduce the ability to revert towards the quiescent-like state, which is an interesting observation if the potential treatment regime should be adjusted to have a more pulsative and not only chronic character, to observe mRNA transcription levels in both cases.

Platelet-derived growth factor receptor- β (PDGFR- β) mediates the activation and increases pro-fibrogenic HSCs' transdifferentiation into myofibroblasts potentiating hepatic fibrosis through its tyrosine kinase activity. Its sudden increase is correlated to fibrotic pathology progression since it influences multiple cellular pathways. A decrease in HSCs activation is hallmarked by PDGFRB expressional reduction and linked to fibrosis progression bettering, and linked to fibrosis progression bettering, and linked to fibrosis progression bettering.

Expression levels of PDGFRB remained constant in active LX-2 acutely treated with CCM, meaning that further activation of LX-2 was not induced post-CCM treatment. In quiescent-like LX-2, S 80 + Oca and S 80 + Ela + Oca CCM caused a minor expression decrease (both ~17%, **Figure 4.13b**), suggesting activation reduction and potential quiescence-reversion that was not statistically significant. Taking into consideration enhanced relatively constant PLIN2 expression with persistent, not significantly changed PDGFRB level, these CCM-treated LX-2 cells could be considered as quiescent-like on the way to the activation since PDFGRB seems to have a quicker transcription response than PLIN2 to external stimuli. The quicker response was observed with Rol+PA re-incubation control, which reduced its expression by ~40% after only 24 h. Once activated cells were treated with Rol+PA, it was also confirmed o that they demonstrated a transcription decrease.

An interesting observation is that Rol+PA, once removed from the treatment medium, as in the case of quiescent-like LX-2-EM control, was not able to reduce the expression level permanently, but only with a re-incubation step, or directly on activated cells, so it seems to have only an acute effect on LX-2. Long-term exposure to Rol+PA and other treatments and study of markers transcription levels were not investigated.

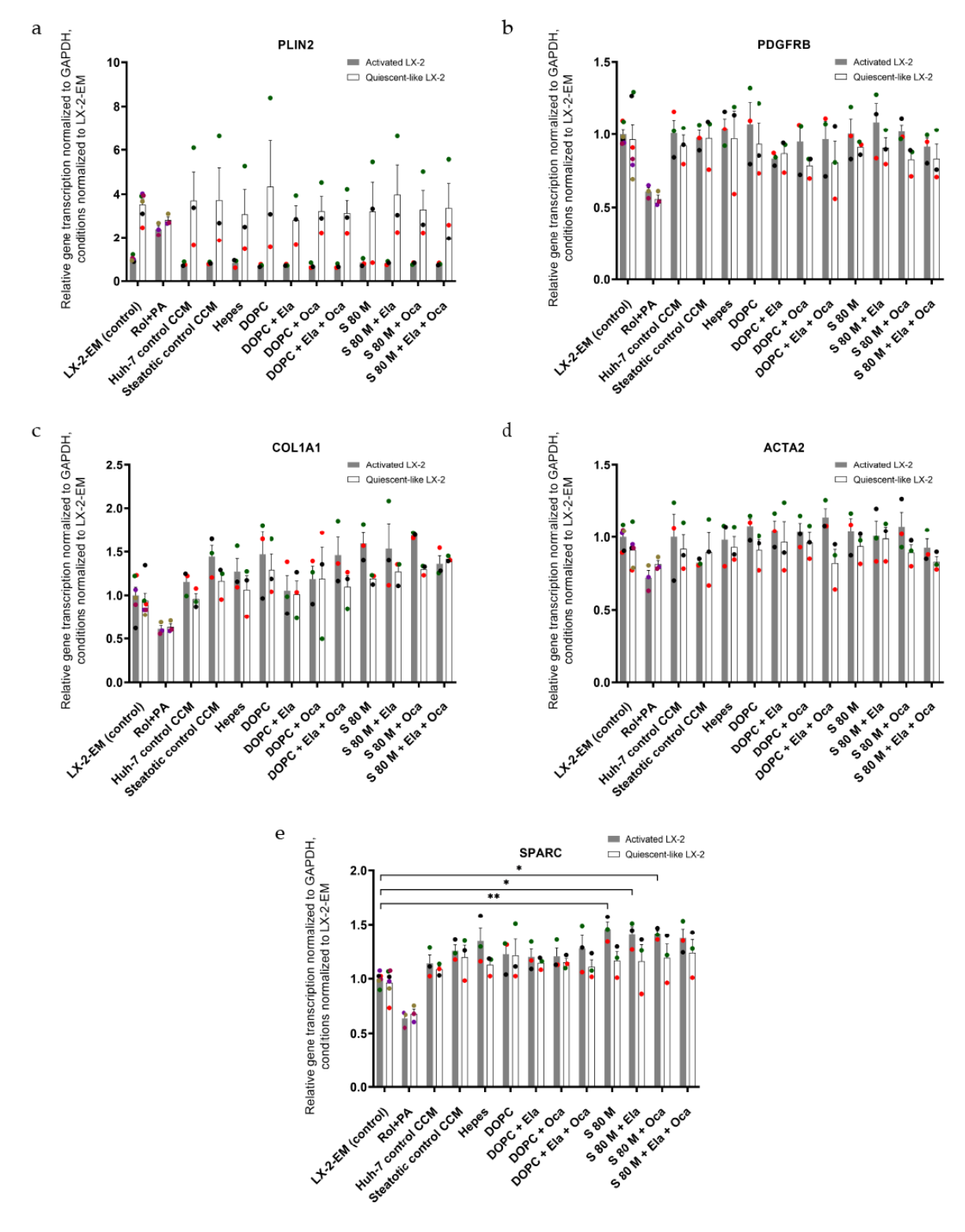


Figure 4.13. Relative mRNA transcription in LX-2 cells of fibrosis markers (a) PLIN2, (b) PDGFRB, (c) COL1A1, (d) ACTA2, (e) SPARC, and normalised to GAPDH mRNA transcription and further normalised to the LX-2-EM (naïve culture) condition after different Huh-7 CCM treatments: LX-2-EM experimental medium (untreated); Huh-7 naïve control and steatotic CCM; DOPC inactive phospholipid used as negative control; S 80 M liposomal PPC formulation. DOPC/S 80 M + Ela, DOPC/S 80 M + Oca, DOPC/S 80 M + Ela + Oca combinations of DOPC and S 80 M with Ela and

Oca, antisteatotic drugs. Mean \pm S.E.M. (n=3-6). In **Figure 4.13e**, only p-values to activated LX-2-EM (control) are reported for convenience. p-values in **Figure 4.13abcd** to activated LX-2-EM are all not significant. p-values: ** p < 0.01, *p < 0.05. All p-values from ordinary one-way ANOVA with post-hoc Tukey's multiple comparison analysis are reported in supplementary tables to this Chapter.

COL1A1 expression in CCM-treated active and quiescent-like LX-2 has shown a slight but not statistically significant increase to control, as reported in **Figure 4.13c** and **Table 4.5**, which was less pronounced in quiescent-like cells, meaning a more fibrotic-activated LX-2 status. In particular, the status of quiescent-like LX-2 treated with various CCMs from steatotic Huh-7, once taken into account PLIN2 and PDGFRB results, their overall status can be described as quiescent-like leaning towards activated, expressing retained lipid-rich phenotype, with slightly increased COL1A1 expression, indicating conserved resistance to external stresses originating from steatotic secretome in Huh-7 CCMs.

ACTA2, one of the hallmarks of the pro-fibrotic expression panel of genes, maintained a steady expression level following any CCM treatments in both LX-2 models (**Figure 4.13d** and **Table 4.5**), meaning there was no significant transdifferentiation towards myofibroblast-like cells, specific to fibrosis. However, Rol+PA control incubation was able to reduce the expression level of COL1A1 and ACTA2 in both activated and quiescent-like LX-2, with reported decreases of 39% and 37% (COL1A1 to controls), and 28% and 10% (ACTA2 to controls) shown in **Figure 4.13cd** and **Table 4.5**, indicating transition towards quiescence in these LX-2 cells, supporting our hypothesis of antifibrotic effect and robustness of model being able to simulate the real biological effect by employing only secretome.

SPARC mRNA expression level increased by ~38-46% in active and ~16-24% in quiescent-like LX-2 incubated with Huh-7 CCMs (**Figure 4.13e**), which could be indirectly compared with an activated LX-2-derived extracellular vesicles SPARC protein expression increase, as reported previously in our group. A significant increase in SPARC mRNA was observed by treating active LX-2 with S 80 M (46%, p=0.0086), S 80 M + Ela (41%, p=0.0358) and S 80 M + Oca (41%, p=0.0326) derived CCM from steatotic Huh-7. As a comparison, Rol+PA control treatment reduced SPARC expression level by 36% in active and 32% in quiescent-like LX-2, which is lower than when cells were treated with CCM originating from PPC and antisteatotic treated Huh-7. However, control values did not reach statistical significance, but evident trends suggest a quiescent-like antifibrotic status of these LX-2s.

Table 4.5. mRNA transcription fold change of chosen experimental conditions all normalised to GAPDH and active LX-2 control. Mean \pm S.E.M. (n=3-6). p-values: ** p < 0.01, *p < 0.05. All p-values from ordinary one-way ANOVA with post-hoc Tukey's multiple comparison analysis are reported in supplementary tables to this Chapter.

Fold change in mRNA expression on active LX-2 control						
mRNA	Active LX-2 control	Rol+PA on active control	S 80 M treated Huh-7 steatotic CCM	S 80 M + Ela treated Huh-7 steatotic CCM	S 80 M + Oca treated Huh-7 steatotic CCM	S 80 M + Ela + Oca treated Huh- 7 steatotic CCM
PLIN2	1.00 ± 0.05	2.41 ± 0.16	0.84 ± 0.10	0.82 ± 0.05	0.80 ± 0.03	0.77 ± 0.03
PDGFRB	1.00 ± 0.03	0.61 ± 0.03	1.00 ± 0.10	1.09 ± 0.13	1.02 ± 0.05	0.91 ± 0.06
COL1A1	1.00 ± 0.09	0.61 ± 0.04	1.60 ± 0.12	1.53 ± 0.29	1.69 ± 0.02	1.36 ± 0.09
ACTA2	1.00 ± 0.03	0.72 ± 0.05	1.04 ± 0.09	1.01 ± 0.10	1.07 ± 0.10	0.93 ± 0.06
SPARC	1.00 ± 0.02	0.64 ± 0.04	1.46 ± 0.07 ** p=0.0086	1.41 ± 0.07 * p=0.0358	1.41 ± 0.03 * p=0.0326	1.38 ± 0.08
Fold change in mRNA expression on quiescent-like LX-2 control						
mRNA	Quiescent- like LX-2 control	Rol+PA on quiescent-like control	S 80 M treated Huh-7 steatotic CCM	S 80 M + Ela treated Huh-7 steatotic CCM	S 80 M + Oca treated Huh-7 steatotic CCM	S 80 M + Ela + Oca treated Huh- 7 steatotic CCM
PLIN2	3.53 ± 0.25	2.83 ± 0.14	3.21 ± 1.34	3.98 ± 1.34	3.30 ± 0.87	3.38 ± 1.11
PDGFRB	0.96 ± 0.10	0.56 ± 0.03	0.91 ± 0.03	0.91 ± 0.07	0.83 ± 0.06	0.83 ± 0.10
COL1A1	0.94 ± 0.08	0.63 ± 0.04	1.19 ± 0.03	1.27 ± 0.08	1.30 ± 0.03	1.42 ± 0.02
ACTA2	0.91 ± 0.05	0.81 ± 0.02	0.94 ± 0.06	0.99 ± 0.08	0.89 ± 0.05	0.83 ± 0.04
SPARC	0.96 ± 0.05	0.68 ± 0.04	1.17 ± 0.08	1.16 ± 0.15	1.19 ± 0.13	1.24 ± 0.12

Given the complexity of the interplay of various fibrosis-involved factors, more than 150 were identified only in HSCs, 427 it is challenging to make a definitive conclusion on LX-2 cell status based on observing only one marker. Hypotheses can only be made when considering multiple factors, as reported above in the discussion, sometimes only evident with observing specific trends or trends than more than one marker. Further studies, with a broader screening panel such as full lipidome, proteome and transcriptome, should be performed to make noticeable less prominent differences and ratios between various fibrotic mediators that might not be readily observable to give a definitive evaluation of quiescent-like or activated HSCs state.

4.3.7 Effect of control-treated LX-2 CCMs on steatotic Huh-7 cells (Model E)

We finally investigate the feasibility of transferring CCM from quiescent-like LX-2 to steatotic Huh-7 to understand whether steatosis could be reverted in this way. To perform this experiment, LX-2 were first treated with Rol+PA, then washed and kept in EM for 24 h. Their CCM was finally used to treat steatotic Huh-7 directly for 24 h. CCMs from control and perpetuated LX-2 were also used as additional conditions.

The treatment of steatotic Huh-7 with LX-2 CCM induces only two significant changes in Huh-7 cell viability (**Figure 4.14a**). First, quiescent-like LX-2 CCM slightly increased cell metabolic activity of naïve Huh-7 compared to naïve treated already steatotic Huh-7 (p= 0.0375). When naïve Huh-7 cells were treated with CCM from quiescent-like LX-2, we observed significantly higher cell viability (p=0.0397) than when perpetuated-like LX-2 CCM was used to treat steatotic Huh-7. Once more, it is essential to notice that Huh-7 and LX-2 cells are cultivated in different composition mediums that might contribute to or alter the bioactivity of the LX-2 secretome contained in this medium. However, it was not evident and significant from the results of the metabolic assay (**Figure 4.14a**).

CCM from quiescent LX-2 did not decrease the lipid droplet content of steatotic Huh-7 (**Figure 4.14bd**). Hence it did not improve the steatotic cell state since there was no observable or measurable difference in lipid content using ORO staining. Interestingly, on the contrary, CCM originating from perpetuated LX-2 increased steatosis compared to na $\ddot{\text{u}}$ edium-treated steatotic hepatocytes (FRI 150.50 \pm 72.89 compared to 102.00 \pm 3.84) but was not statistically significant. This result concludes that perpetuated, myofibroblast-like LX-2 can further enhance steatotic progression in Huh-7 as a chain reaction from pathologic HSCs to steatotic Huh-7 via the respective secretome.

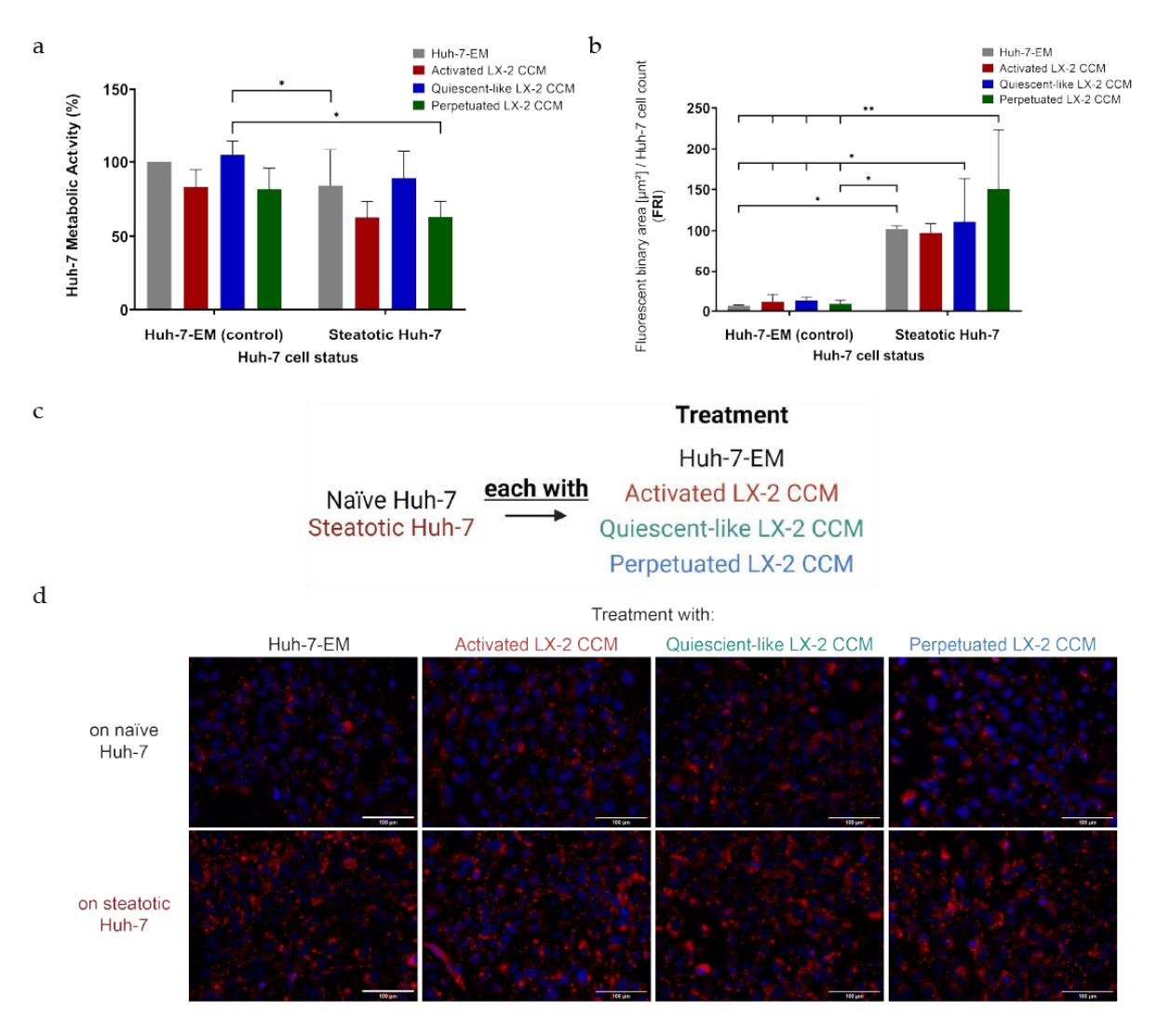


Figure 4.14. (a) Huh-7 cell viability (%) using CCK-8 assay. (b, d) ORO staining of Huh-7 cells treated with control or LX-2 CCMs: Huh-7-EM experimental medium (untreated); steatotic Huh-7 cells; LX-2 naïve control activated, Rol+PA induced quiescent-like, and TGF- $β_1$ induced pro-fibrotic perpetuated CCM. (b) Quantification of the ORO fluorescence normalised to the number of Huh-7 cells in the DAPI field (FRI). (c) Schematic of the experimental setup of Model E. (d) Representative fluorescence images of Huh-7 cells in which lipid droplets can be visualised as red spots and the nuclei are counterstained with blue DAPI. Mean ± S.D. (n=3). p-values: ** p < 0.01, *p < 0.05. All p-values from ordinary one-way ANOVA with post-hoc Tukey's multiple comparison analysis are reported in supplementary tables to this Chapter.

4.4 Conclusion

We developed and optimised a dual cell culture using a conditioned medium, employing Huh-7 and LX-2 cells, put in indirect asynchronous contact through CCM containing steatotic hepatocyte secretome. Huh-7 steatosis induction was validated to obtain the optimal combination and concentration off FFAs to induce a pathologic state and collect CCM.

In the case of the CCM experimental setup, various models of different incubation sequences, as presented in the CCM protocols, provide a solid, validated framework to test compounds of interest on LX-2 and Huh-7 in this NAFLD model. The first three models (**A-C**) investigated a basic validation of our proposed system, investigating the bioactivity of well-established controls and previously investigated compounds that were proven successful.

In **Models A** and **B**, activated LX-2 are treated with CCM from steatotic Huh-7 successively and simultaneously with controls, respectively, and observe if they manage to revert LX-2 to a quiescent-like state. Positive quiescence-inducing control Rol+PA managed to revert LX-2 cells to a physiological status by expressing abundant lipid droplets and not changing cell viability, even after or with treatment with Huh-7 steatotic secretome. In **Model C**, activated LX-2 were pre-treated with controls and bioactive PPCs with induction of a quiescent-like LX-2 state. These cells were successively treated with CCM from steatotic Huh-7, and we investigated if they retained their physiological state. We observed PPC antifibrotic activity of all employed PPCs supplemented additionally with silymarin (S 80, S 80 M and S 80 + Sily) by modulating lipid storage of LX-2, which resisted steatotic Huh-7 CCM without affecting cell viability.

Model D allowed us to examine the biological effect of Huh-7 CCM obtained from cells treated sequentially with investigational antisteatotic drugs, Ela and Oca, encapsulated in S 80 M liposomes on active and quiescent-like LX-2. Even though we could not revert activated LX-2 with CCM treatments, they kept their activated state. They did not proceed towards perpetuated state since their cell metabolic rate remained constant, and chosen fibrotic markers were not drastically changed to control conditions indicating activation stop.

CCM-treated quiescent-like LX-2 steadily retained their lipid droplet content and did not express any significant changes in mRNA expression of investigated fibrotic markers PLIN2 and PDGFRB, remaining constant to control conditions, below a cut-off level of statistical significance. There was a slight numerical decrease or constant in COL1A1 and ACTA2 expression suggesting retainment of quiescent-like status. However, Rol+PA positive control direct treatment showed a more prominent decrease trend of such marker mRNA

expressions, which confirms the robustness of the developed experimental setup to replicate *in vivo* biological effects.

Various Huh-7 steatosis induction protocols reported in the literature, our proposed LX-2 treatments and incubation sequences between both cell lines that can sincerely replicate NAFLD pathophysiology pose a significant challenge when developing a new *in vitro* system to investigate PPCs' bioactivity. A thorough screening of experimental conditions was necessary to obtain the optimal and reproducible setup replicating critical disease steps to observe the biological effect of proposed treatments. Considering that two employed cell lines have different culturing conditions was an additional factor to consider to avoid additional intrinsic changes in these models, and the rationale to opt for short-term 24 h direct treatments with various CCM from Huh-7 on different LX-2 states, such as simultaneous treatment with CCM, pre-treatment with PPC followed by CCM incubation, or treatment of activated and quiescent-like induced LX-2 with CCM from steatotic Huh-7 treated with antisteatotic APIs encapsulated in PPC. In this way, our innovation combined two independent cell models and investigated cross-talk between hepatocytes and HSCs employing only the CCM.

Further investigation should include additional assays such as genomics, proteomics, and lipidomics or examining different compounds and adjusting incubation times to screen cellular and molecular mechanisms affected by proposed treatments more thoroughly in this setup. The models presented in this Chapter are feasible to broaden and enhance the scope of the bioactivity investigation of various potentially anti-NAFLD and antisteatosis compounds. These extensions and modifications offer the opportunity to gather more comprehensive insights into complex NAFLD and further complement the research efforts to combat this ever-growing pathological condition.

Lastly, the opposite CCM system, CCM from activated LX-2 incubated on steatotic Huh-7, could not reduce the extent of steatosis in Huh-7. Further studies should be performed to investigate if there is a way to modulate involved pathways to revert hepatocytes' steatosis employing communication with quiescent-like HSCs.

We are confident that our findings shed light on the intricate nature of this NAFLD *in vitro* model and the biological activity of PPC-based formulations in this experimental setup. Our research serves as a valuable foundation and framework to investigate efficiently and rapidly the cross-talk among various liver cells concerning assessing the bioactivity of potentially effective APIs by employing cell-conditioned medium.

Chapter 5. Conclusions and Outlook

Non-alcoholic fatty liver disease (NAFLD) is the most common chronic liver condition globally. Its prevalence exceeds 25% worldwide and continues to rise steadily, making it an increasingly concerning pathology. The modern lifestyle and numerous epigenetic changes experienced by today's population contribute to this alarming trend. It can be estimated that within the next 15-20 years, this pathological condition will affect an evergrowing part of the world's population. NAFLD typically manifests with mild clinical symptoms, often presenting as an almost asymptomatic condition diagnosed during routine liver examinations. However, delayed NAFLD detection can result in a more pronounced and significant disease progression, leading to extensive tissue damage resolvable only by liver transplant if not treated in time. 57,58

Several APIs have been tested for treating chronic liver diseases in the last quarter of the century. However, no approved pharmacological treatment specifically targeting NAFLD exists. 92-94

The NAFLD complexity, along with the intricate interplay between different cell types, particularly hepatocytes and hepatic stellate cells (HSCs), further complicates therapeutic approaches to address NAFLD. Hepatocytes serve as a central metabolic core of the human body. At the same time, HSCs function as storage cells for vitamin A (retinol) and regulators of liver architecture. The "lipid paradox" in the liver also plays a significant role in the pathophysiologic modulation of this system. Even slight changes in the hepatocytes' status, such as minor steatosis, can trigger a complete rearrangement in HSCs, leading them to an activated pro-fibrotic state. Keeping a delicate physiological balance is crucial for maintaining a healthy state that potential therapy must comply with.

Chapter 1 introduces the liver and its pathological conditions, focusing on the underlying cellular and molecular mechanisms. It also contains an overview of the current state of antisteatotic and antifibrotic therapy, with listed clinical trials and the pharmacological mechanisms targeted by various drug classes. Additionally, an introduction to the key compounds in this dissertation, namely PPC, elafibranor and obeticholic acid, provides relevant background information on their usage and potential benefits in the research context. In **Chapter 2**, an extensive critical review of available human *in vitro* systems reproducing steatosis, a starting phase of NAFLD, is given, with a complete overview of the most used hepatocyte-like cell lines, steatosis induction experimental setups also focusing on technical details of incubation and steatogenic medium preparation with the list of all steatogenic compounds used.

The research in this dissertation focuses on two main parts. The first part in **Chapter 3** investigated a formulation of a new PPC-based tablet dosage form that exhibits bioactivity in the fibrotic liver. Development started from a newly available soybean PPC complex with magnesium salt, S 80 M, with favourable technological properties. This formulation can be a starting point for encapsulation with another API, active against NAFLD and fibrosis. It aims to reduce potential toxicity and enhance the inclusion of hydrophobic compounds.

Building upon a granule formulation previously formulated within our research group, extensive optimisation studies have been conducted by employing different excipients and using a Quality-by-Design/Design of Experiment approach to obtain the optimal high-lipid-content formulation that meets pharmacopoeial quality requirements. The final formulation underwent thorough physico-chemical and pharmacopoeial characterisation to evaluate all formulation properties critically.

PPCs were only available in the market for over three decades as hard capsules. These capsules have been traditionally used as nutraceuticals and supportive therapy for patients with various liver disorders. Our tablet formulation represents a novel development in the PPC formulation of phosphatidylcholine since the conversion of PPC into tablets was not previously explored due to its soft material appearance, low phase transition temperature, and high level of lipid unsaturation. The introduction of PPC tablets offers a new perspective. It opens avenues for formulating phospholipid-based tablets by carefully selecting excipients and modifying the preparation atmosphere.

Tablets are a preferred pharmaceutical form over hard capsules due to patient high compliance, more manageable and cost-effective production process. The PPC S 80 M tablet formulation, described as a bioactive excipient formulation, has demonstrated positive biological antifibrotic effects. It acts as an excipient, allowing another predominantly lipophilic API to be added, and itself as an API with established antifibrotic activity. Achieving a high lipid quantity of 70% provides ample flexibility for modifying the formulation for various purposes.

Soy PPC has traditionally been used as an emulsifier, particularly in the food industry. This property can be leveraged to develop a self-emulsifying drug delivery system that can be directly compressed or 3D printed into tablet form. Ongoing research in our group aims to optimise the S 80 M formulation with silymarin extract, creating a synergistic activity tablet to support patients with liver deficiencies.

Furthermore, *in vitro* validation of PPC bioactivity after tablet compression was performed using our well-established model of liver fibrosis in LX-2 cells. The experiments involved the

addition of cirrhotic primary rat hepatic stellate cells. They showed consistent trends of antifibrotic activity, including an increase in lipid droplet content in HSCs and a reduction in the expression level of the fibrotic activation marker PDGFRB.

The follow-up investigation of this research can include formulation incorporation with additional APIs indicated for antisteatotic and antifibrotic therapy. *In vivo* testing on a more biologically relevant rodent model of steatosis/NAFLD/cirrhosis is necessary to clarify further the biological activity of the current and potential future formulations. Such testing would provide a more comprehensive understanding of the effects and mechanisms of PPC treatment on a larger scale. Assays such as lipidomics, proteomics, and transcriptomics could enhance the biological activity characterisation of these tablet formulations and their potential therapeutic benefit.

Chapter 4 described the developing and optimising a dual cell culture system using a cell-conditioned medium (CCM) to investigate the cross-talk of steatotic hepatocytes and activated pro-fibrotic HSCs in indirect asynchronous contact. We explored the possibility of modulating this system by utilising antifibrotic and antisteatotic compounds. Steatosis induction in Huh-7 cells was validated to obtain the optimal combination and concentration of fatty acids to induce a pathological state and collect respective CCM.

The experimental setup utilised different incubation sequences to test compounds of interest on LX-2 and Huh-7. Activated or quiescent-like LX-2 treated with CCM from steatotic Huh-7, with various controls and compounds, to investigate their biological activity.

The results showed that positive controls successfully reverted LX-2 cells to a quiescent-like state even after or together with treatment with CCM from steatotic Huh-7, indicating potential therapeutic effects and showing an antifibrotic activity. This effect was retained in case LX-2 were pre-treated with PPC-based formulations. LX-2 remained quiescent-like, characterised by abundant lipid droplet content, after treatment with CCM from steatotic Huh-7.

Another model studied the biological effect of CCM originating from steatotic Huh-7 treated successively with investigational antisteatotic drugs, elafibranor and obeticholic acid, encapsulated in PPC-based liposomes. The results showed that the CCM treatments did not revert activated LX-2 but prevented them from progressing to a perpetuated state, and quiescent-like LX-2 did not lose their lipid-rich phenotype and transdifferentiated to an activated state. Chosen hallmark fibrotic markers mRNA transcription levels remained relatively constant in all cells, suggesting retention of the cell status.

Lastly, the additional model showed that reversing hepatocyte steatosis by using CCM from quiescent-like LX-2 was not successful, and further studies are needed to explore potential pathways for this reversal.

This study's innovative approach combined two independent cell models to investigate cross-talk between hepatocytes and HSCs using only the CCM, presenting a feasible and reproducible setup to investigate various compounds' bioactivity in NAFLD and fibrosis.

Further investigation is to be performed to better characterise this system, including additional assays, such as proteomics, genomics, lipidomic, and transcriptomics, with eventual adjustments to incubation times and sequences to gain more comprehensive insights into the cellular and molecular mechanisms affected and modulated by proposed treatments in this setup with particular regard to hepatocytes-HSCs interaction.

The described *in vitro* model provides a solid initial platform for conducting preliminary screenings of the bioactivity potential anti-NAFLD and anti-fibrosis therapeutics might exhibit. Future studies should involve testing additional compounds that could effectively treat these conditions. Overall, our findings shed light on the complex nature of the NAFLD *in vitro* model and the biological activity of PPC-based formulations in this experimental setup, providing a valuable foundation and framework for investigating liver cells cross-talk and assessing potential therapeutic compounds using the cell-conditioned medium.

Appendix

Chapter 3

Table A3.1. DoE constraints on components content for the extreme vertices design

	Amount		Proportion		Pseudocomponent	
Component	Lower	Upper	Lower	Upper	Lower	Upper
S 80 M	30.000	79.000	0.30000	0.79000	0.000000	1.000000
MCC	20.000	50.000	0.20000	0.50000	0.000000	0.612245
Neusilin® US2	1.000	20.000	0.01000	0.20000	0.000000	0.387755

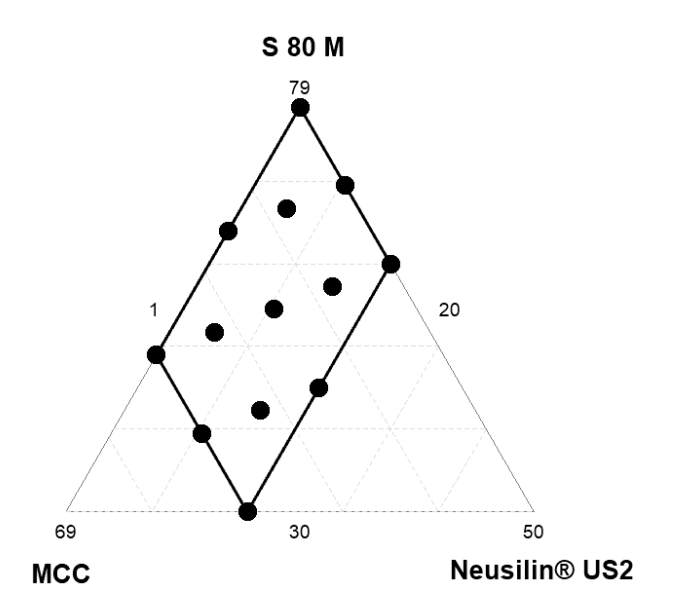


Figure A3.1. Extreme vertices DoE with lower and upper components' limits. The 13 points indicated in this graph identify calculated formulations in **Table 3.2**.

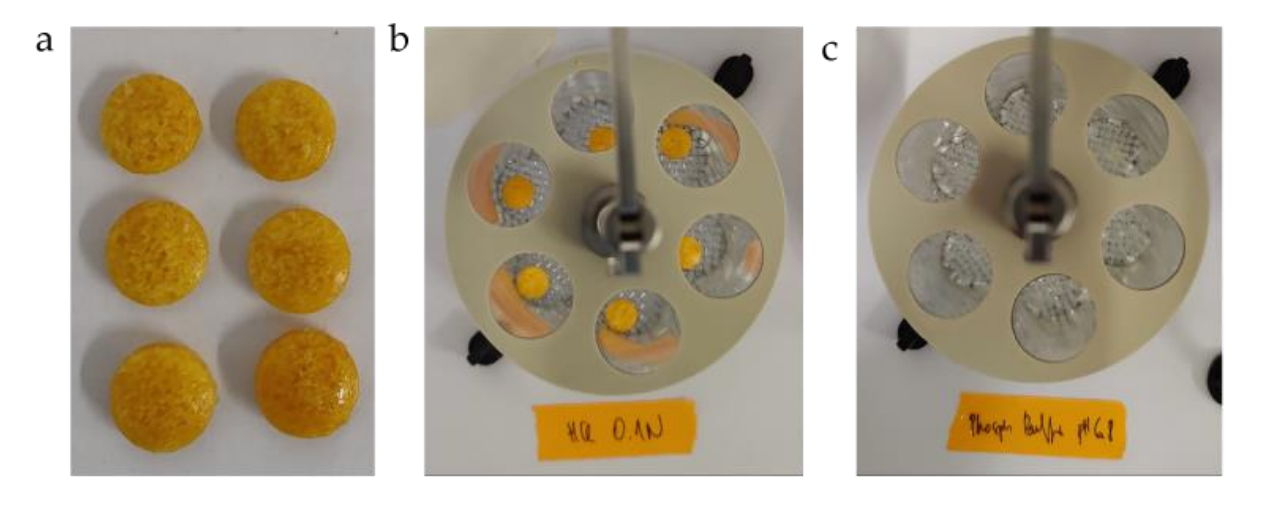


Figure A3.2. Enterically-coated tablets (a) Dried after coating. (b) After 2 hrs in 0.1 N HCl (c) After 1 hr in phosphate buffer pH 6.8.

A3.1 Lipid quantification – HPLC method

S 80 M lipid was extracted from tablets and reconstituted, as described in **Section 3.2.12**. Ultimate 3000 HPLC system (Thermo Fisher Scientific, Reinach, Switzerland) running Chromeleon (version 7.2) and equipped with a quaternary pump (LPG-3400SD), an autosampler (WPS-3000), a thermostatted column compartment (TCC-3000), a DAD (DAD-3000) and a CAD (Corona Veo RS) was used for lipid quantification. The following method has been adapted from the method developed in our lab. Reprospher 200 C18-DE 150 x 2mm with a particle size of 2 μ m and a pore size of 200 Å (Dr. Maisch, Ammerbuch, Germany) was used at 50 °C as the stationary phase. During the analysis, samples were refrigerated at 6 °C in the autosampler. The injection volume was 5 μ L, and the flow rate was constant at 0.5 mL/min. Three different eluents, eluent A: acetonitrile + 0.2 v/v% trifluoroacetic acid (TFA), eluent B: methanol + 0.2 v/v% TFA and eluent C: ultrapure water + 0.2 v/v% was used to create a linear gradient as described in **Table A3.2**. For the Corona Veo RS, the gas evaporation temperature was adjusted to 45 °C, data collection 10 Hz with filter 3.6 and the response rate was set to 100 pA. Palmitic acid (PA; 200 μ g/mL, Sigma Aldrich, Buchs, Switzerland) was used as an internal standard (IS).

Table A3.2. The method used for the analysis of lipids adapted from⁴⁴⁶.

Time (min)	Eluent A (%)	Eluent B (%)	Eluent C (%)
0	25	65	10
27	9.2	89.3	1.5
28	25	65	10
32	25	65	10

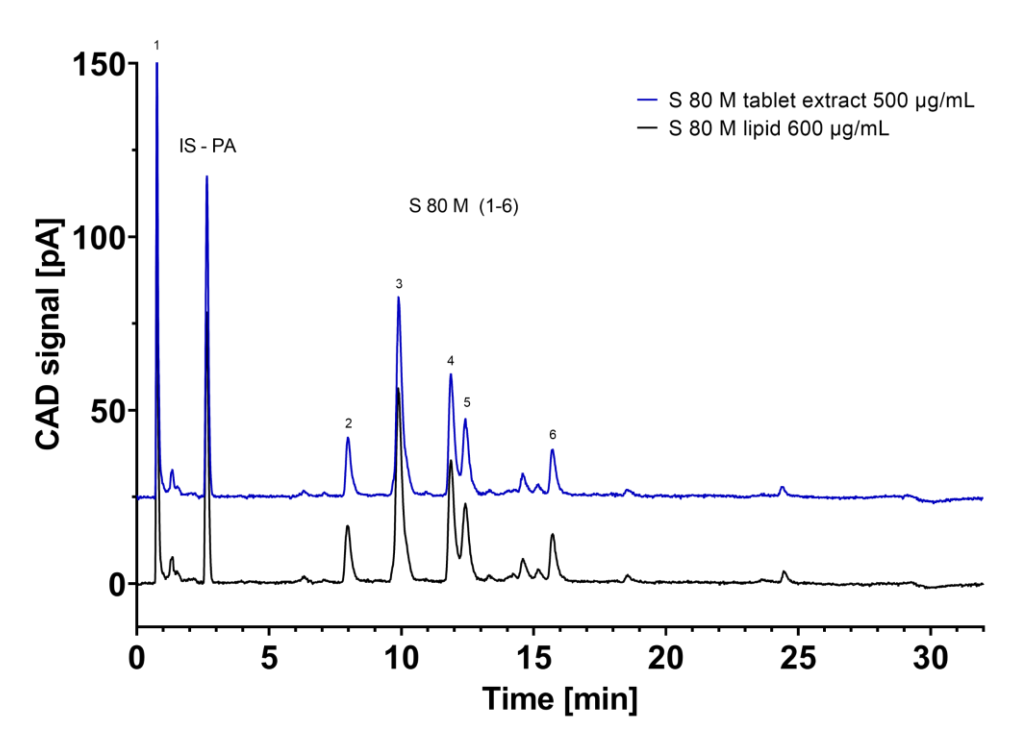


Figure A3.3. An overlay of two representative chromatograms of S 80 M lipid (600 μg/mL) and tablet extract (diluted to 500 μg/mL) obtained by HPLC-CAD. The chromatograms have been vertically offset for display purposes. IS: internal standard; PA: palmitic acid.

A3.2 Preparation and characterisation of liposomes

S 80 M (positive control) and DOPC (negative control) liposomes have been produced to compare their bioactivity with the one obtained from an S 80 M tablet extract to have a consistent internal control.

Liposomes containing the soybean-derived phospholipid S 80 M (S 80 M liposomes) and DOPC were prepared using the film hydration extrusion method. S137,408 Briefly, an appropriate aliquot of S 80 M lipid stock solution in MeOH was evaporated under a nitrogen stream until dry. The resulting thin lipid films were kept under a vacuum overnight to remove further traces of solvent. After hydration with HEPES buffer (10 mM, pH 7.4), the large multilamellar vesicles with a final lipid concentration of 50 mM were extruded 10 times through a 0.2-µm polycarbonate membrane at room temperature (RT) using a LIPEX® extruder. The LIPEX® extruder used to manufacture liposomes was from Transferra Nanosciences Inc. (Burnaby, B.C., Canada). Polycarbonate membranes were from Sterlitech (Auburn, WA, USA), and drain discs were from Whatman (Maidstone, UK).

Liposomes were analysed for the hydrodynamic diameter and the polydispersity index (PDI) with the LitesizerTM 500 (Anton Paar, Austria). Intensity size distribution was typically unimodal; therefore, the autocorrelation function was analysed using the cumulant method.

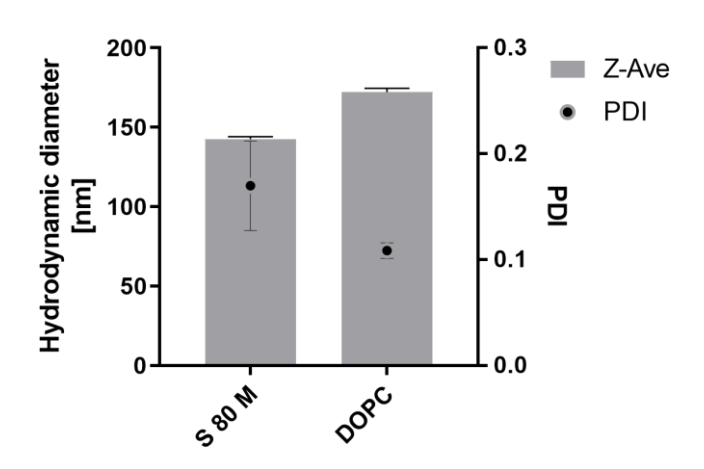


Figure A3.4. Hydrodynamic diameter and PDI for S 80 M and DOPC liposomal formulations immediately after preparation. Mean \pm SD, n = 3.

Table A3.3. Reverse transcription Master Mix composition.

Reagent	Manufacturer	Quantity	
Reverse transcriptase buffer 10x	Agilent	5	μL
DTT 100 mM	Stratagene	5	μL
dNTPs 10 mM	FisherScientific	2	μL
40 U/μL RiboLock RNAse inhibitor	Fermentas	0.5	μL
Reverse transcriptase 200 RXN	Agilent	1	μL
Total volume		13.5	μL

Table A3.4. Overview of the used primer pairs for qPCR.

Primer	Sequence
GAPDH fwd	5'-GAG TCA ACG GAT TTG GTC G-3'
GAPDH rev	5'-GAG GTC AAT GAA GGG GTC AT-3'
PLIN2 fwd	5'-GAT GGC AGA GAA CGG TGT GAA G-3'
PLIN2 rev	5'-CAG GCA TAG GTA TTG GCA ACT GC-3'
COL1A1 fwd	5'-GTT CAG TTT GGG TTG CTT GTC T-3'
COL1A1 rev	5'-CCT GCC CAT CAT CGA TGT G-3'
SPARC fwd	5'-TGC CTG ATG AGA CAG AGG TGG T-3'
SPARC rev	5'-CTT CGG TTT CCT CTG CAC CAT C-3'
ACTA2 fwd	5'-TAG CAC CCA GCA CCA TGA AG-3'
ACTA2 rev	5'-CTG CTG GAA GGT GGA CAG AG-3'
PDGFRB fwd	5'-CCT GCA ATG TGA CGG AGA GT-3'
PDGFRB rev	5'-GGT GCG GTT GTC TTT GAA CC-3'

All primer pairs used for qPCR on LX-2 cells (*Homo sapiens*) are commonly used in our research group and synthesised by Microsynth (Balgach, Switzerland).

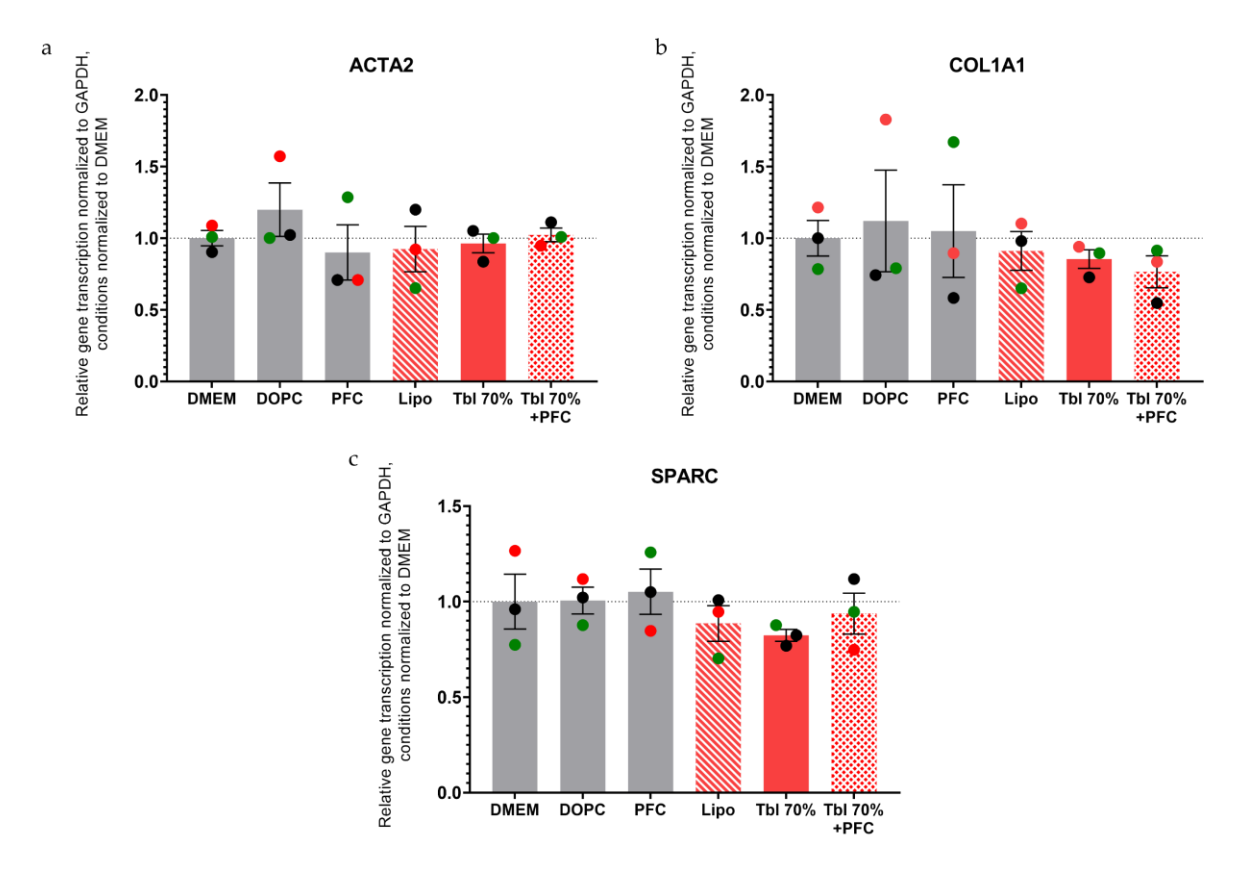


Figure A3.5. Relative mRNA transcription in LX-2 cells of other fibrosis markers (a) ACTA2 coding for α -SMA, (b) COL1A1 coding for collagen type I and (c) SPARC, normalised to GAPDH mRNA transcription and normalised to the DMEM condition after different phospholipid treatments: DMEM experimental medium (untreated); DOPC: inactive phospholipid used as negative control; PFC: protein-free chylomicron-like emulsions without S 80 M; Lipo: S 80 M liposomes; Tbl 70%: S 80 M tablet extract in buffer; Tbl 70% + PFC: tablet extract reconstituted as PFC-like emulsions. Mean ± S.E.M. (n=3).

Complete statistical analyses of **Figures 3.4-3.8** and **A3.5** are deposited in the general repository Zenodo and can be downloaded at this link: https://doi.org/10.5281/zenodo.8152217.

Chapter 4

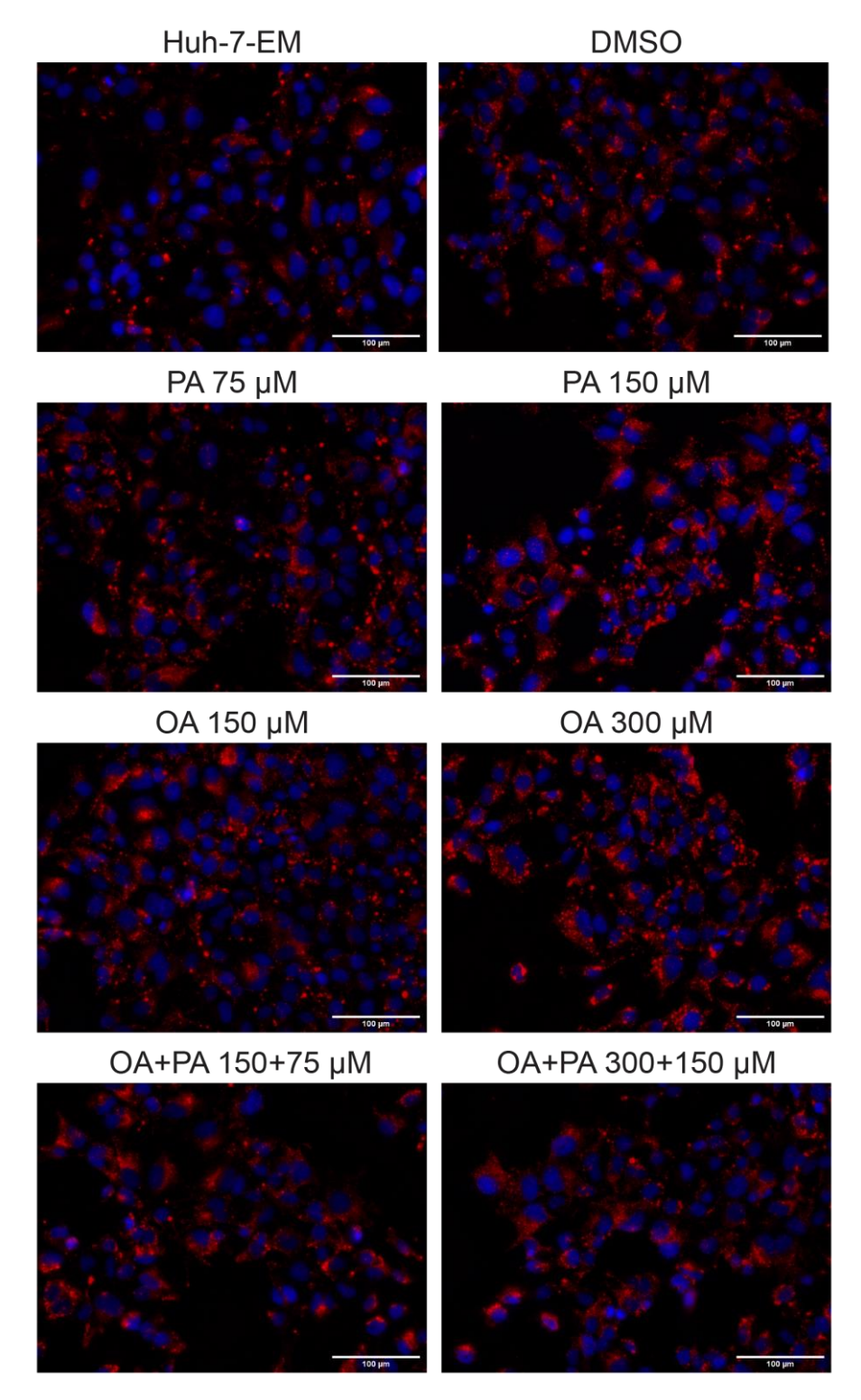


Figure A4.1. ORO staining of Huh-7 cells treated with various FFAs supplemented to Huh-7-EM: Huh-7-EM (untreated); DMSO vehicle control; PA palmitic acid; OA oleic acid.

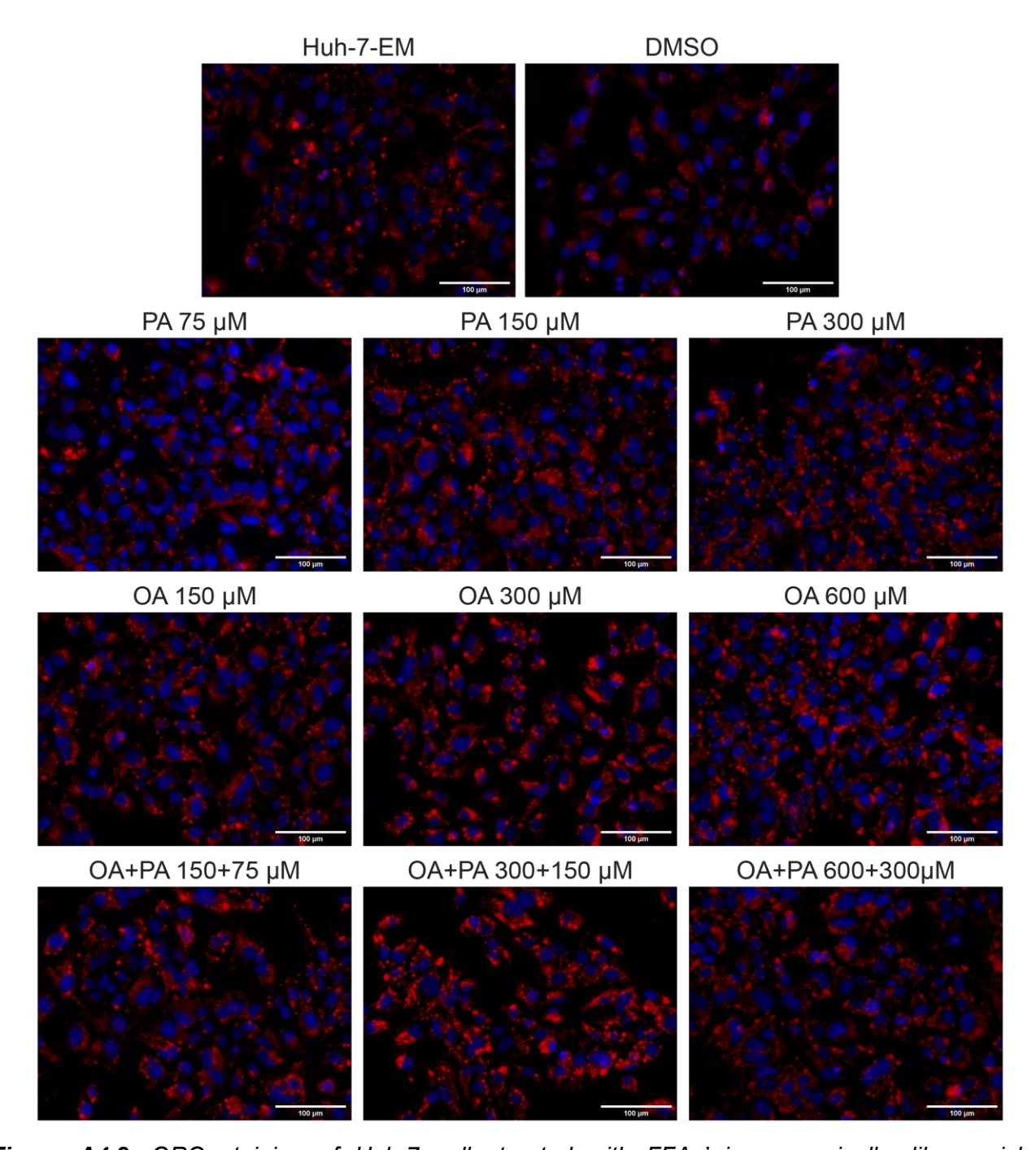


Figure A4.2. ORO staining of Huh-7 cells treated with FFAs' inverse micelles-like vesicles supplemented to Huh-7-EM. Huh-7-EM (untreated); DMSO vehicle control; PA palmitic acid; OA oleic acid.

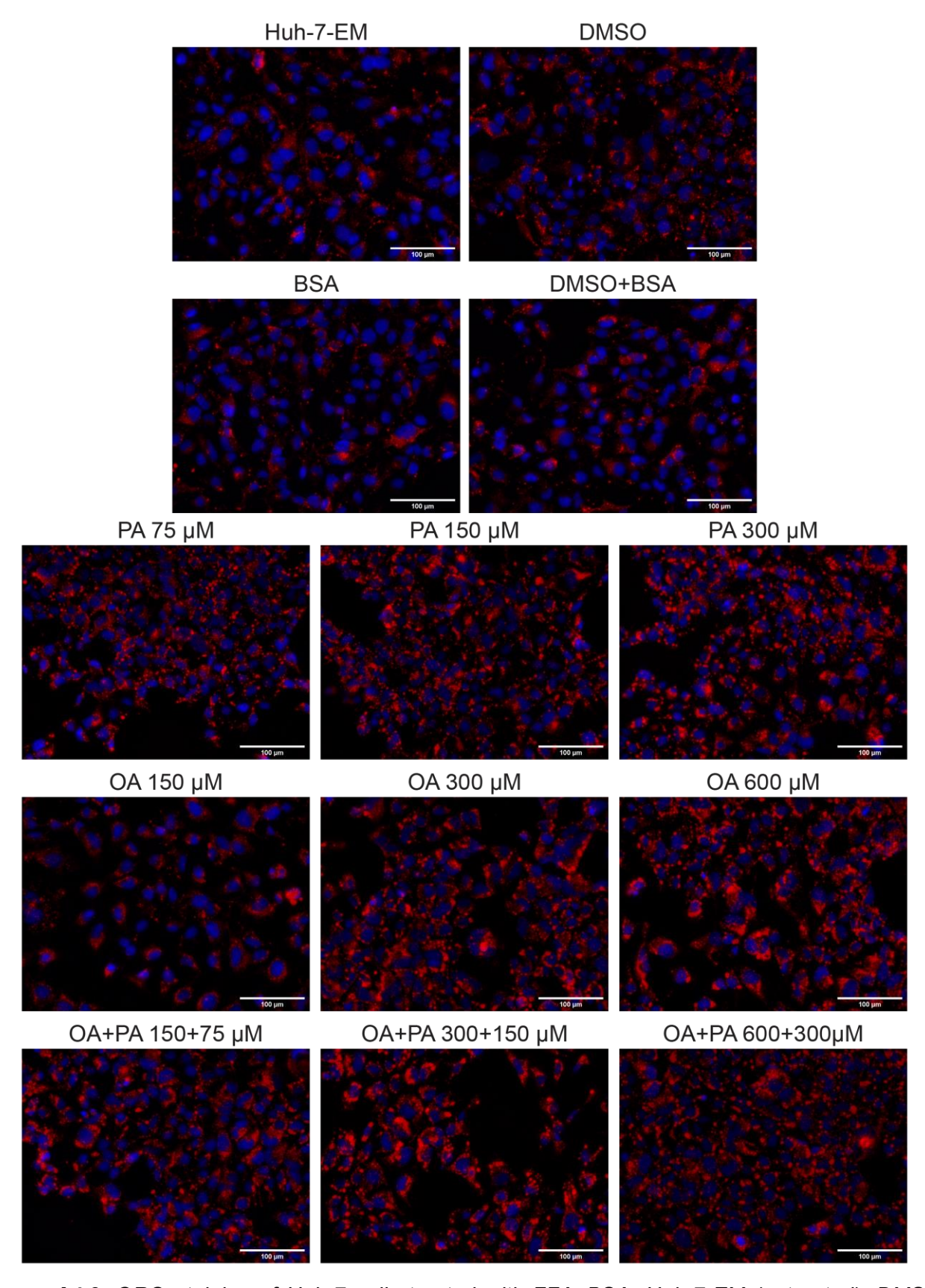


Figure A4.3. ORO staining of Huh-7 cells treated with FFA+BSA: Huh-7-EM (untreated); DMSO, BSA, and DMSO+BSA vehicle control; PA palmitic acid; OA oleic acid.

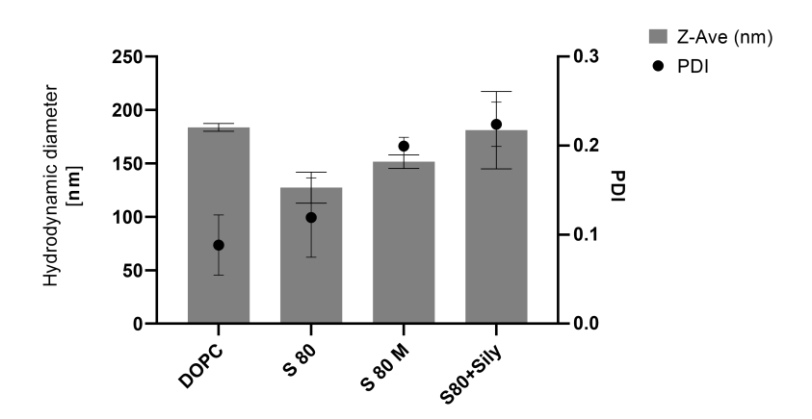


Figure A4.4. Hydrodynamic diameter and PDI for S 80, S 80 M, S80 + Sily and DOPC liposomal formulations immediately after preparation (**Sections 4.2.5.1 and 4.2.5.2**). Mean \pm SD, n = 3-6.

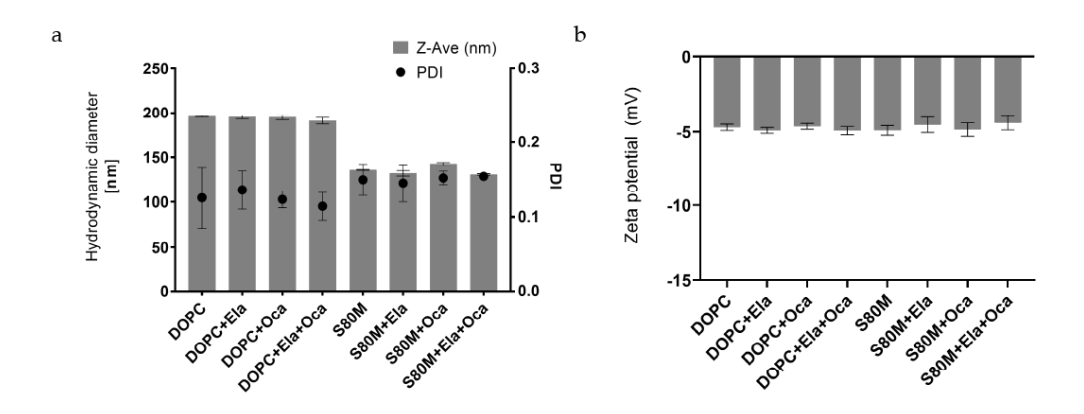


Figure A4.5. (a) Hydrodynamic diameter and PDI and (b) Zeta potential for DOPC and S 80 M with Ela and Oca liposomal formulations on Day 1 after preparation. Mean \pm SD, n = 3.

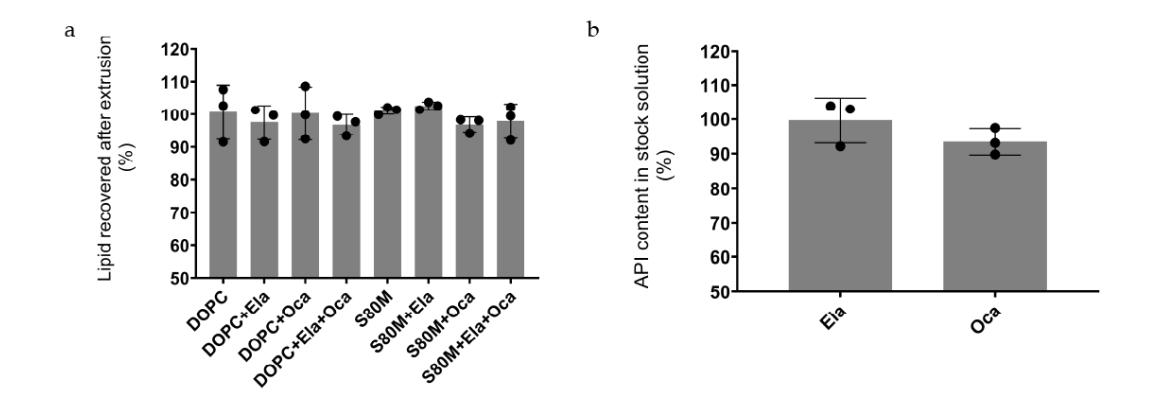


Figure A4.6. (a) Lipid recovery (%) after liposomes extrusion (**Section 4.2.5.3**) and (b) API content (%) in Ela and Oca stock solutions (**Section 4.2.3**) used to prepare these liposomes determined by HPLC-CAD method (**Section 4.2.9**). Mean \pm SD, n = 3.

A4.1 Direct treatment of naïve Huh-7 with antisteatotic liposomal formulations

The medium from seeded Huh-7 cells was discarded the day after cell seeding, the cells were washed once with PBS, and the steatogenic medium, prepared as described in **Section 4.2.4.3**, was added. Cells were incubated at 37 °C in a 5% CO₂ humidified atmosphere for 24 h. Control wells received equal volumes of naïve control Huh-7-EM.

Huh-7 control and steatogenic medium were discarded, cells were washed three times with PBS, and liposomal antisteatotic treatments (**Section 4.2.5.3**) were diluted with fresh naïve Huh-7-EM was resupplied to all the cells, left incubating for the following 24 h, and were assayed afterwards. Control wells received equal volumes of naïve control Huh-7-EM.

Naïve and steatotic Huh-7 cell viability was not affected by any treatments, excluding any possible toxicity of S 80 M, Ela, and Oca in this experimental setup.

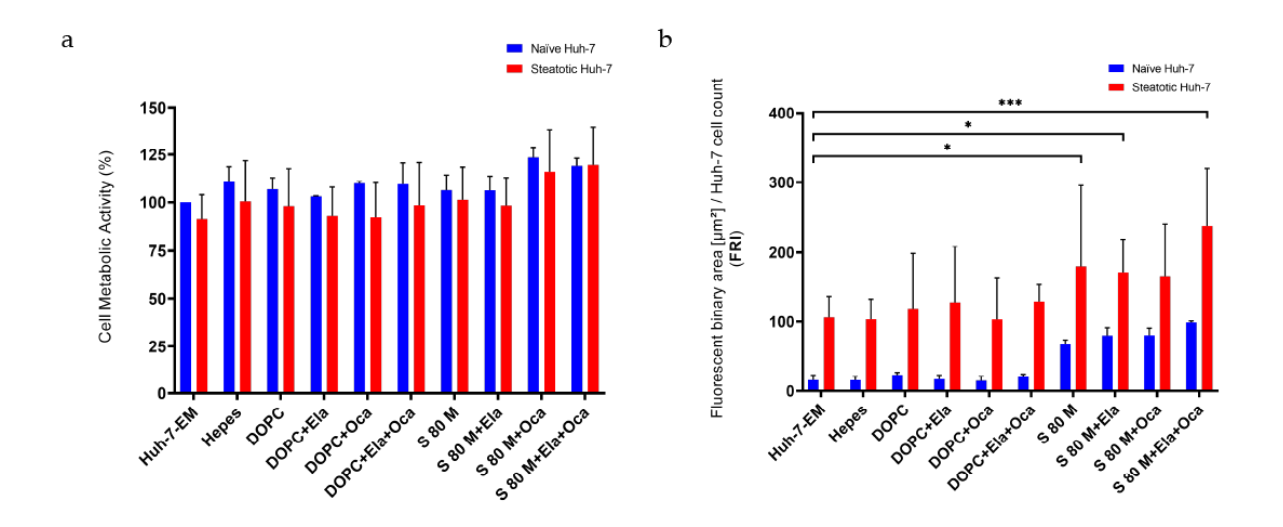


Figure A4.7. Direct treatment of naïve Huh-7 with antisteatotic liposomal formulations. (a) Huh-7 cell viability (%) using CCK-8 assay. (b) Quantification of the ORO staining fluorescence normalised to the number of Huh-7 cells in the DAPI field (FRI). Mean \pm S.D. (n=3). All comparisons in **Figure A4.7a** are not statistically significant. In **Figure A4.7b**, only p-values to naïve Huh-7-EM (control) are reported for convenience. p-values: *** p < 0.001, *p < 0.05. All p-values from ordinary one-way ANOVA with post-hoc Tukey's multiple comparison analysis are reported in supplementary tables to this Chapter.

The incubation of naïve Huh-7 cells with S 80 M-based liposomal formulations induced not statistically significant lipid accumulation, reported FRI 67.38, 80.10, 80.37, and 98.81 for S 80 M, S 80 M + Ela, S 80 M + Oca, and S 80 M + Ela + Oca, respectively. DOPC-based liposomes with or without antisteatotic APIs did not induce an increase in lipid droplet number

23.08 FRI (DOPC), 17.02 FRI (DOPC + Ela), 14.77 FRI (DOPC + Oca), and 21.00 FRI (DOPC + Ela + Oca) compared to 15.71 FRI (naïve Huh-7-EM control).

In the case of steatotic hepatocytes, a similar trend was observed, where S 80-based treatments show a slight numerical, but not statistically significant increase in the number of lipid droplet FRI of 180.10 (S 80 M), 171.30 (S 80 M + Ela), 165.90 (S 80 M + Oca), and 238.20 (S 80 M + Ela + Oca) are reported, in comparison to Huh-7-EM on steatotic cells 106.00 FRI. DOPC-based liposomes retained a level of lipid content at steatotic control. Interestingly both naïve and steatotic Huh-7 treated with S 80 M + Oca showed the highest numerical increase in FRI, which was not statistically different from other S 80 M-based formulations.

Complete statistical analyses of **Figures 4.7-4.11**, **4.13-4.14**, and **A4.7** are deposited in the general repository Zenodo and can be downloaded at this link: https://doi.org/10.5281/zenodo.8152217.

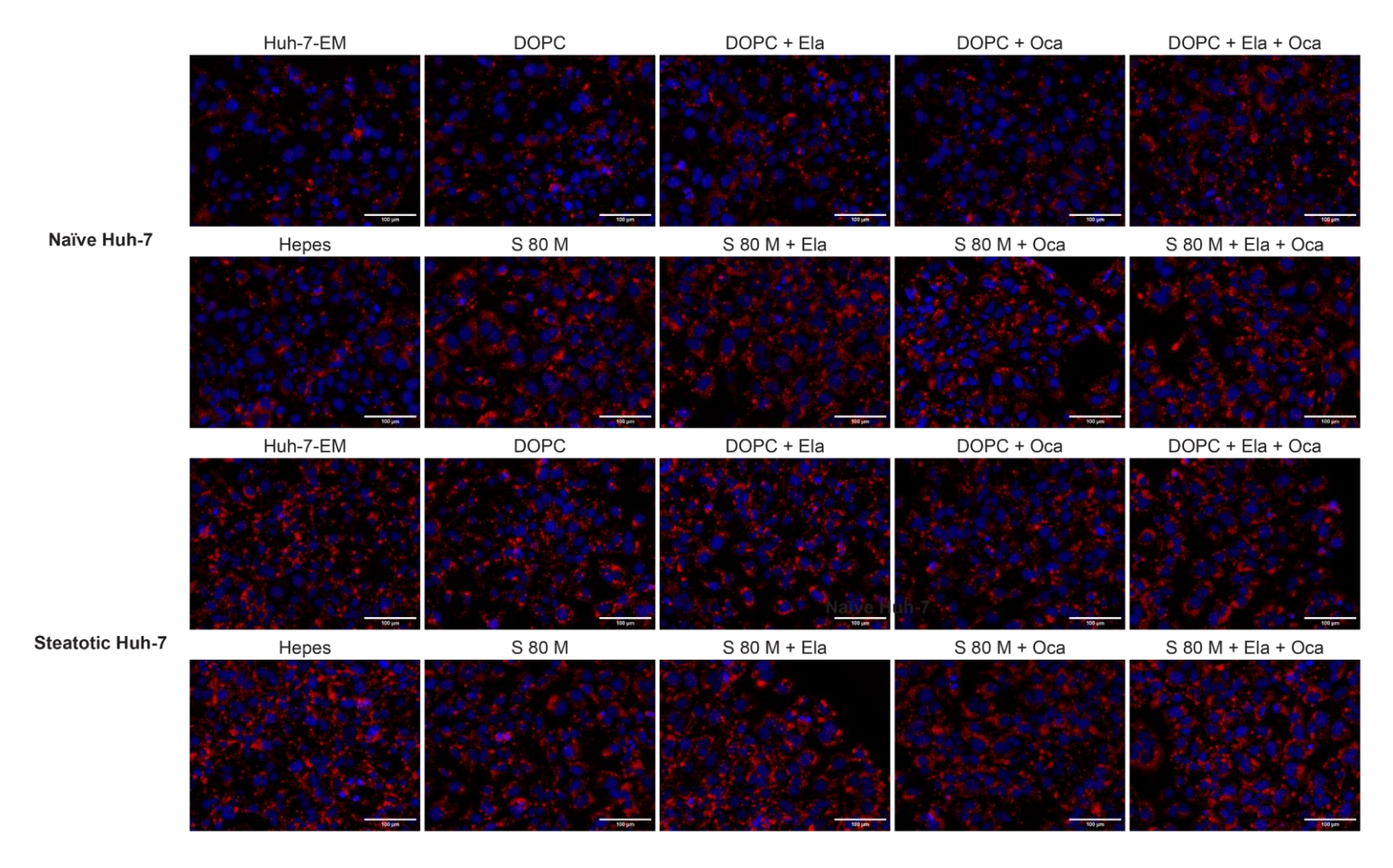


Figure A4.8. Direct treatment of naïve Huh-7 with antisteatotic liposomal formulations. Representative fluorescent images of ORO staining of Huh-7 cells treated with DOPC/S 80 M + Ela/Oca liposomes (Section 4.2.5.3): Huh-7-EM (untreated); HEPES vehicle control; DOPC inactive phospholipid used as negative control; S 80 M liposomal PPC formulation. DOPC/S 80 M + Ela, DOPC/S 80 M + Oca, DOPC/S 80 M + Ela + Oca combinations of DOPC and S 80 M with Ela and Oca, antisteatotic drugs. Lipid droplets can be visualised as red spots, and the nuclei are counterstained with blue DAPI.

List of abbreviations

17β-HSD13 – 17-β-hydroxysteroid dehydrogenase-DAG - diacylglycerol 13 DAPI - 4',6-diamidino-2-phenylindole 3D - three-dimensional DGAT1 - diacylglycerol-O-acyltransferase 1 3TC - lamivudine DoE - design-of-experiment AA – arachidonic acid (C20:4 ω -6) DHA – docosahexaenoic acid (C22:6, ω-3) AASLD - American Association for the Study of DLPC – 1,2-dilinoleoylphosphatidylcholine Liver Diseases DMEM-HG - Dulbecco's Modified Eagle Medium AAT - alanine aminotransferase with high glucose concentration (4.5 g/L), LX-2 ACN - acetonitrile medium ACTA2 – α-smooth muscle actin coding mRNA DMEM-LG - Dulbecco's Modified Eagle Medium AFP - alpha-1-fetoprotein with low glucose concentration (1 g/L), Huh-7 medium AIDS – acquired immune deficiency syndrome ALEH - La Asociación Latinoamericana para el DMSO - dimethyl sulfoxide Estudio del Hígado DOPC – 1,2-dioleoyl-sn-glycero-3-phosphocholine ALP - alkaline phosphatase DPH – 1,6-Diphenyl-1,3,5-hexatriene AMPK - 5' adenosine monophosphate-activated EASL - European Association for the Study of the protein kinase Liver ECM – extracellular matrix ANOVA – analysis of variance AP-1 - activator protein 1 Ela – elafibranor API – active pharmaceutical ingredient EPA - eicosapentaenoic acid (C20:5, ω-3) AZT or ZDV - zidovudine (from other name EPL - essential phospholipid azidothymidine) ER – endoplasmic reticulum BD - bulk density ESC - embryonal stem cell BSA - bovine serum albumin EtOH - ethanol EV - extracellular vesicle CAR – constitutive androstane receptor FaSSIF - fasted simulated state intestinal fluid CCK-8 - Cell Counting Kit-8 CCM - cell-conditioned medium FaSSGF - fasted state simulated gastric fluid cDNA - complementary deoxyribonucleic acid FBS – foetal bovine serum CHCl₃ - chloroform FDA – United States Food and Drug Administration CHOP - C/EBP homologous protein FFA - free fatty acid CI - compressibility index FRI – fluorescent Oil Red O relative intensity CIDE – cell death-inducing DFFA-like effector fwd - forward primer CLD - chronic liver disease FXR - farnesoid X receptor

COL1A1 - collagen type I coding mRNA

CTGF - connective tissue growth factor

CYP or CYP450 - cytochrome P450

d4T - stavudine

3-phosphate

g/mg/µg – gram/milligram/microgram

GAPDH

dehydrogenase

g/rcf - in centrifugation, the relative centrifugal field

glyceraldehyde

GRP78 – glucose-regulated protein 78 LDL-C – low-density lipoprotein cholesterin LSEC - liver sinusoidal endothelial cells GGT - y-glutamyltransferase GLP-1 – glucagon-like peptide 1 LX-2-CM/-EM/-TM - LX-2 complete medium, GLUT2 – glucose transporter 2 experimental medium, treatment medium GRAS - generally recognised as safe LXR - liver X receptor GSH - glutathione M / mM / µM / nM - molar / millimolar / micromolar h/min/sec - hour/minute/second / nanomolar HAEC - primary human aortic endothelial cell MASH _ dysfunction-associated metabolic HBV - hepatitis B virus steatohepatitis HCC - hepatocellular carcinoma MASLD – metabolic dysfunction-associated HCI - hydrochloric acid steatotic liver disease HCV - hepatitis C virus MCC - microcrystalline cellulose HDL – high-density lipoprotein MeOH - methanol HEPES - 4-(2-hydroxyethyl) piperazine-1-ethane MetALD - metabolic dysfunction-associated liver sulfonic acid sodium disease HIEC - human intestine epithelial cells MM - Master Mix HIV - human immunodeficiency virus MMP - matrix metalloprotease HLC - hepatocyte-like cell MMP-2 - matrix metalloprotease 2 **HPLC-CAD** high-performance liquid mTorr - millitorr (1 mTorr = 0.133322 Pa) chromatography-charged aerosol detector N – newton NADPH - nicotinamide adenine dinucleotide HR - Hausner's ratio HSC - hepatic stellate cell phosphate **HSPC** hydrogenated soybean NAFLD - non-alcoholic fatty liver diseases phosphatidylcholine NAFL - non-alcoholic fatty liver hTERT - human telomerase reverse transcriptase NaOH - sodium hydroxide Huh-7-CM/-EM - Huh-7 complete medium, NASH - non-alcoholic steatohepatitis experimental medium NF-κB – nuclear factor kappa-light-chain-enhancer I_{II} – parallel fluorescent intensity of activated B cells Nrf2/CES1 - nuclear factor erythroid 2-related factor I_⊥– perpendicular fluorescent intensity IL - interleukin 2 - carboxylesterase 1 IMDM - Iscove's Modified Dulbecco's Medium n.s. - statistically non-significant OA – oleic acid (C18:1, ω -9), oleate iNOS - inducible nitric oxide synthase iPSC - induced pluripotent stem cell Oca - obeticholic acid OD - optical density IS – internal standard (in HPLC-CAD) ORO - Oil Red O staining JAK-STAT3 – Janus kinase – signal transducer and activator of transcription 3 PA – palmitic acid (C16:0), palmitate JNK - c-Jun N-terminal kinase PB - phosphate buffer L/mL/µL - litre PBC - primary biliary cholangitis PBS - phosphate buffer saline pH 7.4, without LD – lipid droplet Ca/Mg LDL - low-density lipoprotein

PC - phosphatidylcholine

PDGF - platelet-derived growth factor

PDGFR- β – platelet-derived growth factor receptor-

β

PDGFRB - platelet-derived growth factor receptor

β coding mRNA

PDI – polydispersity index

PFC – protein-free chylomicron-like emulsions

Ph. Eur. – European Pharmacopoeia 11th edition

PHH - primary human hepatocyte

PHHSC - primary human hepatic stellate cell

PKC - phosphokinase C

PLC/PRF/5 - Primary Liver

Carcinoma/Poliomyelitis Research Foundation/5

(hepatocarcinoma cell line)

PLIN2 - perilipin 2

PO – palmitoleic acid (C16:1, ω-7), palmitoleate

PPAR - peroxisome proliferator-activated receptor

PPC - polyenylphosphatidylcholine

PRHSC - primary rat hepatic stellate cells

PXR - Pregnane X receptor

QbD - quality by design

qPCR - quantitative polymerase chain reaction

r - calculated fluorescent anisotropy

RAR - retinoic acid receptor

rev - reverse primer

RH – relative humidity

RNA - ribonucleic acid

Rol – retinol

ROS - reactive oxygen species

rpm - revolutions per minute

RPV - rilpivirine

RRID - Cellosaurus cell line research resource

identifier

RT - room temperature

RXR - retinoid X receptor

S 80 - Soybean phospholipid with 75%

phosphatidylcholine

S 80 M - Soluthin® S 80 M, soybean phospholipid

80% complexed with MgCl $_{\!2}$

SA – stearic acid (C18:0), stearate

S.D. - standard deviation

S.E.M. – standard error of the mean

SGLT-2 – sodium-glucose linked transporter 2

Sily - silymarin extract from Silybum marianum

SPARC - secreted protein acidic and rich in

cysteine

SPC – saturated phosphatidylcholine

SREBP-1 - sterol regulatory element-binding

protein

T2DM - type 2 diabetes mellitus

TAA - thioacetamide

TAG - triacylglycerol

TCDD – 2,3,7,8-tetrachlorodibenzo-p-dioxin

TD - tapped density

TFA - trifluoroacetic acid

TGA - thermogravimetry

 $TGF-\beta_1$ – transforming growth factor β_1

TIMP - tissue inhibitors of metalloproteinases

TMA-DPH - N,N,N-trimethyl-4-(6-phenyl-1,3,5-

hexatrien-1-yl)-phenyl-ammonium-p-

toluolsulfonate

TNF-α – tumour necrosis factor-alpha

U/mL – units per millilitre

UDCA - ursodeoxycholic acid

UK - United Kingdom

US/USA - United States of America

VA - valproic acid, valproate

VEGFA - vascular endothelial growth factor A

v/v – volume-to-volume (concentration)

w/v - weight-to-volume (concentration)

w/w – weight-to-weight (concentration)

WB - Western blot

XRPD - X-ray powder diffraction

 α -SMA – α -smooth muscle actin

 λ_{em} – emission wavelength in nm

λ_{ex} – excitation wavelength in nm

 ω - omega, in the designation of fatty acids,

location of the first double bond

Bibliography

- Trefts, E., Gannon, M. & Wasserman, D. H. The liver. *Curr. Biol.* **27**, R1147-R1151, doi:10.1016/j.cub.2017.09.019 (2017).
- Nagy, P., Thorgeirsson, S. S. & Grisham, J. W. in *The Liver* 1-13 (2020).
- Gao, B., Jeong, W. I. & Tian, Z. Liver: An organ with predominant innate immunity. *Hepatology* **47**, 729-736, doi:10.1002/hep.22034 (2008).
- Willekens, F. L. *et al.* Liver Kupffer cells rapidly remove red blood cell-derived vesicles from the circulation by scavenger receptors. *Blood* **105**, 2141-2145, doi:10.1182/blood-2004-04-1578 (2005).
- 5 Nguyen, P. *et al.* Liver lipid metabolism. *J. Anim. Physiol. Anim. Nutr. (Berl.)* **92**, 272-283, doi:10.1111/j.1439-0396.2007.00752.x (2008).
- Gu, X. & Manautou, J. E. Molecular mechanisms underlying chemical liver injury. *Expert Rev. Mol. Med.* **14**, e4, doi:10.1017/S1462399411002110 (2012).
- 7 Klaunig, J. E., Li, X. & Wang, Z. Role of xenobiotics in the induction and progression of fatty liver disease. *Toxicol Res (Camb)* **7**, 664-680, doi:10.1039/c7tx00326a (2018).
- 8 Abdel-Misih, S. R. & Bloomston, M. Liver anatomy. *Surg. Clin. North Am.* **90**, 643-653, doi:10.1016/j.suc.2010.04.017 (2010).
- 9 Molina, D. K. & DiMaio, V. J. M. Normal Organ Weights in Men Part II-The Brain, Lungs, Liver, Spleen, and Kidneys. *Am. J. Forensic Med. Pathol.* **33**, 368-372, doi:10.1097/PAF.0b013e31823d29ad (2012).
- Rappaport, A. M., Borowy, Z. J., Lougheed, W. M. & Lotto, W. N. Subdivision of hexagonal liver lobules into a structural and functional unit; role in hepatic physiology and pathology. *Anat. Rec.* **119**, 11-33, doi:10.1002/ar.1091190103 (1954).
- Eipel, C., Abshagen, K. & Vollmar, B. Regulation of hepatic blood flow: the hepatic arterial buffer response revisited. *World J. Gastroenterol.* **16**, 6046-6057, doi:10.3748/wjg.v16.i48.6046 (2010).
- Vollmar, B. & Menger, M. D. The hepatic microcirculation: mechanistic contributions and therapeutic targets in liver injury and repair. *Physiol. Rev.* **89**, 1269-1339, doi:10.1152/physrev.00027.2008 (2009).
- Carneiro, C. *et al.* All about portal vein: a pictorial display to anatomy, variants and physiopathology. *Insights Imaging* **10**, 38, doi:10.1186/s13244-019-0716-8 (2019).
- Sera, T., Sumii, T., Fujita, R. & Kudo, S. Effect of shear stress on the migration of hepatic stellate cells. *In Vitro Cell. Dev. Biol. Anim.* **54**, 11-22, doi:10.1007/s11626-017-0202-x (2018).
- Wang, L. & Boyer, J. L. The maintenance and generation of membrane polarity in hepatocytes. *Hepatology* **39**, 892-899, doi:10.1002/hep.20039 (2004).
- 16 Cunningham, R. P. & Porat-Shliom, N. Liver Zonation Revisiting Old Questions With New Technologies. *Front. Physiol.* **12**, 732929, doi:10.3389/fphys.2021.732929 (2021).
- Jungermann, K. & Katz, N. Functional specialization of different hepatocyte populations. *Physiol. Rev.* **69**, 708-764, doi:10.1152/physrev.1989.69.3.708 (1989).
- 18 Krishna, M. Microscopic anatomy of the liver. *Clin Liver Dis (Hoboken)* **2**, S4-S7, doi:10.1002/cld.147 (2013).
- Manco, R., Leclercq, I. A. & Clerbaux, L. A. Liver Regeneration: Different Sub-Populations of Parenchymal Cells at Play Choreographed by an Injury-Specific Microenvironment. *Int. J. Mol. Sci.* **19**, doi:10.3390/ijms19124115 (2018).
- Damm, G. *et al.* Human parenchymal and non-parenchymal liver cell isolation, culture and characterization. *Hepatol. Int.* **7**, 951-958, doi:10.1007/s12072-013-9475-7 (2013).
- 21 Kmiec, Z. Cooperation of liver cells in health and disease. *Adv. Anat. Embryol. Cell Biol.* **161**, III-XIII, 1-151, doi:10.1007/978-3-642-56553-3 (2001).
- 22 Atzori, L., Poli, G. & Perra, A. Hepatic stellate cell: a star cell in the liver. *Int. J. Biochem. Cell Biol.* **41**, 1639-1642, doi:10.1016/j.biocel.2009.03.001 (2009).
- Puche, J. E., Saiman, Y. & Friedman, S. L. Hepatic stellate cells and liver fibrosis. *Compr Physiol* **3**, 1473-1492, doi:10.1002/cphy.c120035 (2013).
- Friedman, S. L. Hepatic stellate cells: protean, multifunctional, and enigmatic cells of the liver. *Physiol. Rev.* **88**, 125-172, doi:10.1152/physrev.00013.2007 (2008).
- 25 Senoo, H., Mezaki, Y. & Fujiwara, M. The stellate cell system (vitamin A-storing cell system). *Anat Sci Int* **92**, 387-455, doi:10.1007/s12565-017-0395-9 (2017).
- Cai, X. *et al.* Intercellular crosstalk of hepatic stellate cells in liver fibrosis: New insights into therapy. *Pharmacol. Res.* **155**, 104720, doi:10.1016/j.phrs.2020.104720 (2020).
- Blaner, W. S. *et al.* Hepatic stellate cell lipid droplets: a specialized lipid droplet for retinoid storage. *Biochim. Biophys. Acta* **1791**, 467-473, doi:10.1016/j.bbalip.2008.11.001 (2009).
- Wake, K. Hepatic stellate cells: Three-dimensional structure, localization, heterogeneity and development. *Proc. Jpn. Acad. Ser. B Phys. Biol. Sci.* **82**, 155-164, doi:10.2183/pjab.82.155 (2006).

- 29 Higashi, N. *et al.* Vitamin A storage in hepatic stellate cells in the regenerating rat liver: with special reference to zonal heterogeneity. *Anat. Rec. A. Discov. Mol. Cell. Evol. Biol.* **286**, 899-907, doi:10.1002/ar.a.20230 (2005).
- Pellicoro, A., Ramachandran, P., Iredale, J. P. & Fallowfield, J. A. Liver fibrosis and repair: immune regulation of wound healing in a solid organ. *Nat. Rev. Immunol.* **14**, 181-194, doi:10.1038/nri3623 (2014).
- Pinzani, M. *et al.* Expression of platelet-derived growth factor and its receptors in normal human liver and during active hepatic fibrogenesis. *Am. J. Pathol.* **148**, 785-800 (1996).
- Cordero-Espinoza, L. & Huch, M. The balancing act of the liver: tissue regeneration versus fibrosis. *J. Clin. Invest.* **128**, 85-96, doi:10.1172/JCl93562 (2018).
- Michalopoulos, G. K. & Bhushan, B. Liver regeneration: biological and pathological mechanisms and implications. *Nat. Rev. Gastroenterol. Hepatol.* **18**, 40-55, doi:10.1038/s41575-020-0342-4 (2021).
- Parola, M. & Pinzani, M. Hepatic wound repair. *Fibrogenesis Tissue Repair* **2**, 4, doi:10.1186/1755-1536-2-4 (2009).
- Kurokawa, T. & Ohkohchi, N. in *Stem Cells and Cancer in Hepatology* (ed Yun-Wen Zheng) 159-177 (Academic Press, 2018).
- Heidelbaugh, J. J. & Bruderly, M. Cirrhosis and chronic liver failure: part I. Diagnosis and evaluation. *Am. Fam. Physician* **74**, 756-762 (2006).
- Du, T. et al. Vitamin D improves hepatic steatosis in NAFLD via regulation of fatty acid uptake and betaoxidation. Front. Endocrinol. (Lausanne) **14**, 1138078, doi:10.3389/fendo.2023.1138078 (2023).
- 38 Asrani, S. K., Devarbhavi, H., Eaton, J. & Kamath, P. S. Burden of liver diseases in the world. *J. Hepatol.* **70**, 151-171, doi:10.1016/j.jhep.2018.09.014 (2019).
- 39 Schaffner, F. & Thaler, H. Nonalcoholic fatty liver disease. *Prog. Liver Dis.* 8, 283-298 (1986).
- Hashimoto, E., Tokushige, K. & Ludwig, J. Diagnosis and classification of non-alcoholic fatty liver disease and non-alcoholic steatohepatitis: Current concepts and remaining challenges. *Hepatol. Res.* **45**, 20-28, doi:10.1111/hepr.12333 (2015).
- Rombouts, K. & Marra, F. Molecular mechanisms of hepatic fibrosis in non-alcoholic steatohepatitis. *Dig. Dis.* **28**, 229-235, doi:10.1159/000282094 (2010).
- 42 Rinella, M. E. *et al.* A multi-society Delphi consensus statement on new fatty liver disease nomenclature. *J. Hepatol.*, doi:10.1016/j.jhep.2023.06.003 (2023).
- American Association for the Study of Liver Diseases, L. A. A. f. t. S. o. t. L. E. A. f. t. S. o. t. L. A call for unity: The path towards a more precise and patient-centric nomenclature for NAFLD. *Hepatology* **78** (2023).
- American Association for the Study of Liver Diseases. Electronic address, g. I. o., Latin American Association for the Study of the, L. & European Association for the Study of the, L. A call for unity: The path towards a more precise and patient-centric nomenclature for NAFLD. *Ann. Hepatol.* **28**, 101115, doi:10.1016/j.aohep.2023.101115 (2023).
- 45 Devarbhavi, H. *et al.* Global burden of Liver Disease: 2023 Update. *J. Hepatol.*, doi:10.1016/j.jhep.2023.03.017 (2023).
- Tryndyak, V. P. *et al.* Non-alcoholic fatty liver disease-associated DNA methylation and gene expression alterations in the livers of Collaborative Cross mice fed an obesogenic high-fat and high-sucrose diet. *Epigenetics* **17**, 1462-1476, doi:10.1080/15592294.2022.2043590 (2022).
- 47 Malnick, S. D., Beergabel, M. & Knobler, H. Non-alcoholic fatty liver: a common manifestation of a metabolic disorder. *QJM* **96**, 699-709, doi:10.1093/qjmed/hcg120 (2003).
- Kneeman, J. M., Misdraji, J. & Corey, K. E. Secondary causes of nonalcoholic fatty liver disease. *Therap. Adv. Gastroenterol.* **5**, 199-207, doi:10.1177/1756283X11430859 (2012).
- 49 Byrne, C. D. & Targher, G. NAFLD: a multisystem disease. *J. Hepatol.* **62**, S47-64, doi:10.1016/j.jhep.2014.12.012 (2015).
- Friedman, S. L., Neuschwander-Tetri, B. A., Rinella, M. & Sanyal, A. J. Mechanisms of NAFLD development and therapeutic strategies. *Nat. Med.* **24**, 908-922, doi:10.1038/s41591-018-0104-9 (2018).
- Buzzetti, E., Pinzani, M. & Tsochatzis, E. A. The multiple-hit pathogenesis of non-alcoholic fatty liver disease (NAFLD). *Metabolism* **65**, 1038-1048, doi:10.1016/j.metabol.2015.12.012 (2016).
- Tilg, H. & Moschen, A. R. Evolution of inflammation in nonalcoholic fatty liver disease: the multiple parallel hits hypothesis. *Hepatology* **52**. 1836-1846. doi:10.1002/hep.24001 (2010).
- Farrell, G. C., Haczeyni, F. & Chitturi, S. Pathogenesis of NASH: How Metabolic Complications of Overnutrition Favour Lipotoxicity and Pro-Inflammatory Fatty Liver Disease. *Adv. Exp. Med. Biol.* **1061**, 19-44, doi:10.1007/978-981-10-8684-7 3 (2018).
- Matteoni, C. A. *et al.* Nonalcoholic fatty liver disease: a spectrum of clinical and pathological severity. *Gastroenterology* **116**, 1413-1419, doi:10.1016/s0016-5085(99)70506-8 (1999).

- Yu, S. *et al.* Pathogenesis from Inflammation to Cancer in NASH-Derived HCC. *J Hepatocell Carcinoma* **9**, 855-867, doi:10.2147/JHC.S377768 (2022).
- Singh, S. *et al.* Fibrosis progression in nonalcoholic fatty liver vs nonalcoholic steatohepatitis: a systematic review and meta-analysis of paired-biopsy studies. *Clin. Gastroenterol. Hepatol.* **13**, 643-654 e641-649; quiz e639-640, doi:10.1016/j.cgh.2014.04.014 (2015).
- 57 Pratt, D. S. & Kaplan, M. M. Evaluation of abnormal liver-enzyme results in asymptomatic patients. *N. Engl. J. Med.* **342**, 1266-1271, doi:10.1056/NEJM200004273421707 (2000).
- Arendt, B. M. *et al.* Altered hepatic gene expression in nonalcoholic fatty liver disease is associated with lower hepatic n-3 and n-6 polyunsaturated fatty acids. *Hepatology* **61** (2015).
- Tilg, H., Adolph, T. E., Dudek, M. & Knolle, P. Non-alcoholic fatty liver disease: the interplay between metabolism, microbes and immunity. *Nat Metab* **3**, 1596-1607, doi:10.1038/s42255-021-00501-9 (2021).
- Grossini, E. *et al.* Exposure to Plasma From Non-alcoholic Fatty Liver Disease Patients Affects Hepatocyte Viability, Generates Mitochondrial Dysfunction, and Modulates Pathways Involved in Fat Accumulation and Inflammation. *Front Med (Lausanne)* **8**, 693997, doi:10.3389/fmed.2021.693997 (2021).
- Robinson, K. E. & Shah, V. H. Pathogenesis and pathways: nonalcoholic fatty liver disease & alcoholic liver disease. *Transl Gastroenterol Hepatol* **5**, 49, doi:10.21037/tgh.2019.12.05 (2020).
- Nassir, F., Rector, R. S., Hammoud, G. M. & Ibdah, J. A. Pathogenesis and Prevention of Hepatic Steatosis. *Gastroenterol Hepatol (N Y)* **11**, 167-175 (2015).
- Ress, C. & Kaser, S. Mechanisms of intrahepatic triglyceride accumulation. *World J. Gastroenterol.* **22**, 1664-1673, doi:10.3748/wjg.v22.i4.1664 (2016).
- Takahashi, Y. & Fukusato, T. Histopathology of nonalcoholic fatty liver disease/nonalcoholic steatohepatitis. *World J. Gastroenterol.* **20**, 15539-15548, doi:10.3748/wjg.v20.i42.15539 (2014).
- 65 Caldwell, S. *et al.* Hepatocellular ballooning in NASH. *J. Hepatol.* **53**, 719-723, doi:10.1016/j.jhep.2010.04.031 (2010).
- Trautwein, C., Friedman, S. L., Schuppan, D. & Pinzani, M. Hepatic fibrosis: Concept to treatment. *J. Hepatol.* **62**, S15-24, doi:10.1016/j.jhep.2015.02.039 (2015).
- 67 Bataller, R. & Brenner, D. A. Liver fibrosis. *J. Clin. Invest.* **115**, 209-218, doi:10.1172/JCl24282 (2005).
- Tsuchida, T. & Friedman, S. L. Mechanisms of hepatic stellate cell activation. *Nat. Rev. Gastroenterol. Hepatol.* **14**, 397-411, doi:10.1038/nrgastro.2017.38 (2017).
- Lee, U. E. & Friedman, S. L. Mechanisms of hepatic fibrogenesis. *Best Pract. Res. Clin. Gastroenterol.* **25**, 195-206, doi:10.1016/j.bpg.2011.02.005 (2011).
- Smith-Cortinez, N. *et al.* Collagen release by human hepatic stellate cells requires vitamin C and is efficiently blocked by hydroxylase inhibition. *FASEB J.* **35**, e21219, doi:10.1096/fj.202001564RR (2021).
- Trivedi, P., Wang, S. & Friedman, S. L. The Power of Plasticity-Metabolic Regulation of Hepatic Stellate Cells. *Cell Metab.* **33**, 242-257, doi:10.1016/j.cmet.2020.10.026 (2021).
- Schumacher, J. D. & Guo, G. L. Regulation of Hepatic Stellate Cells and Fibrogenesis by Fibroblast Growth Factors. *Biomed Res Int* **2016**, 8323747, doi:10.1155/2016/8323747 (2016).
- Wobser, H. *et al.* Lipid accumulation in hepatocytes induces fibrogenic activation of hepatic stellate cells. *Cell Res.* **19**, 996-1005, doi:10.1038/cr.2009.73 (2009).
- Zhang, C. Y., Yuan, W. G., He, P., Lei, J. H. & Wang, C. X. Liver fibrosis and hepatic stellate cells: Etiology, pathological hallmarks and therapeutic targets. *World J. Gastroenterol.* **22**, 10512-10522, doi:10.3748/wjg.v22.i48.10512 (2016).
- 75 Haussinger, D. & Kordes, C. Space of Disse: a stem cell niche in the liver. *Biol. Chem.* **401**, 81-95, doi:10.1515/hsz-2019-0283 (2019).
- Barcena-Varela, M., Colyn, L. & Fernandez-Barrena, M. G. Epigenetic Mechanisms in Hepatic Stellate Cell Activation During Liver Fibrosis and Carcinogenesis. *Int. J. Mol. Sci.* **20** (2019).
- Friedman, S. L. Evolving challenges in hepatic fibrosis. *Nat. Rev. Gastroenterol. Hepatol.* **7**, 425-436, doi:10.1038/nrgastro.2010.97 (2010).
- Reeves, H. L. & Friedman, S. L. Activation of hepatic stellate cells--a key issue in liver fibrosis. *Front. Biosci.* **7**, d808-826, doi:10.2741/reeves (2002).
- Fil Taghdouini, A., Najimi, M., Sancho-Bru, P., Sokal, E. & van Grunsven, L. A. In vitro reversion of activated primary human hepatic stellate cells. *Fibrogenesis Tissue Repair* **8**, 14, doi:10.1186/s13069-015-0031-z (2015).
- Hernandez-Gea, V. & Friedman, S. L. Pathogenesis of liver fibrosis. *Annu. Rev. Pathol.* **6**, 425-456, doi:10.1146/annurev-pathol-011110-130246 (2011).

- Jophlin, L. L., Koutalos, Y., Chen, C., Shah, V. & Rockey, D. C. Hepatic stellate cells retain retinoid-laden lipid droplets after cellular transdifferentiation into activated myofibroblasts. *Am. J. Physiol. Gastrointest. Liver Physiol.* **315**, G713-G721, doi:10.1152/ajpgi.00251.2017 (2018).
- Seebacher, F., Zeigerer, A., Kory, N. & Krahmer, N. Hepatic lipid droplet homeostasis and fatty liver disease. *Semin. Cell Dev. Biol.* **108**, 72-81, doi:10.1016/j.semcdb.2020.04.011 (2020).
- Lemoinne, S., Cadoret, A., El Mourabit, H., Thabut, D. & Housset, C. Origins and functions of liver myofibroblasts. *Biochim. Biophys. Acta* **1832**, 948-954, doi:10.1016/j.bbadis.2013.02.019 (2013).
- 84 Ellis, E. L. & Mann, D. A. Clinical evidence for the regression of liver fibrosis. *J. Hepatol.* **56**, 1171-1180, doi:10.1016/j.jhep.2011.09.024 (2012).
- Higashi, T., Friedman, S. L. & Hoshida, Y. Hepatic stellate cells as key target in liver fibrosis. *Adv Drug Deliv Rev* **121**, 27-42, doi:10.1016/j.addr.2017.05.007 (2017).
- de Oliveira da Silva, B., Ramos, L. F. & Moraes, K. C. M. Molecular interplays in hepatic stellate cells: apoptosis, senescence, and phenotype reversion as cellular connections that modulate liver fibrosis. *Cell Biol. Int.* **41**, 946-959, doi:10.1002/cbin.10790 (2017).
- Mabuchi, A. *et al.* Role of hepatic stellate cell/hepatocyte interaction and activation of hepatic stellate cells in the early phase of liver regeneration in the rat. *J. Hepatol.* **40**, 910-916, doi:10.1016/j.jhep.2004.02.005 (2004).
- Hanna, R. F. *et al.* Cirrhosis-associated hepatocellular nodules: correlation of histopathologic and MR imaging features. *Radiographics* **28**, 747-769, doi:10.1148/rg.283055108 (2008).
- Khomich, O., Ivanov, A. V. & Bartosch, B. Metabolic Hallmarks of Hepatic Stellate Cells in Liver Fibrosis. *Cells* **9**, doi:10.3390/cells9010024 (2019).
- 90 Kisseleva, T. & Brenner, D. A. Hepatic stellate cells and the reversal of fibrosis. *J. Gastroenterol. Hepatol.* **21 Suppl 3**, S84-87, doi:10.1111/j.1440-1746.2006.04584.x (2006).
- 91 Friedman, S. L. Liver fibrosis -- from bench to bedside. *J. Hepatol.* **38 Suppl 1**, S38-53, doi:10.1016/s0168-8278(02)00429-4 (2003).
- 92 Mantovani, A. & Dalbeni, A. Treatments for NAFLD: State of Art. *Int. J. Mol. Sci.* **22**, 2350, doi:10.3390/ijms22052350 (2021).
- 93 Ratziu, V. Novel Pharmacotherapy Options for NASH. *Dig. Dis. Sci.* **61**, 1398-1405, doi:10.1007/s10620-016-4128-z (2016).
- Brown, E., Hydes, T., Hamid, A. & Cuthbertson, D. J. Emerging and Established Therapeutic Approaches for Nonalcoholic Fatty Liver Disease. *Clin. Ther.* **43**, 1476-1504, doi:10.1016/j.clinthera.2021.07.013 (2021).
- Paternostro, R. & Trauner, M. Current treatment of non-alcoholic fatty liver disease. *J. Intern. Med.* **292**, 190-204, doi:10.1111/joim.13531 (2022).
- European Association for the Study of the, L., European Association for the Study of, D. & European Association for the Study of, O. EASL-EASD-EASO Clinical Practice Guidelines for the management of non-alcoholic fatty liver disease. *J. Hepatol.* **64**, 1388-1402, doi:10.1016/j.jhep.2015.11.004 (2016).
- 97 Chalasani, N. *et al.* The diagnosis and management of nonalcoholic fatty liver disease: Practice guidance from the American Association for the Study of Liver Diseases. *Hepatology* **67**, 328-357, doi:10.1002/hep.29367 (2018).
- 98 Belfort, R. *et al.* A placebo-controlled trial of pioglitazone in subjects with nonalcoholic steatohepatitis. *N. Engl. J. Med.* **355**, 2297-2307, doi:10.1056/NEJMoa060326 (2006).
- 99 Francque, S. *et al.* Nonalcoholic steatohepatitis: the role of peroxisome proliferator-activated receptors. *Nat. Rev. Gastroenterol. Hepatol.* **18**, 24-39, doi:10.1038/s41575-020-00366-5 (2021).
- Sanyal, A. J. *et al.* Pioglitazone, vitamin E, or placebo for nonalcoholic steatohepatitis. *N. Engl. J. Med.* **362**, 1675-1685, doi:10.1056/NEJMoa0907929 (2010).
- Aithal, G. P. *et al.* Randomized, placebo-controlled trial of pioglitazone in nondiabetic subjects with nonalcoholic steatohepatitis. *Gastroenterology* **135**, 1176-1184, doi:10.1053/j.gastro.2008.06.047 (2008).
- Hsiao, P. J. *et al.* Pioglitazone Enhances Cytosolic Lipolysis, beta-oxidation and Autophagy to Ameliorate Hepatic Steatosis. *Sci. Rep.* **7**, 9030, doi:10.1038/s41598-017-09702-3 (2017).
- Mantovani, A., Byrne, C. D., Scorletti, E., Mantzoros, C. S. & Targher, G. Efficacy and safety of anti-hyperglycaemic drugs in patients with non-alcoholic fatty liver disease with or without diabetes: An updated systematic review of randomized controlled trials. *Diabetes Metab.* **46**, 427-441, doi:10.1016/j.diabet.2019.12.007 (2020).
- 104 Cholankeril, R. *et al.* Anti-Diabetic Medications for the Pharmacologic Management of NAFLD. *Diseases* **6**, doi:10.3390/diseases6040093 (2018).
- 105 Raschi, E., Mazzotti, A., Poluzzi, E., De Ponti, F. & Marchesini, G. Pharmacotherapy of type 2 diabetes in patients with chronic liver disease: focus on nonalcoholic fatty liver disease. *Expert Opin. Pharmacother.* **19**, 1903-1914, doi:10.1080/14656566.2018.1531126 (2018).

- Pingitore, P. *et al.* Human Multilineage 3D Spheroids as a Model of Liver Steatosis and Fibrosis. *Int. J. Mol. Sci.* **20**, doi:10.3390/ijms20071629 (2019).
- El Hadi, H., Vettor, R. & Rossato, M. Vitamin E as a Treatment for Nonalcoholic Fatty Liver Disease: Reality or Myth? *Antioxidants (Basel)* **7**, doi:10.3390/antiox7010012 (2018).
- He, W. *et al.* Vitamin E Ameliorates Lipid Metabolism in Mice with Nonalcoholic Fatty Liver Disease via Nrf2/CES1 Signaling Pathway. *Dig. Dis. Sci.* **64**, 3182-3191, doi:10.1007/s10620-019-05657-9 (2019).
- Uchida, D., Takaki, A., Adachi, T. & Okada, H. Beneficial and Paradoxical Roles of Anti-Oxidative Nutritional Support for Non-Alcoholic Fatty Liver Disease. *Nutrients* **10**, doi:10.3390/nu10080977 (2018).
- Lavine, J. E. *et al.* Effect of vitamin E or metformin for treatment of nonalcoholic fatty liver disease in children and adolescents: the TONIC randomized controlled trial. *JAMA* **305**, 1659-1668, doi:10.1001/jama.2011.520 (2011).
- 111 Khurana, A., Navik, U., Allawadhi, P., Yadav, P. & Weiskirchen, R. Spotlight on liver macrophages for halting liver disease progression and injury. *Expert Opin. Ther. Targets* **26**, 707-719, doi:10.1080/14728222.2022.2133699 (2022).
- 112 Drucker, D. J. The biology of incretin hormones. *Cell Metab.* **3**, 153-165, doi:10.1016/j.cmet.2006.01.004 (2006).
- Ding, X., Saxena, N. K., Lin, S., Gupta, N. A. & Anania, F. A. Exendin-4, a glucagon-like protein-1 (GLP-1) receptor agonist, reverses hepatic steatosis in ob/ob mice. *Hepatology* **43**, 173-181, doi:10.1002/hep.21006 (2006).
- Gupta, N. A. *et al.* Glucagon-like peptide-1 receptor is present on human hepatocytes and has a direct role in decreasing hepatic steatosis in vitro by modulating elements of the insulin signaling pathway. *Hepatology* **51**, 1584-1592, doi:10.1002/hep.23569 (2010).
- 115 Mantovani, A. *et al.* Glucagon-Like Peptide-1 Receptor Agonists for Treatment of Nonalcoholic Fatty Liver Disease and Nonalcoholic Steatohepatitis: An Updated Meta-Analysis of Randomized Controlled Trials. *Metabolites* **11**, doi:10.3390/metabo11020073 (2021).
- Mantovani, A., Petracca, G., Csermely, A., Beatrice, G. & Targher, G. Sodium-Glucose Cotransporter-2 Inhibitors for Treatment of Nonalcoholic Fatty Liver Disease: A Meta-Analysis of Randomized Controlled Trials. *Metabolites* **11**, doi:10.3390/metabo11010022 (2020).
- Malehmir, M. *et al.* Platelet GPIbalpha is a mediator and potential interventional target for NASH and subsequent liver cancer. *Nat. Med.* **25**, 641-655, doi:10.1038/s41591-019-0379-5 (2019).
- Simon, T. G. *et al.* Daily Aspirin Use Associated With Reduced Risk For Fibrosis Progression In Patients With Nonalcoholic Fatty Liver Disease. *Clin. Gastroenterol. Hepatol.* **17**, 2776-2784 e2774, doi:10.1016/j.cgh.2019.04.061 (2019).
- 119 Ratziu, V. *et al.* Elafibranor, an Agonist of the Peroxisome Proliferator-Activated Receptor-alpha and delta, Induces Resolution of Nonalcoholic Steatohepatitis Without Fibrosis Worsening. *Gastroenterology* **150**, 1147-1159 e1145, doi:10.1053/j.gastro.2016.01.038 (2016).
- Neuschwander-Tetri, B. A. *et al.* Farnesoid X nuclear receptor ligand obeticholic acid for non-cirrhotic, non-alcoholic steatohepatitis (FLINT): a multicentre, randomised, placebo-controlled trial. *Lancet* **385**, 956-965, doi:10.1016/S0140-6736(14)61933-4 (2015).
- Younossi, Z. M. *et al.* Obeticholic acid for the treatment of non-alcoholic steatohepatitis: interim analysis from a multicentre, randomised, placebo-controlled phase 3 trial. *Lancet* **394**, 2184-2196, doi:10.1016/S0140-6736(19)33041-7 (2019).
- Zivko, C., Witt, F., Koeberle, A., Fuhrmann, G. & Luciani, P. Formulating elafibranor and obeticholic acid with phospholipids decreases drug-induced association of SPARC to extracellular vesicles from LX-2 human hepatic stellate cells. *Eur. J. Pharm. Biopharm.* **182**, 32-40, doi:10.1016/j.ejpb.2022.11.025 (2023).
- Luchtenborg, C., Niederhaus, B., Brugger, B., Popovic, B. & Fricker, G. Lipid Profiles of Five Essential Phospholipid Preparations for the Treatment of Nonalcoholic Fatty Liver Disease: A Comparative Study. *Lipids* **55**, 271-278, doi:10.1002/lipd.12236 (2020).
- van Hoogevest, P. & Wendel, A. The use of natural and synthetic phospholipids as pharmaceutical excipients. *Eur. J. Lipid Sci. Technol.* **116**, 1088-1107, doi:10.1002/ejlt.201400219 (2014).
- Gundermann, K. J., Gundermann, S., Drozdzik, M. & Mohan Prasad, V. G. Essential phospholipids in fatty liver: a scientific update. *Clin. Exp. Gastroenterol.* **9**, 105-117, doi:10.2147/CEG.S96362 (2016).
- Gundermann, K. J., Kuenker, A., Kuntz, E. & Drozdzik, M. Activity of essential phospholipids (EPL) from soybean in liver diseases. *Pharmacol. Rep.* **63**, 643-659, doi:10.1016/s1734-1140(11)70576-x (2011).
- Lieber, C. S. *et al.* Phosphatidylcholine protects against fibrosis and cirrhosis in the baboon. *Gastroenterology* **106**, 152-159, doi:10.1016/s0016-5085(94)95023-7 (1994).

- Varganova, D. L., Pavlov, C. S., Casazza, G., Nikolova, D. & Gluud, C. Essential phospholipids for people with non-alcoholic fatty liver disease. *Cochrane Database of Systematic Reviews*, doi:10.1002/14651858.cd013301 (2019).
- Anstee, Q. M. & Day, C. P. A lipid to treat non-alcoholic fatty liver disease the dawn of 'liporehabilitation'? *J. Hepatol.* **56**, 987-989, doi:10.1016/j.jhep.2011.10.002 (2012).
- 130 Ingraham, H. A. Metabolism: A lipid for fat disorders. *Nature* **474**, 455-456, doi:10.1038/474455a (2011).
- Fex, G. Metabolism of phosphatidyl choline, phosphatidyl ethanolamine and sphingomyelin in regenerating rat liver. *Biochim. Biophys. Acta* **231**, 161-169, doi:10.1016/0005-2760(71)90264-5 (1971).
- The "Essential" Phospholipids as a Membrane Therapeutic. (Polish Section of European Society of Biochemical Pharmacology Institute of Pharmacology and Toxicology, Medical Academy, 1993).
- Cao, Q., Mak, K. M. & Lieber, C. S. DLPC and SAMe prevent alpha1(I) collagen mRNA up-regulation in human hepatic stellate cells, whether caused by leptin or menadione. *Biochem. Biophys. Res. Commun.* **350**, 50-55, doi:10.1016/j.bbrc.2006.08.174 (2006).
- Poniachik, J., Baraona, E., Zhao, J. & Lieber, C. S. Dilinoleoylphosphatidylcholine decreases hepatic stellate cell activation. *J. Lab. Clin. Med.* **133**, 342-348, doi:10.1016/s0022-2143(99)90064-1 (1999).
- 135 Ikeda, R. *et al.* Reactive oxygen species and NADPH oxidase 4 induced by transforming growth factor beta1 are the therapeutic targets of polyenylphosphatidylcholine in the suppression of human hepatic stellate cell activation. *Inflamm. Res.* **60**, 597-604, doi:10.1007/s00011-011-0309-6 (2011).
- Nicolson, G. L. & Ash, M. E. Lipid Replacement Therapy: a natural medicine approach to replacing damaged lipids in cellular membranes and organelles and restoring function. *Biochim. Biophys. Acta* **1838**, 1657-1679, doi:10.1016/j.bbamem.2013.11.010 (2014).
- Valentino, G., Zivko, C., Weber, F., Brulisauer, L. & Luciani, P. Synergy of Phospholipid-Drug Formulations Significantly Deactivates Profibrogenic Human Hepatic Stellate Cells. *Pharmaceutics* **11**, 676, doi:10.3390/pharmaceutics11120676 (2019).
- Zivko, C., Fuhrmann, K., Fuhrmann, G. & Luciani, P. Tracking matricellular protein SPARC in extracellular vesicles as a non-destructive method to evaluate lipid-based antifibrotic treatments. *Commun Biol* **5**, 1155, doi:10.1038/s42003-022-04123-z (2022).
- Westerouen Van Meeteren, M. J., Drenth, J. P. H. & Tjwa, E. Elafibranor: a potential drug for the treatment of nonalcoholic steatohepatitis (NASH). *Expert Opin Investig Drugs* **29**, 117-123, doi:10.1080/13543784.2020.1668375 (2020).
- Wang, Y., Nakajima, T., Gonzalez, F. J. & Tanaka, N. PPARs as Metabolic Regulators in the Liver: Lessons from Liver-Specific PPAR-Null Mice. *Int. J. Mol. Sci.* **21**, doi:10.3390/ijms21062061 (2020).
- Pawlak, M., Lefebvre, P. & Staels, B. Molecular mechanism of PPARalpha action and its impact on lipid metabolism, inflammation and fibrosis in non-alcoholic fatty liver disease. *J. Hepatol.* **62**, 720-733, doi:10.1016/j.jhep.2014.10.039 (2015).
- Bojic, L. A. & Huff, M. W. Peroxisome proliferator-activated receptor delta: a multifaceted metabolic player. *Curr. Opin. Lipidol.* **24**, 171-177, doi:10.1097/MOL.0b013e32835cc949 (2013).
- Odegaard, J. I. *et al.* Alternative M2 activation of Kupffer cells by PPARdelta ameliorates obesity-induced insulin resistance. *Cell Metab.* **7**, 496-507, doi:10.1016/j.cmet.2008.04.003 (2008).
- Riserus, U. *et al.* Activation of peroxisome proliferator-activated receptor (PPAR)delta promotes reversal of multiple metabolic abnormalities, reduces oxidative stress, and increases fatty acid oxidation in moderately obese men. *Diabetes* **57**, 332-339, doi:10.2337/db07-1318 (2008).
- Ahmadian, M. *et al.* PPARgamma signaling and metabolism: the good, the bad and the future. *Nat. Med.* **19**, 557-566, doi:10.1038/nm.3159 (2013).
- 146 Nadra, K. *et al.* PPARgamma in placental angiogenesis. *Endocrinology* **151**, 4969-4981, doi:10.1210/en.2010-0131 (2010).
- Prikhodko, V. A., Bezborodkina, N. N. & Okovityi, S. V. Pharmacotherapy for Non-Alcoholic Fatty Liver Disease: Emerging Targets and Drug Candidates. *Biomedicines* **10**, doi:10.3390/biomedicines10020274 (2022).
- Guirguis, E., Grace, Y., Bolson, A., DellaVecchia, M. J. & Ruble, M. Emerging therapies for the treatment of nonalcoholic steatohepatitis: A systematic review. *Pharmacotherapy* **41**, 315-328, doi:10.1002/phar.2489 (2021).
- Schattenberg, J. M. *et al.* A randomized placebo-controlled trial of elafibranor in patients with primary biliary cholangitis and incomplete response to UDCA. *J. Hepatol.* **74**, 1344-1354, doi:10.1016/j.jhep.2021.01.013 (2021).
- D'Amato, D. *et al.* Real-world experience with obeticholic acid in patients with primary biliary cholangitis. *JHEP Rep* **3**, 100248, doi:10.1016/j.jhepr.2021.100248 (2021).
- Zhou, W. C., Zhang, Q. B. & Qiao, L. Pathogenesis of liver cirrhosis. World J. Gastroenterol. 20, 7312-7324, doi:10.3748/wjg.v20.i23.7312 (2014).

- Heyens, L. J. M., Busschots, D., Koek, G. H., Robaeys, G. & Francque, S. Liver Fibrosis in Non-alcoholic Fatty Liver Disease: From Liver Biopsy to Non-invasive Biomarkers in Diagnosis and Treatment. *Front Med (Lausanne)* **8**, 615978, doi:10.3389/fmed.2021.615978 (2021).
- Mudaliar, S. *et al.* Efficacy and safety of the farnesoid X receptor agonist obeticholic acid in patients with type 2 diabetes and nonalcoholic fatty liver disease. *Gastroenterology* **145**, 574-582 e571, doi:10.1053/j.gastro.2013.05.042 (2013).
- Modica, S., Gadaleta, R. M. & Moschetta, A. Deciphering the nuclear bile acid receptor FXR paradigm. *Nucl Recept Signal* **8**, e005, doi:10.1621/nrs.08005 (2010).
- 155 Cipriani, S., Mencarelli, A., Palladino, G. & Fiorucci, S. FXR activation reverses insulin resistance and lipid abnormalities and protects against liver steatosis in Zucker (fa/fa) obese rats. *J. Lipid Res.* **51**, 771-784, doi:10.1194/jlr.M001602 (2010).
- Fickert, P. *et al.* Farnesoid X receptor critically determines the fibrotic response in mice but is expressed to a low extent in human hepatic stellate cells and periductal myofibroblasts. *Am. J. Pathol.* **175**, 2392-2405, doi:10.2353/ajpath.2009.090114 (2009).
- 157 Verbeke, L. *et al.* Obeticholic acid, a farnesoid X receptor agonist, improves portal hypertension by two distinct pathways in cirrhotic rats. *Hepatology* **59**, 2286-2298, doi:10.1002/hep.26939 (2014).
- Lindor, K. D. *et al.* Ursodeoxycholic acid for treatment of nonalcoholic steatohepatitis: results of a randomized trial. *Hepatology* **39**, 770-778, doi:10.1002/hep.20092 (2004).
- Intercept Pharmaceuticals, Inc. Press Release Intercept receives complete response letter from FDA for obeticholic acid as a treatment for pre-cirrhotic fibrosis due to NASH, https://ir.interceptpharma.com/news-releases/news-release-details/intercept-receives-complete-response-letter-fda-obeticholic-0 (2023).
- Malhi, H., Bronk, S. F., Werneburg, N. W. & Gores, G. J. Free fatty acids induce JNK-dependent hepatocyte lipoapoptosis. *J. Biol. Chem.* **281**, 12093-12101, doi:10.1074/jbc.M510660200 (2006).
- Joshi-Barve, S. *et al.* Palmitic acid induces production of proinflammatory cytokine interleukin-8 from hepatocytes. *Hepatology* **46**, 823-830, doi:10.1002/hep.21752 (2007).
- Madec, S. *et al.* CYP4F3B expression is associated with differentiation of HepaRG human hepatocytes and unaffected by fatty acid overload. *Drug Metab. Dispos.* **39**, 1987-1996, doi:10.1124/dmd.110.036848 (2011).
- Dornas, W. *et al.* Endotoxin regulates matrix genes increasing reactive oxygen species generation by intercellular communication between palmitate-treated hepatocyte and stellate cell. *J. Cell. Physiol.* **234**, 122-133, doi:10.1002/jcp.27175 (2018).
- Brown, M. V., Compton, S. A., Milburn, M. V., Lawton, K. A. & Cheatham, B. Metabolomic signatures in lipid-loaded HepaRGs reveal pathways involved in steatotic progression. *Obesity (Silver Spring)* **21**, E561-570, doi:10.1002/oby.20440 (2013).
- Mun, S. J. *et al.* Generation of expandable human pluripotent stem cell-derived hepatocyte-like liver organoids. *J. Hepatol.* **71**, 970-985, doi:10.1016/j.jhep.2019.06.030 (2019).
- Graffmann, N. *et al.* Modeling Nonalcoholic Fatty Liver Disease with Human Pluripotent Stem Cell-Derived Immature Hepatocyte-Like Cells Reveals Activation of PLIN2 and Confirms Regulatory Functions of Peroxisome Proliferator-Activated Receptor Alpha. *Stem Cells Dev* **25**, 1119-1133, doi:10.1089/scd.2015.0383 (2016).
- Avior, Y. *et al.* Microbial-derived lithocholic acid and vitamin K2 drive the metabolic maturation of pluripotent stem cells-derived and fetal hepatocytes. *Hepatology* **62**, 265-278, doi:10.1002/hep.27803 (2015)
- Wang, X. L. *et al.* Free fatty acids inhibit insulin signaling-stimulated endothelial nitric oxide synthase activation through upregulating PTEN or inhibiting Akt kinase. *Diabetes* **55**, 2301-2310, doi:10.2337/db05-1574 (2006).
- Maruyama, H., Takahashi, M., Sekimoto, T., Shimada, T. & Yokosuka, O. Linoleate appears to protect against palmitate-induced inflammation in Huh7 cells. *Lipids Health Dis.* **13**, 78, doi:10.1186/1476-511X-13-78 (2014).
- Boteon, Y. L. *et al.* An effective protocol for pharmacological defatting of primary human hepatocytes which is non-toxic to cholangiocytes or intrahepatic endothelial cells. *PLoS One* **13**, e0201419, doi:10.1371/journal.pone.0201419 (2018).
- Li, Y. et al. Sphingomyelin synthase 2 activity and liver steatosis: an effect of ceramide-mediated peroxisome proliferator-activated receptor gamma2 suppression. *Arterioscler. Thromb. Vasc. Biol.* **33**, 1513-1520, doi:10.1161/ATVBAHA.113.301498 (2013).
- Lee, J. S., Mendez, R., Heng, H. H., Yang, Z. Q. & Zhang, K. Pharmacological ER stress promotes hepatic lipogenesis and lipid droplet formation. *American journal of translational research* **4**, 102-113 (2012).

- Cuykx, M., Claes, L., Rodrigues, R. M., Vanhaecke, T. & Covaci, A. Metabolomics profiling of steatosis progression in HepaRG((R)) cells using sodium valproate. *Toxicol. Lett.* **286**, 22-30, doi:10.1016/j.toxlet.2017.12.015 (2018).
- Antherieu, S., Rogue, A., Fromenty, B., Guillouzo, A. & Robin, M. A. Induction of vesicular steatosis by amiodarone and tetracycline is associated with up-regulation of lipogenic genes in HepaRG cells. *Hepatology* **53**, 1895-1905, doi:10.1002/hep.24290 (2011).
- Antherieu, S., Chesne, C., Li, R., Guguen-Guillouzo, C. & Guillouzo, A. Optimization of the HepaRG cell model for drug metabolism and toxicity studies. *Toxicol. In Vitro* **26**, 1278-1285, doi:10.1016/j.tiv.2012.05.008 (2012).
- Bell, C. C. *et al.* Characterization of primary human hepatocyte spheroids as a model system for druginduced liver injury, liver function and disease. *Sci. Rep.* **6**, 25187, doi:10.1038/srep25187 (2016).
- 177 Mehta, S. R., Thomas, E. L., Bell, J. D., Johnston, D. G. & Taylor-Robinson, S. D. Non-invasive means of measuring hepatic fat content. *World J. Gastroenterol.* **14**, 3476-3483, doi:10.3748/wjg.14.3476 (2008).
- Powell, E. E., Jonsson, J. R. & Clouston, A. D. Steatosis: co-factor in other liver diseases. *Hepatology* **42**, 5-13, doi:10.1002/hep.20750 (2005).
- Zadoorian, A., Du, X. & Yang, H. Lipid droplet biogenesis and functions in health and disease. *Nature Reviews Endocrinology*, doi:10.1038/s41574-023-00845-0 (2023).
- De, A. & Duseja, A. Natural History of Simple Steatosis or Nonalcoholic Fatty Liver. *J. Clin. Exp. Hepatol.* **10**, 255-262, doi:10.1016/j.jceh.2019.09.005 (2020).
- Mendez-Sanchez, N. *et al.* New Aspects of Lipotoxicity in Nonalcoholic Steatohepatitis. *Int. J. Mol. Sci.* **19**, doi:10.3390/ijms19072034 (2018).
- 182 Chavez-Tapia, N. C., Rosso, N. & Tiribelli, C. Effect of intracellular lipid accumulation in a new model of non-alcoholic fatty liver disease. *BMC Gastroenterol.* **12**, 20, doi:10.1186/1471-230X-12-20 (2012).
- Barbero-Becerra, V. J. *et al.* The interplay between hepatic stellate cells and hepatocytes in an in vitro model of NASH. *Toxicol. In Vitro* **29**, 1753-1758, doi:10.1016/j.tiv.2015.07.010 (2015).
- Solinas, G. & Becattini, B. JNK at the crossroad of obesity, insulin resistance, and cell stress response. *Mol Metab* **6**, 174-184, doi:10.1016/j.molmet.2016.12.001 (2017).
- Schulze, R. J., Schott, M. B., Casey, C. A., Tuma, P. L. & McNiven, M. A. The cell biology of the hepatocyte: A membrane trafficking machine. *J. Cell Biol.* **218**, 2096-2112, doi:10.1083/jcb.201903090 (2019).
- Fielding, C. M. & Angulo, P. Hepatic steatosis and steatohepatitis: Are they really two distinct entities? *Curr Hepatol Rep* **13**, 151-158, doi:10.1007/s11901-014-0227-5 (2014).
- Svegliati-Baroni, G. *et al.* Lipidomic biomarkers and mechanisms of lipotoxicity in non-alcoholic fatty liver disease. *Free Radic. Biol. Med.* **144**, 293-309, doi:10.1016/j.freeradbiomed.2019.05.029 (2019).
- Li, Z. & Olzmann, J. A. A Proteomic Map to Navigate Subcellular Reorganization in Fatty Liver Disease. *Dev. Cell* **47**, 139-141, doi:10.1016/j.devcel.2018.10.006 (2018).
- Krahmer, N. *et al.* Organellar Proteomics and Phospho-Proteomics Reveal Subcellular Reorganization in Diet-Induced Hepatic Steatosis. *Dev. Cell* **47**, 205-221 e207, doi:10.1016/j.devcel.2018.09.017 (2018).
- Wang, L., Liu, J., Miao, Z., Pan, Q. & Cao, W. Lipid droplets and their interactions with other organelles in liver diseases. *Int. J. Biochem. Cell Biol.* **133**, 105937, doi:10.1016/j.biocel.2021.105937 (2021).
- Murphy, D. J. The biogenesis and functions of lipid bodies in animals, plants and microorganisms. *Prog. Lipid Res.* **40**, 325-438, doi:10.1016/s0163-7827(01)00013-3 (2001).
- Sanjabi, B. et al. Lipid droplets hypertrophy: a crucial determining factor in insulin regulation by adipocytes. *Sci. Rep.* **5**, 8816, doi:10.1038/srep08816 (2015).
- Huang, Y. L. *et al.* Administration of Secretome Derived from Human Mesenchymal Stem Cells Induces Hepatoprotective Effects in Models of Idiosyncratic Drug-Induced Liver Injury Caused by Amiodarone or Tamoxifen. *Cells* **12**, doi:10.3390/cells12040636 (2023).
- Mashek, D. G. Hepatic lipid droplets: A balancing act between energy storage and metabolic dysfunction in NAFLD. *Mol Metab* **50**, 101115, doi:10.1016/j.molmet.2020.101115 (2021).
- Xu, W. et al. Differential Roles of Cell Death-inducing DNA Fragmentation Factor-alpha-like Effector (CIDE) Proteins in Promoting Lipid Droplet Fusion and Growth in Subpopulations of Hepatocytes. *J. Biol. Chem.* **291**, 4282-4293, doi:10.1074/jbc.M115.701094 (2016).
- Langhi, C. & Baldan, A. CIDEC/FSP27 is regulated by peroxisome proliferator-activated receptor alpha and plays a critical role in fasting- and diet-induced hepatosteatosis. *Hepatology* **61**, 1227-1238, doi:10.1002/hep.27607 (2015).
- Wilfling, F. *et al.* Triacylglycerol synthesis enzymes mediate lipid droplet growth by relocalizing from the ER to lipid droplets. *Dev. Cell* **24**, 384-399, doi:10.1016/j.devcel.2013.01.013 (2013).

- 198 Chen, K. *et al.* Advancing the understanding of NAFLD to hepatocellular carcinoma development: From experimental models to humans. *Biochim Biophys Acta Rev Cancer* **1871**, 117-125, doi:10.1016/j.bbcan.2018.11.005 (2019).
- Fu, S. *et al.* Aberrant lipid metabolism disrupts calcium homeostasis causing liver endoplasmic reticulum stress in obesity. *Nature* **473**, 528-531, doi:10.1038/nature09968 (2011).
- Yamamoto, K. *et al.* Induction of liver steatosis and lipid droplet formation in ATF6alpha-knockout mice burdened with pharmacological endoplasmic reticulum stress. *Mol. Biol. Cell* **21**, 2975-2986, doi:10.1091/mbc.E09-02-0133 (2010).
- Xu, S. *et al.* Perilipin 2 and lipid droplets provide reciprocal stabilization. *Biophysics Reports* **5**, 145-160, doi:10.1007/s41048-019-0091-5 (2019).
- Straub, B. K., Stoeffel, P., Heid, H., Zimbelmann, R. & Schirmacher, P. Differential pattern of lipid droplet-associated proteins and de novo perilipin expression in hepatocyte steatogenesis. *Hepatology* **47**, 1936-1946, doi:10.1002/hep.22268 (2008).
- Zhou, L. *et al.* Cidea promotes hepatic steatosis by sensing dietary fatty acids. *Hepatology* **56**, 95-107, doi:10.1002/hep.25611 (2012).
- Su, W. et al. Liver X receptor alpha induces 17beta-hydroxysteroid dehydrogenase-13 expression through SREBP-1c. *Am. J. Physiol. Endocrinol. Metab.* **312**, E357-E367, doi:10.1152/ajpendo.00310.2016 (2017).
- Su, W. et al. Comparative proteomic study reveals 17beta-HSD13 as a pathogenic protein in nonalcoholic fatty liver disease. *Proc. Natl. Acad. Sci. U. S. A.* **111**, 11437-11442, doi:10.1073/pnas.1410741111 (2014).
- Mak, K. M., Wu, C. & Cheng, C. P. Lipid droplets, the Holy Grail of hepatic stellate cells: In health and hepatic fibrosis. *Anat Rec (Hoboken)* **306**, 983-1010, doi:10.1002/ar.25138 (2023).
- 207 Molenaar, M. R., Vaandrager, A. B. & Helms, J. B. Some Lipid Droplets Are More Equal Than Others: Different Metabolic Lipid Droplet Pools in Hepatic Stellate Cells. *Lipid Insights* **10**, 1178635317747281, doi:10.1177/1178635317747281 (2017).
- Bobowski-Gerard, M., Zummo, F. P., Staels, B., Lefebvre, P. & Eeckhoute, J. Retinoids Issued from Hepatic Stellate Cell Lipid Droplet Loss as Potential Signaling Molecules Orchestrating a Multicellular Liver Injury Response. *Cells* **7**, doi:10.3390/cells7090137 (2018).
- Geerts, A., Bouwens, L. & Wisse, E. Ultrastructure and function of hepatic fat-storing and pit cells. *J. Electron Microsc. Tech.* **14**, 247-256, doi:10.1002/jemt.1060140306 (1990).
- Libby, A. E., Bales, E., Orlicky, D. J. & McManaman, J. L. Perilipin-2 Deletion Impairs Hepatic Lipid Accumulation by Interfering with Sterol Regulatory Element-binding Protein (SREBP) Activation and Altering the Hepatic Lipidome. *J. Biol. Chem.* **291**, 24231-24246, doi:10.1074/jbc.M116.759795 (2016).
- Lee, T. F. *et al.* Downregulation of hepatic stellate cell activation by retinol and palmitate mediated by adipose differentiation-related protein (ADRP). *J. Cell. Physiol.* **223**, 648-657, doi:10.1002/jcp.22063 (2010).
- Najt, C. P. *et al.* Liver-specific loss of Perilipin 2 alleviates diet-induced hepatic steatosis, inflammation, and fibrosis. *Am. J. Physiol. Gastrointest. Liver Physiol.* **310**, G726-738, doi:10.1152/ajpgi.00436.2015 (2016).
- Molenaar, M. R., Penning, L. C. & Helms, J. B. Playing Jekyll and Hyde-The Dual Role of Lipids in Fatty Liver Disease. *Cells* **9**, doi:10.3390/cells9102244 (2020).
- Stanger, B. Z. Cellular homeostasis and repair in the mammalian liver. *Annu. Rev. Physiol.* **77**, 179-200, doi:10.1146/annurev-physiol-021113-170255 (2015).
- Green, C. J. *et al.* The isolation of primary hepatocytes from human tissue: optimising the use of small non-encapsulated liver resection surplus. *Cell Tissue Bank* **18**, 597-604, doi:10.1007/s10561-017-9641-6 (2017).
- Mitry, R. R., Hughes, R. D. & Dhawan, A. Progress in human hepatocytes: isolation, culture & cryopreservation. *Semin. Cell Dev. Biol.* **13**, 463-467, doi:10.1016/s1084952102001350 (2002).
- Feaver, R. E. *et al.* Development of an in vitro human liver system for interrogating nonalcoholic steatohepatitis. *JCI Insight* 1, e90954, doi:10.1172/jci.insight.90954 (2016).
- Mahli, A. *et al.* Iso-alpha acids from hops (Humulus lupulus) inhibit hepatic steatosis, inflammation, and fibrosis. *Lab. Invest.* **98**, 1614-1626, doi:10.1038/s41374-018-0112-x (2018).
- Kawamoto, M. *et al.* Identification of Characteristic Genomic Markers in Human Hepatoma HuH-7 and Huh7.5.1-8 Cell Lines, *Front Genet* **11**, 546106, doi:10.3389/fgene.2020.546106 (2020).
- Nakabayashi, H., Taketa, K., Miyano, K., Yamane, T. & Sato, J. Growth of human hepatoma cells lines with differentiated functions in chemically defined medium. *Cancer Res.* **42**, 3858-3863 (1982).
- Blight, K. J., McKeating, J. A. & Rice, C. M. Highly permissive cell lines for subgenomic and genomic hepatitis C virus RNA replication. *J. Virol.* **76**, 13001-13014, doi:10.1128/jvi.76.24.13001-13014.2002 (2002).

- Aden, D. P., Fogel, A., Plotkin, S., Damjanov, I. & Knowles, B. B. Controlled synthesis of HBsAg in a differentiated human liver carcinoma-derived cell line. *Nature* **282**, 615-616, doi:10.1038/282615a0 (1979).
- Lopez-Terrada, D., Cheung, S. W., Finegold, M. J. & Knowles, B. B. Hep G2 is a hepatoblastoma-derived cell line. *Hum. Pathol.* **40**, 1512-1515, doi:10.1016/j.humpath.2009.07.003 (2009).
- Freitas, N., Cunha, C., Menne, S. & Gudima, S. O. Envelope proteins derived from naturally integrated hepatitis B virus DNA support assembly and release of infectious hepatitis delta virus particles. *J. Virol.* **88**, 5742-5754, doi:10.1128/JVI.00430-14 (2014).
- 225 Gripon, P. *et al.* Infection of a human hepatoma cell line by hepatitis B virus. *Proc. Natl. Acad. Sci. U. S. A.* **99**, 15655-15660, doi:10.1073/pnas.232137699 (2002).
- Guillouzo, A. *et al.* The human hepatoma HepaRG cells: a highly differentiated model for studies of liver metabolism and toxicity of xenobiotics. *Chem. Biol. Interact.* **168**, 66-73, doi:10.1016/j.cbi.2006.12.003 (2007).
- Marion, M.-J., Hantz, O. & Durantel, D. in *Hepatocytes: Methods and Protocols* (ed P. Maurel) 261-272 (Humana Press, 2010).
- Kelly, J. H. Permanent human hepatocyte cell line and its use in a liver assist device (LAD). United States of America patent US5290684A (1992).
- Murakami, T., Yano, H., Maruiwa, M., Sugihara, S. & Kojiro, M. Establishment and characterization of a human combined hepatocholangiocarcinoma cell line and its heterologous transplantation in nude mice. *Hepatology* **7**, 551-556, doi:10.1002/hep.1840070322 (1987).
- Yano, H. *et al.* A human combined hepatocellular and cholangiocarcinoma cell line (KMCH-2) that shows the features of hepatocellular carcinoma or cholangiocarcinoma under different growth conditions. *J. Hepatol.* **24**, 413-422, doi:10.1016/s0168-8278(96)80161-9 (1996).
- 231 Ikeda, M. *et al.* Efficient replication of a full-length hepatitis C virus genome, strain O, in cell culture, and development of a luciferase reporter system. *Biochem. Biophys. Res. Commun.* **329**, 1350-1359, doi:10.1016/j.bbrc.2005.02.138 (2005).
- Alexander, J. J., Bey, E. M., Geddes, E. W. & Lecatsas, G. Establishment of a continuously growing cell line from primary carcinoma of the liver. *S. Afr. Med. J.* **50**, 2124-2128 (1976).
- Chen, C. C. et al. Pacbio Sequencing of PLC/PRF/5 Cell Line and Clearance of HBV Integration Through CRISPR/Cas-9 System. Front Mol Biosci 8, 676957, doi:10.3389/fmolb.2021.676957 (2021).
- Ouchi, R. *et al.* Modeling Steatohepatitis in Humans with Pluripotent Stem Cell-Derived Organoids. *Cell Metab.* **30**, 374-384 e376, doi:10.1016/j.cmet.2019.05.007 (2019).
- Anfuso, B., Giraudi, P. J., Tiribelli, C. & Rosso, N. Silybin Modulates Collagen Turnover in an In Vitro Model of NASH. *Molecules* **24**. doi:10.3390/molecules24071280 (2019).
- Davidson, M. D., Kukla, D. A. & Khetani, S. R. Microengineered cultures containing human hepatic stellate cells and hepatocytes for drug development. *Integr. Biol. (Camb.)* **9**, 662-677, doi:10.1039/c7ib00027h (2017).
- 237 Donati, B. & Valenti, L. Telomeres, NAFLD and Chronic Liver Disease. *Int. J. Mol. Sci.* **17**, 383, doi:10.3390/ijms17030383 (2016).
- Calado, R. T. *et al.* A spectrum of severe familial liver disorders associate with telomerase mutations. *PLoS One* **4**, e7926, doi:10.1371/journal.pone.0007926 (2009).
- Sinton, M. C. *et al.* A human pluripotent stem cell model for the analysis of metabolic dysfunction in hepatic steatosis. *iScience* **24**, 101931, doi:10.1016/j.isci.2020.101931 (2021).
- Duwaerts, C. C. *et al.* Induced Pluripotent Stem Cell-derived Hepatocytes From Patients With Nonalcoholic Fatty Liver Disease Display a Disease-specific Gene Expression Profile. *Gastroenterology* **160**, 2591-2594 e2596, doi:10.1053/j.gastro.2021.02.050 (2021).
- 241 Kozyra, M. *et al.* Human hepatic 3D spheroids as a model for steatosis and insulin resistance. *Sci. Rep.* **8**, 14297, doi:10.1038/s41598-018-32722-6 (2018).
- Kostrzewski, T. *et al.* Three-dimensional perfused human in vitro model of non-alcoholic fatty liver disease. *World J. Gastroenterol.* **23**, 204-215, doi:10.3748/wjg.v23.i2.204 (2017).
- Gori, M. *et al.* Investigating Nonalcoholic Fatty Liver Disease in a Liver-on-a-Chip Microfluidic Device. *PLoS One* **11**, e0159729, doi:10.1371/journal.pone.0159729 (2016).
- Maharjan, S. *et al.* 3D human nonalcoholic hepatic steatosis and fibrosis models. *Bio-Design and Manufacturing* **4**, 157-170, doi:10.1007/s42242-020-00121-4 (2021).
- Soret, P. A., Magusto, J., Housset, C. & Gautheron, J. In Vitro and In Vivo Models of Non-Alcoholic Fatty Liver Disease: A Critical Appraisal. *J Clin Med* **10**, doi:10.3390/jcm10010036 (2020).
- Ramos, M. J., Bandiera, L., Menolascina, F. & Fallowfield, J. A. In vitro models for non-alcoholic fatty liver disease: Emerging platforms and their applications. *iScience* **25**, 103549, doi:10.1016/j.isci.2021.103549 (2022).

- Wang, Y. et al. Modeling Human Nonalcoholic Fatty Liver Disease (NAFLD) with an Organoids-on-a-Chip System. ACS Biomater Sci Eng 6, 5734-5743, doi:10.1021/acsbiomaterials.0c00682 (2020).
- Ferramosca, A. & Zara, V. Modulation of hepatic steatosis by dietary fatty acids. *World J. Gastroenterol.* **20**, 1746-1755, doi:10.3748/wjg.v20.i7.1746 (2014).
- Juarez-Hernandez, E., Chavez-Tapia, N. C., Uribe, M. & Barbero-Becerra, V. J. Role of bioactive fatty acids in nonalcoholic fatty liver disease. *Nutr. J.* **15**, 72, doi:10.1186/s12937-016-0191-8 (2016).
- Ricchi, M. *et al.* Differential effect of oleic and palmitic acid on lipid accumulation and apoptosis in cultured hepatocytes. *J. Gastroenterol. Hepatol.* **24**, 830-840, doi:10.1111/j.1440-1746.2008.05733.x (2009).
- Nissar, A. U., Sharma, L. & Tasduq, S. A. Palmitic acid induced lipotoxicity is associated with altered lipid metabolism, enhanced CYP450 2E1 and intracellular calcium mediated ER stress in human hepatoma cells. *Toxicology Research* **4**, 1344-1358, doi:10.1039/c5tx00101c (2015).
- Luo, Y., Rana, P. & Will, Y. Cyclosporine A and palmitic acid treatment synergistically induce cytotoxicity in HepG2 cells. *Toxicol. Appl. Pharmacol.* **261**, 172-180, doi:10.1016/j.taap.2012.03.022 (2012).
- Ganji, S. H., Kashyap, M. L. & Kamanna, V. S. Niacin inhibits fat accumulation, oxidative stress, and inflammatory cytokine IL-8 in cultured hepatocytes: Impact on non-alcoholic fatty liver disease. *Metabolism* **64**, 982-990, doi:10.1016/j.metabol.2015.05.002 (2015).
- Sanyal, A. J. *et al.* Nonalcoholic steatohepatitis: association of insulin resistance and mitochondrial abnormalities. *Gastroenterology* **120**, 1183-1192, doi:10.1053/gast.2001.23256 (2001).
- Wanninger, J. et al. Lipid accumulation impairs adiponectin-mediated induction of activin A by increasing TGFbeta in primary human hepatocytes. *Biochim. Biophys. Acta* **1811**, 626-633, doi:10.1016/j.bbalip.2010.11.001 (2011).
- Dashti, N. & Wolfbauer, G. Secretion of lipids, apolipoproteins, and lipoproteins by human hepatoma cell line, HepG2: effects of oleic acid and insulin. *J. Lipid Res.* **28**, 423-436, doi:10.1016/s0022-2275(20)38686-7 (1987).
- Lin, Y. et al. Differential effects of eicosapentaenoic acid on glycerolipid and apolipoprotein B metabolism in primary human hepatocytes compared to HepG2 cells and primary rat hepatocytes. *Biochim. Biophys. Acta* **1256**, 88-96, doi:10.1016/0005-2760(95)00006-x (1995).
- Okamoto, Y., Tanaka, S. & Haga, Y. Enhanced GLUT2 gene expression in an oleic acid-induced in vitro fatty liver model. *Hepatol. Res.* **23**, 138-144, doi:10.1016/s1386-6346(01)00172-3 (2002).
- Rao, Y. *et al.* Bouchardatine analogue alleviates non-alcoholic hepatic fatty liver disease/non-alcoholic steatohepatitis in high-fat fed mice by inhibiting ATP synthase activity. *Br. J. Pharmacol.* **176**, 2877-2893, doi:10.1111/bph.14713 (2019).
- Rojas, A. *et al.* Natural Extracts Abolished Lipid Accumulation in Cells Harbouring non-favourable PNPLA3 genotype. *Ann. Hepatol.* **17**, 242-249, doi:10.5604/01.3001.0010.8642 (2018).
- Cui, W., Chen, S. L. & Hu, K. Q. Quantification and mechanisms of oleic acid-induced steatosis in HepG2 cells. *American journal of translational research* **2**, 95-104 (2010).
- Michaut, A. *et al.* A cellular model to study drug-induced liver injury in nonalcoholic fatty liver disease: Application to acetaminophen. *Toxicol. Appl. Pharmacol.* **292**, 40-55, doi:10.1016/j.taap.2015.12.020 (2016).
- Malhi, H., Barreyro, F. J., Isomoto, H., Bronk, S. F. & Gores, G. J. Free fatty acids sensitise hepatocytes to TRAIL mediated cytotoxicity. *Gut* **56**, 1124-1131, doi:10.1136/gut.2006.118059 (2007).
- Akazawa, Y. *et al.* Palmitoleate attenuates palmitate-induced Bim and PUMA up-regulation and hepatocyte lipoapoptosis. *J. Hepatol.* **52**, 586-593, doi:10.1016/j.jhep.2010.01.003 (2010).
- Sharma, S., Mells, J. E., Fu, P. P., Saxena, N. K. & Anania, F. A. GLP-1 analogs reduce hepatocyte steatosis and improve survival by enhancing the unfolded protein response and promoting macroautophagy. *PLoS One* **6**, e25269, doi:10.1371/journal.pone.0025269 (2011).
- Araya, J. *et al.* Increase in long-chain polyunsaturated fatty acid n 6/n 3 ratio in relation to hepatic steatosis in patients with non-alcoholic fatty liver disease. *Clin. Sci. (Lond.)* **106**, 635-643, doi:10.1042/CS20030326 (2004).
- Tanner, N. *et al.* Regulation of Drug Metabolism by the Interplay of Inflammatory Signaling, Steatosis, and Xeno-Sensing Receptors in HepaRG Cells. *Drug Metab. Dispos.* **46**, 326-335, doi:10.1124/dmd.117.078675 (2018).
- AlGhamdi, S., Leoncikas, V., Plant, K. E. & Plant, N. J. Synergistic interaction between lipid-loading and doxorubicin exposure in Huh7 hepatoma cells results in enhanced cytotoxicity and cellular oxidative stress: implications for acute and chronic care of obese cancer patients. *Toxicol Res (Camb)* **4**, 1479-1487, doi:10.1039/c5tx00173k (2015).
- Nehra, V., Angulo, P., Buchman, A. L. & Lindor, K. D. Nutritional and metabolic considerations in the etiology of nonalcoholic steatohepatitis. *Dig. Dis. Sci.* **46**, 2347-2352, doi:10.1023/a:1012338828418 (2001).

- 270 Richieri, G. V. & Kleinfeld, A. M. Unbound free fatty acid levels in human serum. *J. Lipid Res.* **36**, 229-240, doi:10.1016/s0022-2275(20)39899-0 (1995).
- Basak, M. et al. RGS7-ATF3-Tip60 Complex Promotes Hepatic Steatosis and Fibrosis by Directly Inducing TNFalpha. *Antioxid. Redox Signal.* **38**, 137-159, doi:10.1089/ars.2021.0174 (2023).
- Chong, L. W. *et al.* Fluvastatin attenuates hepatic steatosis-induced fibrogenesis in rats through inhibiting paracrine effect of hepatocyte on hepatic stellate cells. *BMC Gastroenterol.* **15**, 22, doi:10.1186/s12876-015-0248-8 (2015).
- Song, Z. *et al.* Silymarin prevents palmitate-induced lipotoxicity in HepG2 cells: involvement of maintenance of Akt kinase activation. *Basic Clin. Pharmacol. Toxicol.* **101**, 262-268, doi:10.1111/j.1742-7843.2007.00116.x (2007).
- Khamphaya, T. *et al.* Nonalcoholic fatty liver disease impairs expression of the type II inositol 1,4,5-trisphosphate receptor. *Hepatology* **67**, 560-574, doi:10.1002/hep.29588 (2018).
- Lee, J. *et al.* Exendin-4 improves steatohepatitis by increasing Sirt1 expression in high-fat diet-induced obese C57BL/6J mice. *PLoS One* **7**, e31394, doi:10.1371/journal.pone.0031394 (2012).
- Li, Y. *et al.* CD36 plays a negative role in the regulation of lipophagy in hepatocytes through an AMPK-dependent pathway. *J. Lipid Res.* **60**, 844-855, doi:10.1194/jlr.M090969 (2019).
- Liu, P. Y. *et al.* E3 ubiquitin ligase Grail promotes hepatic steatosis through Sirt1 inhibition. *Cell Death Dis.* **12**, 323, doi:10.1038/s41419-021-03608-9 (2021).
- Kim, J. H. *et al.* Regulated in Development and DNA Damage Response 1 Protects Hepatocytes Against Palmitate-induced Lipotoxicity. *Biotechnology and Bioprocess Engineering* **27**, 70-78, doi:10.1007/s12257-021-0140-z (2022).
- Cao, J. *et al.* Saturated fatty acid induction of endoplasmic reticulum stress and apoptosis in human liver cells via the PERK/ATF4/CHOP signaling pathway. *Mol. Cell. Biochem.* **364**, 115-129, doi:10.1007/s11010-011-1211-9 (2012).
- Fang, Z. et al. Sestrin Proteins Protect Against Lipotoxicity-Induced Oxidative Stress in the Liver via Suppression of C-Jun N-Terminal Kinases. *Cell Mol Gastroenterol Hepatol* **12**, 921-942, doi:10.1016/j.jcmgh.2021.04.015 (2021).
- 281 Cazanave, S. C. *et al.* Death receptor 5 signaling promotes hepatocyte lipoapoptosis. *J. Biol. Chem.* **286**, 39336-39348, doi:10.1074/jbc.M111.280420 (2011).
- Chang, E. *et al.* Ezetimibe improves hepatic steatosis in relation to autophagy in obese and diabetic rats. *World J. Gastroenterol.* **21**, 7754-7763, doi:10.3748/wjg.v21.i25.7754 (2015).
- Gonzalez-Rodriguez, A. et al. Impaired autophagic flux is associated with increased endoplasmic reticulum stress during the development of NAFLD. *Cell Death Dis.* **5**, e1179, doi:10.1038/cddis.2014.162 (2014).
- Ito, K., Yoshida, K., Maruyama, H., Mamou, J. & Yamaguchi, T. Acoustic Impedance Analysis with High-Frequency Ultrasound for Identification of Fatty Acid Species in the Liver. *Ultrasound Med. Biol.* **43**, 700-711, doi:10.1016/j.ultrasmedbio.2016.11.011 (2017).
- Koletzko, L., Mahli, A. & Hellerbrand, C. Development of an in vitro model to study hepatitis C virus effects on hepatocellular lipotoxicity and lipid metabolism. *Pathol. Res. Pract.* **214**, 1700-1706, doi:10.1016/j.prp.2018.08.013 (2018).
- Liu, X. L. *et al.* miR-192-5p regulates lipid synthesis in non-alcoholic fatty liver disease through SCD-1. *World J. Gastroenterol.* **23**, 8140-8151, doi:10.3748/wjg.v23.i46.8140 (2017).
- Maruyama, H., Kiyono, S., Kondo, T., Sekimoto, T. & Yokosuka, O. Palmitate-induced Regulation of PPARgamma via PGC1alpha: a Mechanism for Lipid Accumulation in the Liver in Nonalcoholic Fatty Liver Disease. *Int. J. Med. Sci.* **13**, 169-178, doi:10.7150/ijms.13581 (2016).
- 288 Masuoka, H. C. *et al.* Mcl-1 degradation during hepatocyte lipoapoptosis. *J. Biol. Chem.* **284**, 30039-30048, doi:10.1074/jbc.M109.039545 (2009).
- Takahara, I. *et al.* Toyocamycin attenuates free fatty acid-induced hepatic steatosis and apoptosis in cultured hepatocytes and ameliorates nonalcoholic fatty liver disease in mice. *PLoS One* **12**, e0170591, doi:10.1371/journal.pone.0170591 (2017).
- Takaki, H. *et al.* Hepatitis C Virus Infection Increases c-Jun N-Terminal Kinase (JNK) Phosphorylation and Accentuates Hepatocyte Lipoapoptosis. *Med. Sci. Monit.* **23**, 4526-4532, doi:10.12659/msm.903210 (2017).
- 291 Kirovski, G. *et al.* Hepatic steatosis causes induction of the chemokine RANTES in the absence of significant hepatic inflammation. *Int. J. Clin. Exp. Pathol.* **3**, 675-680 (2010).
- Xiong, Y. *et al.* Icaritin ameliorates hepatic steatosis via promoting fatty acid beta-oxidation and insulin sensitivity. *Life Sci.* **268**, 119000, doi:10.1016/j.lfs.2020.119000 (2021).
- 293 Hashimoto, T., Sugihara, T., Kanda, T., Takata, T. & Isomoto, H. 5-Aminolevulinic Acid Attenuates Glucose-Regulated Protein 78 Expression and Hepatocyte Lipoapoptosis via Heme Oxygenase-1 Induction. *Int. J. Mol. Sci.* **22**, doi:10.3390/ijms222111405 (2021).

- Docke, S. *et al.* Elevated hepatic chemerin mRNA expression in human non-alcoholic fatty liver disease. *Eur. J. Endocrinol.* **169**, 547-557, doi:10.1530/EJE-13-0112 (2013).
- Krautbauer, S. *et al.* Manganese superoxide dismutase is reduced in the liver of male but not female humans and rodents with non-alcoholic fatty liver disease. *Exp. Mol. Pathol.* **95**, 330-335, doi:10.1016/j.yexmp.2013.10.003 (2013).
- Levada, K. *et al.* Hsp72 protects against liver injury via attenuation of hepatocellular death, oxidative stress, and JNK signaling. *J. Hepatol.* **68**, 996-1005, doi:10.1016/j.jhep.2018.01.003 (2018).
- Lozano-Bartolome, J. *et al.* Reduced circulating levels of sTWEAK are associated with NAFLD and may affect hepatocyte triglyceride accumulation. *Int. J. Obes. (Lond.)* **40**, 1337-1345, doi:10.1038/ijo.2016.73 (2016).
- Shiragannavar, V. D. *et al.* The ameliorating effect of withaferin A on high-fat diet-induced non-alcoholic fatty liver disease by acting as an LXR/FXR dual receptor activator. *Front. Pharmacol.* **14**, 1135952, doi:10.3389/fphar.2023.1135952 (2023).
- Bartolini, D. *et al.* Wheat germ oil vitamin E cytoprotective effect and its nutrigenomics signature in human hepatocyte lipotoxicity. *Heliyon* **8**, e10748, doi:10.1016/j.heliyon.2022.e10748 (2022).
- Bai, X. et al. Valproate induced hepatic steatosis by enhanced fatty acid uptake and triglyceride synthesis. *Toxicol. Appl. Pharmacol.* **324**, 12-25, doi:10.1016/j.taap.2017.03.022 (2017).
- Meex, S. J., Andreo, U., Sparks, J. D. & Fisher, E. A. Huh-7 or HepG2 cells: which is the better model for studying human apolipoprotein-B100 assembly and secretion? *J. Lipid Res.* **52**, 152-158, doi:10.1194/jlr.D008888 (2011).
- Wu, X., Shang, A., Jiang, H. & Ginsberg, H. N. Low rates of apoB secretion from HepG2 cells result from reduced delivery of newly synthesized triglyceride to a "secretion-coupled" pool. *J. Lipid Res.* **37**, 1198-1206, doi:10.1016/s0022-2275(20)39149-5 (1996).
- Wang, S. R. *et al.* Lipid and lipoprotein metabolism in Hep G2 cells. *Biochim. Biophys. Acta* **961**, 351-363, doi:10.1016/0005-2760(88)90082-3 (1988).
- El-Ekiaby, N. M. *et al.* Epigenetic harnessing of HCV via modulating the lipid droplet-protein, TIP47, in HCV cell models. *FEBS Lett.* **589**, 2266-2273, doi:10.1016/j.febslet.2015.06.040 (2015).
- Omanovic Kolaric, T. *et al.* Liraglutide Exerts Protective Effects by Downregulation of PPARgamma, ACSL1 and SREBP-1c in Huh7 Cell Culture Models of Non-Alcoholic Steatosis and Drug-Induced Steatosis. *Curr. Issues Mol. Biol.* **44**, 3465-3480, doi:10.3390/cimb44080239 (2022).
- Tolosa, L. *et al.* Advantageous use of HepaRG cells for the screening and mechanistic study of druginduced steatosis. *Toxicol. Appl. Pharmacol.* **302**, 1-9, doi:10.1016/j.taap.2016.04.007 (2016).
- Breher-Esch, S., Sahini, N., Trincone, A., Wallstab, C. & Borlak, J. Genomics of lipid-laden human hepatocyte cultures enables drug target screening for the treatment of non-alcoholic fatty liver disease. *BMC Med. Genomics* **11**, 111, doi:10.1186/s12920-018-0438-7 (2018).
- Cole, B. K., Feaver, R. E., Wamhoff, B. R. & Dash, A. Non-alcoholic fatty liver disease (NAFLD) models in drug discovery. *Expert Opin Drug Discov* **13**, 193-205, doi:10.1080/17460441.2018.1410135 (2018).
- Gomez-Lechon, M. J. *et al.* A human hepatocellular in vitro model to investigate steatosis. *Chem. Biol. Interact.* **165**, 106-116, doi:10.1016/j.cbi.2006.11.004 (2007).
- Long, J. K., Dai, W., Zheng, Y. W. & Zhao, S. P. miR-122 promotes hepatic lipogenesis via inhibiting the LKB1/AMPK pathway by targeting Sirt1 in non-alcoholic fatty liver disease. *Mol. Med.* **25**, 26, doi:10.1186/s10020-019-0085-2 (2019).
- Sun, Y. *et al.* Berberine ameliorates fatty acid-induced oxidative stress in human hepatoma cells. *Sci. Rep.* **7**, 11340, doi:10.1038/s41598-017-11860-3 (2017).
- Wu, G. Y. *et al.* MicroRNA-122 Inhibits Lipid Droplet Formation and Hepatic Triglyceride Accumulation via Yin Yang 1. *Cell. Physiol. Biochem.* **44**, 1651-1664, doi:10.1159/000485765 (2017).
- Campos-Espinosa, A. & Guzman, C. A Model of Experimental Steatosis In Vitro: Hepatocyte Cell Culture in Lipid Overload-Conditioned Medium. *J Vis Exp*, doi:10.3791/62543 (2021).
- Pipitone, R. M. *et al.* Curcumin and Andrographolide Co-Administration Safely Prevent Steatosis Induction and ROS Production in HepG2 Cell Line. *Molecules* **28**, doi:10.3390/molecules28031261 (2023).
- 315 Hu, Z., Li, Y., Ma, B., Lei, S. & Wang, X. Iron metabolism mediates the relationship between Vitamin C and hepatic steatosis and fibrosis in NAFLD. *Front Nutr* **9**, 952056, doi:10.3389/fnut.2022.952056 (2022).
- Patil, N. Y. *et al.* Cinnabarinic Acid Provides Hepatoprotection Against Nonalcoholic Fatty Liver Disease. *J. Pharmacol. Exp. Ther.* **383**, 32-43, doi:10.1124/jpet.122.001301 (2022).
- 317 Cazanave, S. C. *et al.* JNK1-dependent PUMA expression contributes to hepatocyte lipoapoptosis. *J. Biol. Chem.* **284**, 26591-26602, doi:10.1074/jbc.M109.022491 (2009).
- Cazanave, S. C. *et al.* CHOP and AP-1 cooperatively mediate PUMA expression during lipoapoptosis. *Am. J. Physiol. Gastrointest. Liver Physiol.* **299**, G236-243, doi:10.1152/ajpgi.00091.2010 (2010).

- 319 Cazanave, S. C. *et al.* A role for miR-296 in the regulation of lipoapoptosis by targeting PUMA. *J. Lipid Res.* **52**, 1517-1525, doi:10.1194/jlr.M014654 (2011).
- Feldstein, A. E. *et al.* Diet associated hepatic steatosis sensitizes to Fas mediated liver injury in mice. *J. Hepatol.* **39**, 978-983, doi:10.1016/s0168-8278(03)00460-4 (2003).
- 321 Kim, M. S. *et al.* Compound K modulates fatty acid-induced lipid droplet formation and expression of proteins involved in lipid metabolism in hepatocytes. *Liver Int* **33**, 1583-1593, doi:10.1111/liv.12287 (2013).
- Kurt, R. *et al.* Chaperone-Mediated Autophagy Targets IFNAR1 for Lysosomal Degradation in Free Fatty Acid Treated HCV Cell Culture. *PLoS One* **10**, e0125962, doi:10.1371/journal.pone.0125962 (2015).
- Sahini, N. & Borlak, J. Genomics of human fatty liver disease reveal mechanistically linked lipid droplet-associated gene regulations in bland steatosis and nonalcoholic steatohepatitis. *Transl. Res.* **177**, 41-69, doi:10.1016/j.trsl.2016.06.003 (2016).
- Tse, E. *et al.* Fatty Acids Induce a Pro-Inflammatory Gene Expression Profile in Huh-7 Cells That Attenuates the Anti-HCV Action of Interferon. *J. Interferon Cytokine Res.* **35**, 392-400, doi:10.1089/jir.2014.0165 (2015).
- Woolsey, S. J., Mansell, S. E., Kim, R. B., Tirona, R. G. & Beaton, M. D. CYP3A Activity and Expression in Nonalcoholic Fatty Liver Disease. *Drug Metab. Dispos.* **43**, 1484-1490, doi:10.1124/dmd.115.065979 (2015).
- Infante-Menendez, J. *et al.* Increased let-7d-5p in non-alcoholic fatty liver promotes insulin resistance and is a potential blood biomarker for diagnosis. *Liver Int* **n/a**, doi:10.1111/liv.15581 (2023).
- Gunduz, F. *et al.* Free fatty acids induce ER stress and block antiviral activity of interferon alpha against hepatitis C virus in cell culture. *Virol J.* **9**, 143, doi:10.1186/1743-422X-9-143 (2012).
- Donato, M. T. *et al.* Effects of steatosis on drug-metabolizing capability of primary human hepatocytes. *Toxicol. In Vitro* **21**, 271-276, doi:10.1016/j.tiv.2006.07.008 (2007).
- Donato, M. T. *et al.* Potential impact of steatosis on cytochrome P450 enzymes of human hepatocytes isolated from fatty liver grafts. *Drug Metab. Dispos.* **34**, 1556-1562, doi:10.1124/dmd.106.009670 (2006).
- Prill, S. *et al.* The TM6SF2 E167K genetic variant induces lipid biosynthesis and reduces apolipoprotein B secretion in human hepatic 3D spheroids. *Sci. Rep.* **9**, 11585, doi:10.1038/s41598-019-47737-w (2019).
- Rey-Bedon, C. *et al.* CYP450 drug inducibility in NAFLD via an in vitro hepatic model: Understanding drug-drug interactions in the fatty liver. *Biomed. Pharmacother.* **146**, 112377, doi:10.1016/j.biopha.2021.112377 (2022).
- Bucher, S. *et al.* Possible Involvement of Mitochondrial Dysfunction and Oxidative Stress in a Cellular Model of NAFLD Progression Induced by Benzo[a]pyrene/Ethanol CoExposure. *Oxid. Med. Cell. Longev.* **2018**, 4396403, doi:10.1155/2018/4396403 (2018).
- Bucher, S. *et al.* Co-exposure to benzo[a]pyrene and ethanol induces a pathological progression of liver steatosis in vitro and in vivo. *Sci. Rep.* **8**, 5963, doi:10.1038/s41598-018-24403-1 (2018).
- Koenen, M. T. *et al.* Extracellular Vesicles from Steatotic Hepatocytes Provoke Pro-Fibrotic Responses in Cultured Stellate Cells. *Biomolecules* **12**, doi:10.3390/biom12050698 (2022).
- Longato, L., Tong, M., Wands, J. R. & de la Monte, S. M. High fat diet induced hepatic steatosis and insulin resistance: Role of dysregulated ceramide metabolism. *Hepatol. Res.* **42**, 412-427, doi:10.1111/j.1872-034X.2011.00934.x (2012).
- Cordero-Herrera, I. *et al.* AMP-activated protein kinase activation and NADPH oxidase inhibition by inorganic nitrate and nitrite prevent liver steatosis. *Proc. Natl. Acad. Sci. U. S. A.* **116**, 217-226, doi:10.1073/pnas.1809406115 (2019).
- van der Vusse, G. J. Albumin as fatty acid transporter. *Drug Metab. Pharmacokinet.* **24**, 300-307, doi:10.2133/dmpk.24.300 (2009).
- Silva, M. F. *et al.* Valproic acid metabolism and its effects on mitochondrial fatty acid oxidation: a review. *J. Inherit. Metab. Dis.* **31**, 205-216, doi:10.1007/s10545-008-0841-x (2008).
- Donato, M. T. & Gomez-Lechon, M. J. Drug-induced liver steatosis and phospholipidosis: cell-based assays for early screening of drug candidates. *Curr. Drug Metab.* **13**, 1160-1173, doi:10.2174/138920012802850001 (2012).
- Kohonen, P. *et al.* The ToxBank Data Warehouse: Supporting the Replacement of In Vivo Repeated Dose Systemic Toxicity Testing. *Mol. Inform.* **32**, 47-63, doi:10.1002/minf.201200114 (2013).
- Jennings, P. *et al.* SEURAT-1 liver gold reference compounds: a mechanism-based review. *Arch. Toxicol.* **88**, 2099-2133, doi:10.1007/s00204-014-1410-8 (2014).
- Willebrords, J. *et al.* Strategies, models and biomarkers in experimental non-alcoholic fatty liver disease research. *Prog. Lipid Res.* **59**, 106-125, doi:10.1016/j.plipres.2015.05.002 (2015).

- Knapp, A. C. *et al.* Toxicity of valproic acid in mice with decreased plasma and tissue carnitine stores. *J. Pharmacol. Exp. Ther.* **324**, 568-575, doi:10.1124/jpet.107.131185 (2008).
- Fromenty, B. & Pessayre, D. Inhibition of mitochondrial beta-oxidation as a mechanism of hepatotoxicity. *Pharmacol. Ther.* **67**, 101-154, doi:10.1016/0163-7258(95)00012-6 (1995).
- Amacher, D. E. Strategies for the early detection of drug-induced hepatic steatosis in preclinical drug safety evaluation studies. *Toxicology* **279**, 10-18, doi:10.1016/j.tox.2010.10.006 (2011).
- Freneaux, E. *et al.* Inhibition of the mitochondrial oxidation of fatty acids by tetracycline in mice and in man: possible role in microvesicular steatosis induced by this antibiotic. *Hepatology* **8**, 1056-1062, doi:10.1002/hep.1840080513 (1988).
- Lewis, J. H. *et al.* Histopathologic analysis of suspected amiodarone hepatotoxicity. *Hum. Pathol.* **21**, 59-67, doi:10.1016/0046-8177(90)90076-h (1990).
- Krensky, A. M., Azzi, J. R. & Hafler, D. A. in *Goodman & Gilman's: The Pharmacological Basis of Therapeutics, 13e* (eds Laurence L. Brunton, Randa Hilal-Dandan, & Björn C. Knollmann) (McGraw-Hill Education, 2017).
- Donato, M. T., Tolosa, L., Jimenez, N., Castell, J. V. & Gomez-Lechon, M. J. High-content imaging technology for the evaluation of drug-induced steatosis using a multiparametric cell-based assay. *J. Biomol. Screen.* **17**, 394-400, doi:10.1177/1087057111427586 (2012).
- Rezzani, R. Exploring cyclosporine A-side effects and the protective role-played by antioxidants: the morphological and immunohistochemical studies. *Histol. Histopathol.* **21**, 301-316, doi:10.14670/HH-21.301 (2006).
- Garcia-Roman, R. & Frances, R. Acetaminophen-Induced Liver Damage in Hepatic Steatosis. *Clin. Pharmacol. Ther.* **107**, 1068-1081, doi:10.1002/cpt.1701 (2020).
- McGill, M. R. & Jaeschke, H. Metabolism and disposition of acetaminophen: recent advances in relation to hepatotoxicity and diagnosis. *Pharm. Res.* **30**, 2174-2187, doi:10.1007/s11095-013-1007-6 (2013).
- Bucher, S. *et al.* Bisphenol a induces steatosis in HepaRG cells using a model of perinatal exposure. *Environ. Toxicol.* **32**, 1024-1036, doi:10.1002/tox.22301 (2017).
- Forgacs, A. L., Dere, E., Angrish, M. M. & Zacharewski, T. R. Comparative analysis of temporal and dose-dependent TCDD-elicited gene expression in human, mouse, and rat primary hepatocytes. *Toxicol. Sci.* **133**, 54-66, doi:10.1093/toxsci/kft028 (2013).
- Lichtenstein, D. *et al.* Transcript and protein marker patterns for the identification of steatotic compounds in human HepaRG cells. *Food Chem. Toxicol.* **145**, 111690, doi:10.1016/j.fct.2020.111690 (2020).
- Lin, Y. et al. Downregulation of miR-192 causes hepatic steatosis and lipid accumulation by inducing SREBF1: Novel mechanism for bisphenol A-triggered non-alcoholic fatty liver disease. *Biochim Biophys Acta Mol Cell Biol Lipids* **1862**, 869-882, doi:10.1016/j.bbalip.2017.05.001 (2017).
- Luckert, C. *et al.* Adverse Outcome Pathway-Driven Analysis of Liver Steatosis in Vitro: A Case Study with Cyproconazole. *Chem. Res. Toxicol.* **31**, 784-798, doi:10.1021/acs.chemrestox.8b00112 (2018).
- Wandrer, F. *et al.* Autophagy alleviates amiodarone-induced hepatotoxicity. *Arch. Toxicol.* **94**, 3527-3539, doi:10.1007/s00204-020-02837-9 (2020).
- Parmentier, C. *et al.* Transcriptomic hepatotoxicity signature of chlorpromazine after short- and long-term exposure in primary human sandwich cultures. *Drug Metab. Dispos.* **41**, 1835-1842, doi:10.1124/dmd.113.052415 (2013).
- Stankov, M. V. *et al.* Autophagy inhibition due to thymidine analogues as novel mechanism leading to hepatocyte dysfunction and lipid accumulation. *AIDS* **26**, 1995-2006, doi:10.1097/QAD.0b013e32835804f9 (2012).
- Leite, S. B. *et al.* Novel human hepatic organoid model enables testing of drug-induced liver fibrosis in vitro. *Biomaterials* **78**, 1-10, doi:10.1016/j.biomaterials.2015.11.026 (2016).
- Yan, L. *et al.* PXR-mediated expression of FABP4 promotes valproate-induced lipid accumulation in HepG2 cells. *Toxicol. Lett.* **346**, 47-56, doi:10.1016/j.toxlet.2021.04.016 (2021).
- Elphick, L. M. *et al.* Conserved valproic-acid-induced lipid droplet formation in Dictyostelium and human hepatocytes identifies structurally active compounds. *Dis. Model. Mech.* **5**, 231-240, doi:10.1242/dmm.008391 (2012).
- van Breda, S. G. J. *et al.* Integrative omics data analyses of repeated dose toxicity of valproic acid in vitro reveal new mechanisms of steatosis induction. *Toxicology* **393**, 160-170, doi:10.1016/j.tox.2017.11.013 (2018).
- Reimer, K. C., Wree, A., Roderburg, C. & Tacke, F. New drugs for NAFLD: lessons from basic models to the clinic. *Hepatol. Int.* **14**, 8-23, doi:10.1007/s12072-019-10001-4 (2020).
- 366 Dufour, J. F. *et al.* Current therapies and new developments in NASH. *Gut* **71**, 2123-2134, doi:10.1136/gutjnl-2021-326874 (2022).

- Chen, J. Y. S., Chua, D., Lim, C. O., Ho, W. X. & Tan, N. S. Lessons on Drug Development: A Literature Review of Challenges Faced in Nonalcoholic Fatty Liver Disease (NAFLD) Clinical Trials. *Int. J. Mol. Sci.* **24**, doi:10.3390/ijms24010158 (2022).
- Vuppalanchi, R., Noureddin, M., Alkhouri, N. & Sanyal, A. J. Therapeutic pipeline in nonalcoholic steatohepatitis. *Nat. Rev. Gastroenterol. Hepatol.* **18**, 373-392, doi:10.1038/s41575-020-00408-y (2021).
- Marxer, R. A. Design of novel lipid-based solid oral formulations for the therapy of liver fibrosis MSc in Pharmacy thesis, University of Bern, (2021).
- 370 Maev, I. V. *et al.* Real-world comorbidities and treatment patterns among patients with non-alcoholic fatty liver disease receiving phosphatidylcholine as adjunctive therapy in Russia. *BMJ Open Gastroenterol* **6**, e000307, doi:10.1136/bmjgast-2019-000307 (2019).
- Valentino, G. *Oral Lipid-based Formulations Designed for the Treatment of Chronic Liver Pathologies*PhD in Chemistry and Molecular Sciences thesis, University of Bern, (2020).
- Grune, L. & Bunjes, H. Suitability of phosphatidylcholine-based formulations for liquid filling in hard capsules. *Eur. J. Pharm. Sci.* **153**, 105470, doi:10.1016/j.ejps.2020.105470 (2020).
- Oral Lipid-Based Formulations: Enhancing the Bioavailability of Poorly Water-Soluble Drugs. 1 edn, (CRC Press, 2007).
- Kuentz, M. Lipid-based formulations for oral delivery of lipophilic drugs. *Drug Discov Today Technol* **9**, e71-e174, doi:10.1016/j.ddtec.2012.03.002 (2012).
- van Hoogevest, P. Review An update on the use of oral phospholipid excipients. *Eur. J. Pharm. Sci.* **108**, 1-12, doi:10.1016/j.ejps.2017.07.008 (2017).
- Koch, N., Jennotte, O., Toussaint, C., Lechanteur, A. & Evrard, B. Production challenges of tablets containing lipid excipients: Case study using cannabidiol as drug model. *Int. J. Pharm.* **633**, 122639, doi:10.1016/j.ijpharm.2023.122639 (2023).
- 377 European Pharmacopoeia 11. 11 edn, (European Directorate for the Quality of Medicines & HealthCare, 2023).
- Gillessen, A. & Schmidt, H. H. Silymarin as Supportive Treatment in Liver Diseases: A Narrative Review. *Adv. Ther.* **37**, 1279-1301, doi:10.1007/s12325-020-01251-y (2020).
- Federico, A., Dallio, M. & Loguercio, C. Silymarin/Silybin and Chronic Liver Disease: A Marriage of Many Years. *Molecules* **22**, doi:10.3390/molecules22020191 (2017).
- Snee, R. D. Experimental designs for mixture systems with multicomponent constraints. *Communications in Statistics Theory and Methods* **8**, 303-326, doi:10.1080/03610927908827762 (1979).
- 381 Snee, R. D. & Marquardt, D. W. Extreme Vertices Designs for Linear Mixture Models. *Technometrics* **16**, 399-408, doi:10.1080/00401706.1974.10489209 (1974).
- Mortimer, B. C. *et al.* Features of Cholesterol Structure That Regulate the Clearance of Chylomicron-Like Lipid Emulsions. *J. Lipid Res.* **36**, 2038-2053, doi:10.1016/S0022-2275(20)41121-6 (1995).
- Fernandez-Iglesias, A., Ortega-Ribera, M., Guixe-Muntet, S. & Gracia-Sancho, J. 4 in 1: Antibody-free protocol for isolating the main hepatic cells from healthy and cirrhotic single rat livers. *J. Cell. Mol. Med.* **23**, 877-886, doi:10.1111/jcmm.13988 (2019).
- 384 Schindelin, J. *et al.* Fiji: an open-source platform for biological-image analysis. *Nat. Methods* **9**, 676-682, doi:10.1038/nmeth.2019 (2012).
- Livak, K. J. & Schmittgen, T. D. Analysis of relative gene expression data using real-time quantitative PCR and the 2(-Delta Delta C(T)) Method. *Methods* **25**, 402-408, doi:10.1006/meth.2001.1262 (2001).
- Tan, A., Rao, S. & Prestidge, C. A. Transforming lipid-based oral drug delivery systems into solid dosage forms: an overview of solid carriers, physicochemical properties, and biopharmaceutical performance. *Pharm. Res.* **30**, 2993-3017, doi:10.1007/s11095-013-1107-3 (2013).
- Hentzschel, C. M., Sakmann, A. & Leopold, C. S. Suitability of various excipients as carrier and coating materials for liquisolid compacts. *Drug Dev. Ind. Pharm.* **37**, 1200-1207, doi:10.3109/03639045.2011.564184 (2011).
- Chakraborty, S., Shukla, D., Vuddanda, P. R., Mishra, B. & Singh, S. Utilization of adsorption technique in the development of oral delivery system of lipid based nanoparticles. *Colloids Surf. B. Biointerfaces* **81**, 563-569, doi:10.1016/j.colsurfb.2010.07.058 (2010).
- Gumaste, S. G. *et al.* Development of Solid SEDDS, IV: Effect of Adsorbed Lipid and Surfactant on Tableting Properties and Surface Structures of Different Silicates. *Pharm. Res.* **30**, 3170-3185, doi:10.1007/s11095-013-1114-4 (2013).
- Gumaste, S. G., Dalrymple, D. M. & Serajuddin, A. T. Development of Solid SEDDS, V: Compaction and Drug Release Properties of Tablets Prepared by Adsorbing Lipid-Based Formulations onto Neusilin(R) US2. *Pharm. Res.* **30**, 3186-3199, doi:10.1007/s11095-013-1106-4 (2013).

- Gumaste, S. G., Freire, B. O. S. & Serajuddin, A. T. M. Development of solid SEDDS, VI: Effect of precoating of Neusilin((R)) US2 with PVP on drug release from adsorbed self-emulsifying lipid-based formulations. *Eur. J. Pharm. Sci.* **110**, 124-133, doi:10.1016/j.ejps.2017.02.022 (2017).
- Williams, H. D., Van Speybroeck, M., Augustijns, P. & Porter, C. J. Lipid-based formulations solidified via adsorption onto the mesoporous carrier Neusilin(R) US2: effect of drug type and formulation composition on in vitro pharmaceutical performance. *J. Pharm. Sci.* **103**, 1734-1746, doi:10.1002/jps.23970 (2014).
- de Avelar, C. R. *et al.* Efficacy of silymarin in patients with non-alcoholic fatty liver disease the Siliver trial: a study protocol for a randomized controlled clinical trial. *Trials* **24**, 177, doi:10.1186/s13063-023-07210-6 (2023).
- 394 Kapoor, D. et al. in Drug Delivery Systems (ed Rakesh K. Tekade) 665-719 (Academic Press, 2020).
- 395 Chapman, D. & Collin, D. T. Differential thermal analysis of phospholipids. *Nature* **206**, 189, doi:10.1038/206189a0 (1965).
- Thoorens, G., Krier, F., Leclercq, B., Carlin, B. & Evrard, B. Microcrystalline cellulose, a direct compression binder in a quality by design environment--a review. *Int. J. Pharm.* **473**, 64-72, doi:10.1016/j.ijpharm.2014.06.055 (2014).
- Trache, D. *et al.* Microcrystalline cellulose: Isolation, characterization and bio-composites application-A review. *Int. J. Biol. Macromol.* **93**, 789-804, doi:10.1016/j.ijbiomac.2016.09.056 (2016).
- Kolbina, M., Bodmeier, R. & Korber, M. Saturated phosphatidylcholine as matrix former for oral extended release dosage forms. *Eur. J. Pharm. Sci.* **108**, 86-92, doi:10.1016/j.ejps.2017.07.017 (2017).
- Porter, C. J. H. & Charman, W. N. Uptake of drugs into the intestinal lymphatics after oral administration. *Adv. Drug Del. Rev.* **25**, 71-89, doi:Doi 10.1016/S0169-409x(96)00492-9 (1997).
- Tso, P. & Balint, J. A. Formation and transport of chylomicrons by enterocytes to the lymphatics. *Am. J. Physiol.* **250**, G715-726, doi:10.1152/ajpqi.1986.250.6.G715 (1986).
- Nayak, N., Harrison, E. H. & Hussain, M. M. Retinyl ester secretion by intestinal cells: a specific and regulated process dependent on assembly and secretion of chylomicrons. *J. Lipid Res.* **42**, 272-280, doi:10.1016/S0022-2275(20)31689-8 (2001).
- Sautot, P. *et al.* Structural, hydration, and phase transition properties of phosphatidylcholine from salmon heads. *Eur. J. Lipid Sci. Technol.* **113**, 744-755, doi:10.1002/ejlt.201000449 (2011).
- Kolbina, M., Schulte, A., van Hoogevest, P., Korber, M. & Bodmeier, R. Evaluation of Hydrogenated Soybean Phosphatidylcholine Matrices Prepared by Hot Melt Extrusion for Oral Controlled Delivery of Water-Soluble Drugs. *AAPS PharmSciTech* **20**, 159, doi:10.1208/s12249-019-1366-3 (2019).
- Pence, I. & Mahadevan-Jansen, A. Clinical instrumentation and applications of Raman spectroscopy. *Chem. Soc. Rev.* **45**, 1958-1979, doi:10.1039/c5cs00581g (2016).
- Azad, M., Moreno, J. & Dave, R. Stable and Fast-Dissolving Amorphous Drug Composites Preparation via Impregnation of Neusilin((R)) UFL2. *J. Pharm. Sci.* **107**, 170-182, doi:10.1016/j.xphs.2017.10.007 (2018).
- Kochan, K. *et al.* IR and Raman imaging of murine brains from control and ApoE/LDLR(-/-) mice with advanced atherosclerosis. *Analyst* **141**, 5329-5338, doi:10.1039/c6an00107f (2016).
- Bligh, E. G. & Dyer, W. J. A rapid method of total lipid extraction and purification. *Can. J. Biochem. Physiol.* **37**, 911-917, doi:10.1139/o59-099 (1959).
- 408 Rahnfeld, L., Thamm, J., Steiniger, F., van Hoogevest, P. & Luciani, P. Study on the in situ aggregation of liposomes with negatively charged phospholipids for use as injectable depot formulation. *Colloids Surf. B. Biointerfaces* **168**, 10-17, doi:10.1016/j.colsurfb.2018.02.023 (2018).
- Tso, P., Lindstrom, M. B. & Borgstrom, B. Factors regulating the formation of chylomicrons and very-low-density lipoproteins by the rat small intestine. *Biochim. Biophys. Acta* **922**, 304-313, doi:10.1016/0005-2760(87)90053-1 (1987).
- Londos, C., Sztalryd, C., Tansey, J. T. & Kimmel, A. R. Role of PAT proteins in lipid metabolism. *Biochimie* 87, 45-49, doi:10.1016/j.biochi.2004.12.010 (2005).
- Kocabayoglu, P. *et al.* beta-PDGF receptor expressed by hepatic stellate cells regulates fibrosis in murine liver injury, but not carcinogenesis. *J. Hepatol.* **63**, 141-147, doi:10.1016/j.jhep.2015.01.036 (2015).
- Kikuchi, A. *et al.* Hepatic Stellate Cell-Specific Platelet-Derived Growth Factor Receptor-alpha Loss Reduces Fibrosis and Promotes Repair after Hepatocellular Injury. *Am. J. Pathol.* **190**, 2080-2094, doi:10.1016/j.ajpath.2020.06.006 (2020).
- Lambrecht, J. *et al.* A PDGFRbeta-based score predicts significant liver fibrosis in patients with chronic alcohol abuse, NAFLD and viral liver disease. *EBioMedicine* **43**, 501-512, doi:10.1016/j.ebiom.2019.04.036 (2019).
- Donovan, J., Abraham, D. & Norman, J. Platelet-derived growth factor signaling in mesenchymal cells. Front Biosci (Landmark Ed) 18, 106-119, doi:10.2741/4090 (2013).

- Rovida, E., Navari, N., Caligiuri, A., Dello Sbarba, P. & Marra, F. ERK5 differentially regulates PDGF-induced proliferation and migration of hepatic stellate cells. *J. Hepatol.* **48**, 107-115, doi:10.1016/j.jhep.2007.08.010 (2008).
- Jeng, K. S., Lu, S. J., Wang, C. H. & Chang, C. F. Liver Fibrosis and Inflammation under the Control of ERK2. *Int. J. Mol. Sci.* **21**, 3796, doi:10.3390/ijms21113796 (2020).
- Kim, Y. *et al.* Anti-fibrotic activity and enhanced interleukin-6 production by hepatic stellate cells in response to imatinib mesylate. *Liver Int* **32**, 1008-1017, doi:10.1111/j.1478-3231.2012.02806.x (2012).
- Reichenbach, V. *et al.* Adenoviral dominant-negative soluble PDGFRbeta improves hepatic collagen, systemic hemodynamics, and portal pressure in fibrotic rats. *J. Hepatol.* **57**, 967-973, doi:10.1016/j.jhep.2012.07.012 (2012).
- Borkham-Kamphorst, E. *et al.* Platelet-derived growth factor isoform expression in carbon tetrachloride-induced chronic liver injury. *Lab. Invest.* **88**, 1090-1100, doi:10.1038/labinvest.2008.71 (2008).
- Neef, M. *et al.* Oral imatinib treatment reduces early fibrogenesis but does not prevent progression in the long term. *J. Hepatol.* **44**, 167-175, doi:10.1016/j.jhep.2005.06.015 (2006).
- Barker, T. H. *et al.* SPARC regulates extracellular matrix organization through its modulation of integrin-linked kinase activity. *J. Biol. Chem.* **280**, 36483-36493, doi:10.1074/jbc.M504663200 (2005).
- Trombetta-Esilva, J. & Bradshaw, A. D. The Function of SPARC as a Mediator of Fibrosis. *Open Rheumatol. J.* **6**, 146-155, doi:10.2174/1874312901206010146 (2012).
- 423 Camino, A. M. *et al.* Adenovirus-mediated inhibition of SPARC attenuates liver fibrosis in rats. *J. Gene Med.* **10**, 993-1004, doi:10.1002/jgm.1228 (2008).
- Wang, J., Ding, Y. & Zhou, W. Albumin self-modified liposomes for hepatic fibrosis therapy via SPARC-dependent pathways. *Int. J. Pharm.* **574**, 118940, doi:10.1016/j.ijpharm.2019.118940 (2020).
- A, M. O. *et al.* SPARC inhibition accelerates NAFLD-associated hepatocellular carcinoma development by dysregulating hepatic lipid metabolism. *Liver Int* **41**, 1677-1693, doi:10.1111/liv.14857 (2021).
- Mazzolini, G. *et al.* SPARC expression is associated with hepatic injury in rodents and humans with non-alcoholic fatty liver disease. *Sci. Rep.* **8**, 725, doi:10.1038/s41598-017-18981-9 (2018).
- He, L., Yuan, H., Liang, J., Hong, J. & Qu, C. Expression of hepatic stellate cell activation-related genes in HBV-, HCV-, and nonalcoholic fatty liver disease-associated fibrosis. *PLoS One* **15**, e0233702, doi:10.1371/journal.pone.0233702 (2020).
- O'Mahony, F. *et al.* Liver X receptors balance lipid stores in hepatic stellate cells through Rab18, a retinoid responsive lipid droplet protein. *Hepatology* **62**, 615-626, doi:10.1002/hep.27645 (2015).
- do Canto, A. *et al.* Diphenylhexatriene membrane probes DPH and TMA-DPH: A comparative molecular dynamics simulation study. *Biochim. Biophys. Acta* **1858**, 2647-2661, doi:10.1016/j.bbamem.2016.07.013 (2016).
- 430 Saneyasu, T., Akhtar, R. & Sakai, T. Molecular Cues Guiding Matrix Stiffness in Liver Fibrosis. *Biomed Res Int* **2016**, 2646212, doi:10.1155/2016/2646212 (2016).
- Sakata, R., Ueno, T., Nakamura, T., Ueno, H. & Sata, M. Mechanical stretch induces TGF-beta synthesis in hepatic stellate cells. *Eur. J. Clin. Invest.* **34**, 129-136, doi:10.1111/j.1365-2362.2004.01302.x (2004).
- Chiabotto, G., Ceccotti, E. & Bruno, S. Narrative review of in vitro experimental models of hepatic fibrogenesis. *Digestive Medicine Research* **5**, 33-33, doi:10.21037/dmr-21-102 (2022).
- Wu, X. *et al.* Precision-cut human liver slice cultures as an immunological platform. *J. Immunol. Methods* **455**, 71-79, doi:10.1016/j.jim.2018.01.012 (2018).
- Palma, E., Doornebal, E. J. & Chokshi, S. Precision-cut liver slices: a versatile tool to advance liver research. *Hepatol. Int.* **13**, 51-57, doi:10.1007/s12072-018-9913-7 (2019).
- Dowling, P. & Clynes, M. Conditioned media from cell lines: a complementary model to clinical specimens for the discovery of disease-specific biomarkers. *Proteomics* **11**, 794-804, doi:10.1002/pmic.201000530 (2011).
- Shen, H. et al. Hepatocyte-derived VEGFA accelerates the progression of non-alcoholic fatty liver disease to hepatocellular carcinoma via activating hepatic stellate cells. *Acta Pharmacol. Sin.* **43**, 2917-2928, doi:10.1038/s41401-022-00907-5 (2022).
- Wijayasiri, P. *et al.* Role of Hepatocyte Senescence in the Activation of Hepatic Stellate Cells and Liver Fibrosis Progression. *Cells* **11**, doi:10.3390/cells11142221 (2022).
- Li, Z. et al. A non-autonomous role of MKL1 in the activation of hepatic stellate cells. Biochim Biophys Acta Gene Regul Mech **1862**. 609-618. doi:10.1016/j.bbagrm.2019.03.001 (2019).
- Mekala, S. *et al.* Cellular crosstalk mediated by platelet-derived growth factor BB and transforming growth factor beta during hepatic injury activates hepatic stellate cells. *Can. J. Physiol. Pharmacol.* **96**, 728-741, doi:10.1139/cjpp-2017-0768 (2018).
- Schulze-Krebs, A. *et al.* Hepatitis C virus-replicating hepatocytes induce fibrogenic activation of hepatic stellate cells. *Gastroenterology* **129**, 246-258, doi:10.1053/j.gastro.2005.03.089 (2005).

- Marti-Rodrigo, A. *et al.* Rilpivirine attenuates liver fibrosis through selective STAT1-mediated apoptosis in hepatic stellate cells. *Gut* **69**, 920-932, doi:10.1136/gutjnl-2019-318372 (2020).
- Wang, H., Lafdil, F., Kong, X. & Gao, B. Signal transducer and activator of transcription 3 in liver diseases: a novel therapeutic target. *Int. J. Biol. Sci.* **7**, 536-550, doi:10.7150/ijbs.7.536 (2011).
- Gandhi, C. R. Hepatic stellate cell activation and pro-fibrogenic signals. *J. Hepatol.* **67**, 1104-1105, doi:10.1016/j.jhep.2017.06.001 (2017).
- Castilla, A., Prieto, J. & Fausto, N. Transforming growth factors beta 1 and alpha in chronic liver disease. Effects of interferon alfa therapy. *N. Engl. J. Med.* **324**, 933-940, doi:10.1056/NEJM199104043241401 (1991).
- Dewidar, B., Meyer, C., Dooley, S. & Meindl-Beinker, A. N. TGF-beta in Hepatic Stellate Cell Activation and Liver Fibrogenesis-Updated 2019. *Cells* **8**, doi:10.3390/cells8111419 (2019).
- Weber, F., Rahnfeld, L. & Luciani, P. Analytical profiling and stability evaluation of liposomal drug delivery systems: A rapid UHPLC-CAD-based approach for phospholipids in research and quality control. *Talanta* **220**, 121320, doi:10.1016/j.talanta.2020.121320 (2020).

Acknowledgements

Since I have told my long research story in the previous pages, it is a time and place to thank certain people that were part of my challenging 3.5-year-long PhD journey.

I express my sincere gratitude to Prof. Dr. Paola Luciani, Prof. Dr. Francesca Paradisi, and Prof. Dr. Francesca Ridi for their valuable time and commitment to evaluating my doctoral dissertation and being part of my PhD defence committee.

I would really like to thank Prof. Dr. Paola Luciani for giving me the opportunity to work in her laboratory and for all support he provided. She was always available to guide me through a very complex labyrinth that every PhD student experiences on their way, pursuing different projects and having a pragmatic approach to sometimes very challenging experiments and timelines by employing a principle that no goal is distant enough if we put ourselves to it. Despite encountering some challenging moments, I am immensely grateful for the valuable experience I gained throughout this journey. This process has enabled me to develop and grow as a more proficient scientist and well-rounded individual. I appreciate the lessons learned and the personal growth that has occurred because of these trials.

My special thanks go to Prof. Dr. Francesca Ridi, that accepted to be a part of my defence committee but was also available to run a smooth and productive collaboration on the tablet characterisation supervising Dr. Rita Gelli. They showed me by example how scientific collaboration should be done to be fruitful.

Further, thanks go to Prof. Dr. Francesca Paradisi for chairing my PhD defence and following, from a distance, my research from my first presentation at the First Year Graduate Symposium of our Department.

I am deeply thankful to Dr. Gina Valentino, with whom I spent a certain time working together, for all the passion we shared for these and other different projects, and who introduced me to Pharmaceutical Technology working ways in Bern.

Dr. Simone Aleandri's help is highly appreciated for all his scientific expertise and crisis management that happened here and there.

I would like to sincerely thank all current and former members of Luciani Research Group, with particular regard to "my generation" Aymar, Marianna, Gregor, Cristina, and Sarah, for all the valuable scientific discussion and time spent together. I am appreciative to have met Assumpta and that I was able to introduce her to our laboratory for the last few months of my way, and she will continue to investigate where I stopped. I am grateful to Remo for all our discussions, not only on scientific topics and for the non-repeatable exchange of military

Fresspäcklis. I appreciate meeting Christoph for having a great time that first July Praktikum. I am grateful to have met and learnt from Rafaela, Despo, Lisa, Florian, and all the former Masters and Bachelor students in our group.

My distinct thanks go to Roseanne, my master student for working along on our tablets story, Elena, and Glòria, for the moral support. Jedno veliko hvala Ani i Tijani, što su radile zajedno sa mnom na ostvarenju naših zajedničkih ciljeva.

My big thanks go to the Hepatology Research Group of DBMR headed by Prof. Dr. Annalisa Berzigotti for all the provided help with primary rat cells, especially Dr. Eric Felli, Dr. Jordi Gracia, Sonia-Emilia Selicean, Cong Wang, and Yeliduosi Nulan.

Special thanks go to Dr. Sofia Nasif, Nicole Kleinschmidt and Prof. Dr. Oliver Mühlemann for supporting qPCR experiments.

Ich bin sehr dankbar an den Dienstleistungen des DCBPs, Materialausgabe, Hausdienst und Werkstatt, die immer da waren, wenn ich ihnen brauchte. Meine endlosen Anfragen und Anforderungen waren immer prompt erledigt und in einer besten Art. Meine spezielle Merci gehen Marco, Dani, Michel, Heiner, Samuel und Adrian an. Dieses Department würde nie gleich ohne Euch sein! Meine beste Immigrationsberaterin war Beatrice Thoenen. Ich bin Dir sehr dankbar, wenn Du auf meinen Seiten gestanden hast! Merci vielmals!

Moje veliko hvala ide Dr. Zorici Ristić i Vladimiru Savoviću koji su bili kao moja obitelj daleko od kuće a od kojih sam naučio neke ključne stvari kako preživjeti ovdje, a Zürich je ipak samo jedan sat daleko vlakom. I da uspio sam u tome da i ja mogu reći kao i Brajan – I have a story to tell!

Ich bin sehr dankbar an den Prof. Dr. Martin E. Schwab und Dr. Michael Miguel Maurer, die haben in mir ein besonderes Potenzial entdeckt und meine ersten Forschungsschritte vor 4.5 Jahren begleitet. Merci vielmals!

Un grazie speciale va a Federico, per tutto il tempo che ci siamo dati la spalla e che lo continueremo a fare, e che abbiamo affrontato questo viaggio del PhD in diversi ambiti e luoghi, ma nonostante siamo rimasti vicini e ci capiamo come al primo giorno. Ora tocca a te!

My special thanks go to my friend and the best DCBP PhD colleague Alicia, whom I met in the first days of her PhD. We grew together almost as a family in the last 3 years, sharing our experiences, times, flying and our favourite kebab in Ayverdis. Only you will understand how we went A to Ω and will continue so!

Ci ho insegnato tanti studenti di Farmacia negli ultimi 4 Praktikum di Galenica, ma una persona speciale, con la quale ho incrociato le strade, è stata Anna, che mi ha mostrato che

pure io più grande e con più esperienza ci posso imparare da Lei certe cose ed atteggiamenti quando non riuscivo più a distinguere un albero dal bosco. Grazie mille, Signora (futuro) Capitano!

Ein grosses Danke geht an allem RBS, SBB, BLS und Jungfraubahnen Personal, mit denen ich zu tun hatte, wenn ich zur und vor Arbeit oder in meiner Freizeit gefahren bin.

Posebno hvala od srca želim reći, meni vrlo bliskim i posebnim ljudima "s one strane Alpa", koji su bili tu uvijek uz mene, samo jedan poziv, poruku ili sliku udaljenosti, COVID krizu ili druge probleme, uvijek smo nekako našli vremena jedni za druge, a to su David (koji se prebacio s moje strane Alpa u međuvremenu), Ivana, Franka, Marija Magdalena, Tea i Vittorio.

Moja Bern – Bolligen ekipa također ima moju duboku zahvalnost, koji su bili tu uvijek kada mi je trebala jedna glazbena i umjetnička pauza ili logistička podrška. Neki bi rekli "jednom komšija – vazda komšija", a tu ulogu su u najboljem svjetlu i uz harmoniku odigrali Dimitrije, Sale, Uglješa, Anja, Kovida, Elisa, Rachele i Dejan.

Posljednje, ali i najvažnije ogromno hvala ide mojim roditeljima, Sanji i Branku, mom bratu Anđelu i baki Janji, koji su uvijek bili tu za mene, potiču me i prate, vjeruju u mene, podržavaju i trpe sve moje hirove, raspoloženja i razno – razne situacije u zadnjih nešto više od 31 godinu, a posebno, i s nesmanjenom strašću i voljom, sve vrijeme dosadašnje 23 godine školovanja, od Rijeke. Pehlina i Sušaka, do Trsta i kampusa Piazzale Europa, a sve do Züricha i Berna. Hvala Vam još jednom za sve!

Declaration of Consent

on the basis of Article 18 of the PromR Phil.-nat. 19

Name/First Name: Skorup Ivo

Registration Number: 18-798-645

Study program: PhD in Chemistry and Molecular Sciences

Dissertation

Title of the thesis: Oral lipid-based treatments for chronic liver disease: from

formulation characterization to in vitro assays mimicking

pathological conditions

Supervisor: Prof. Dr. Paola Luciani

I declare herewith that this thesis is my own work and that I have not used any sources other than those stated. I have indicated the adoption of quotations as well as thoughts taken from other authors as such in the thesis. I am aware that the Senate pursuant to Article 36 paragraph 1 litera r of the University Act of September 5th, 1996 and Article 69 of the University Statute of June 7th, 2011 is authorized to revoke the doctoral degree awarded on the basis of this thesis. For the purposes of evaluation and verification of compliance with the declaration of originality and the regulations governing plagiarism, I hereby grant the University of Bern the right to process my personal data and to perform the acts of use this requires, in particular, to reproduce the written thesis and to store it permanently in a database, and to use said database, or to make said database available, to enable comparison with theses submitted by others.

Place/Date Signature

Bern, 22.05.2023 Ivo Skorup